To my Parents, Rosa Estela and Heleno
To my brothers, Ivan, Cesar and Karina
To my wife and "complice en la vida" Roshelly
To my people, "Los Latinoamericanos", wherever they are

Hugo Alberto Gutiérrez-Jurado
New Mexico Institute of Mining and Technology
December, 2011

A HOLISTIC EXPLANATION OF THE ECOHYDROLOGIC AND GEOMORPHIC PROPERTIES FOR A SEMIARID BASIN WITH CONTRASTING ECOSYSTEMS

by

Hugo Alberto Gutiérrez-Jurado

Submitted in Partial Fulfillment

of the Requirements for the Degree of

Doctorate of Philosophy in Earth and Environmental Science

With Dissertation in Hydrology

New Mexico Institute of Mining and Technology

Socorro, New Mexico

December, 2011

The rain ...
Eyes of shadow-water
eyes of well-water
eyes of dream-water.
Blue suns, green whirlwinds,
birdbeaks of light pecking open
pomegranate stars.
But tell me, burnt earth,
is there no water?
Only blood, only dust,
only naked footsteps on the thorns?

- Octavio Paz, *Cloudbursts*

ABSTRACT

In semiarid areas with complex topographies, the combination of elevation and aspect promotes variations in the water and energy balance at the surface resulting in slopes with distinct ecologic, hydrologic and geomorphic properties. Although this phenomenon has captivated the attention of numerous researchers for many years, and various hypotheses have been proposed to explain particular aspects of the complex interactions between terrain, vegetation and water and energy fluxes, a holistic explication of the underlying mechanisms responsible for these patterns has yet to be accomplished. Additionally, and in light of the impending effects of climate change on the cycling of water and its impacts on the structure of vegetation mosaics in semiarid landscapes, it is critical to obtain a better understanding of the controls and feedbacks among vegetation-topographic-hydrologic interactions.

This study attempts to explain the primary controls on the observed vegetation contrasts in a semiarid catchment with nearly exact north and south facing aspects. Along this route, the study quantifies energy and water fluxes of the opposing slopes using field observations from an array of sensors deployed on and along the slopes of the study basin, and numeric modeling of various degrees of complexities. Important microclimatic parameters were also measured. The quantification of the differential energy and water balance dynamics of these slopes can provide essential information on the potential effects of climate variability for semiarid landscapes.

The study builds up from previous analyses on the effect of slope-aspect on the distinct degree of soil development and vegetation type, structure, and cover found on the slopes of a small (0.1 km^2) first order catchment in central New Mexico. One-dimensional vadose zone modeling on the opposing slopes, parameterized with soil profile and vegetation and meteorologic data, reveal important soil and vegetation-specific controls on the partitioning of water inputs on the slopes. Marked differences in root zone fluxes in a north-facing juniper (*Juniperus monosperma*) and south-facing creosote (*Larrea tridentata*) ecosystems were found. Differences in the amplitude and frequency of soil water content and pressure between the opposing slopes correspond to changes in soil profile and vegetation characteristics such as different stages of calcium carbonate ($CaCO_3$) and distinct plant water uptake capacities of Junipers and Creosote shrubs. The results at this stage suggest these variations in water fluxes reinforce the development of $CaCO_3$ horizons present in the soil profiles, leading to a feedback between vegetation establishment, soil water fluxes and geomorphic processes in the catchment. In addition, the model results also indicate that soil properties and water fluxes compensate for large differences in evaporative demand, leading to similar actual evapotranspiration (AET) in the opposing slopes.

Analyses on the differential response of the opposing slopes to a geomorphically significant flood from field reconnaissance observations after the event and soil moisture data recorded during and after the rainstorm reveal significantly different responses on the soil moisture dynamics, and rainfall-runoff relations on each slope. These results provide insights on the terrain-soil-vegetation interactions acting on the movement of water and sediments through this semiarid system and motivate the search for potential hydrogeomorphic signatures expressed on the terrain as a result of the observed differential hydrologic and

geomorphic processes occurring at the study site. Performing terrain analyses with high resolution topographic data from the study catchment revealed distinct mechanisms of runoff-erosion processes on the opposing slopes; Hillslope diffusion on north facing ecosystems is due to relatively higher slope, while fluvial erosion is more important on the south facing ecosystems as a result of large contributing areas. High-resolution topographic data was also able to discriminate statistically different sediment transport regimes in north and south facing slopes due to different dominant factors.

To test the hypothesis that large solar irradiance differences are a driving mechanism for the observed vegetation patterns, modeling of the incoming radiation on the study basin was performed using the same set of high-resolution topographic data and a distributed solar radiation model. Topographic-vegetation controls on the annual and seasonal patterns of irradiance were found. The first-order control on the irradiance pattern of each slope is dictated by aspect and slope, with tree cover and its spatial arrangement acting as a second order control on the north facing slope. We found seasonal maximization of the radiation differences for the spring equinox when the combination of tree and topographic shade greatly diminished the energy load on the north facing slopes. It is believed that for these types of ecosystems, irradiance analysis helps to identify the underlying topographic and vegetation controls on microclimate in the opposing slopes, revealing a feedback mechanism reinforcing the differences in vegetation establishment and persistence.

In the final part of this investigation, a series of analyses on the measured water and energy fluxes of the opposing slopes revealed the mechanisms responsible for the observed differences in vegetation cover and microclimatic prop-

erties in the study basin. The analyses show an amplification of seasonal differences in the energy balance that are translated into significant microclimatic differences between the opposing slopes. This results in seasonally enhanced differences in available energy for latent heat transfers, thereby, imposing distinct evapotranspiration (ET) dynamics on the opposing slopes. The already established vegetation cover and soil development of the slopes further accentuate the differences in hydrologic dynamics of each ecosystem and creates a series of feedback mechanisms that self-reinforce the observed contrasts in vegetation and terrain properties. For example, longer soil moisture residence times on the north facing slope benefit a denser vegetation cover that produces and conserves more soil which in turn accommodates and retains more water. Seasonal water balances of the contrasting ecosystems reveal the use of different soil water sources for ET through the year. Larger and more frequent runoff events on the south facing slope contribute to a more active erosive condition, leading to increased rates of soil losses resulting in a decrease of surface moisture storage and vegetation cover. The final result of these vegetation-topographic- hydrologic interactions is a characteristic progression of soil moisture and temperature values along the slope aspect continuum that is preserved throughout the year, going from the wetter and cooler soils on the north facing slope to the drier and warmer soils on the south facing slope. The quantified water and energy fluxes corroborate a conceptual model that incorporates vegetation-terrain-hydrologic interactions (and feedbacks) seeking to explain the differential ecohydrologic dynamics of opposing slopes with contrasting ecosystems of semiarid regions.

Keywords: ecohydrology; hydrogeomorphology; vegetation-topographic-hydrologic interactions; catchment hydrology; semiarid hydrology.

ACKNOWLEDGMENTS

This has been an endeavour in which many people and institutions have participated directly or indirectly, and to all those people and entities I owe my infinite gratitude. My studies at New Mexico Tech have been possible thanks to the generous support from a NASA and NSF grants. Likewise, I would like to acknowledge the New Mexico Geological Society and the New Mexico Tech Graduate Student Association for their support on many of my academic and research activities during this Ph.D. The National Center for Airborne LiDAR Mapping (NCALM) provided a valuable dataset that facilitated enormously a large part of the research I conducted for this dissertation, I am thankful to them. I would also like to acknowledge The Sevilleta National Wildlife Refuge for providing access to the study site.

During my studies at NMT I have found without a doubt the best Professors anyone can have in Graduate School: Dr. Jan Hendrickx, Dr. Robert Bowman, Dr. Fred Phillips, Dr. John Wilson, Dr. Enrique Vivoni, Dr. Bruce Harrison, Dr. Dana Ulmer-Scholle, and Dr. Peter Mozley, each one of them has seeded in me their passion for our science and through their example have inspired me to keep building my own scientific career, and for all of that the least I can do is to make them patent my gratitude, respect and admiration.

I would like to express my recognition to my committee members, whose advice and guidance have been instrumental in the successful completion of this work. My sincere appreciation goes to Dr. Fred Phillips, whose door was always

open to me for guidance and help in every aspect of my academic formation. A Professor whose help was always opportune and whose advice was always useful was that of Dr. Bruce Harrison. His always frank and friendly approach when sharing his insights to many of the problems I faced during my time at NMT I will always remember and try to imitate. One of the Professors whose teachings and counsels had perhaps the most profound influences on my development as a scientist was Dr. John Wilson. However, my admiration and appreciation to him goes beyond the classroom and laboratory as I had the opportunity to work with him and learn from his mentorship style, and recognize him as a Professor who is always genuinely interested in the problems and well being of the students, and to me that means a great deal. If some day I become a Professor, I would be lucky to be half the professor Dr. Wilson is. There is one person whose overall input to this work was not only essential and important, but key to the successful conclusion of this research project and doctorate. This person did not only affect in a positive way the course of my studies and scientific production but has set an example to me of what a scientist should be, and there is probably nothing I could do to repay him sufficiently for the opportunity he gave me to work on this magnificent project. This person was my advisor and friend Enrique Vivoni, to whom I will always remain indebted. I would also like to acknowledge all the help and advice I received from Drs. Dave Breshears and Brent Newman who were also part of my Ph.D. committee, but could not participate in the last part of this dissertation for different reasons.

Many friends and collaborators participated from my efforts and all of them deserve my gratitude. I owe special thanks to Dr. Erkan Istanbulluoglu, for his friendship and camaraderie, and for providing me with valuable comments on my work and giving me a hand with recommendations any time I

needed them. On a similar note I would like to thank Dr. Rafael Bras for his always attentive and invaluable insights on my work. I recognize also from among all my friends those who have shared the magnificent experience of graduate school at New Mexico Tech, and whose friendship I will carry with me to every place I go until we meet again in this big theater of life: Huade Guan, Luis Mendez, Taufique Mahmood, Rob Wyckoff, Carlos Aragon, Alex Rinehart, Bill Tai, Giuseppe Mascaro, Laura Rosales, Sung-Ho Hong, Marty Frisbee, Emily Engle, Jason Heath, Fred Partey, Helga Madrigal, Carlos Ramirez, Hernan Moreno, Laura Alvarez, Mussie Tewelde, Brian Cozzens, Jesus Gomez, Walter Moreno, Agustin Robles, Maya El Hariri, Shari Houston, Aida Quezada and many others to whom I apologize If I missed in this long list. During the course of my studies at NMT many hours of field work were carried, and from those long hours, I recall the best part was the company of friends whose help to either deploy instruments, collect data or maintain equipment I could never thank enough; Phil Turner, Frederick Ennin, Rhonda Trujillo, Christina Hernandez, Colin Cikoski, Luis Mendez, and Carlos Ramirez were all the best field work partners one can ask. In the life of a graduate student many errands and paperwork are tremendously simplified by those persons sitting behind a desk, always with a big smile and the willingness to spare a minute or two of their time to help you. At the NMT E&ES Dept. Pat Mills, Connie Apache, Susan Heath, Leigh Davidson, Pat Valentine and Shari Houston made my life much easier, and they deserve all my gratefulness. During the last couple months of work leading to the completion of this Dissertation, I received the support from many friends and their families (Robles Valencia, Mendez Ortiz, Vivoni Felix), to all of them I want to express my deepest appreciation. I would also like to acknowledge all the help and support I received from CAFERATO Ent. and all its divisions, WALRUS Inc., and Gele-Gele B&B.

From all the people around me, my family has always been there for me, supporting me in every enterprise I start. My parents Rosa Estela and Heleno, and my brothers Ivan, Cesar and Karina, were all a source of inspiration and motivation to reach the finish line and never quit working towards the goals I set to myself. Finally, I would like to thank that person whose love and care accompanied me throughout all these years of constant learning and effort, and whose company has made the load I carried more enjoyable and meaningful, thank you Roshelly for being always on my side providing me your strength, this has become a reality thanks to you.

Muchas Gracias a todos!!

Arrieros somos y en el camino andamos...

-Anónimo

This dissertation was typeset with LaTeX[1] by the author.

[1]The LaTeX document preparation system was developed by Leslie Lamport as a special version of Donald Knuth's TeX program for computer typesetting. TeX is a trademark of the American Mathematical Society. The LaTeX macro package for the New Mexico Institute of Mining and Technology dissertation format was written for the Tech Computer Center by John W. Shipman.

TABLE OF CONTENTS

LIST OF TABLES

LIST OF FIGURES

This dissertation is accepted on behalf of the faculty of the Institute by the following committee:

John L. Wilson, Chair

Enrique R. Vivoni, Co-Chair

Fred M. Phillips

J. Bruce J. Harrison

I release this document to the New Mexico Institute of Mining and Technology.

Hugo Alberto Gutiérrez-Jurado Date

CHAPTER 1

INTRODUCTION

1.1 Introduction and Research Questions

In the hydrologic cycle, vegetation and terrain properties strongly influence the partitioning of water into soil water, groundwater, surface water, and atmospheric water (Dingman, 2000). Moreover, the combination of vegetation and terrain properties along with rainfall characteristics dictate the rates at which hydrologic processes such as infiltration, evapotranspiration, deep percolation, runoff and runon occur (Turnbull et al., 2010.c). Yet, the joint effects of vegetation-terrain properties on the hydrologic cycle, and vice versa, are poorly understood and have not been extensively quantified (Ivanov et al., 2008.a,b; Brooks and Vivoni 2008; Vivoni et al., 2008). Furthermore, few investigations have examined systemically the interactions between physical, topographical and ecological form (Tromp-van Meerveld and McDonnell, 2006). Advancing the understanding of vegetation-topographic interactions on the hydrologic cycle is particularly important for semiarid areas, where the limited availability of water in time and space control ecosystem functions and all the services provided by them to society (Popp et al., 2009; Vivoni et al., 2010).

A potentially fertile avenue to investigate vegetation-topographic-hydrologic interactions is the study of naturally occurring environmental gradients in areas of complex terrain. The quantification of environmental thresholds imposed by

terrain to vegetation communities can shed light into the vulnerability of semiarid ecosystems to changes in hydrologic and climatic regimes expected as a result of a warming climate (Allen et al., 2010). In this regard, Mátyás (2010) recognized the urgent need for a better understanding on the xeric limits of trees and forests in view of the current trends in climate change scenarios, that we review in the following lines.

An ample number of climate models projections indicate that southwestern North America and other subtropical regions will become increasingly arid as a consequence of rising greenhouse gases (Seager et al., 2007). Recent studies predict that large areas in the semiarid southwestern North America will experience increases in land surface temperatures ranging between 1.2-2 °C by the year 2040 (Diffenbaugh et al., 2008) and between 3-5 °C by the end of the 21st century (Christensen et al., 2007). In much of the region, the projected temperature increases will intensify seasonal hot extremes, leading to decreases in warm season soil moisture (Diffenbaugh and Ashfaq, 2010). The permanent emergence of unprecedented heat conditions (Diffenbaugh and Scherer 2011), particularly during the warm season, could result in major changes in vegetation composition (Allen et al., 2010). For example, recent research suggest that relatively minor changes in temperature associated with prolonged droughts could severely impact semiarid ecosystems by killing large numbers of trees (Breshears et al., 2005; Adams et al., 2009; Allen et al., 2010). Furthermore, changes in regional precipitation patterns expected for southwestern North America envisage more intense and less frequent summer moonson storms over large areas (Gutzler et al. 2008). As a result, longer and warmer droughts are expected to occur in the coming years (Gutzler and Robbins 2010). These arguments support the reported tendency of drying in continental interiors during the summer at mid-latitudes (IPCC, 2007).

The consequences of the climatic trends for the preservation and management of natural resources (including water) in arid and semiarid ecosystems are largely unexplored and represent a challenge for ecologists and hydrologists alike.

Although it is conceivable that changes in climatic regimes at the regional level will produce impacts on the structure and hydrologic functioning of arid and semiarid ecosystems, the resulting effects on the local hydrology are not entirely clear. Nevertheless, examples of hydrologic dynamics shifting resulting from alteration of ecosystem structure exist within the realm of woody plant encroachment studies (Huxman et al., 2005; Turnbull et al., 2010a,c). A number of works have documented and investigated the causes and effects of shrubs encroachment in places historically occupied by grasslands (Gao and Reynolds, 2003; Laliberte et al., 2004; Briggs et al., 2005; Knapp et al., 2008; Turnbull et al., 2010a,b,c.). It is known that the conversion of grasslands into shrublands leads to the modification of land surface processes affecting the spatio-temporal availability of water and nutrients (D'Odorico et al., 2010; Turnbull et al., 2010a,b). Specific processes affected by these changes in vegetation with direct implications on the hydrology of arid and semiarid areas are rainfall-runoff relations (Huxman et al., 2005; Turnbull et al., 2010.c; Bedford, 2008), water infiltration (Bedford and Small 2008), deep percolation and groundwater recharge (Seyfried et al., 2005; Sandvig and Phillips 2006), soil deposition, nutrients redistribution and cycling (Turnbull et al., 2010), soil and air temperature regimes (D'Odorico et al., 2010).

While some of these vegetation changes and their associated impacts on the hydrologic cycle can be observed in the short term (i.e., in the scale of months to years), others become evident in the long term (e.g., soil development, water percolation and aquifer recharge)(Gutiérrez-Jurado et al., 2006; Sandvig and

Phillips, 2006). Therefore, studying naturally occurring environmental gradients in areas of complex terrain can not only help elucidate the controls of topographically-modified climatic factors on the dynamics of water and energy fluxes, but may also shed light on the attenuation or amplification effects of spatially varying land surface properties on the magnitude of these fluxes. In this study we attempt to explain in a parsimonious way, how observed terrain-vegetation interactions modify regional hydrologic and energy fluxes within a semiarid catchment with opposing aspect-slopes and sharp vegetation contrasts. In addition, we explore the long term legacy of the differential ecologic-hydrologic dynamics of the basin expressed on the soils and geomorphic properties of the catchment. We pose the hypothesis that a strong coupling must exist between patterns of terrain, vegetation, energy and water balance and propose to answer the following questions:

1. What are the underlying controls driving the characteristic contrasting vegetation patterns observed in semiarid hillslopes with opposing aspects?

2. What are the mechanisms enforced by the coupling of terrain and vegetation patterns on the dynamics of water fluxes in the area?

3. How are the dynamics and magnitudes of the differential hydrologic fluxes and states of opposing ecosystem-slopes, responsible for the observed geomorphic and vegetation patterns of semiarid catchments with contrasting ecosystems?

Answering these questions will provide necessary knowledge on the environmental thresholds imposed by terrain to semiarid vegetation communities that in turn can offer insights into the vulnerability of semiarid ecosystems to changes in hydrologic and climatic regimes expected as a result of a warming climate (Allen et al., 2010). In addition, we expect to obtain information on potential vegetation-hydrologic-terrain feedbacks and parameters to feed and verify

future ecohydrologic and hydrogeomorphic modeling efforts for semiarid areas with complex topographies.

This dissertation is organized as follows. Chapter 2 investigates the effects of topographic position, vegetation and soil development on the hydrologic fluxes in two ecosystems within a semiarid basin in central New Mexico. In chapter 3, we document and analyze the hydrologic response of a semiarid catchment to a geomorphically significant rainfall event defined here as a flood that alters landscape form, and analyze the differential response on soil moisture dynamics of opposing north and south facing slopes. In chapter 4, we study the geomorphological features of north and south facing slopes through the use of improved resolution elevation datasets. Slope-contributing area, and Curvature-Contributing area analyses were used to investigate, quantify and contrast the geomorphic properties of the opposing north and south facing slopes. Similarly, in chapter 5 we used a distributed solar radiation model and a set of sequentially improved elevation datasets to explore the vegetation-topography-radiation interactions in a basin. In chapter 6, we quantify and analyze the differential energy and water dynamics of opposing slopes of a semiarid basin with contrasting ecosystems. Chapter 7 summarizes the role of terrain-vegetation interactions on the modification of land surface properties and processes giving rise to distinct ecohydrologic dynamics supporting the contrasting vegetation communities between the north and south facing slopes.

REFERENCES

Adams, H. D., Guardiola-Claramonte, M., Barron-Gafford, G. a, Villegas, J. C., Breshears, D. D., Zou, C. B., et al. (2009), Temperature sensitivity of drought-induced tree mortality portends increased regional die-off under global-change-type drought. *Proceedings of the National Academy of Sciences of the United States of America, 106*(17), 7063-6. doi: 10.1073/pnas.0901438106.

Allen, C. D., Macalady, A. K., Chenchouni, H., Bachelet, D., McDowell, N., Vennetier, M., et al. (2010), A global overview of drought and heat-induced tree mortality reveals emerging climate change risks for forests. *Forest Ecology and Management, 259*(4), 660-684. doi: 10.1016/j.foreco.2009.09.001.

Bedford, D. (2008), *Effects of vegetation-related soil heterogeneity on runoff, infiltration, and redistribution in semiarid shrubland and grassland landscapes*, Ph.D. Thesis, University of Colorado, 197 pp.

Bedford, D. and Small, E. (2008), Spatial patterns of ecohydrologic properties on a hillslope-alluvial fan transect, central New Mexico. *Catena, 73*(1), 34-48. doi: 10.1016/j.catena.2007.08.005.

Breshears, D. D., Cobb, N. S., Rich, P. M., Price, K. P., Allen, C. D., Balice, R. G., et al. (2005), Regional vegetation die-off in response to global-change-type drought. *Proceedings of the National Academy of Sciences of the United States of America, 102*(42), 15144-8. doi: 10.1073/pnas.0505734102.

Briggs, J. M., Knapp, A. K., Blair, J. M., Heisler, J. L., Hoch, G. a, Lett, M. S., and McCarron, J. K. (2005), An Ecosystem in Transition: Causes and Consequences of the Conversion of Mesic Grassland to Shrubland. *BioScience, 55*(3), 243. doi:10.1641/0006-3568(2005)055[0243:AEITCA]2.0.CO;2

Brooks, P.D. and Vivoni, E.R. (2008), Mountain ecohydrology: quantifying the role of vegetation in the water balance of montane catchments. *Ecohydrology. 1*(3): 187-192.

Christensen, J. H. et al. (2007), *Regional climate projections, in Climate Change 2007: The Physical Science Basis.* Contribution of Working Group I to the Fourth Assessment Report of the Intergovernmental Panel on Climate Change, edited by S. Solomon, et al., chap. 11, pp. 235336, Cambridge Univ. Press, New York.

Diffenbaugh, N. S., and Ashfaq, M. (2010), Intensification of hot extremes in the United States. *Geophysical Research Letters, 37*(15), 1-5. doi: 10.1029/2010GL043888.

Diffenbaugh, N. S., Giorgi, F., and Pal, J. S. (2008), Climate change hotspots in the United States. *Geophysical Research Letters, 35*(16), 1-5. doi: 10.1029/2008GL035075.

Diffenbaugh, N. S., and Scherer, M. (2011), Observational and model evidence of global emergence of permanent, unprecedented heat in the 20th and 21st centuries. *Climatic Change, 107*(3-4), 615-624. doi: 10.1007/s10584-011-0112-y.

Dingman, L. S. (2000), *Physical Hydrology*, 2nd edition, Prentice Hall, 365 pp.

D'Odorico, P., Fuentes J. D., Pockman W. T., Collins S. L., He Y., Medeiros J. A., DeWekker S., and Litvak M. E. (2010), Positive feedback between microclimate and shrub encroachment in the northern Chihuahuan desert, *Ecosphere 1*(6):art17. doi:10.1890/ES10-00073.1

Gao Q., and Reynolds J.F. (2003), Historical shrub-grass transitions in the northern Chihuahan Desert: modeling the effects of shifting rainfall seasonality and event size over a landscape gradient, *Global Change Biology* 9.

Gutiérrez-Jurado H.A., Vivoni E.R., Harrison J.B.J. and Guan H. (2006), Ecohydrology of root zone water fluxes and soil development in complex semiarid rangelands. *Hydrol. Process.*, 20: 32893316, doi: 10.1002/hyp.6333.

Gutzler, D. S., and Robbins, T. O. (2010), Climate variability and projected change in the western United States: regional downscaling and drought statistics. *Climate Dynamics*. doi: 10.1007/s00382-010-0838-7.

Huxman, T. E., Wilcox, B. P., Breshears, D. D., Scott, R. L., Snyder, K. A., Small, E. E., Hultine, K., et al. (2005), Ecohydrological implications of woody plant encroachment. *Ecology*, 86(2), 308-319. doi:10.1890/03-0583

Knapp, A. K., Briggs, J. M., Collins, S. L., Archer, S. R., Bret-Harte, M. S., Ewers, B. E., Peters, D. P., et al. (2008), Shrub encroachment in North American grasslands: shifts in growth form dominance rapidly alters control of ecosystem carbon inputs. *Global Change Biology*, 14(3), 615-623. doi:10.1111/j.1365-2486.2007.01512.x

Laliberte, A. S., Rango, A., Havstad, K. M., Paris, J. F., Beck, R. F., McNeely, R., et al. (2004), Object-oriented image analysis for mapping shrub encroachment from 1937 to 2001 in southern New Mexico, *Remote Sen*, 93, 198-210. doi: 10.1016/j.rse.2004.07.011.

Mátyás C. (2010), Forecasts needed for retreating forests, *Nature*, 464, 1271 pp. doi:10.1038/4641271a

Popp, A., Blaum, N., and Jeltsch, F. (2009), Ecohydrological feedback mechanisms in arid rangelands: Simulating the impacts of topography and land use. *Basic and Applied Ecology*, 10(4), 319-329. Elsevier. doi:10.1016/j.baae.2008.06.002

Sandvig, R.C., and Phillips, F.M. (2006), Ecohydrological controls on soil-moisture fluxes in arid vadose zones: *Water Resour. Res., 42* W08422, doi:10.1029/2005WR004644.

Seager R., Ting M.F., Held I.M., Kushnir Y., Lu J., Vecchi G., Huang H.P., Harnik N., Leetmaa A., Lau N.C., Li C., Velez J., Naik N., (2007), Model projections of an imminent transition to a more arid climate in southwestern North America. *Science*, 316,(5828), 1181 1184. DOI: 10.1126/science.1139601

Seyfried, M. S., Schwinning, S., Walvoord, M. A., Pockman, W. T., Newman, B. D., Jackson, R. B., and Phillips, F. M. (2005), Ecohydrological control of deep drainage in arid and semiarid regions. *Ecology, 86*(2), 277-287. Eco Soc America. doi:10.1890/03-0568

Tromp-van Meerveld, H.J., McDonnell, J.J. (2006), On the interrelations between topography, soil depth, soil moisture, transpiration rates and species distribution at the hillslope scale, *Adv. Water Res.*, 29, 293-310.

Turnbull, L., Wainwright, J., and Brazier, R. E. (2010.a), Hydrology, erosion and nutrient transfers over a transition from semiarid grassland to shrubland in the South-Western USA: A modelling assessment. *Journal of Hydrology, 388*(3-4), 258-272. doi: 10.1016/j.jhydrol.2010.05.005.

Turnbull, L., Wainwright, J., and Brazier, R. E. (2010.b), Nitrogen and phosphorus dynamics during runoff events over a transition from grassland to shrubland in the south-western United States. *Hydrological Processes, 25*(1), 1-17. doi: 10.1002/hyp.7806.

Turnbull, L., Wainwright, J., and Brazier, R. E. (2010.c), Changes in hydrology and erosion over a transition from grassland to shrubland. *Hydrological Processes*, 24, 393- 414. doi: 10.1002/hyp.7491.

Turnbull, L., Wainwright, J., Brazier, R. E., and Bol, R. (2010.d), Biotic and abiotic changes in ecosystem structure over a shrub-encroachment gradient in the southwestern USA. *Ecosystems, 13*(8), 1239-1255. doi: 10.1007/s10021-010-9384-8.

Vivoni, E.R., Rinehart, A.J., Mendez-Barroso, L.A., Aragon, C.A., Bisht, G., Cardenas, M.B., Engle, E., Forman, B.A., Frisbee, M.D., Gutiérrez-Jurado, H.A., Hong, S., Mahmood, T.H., Tai, K. and Wyckoff, R.L. (2008), Vegetation controls on soil moisture distribution in the Valles Caldera, New Mexico, during the North American monsoon. *Ecohydrology, 1*(3): 225-238.

Vivoni, E. R., Rodrguez, J. C., and Watts, C. J. (2010), On the spatiotemporal variability of soil moisture and evapotranspiration in a mountainous basin within the North American monsoon region. *Water Resources Research, 46*(2), 1-18. doi:10.1029/2009WR008240.

CHAPTER 2

ECOHYDROLOGY OF ROOT ZONE WATER FLUXES AND SOIL DEVELOPMENT IN CATCHMENTS OF COMPLEX TERRAIN

(This chapter is published as: Gutiérrez-Jurado H.A., Vivoni E.R., Harrison J.B.J. and Guan H. 2006. Ecohydrology of root zone water fluxes and soil development in complex semiarid rangelands. *Hydrol. Process.* **20**: 32893316, doi: 10.1002/hyp.6333.)

2.1 Introduction

Topographic and soil properties are considered a large determinant of the spatial establishment and persistence of terrestrial plants under a similar climate (e.g., Wierenga et al., 1987; Florinsky and Kuryakova, 1996; Engel et al., 2002; Coblentz and Riitters, 2004; Kim and Eltahir, 2004; Caylor et al., 2005). In arid and semiarid environments, low precipitation amounts lead to conditions where water availability and its interaction with terrain and soil characteristics controls ecosystem processes such as transpiration, growth, species competition, and mortality (e.g., Allen and Breshears, 1998; Wainwright et al., 1999; Rodrguez-Iturbe et al., 2001a; Porporato et al., 2002; Wilcox et al., 2003a; Kerkhoff et al., 2004). As a result, the study of semiarid watersheds characterized by complex terrain requires consideration of the combined effect of topography, soils and vegetation

on the redistribution of available water (Loik et al., 2004; Reynolds et al., 2004; Ludwig et al., 2005; Newman et al., 2005). Despite their importance, interactions and feedbacks between terrain position, soil properties and plant establishment have not been adequately documented in arid and semiarid regions, in particular with respect to the reinforcing effects of the these interactions on soil development. Terrain-soil-plant interactions in water-limited ecosystems is an emerging research issue in ecohydrology which presents a significant opportunity to understand both the short term (e.g., runoff response, seasonal growth) and long term processes (e.g., soil evolution, plant succession) operating within watersheds.

Topographic position is known to create spatial niches for the establishment of specific vegetation types (e.g., grasses, shrubs, trees) through the effects of slope, aspect and curvature on incident radiation and the transport of water and nutrients (Moore et al., 1993; Band et al., 1993; Mackay and Band, 1997; Dirnbock et al., 2002). For example, the effects of topography on soil water redistribution have been widely recognized to create regions of time-varying saturation near channels (Dunne and Black, 1970; Beven and Kirkby, 1979; Western et al., 1999). Differences in lateral moisture distribution also lead to soil catenary relationships along hillslopes and transport of material downslope toward channel reaches (Milne, 1935; Birkeland, 1999). The preferential redistribution of soil water, through overland or subsurface pathways in accordance to landscape position, allows for vegetation species with different water use characteristics to coexist in a particular basin (e.g., Stewart and Harrison, 1987; van Wijk and Rodrguez-Iturbe, 2002; Kim and Eltahir, 2004). Once established, vegetation plays a critical role in modifying the hydrologic dynamics in a watershed over the hillslope and channel reach scale through controls on the water balance and the physical characteristics of the landscape.

Vegetation impacts on hydrologic dynamics include effects on precipitation due to interception and stemflow (Martnez-Mesa and Whitford, 1996; Abrahams et al., 2003); soil surface temperature due to plant shadowing (Breshears et al., 1998); moisture availability due to plant root water extraction (Scott et al., 2000; Small and Kurc, 2003); surface resistance to winds and overland runoff (Reid et al., 1999; Breshears et al., 2003); infiltration capacity due to vegetation patches and root channels (Wilcox et al., 2003b; Bhark and Small, 2003); contributions of plants to evapotranspiration (Boulanger, 2004; Huxman et al., 2005); and deep vadose zone percolation (Walvoord and Phillips, 2004; Seyfried et al., 2005). Since plants play a fundamental role in controlling the surface energy and water balance, the differential establishment of vegetation across a landscape can lead to significant spatial variations in ecohydrological dynamics. While the individual effects of different species on hydrologic dynamics have been investigated, many questions still exist regarding the emergent vegetation patterns arising in semiarid regions (van Wijk and Rodrguez-Iturbe, 2002; Wilcox et al., 2003a; Caylor et al., 2005). In this respect, understanding the controls exerted by topography and soil development may lead to identifying the ecohydrological interactions resulting in vegetation patterns.

Soil properties in the plant root zone are of considerable importance in mediating ecohydrological dynamics (e.g., Fernández-Illescas et al., 2001; Dodd et al., 2002). An often overlooked interaction between soil properties and vegetation are the effects that plants have on material deposition and erosion. Vegetation controls on the production and transport of material have important implications on soil development over long periods (Shreve and Mallery, 1932; Gile et al., 1981). In complex terrain, this is further complicated by pedogenic processes that operate in hillslopes (Milne, 1935; Kirkby, 1978; Birkeland, 1999), with material

transported downslope in response to vegetation-mediated fluxes. As a result, a critical factor in ecohydrological dynamics are the influences that different plants may have on soil formation and the resulting soil properties (e.g., hydraulic conductivity, organic matter, water retention capacity). As soil formation stores a long-term record of surface processes, an analysis of soil properties can provide time-integrated insights on the interaction of coexisting plants with geomorphic processes and the history of water fluxes on complex topographic surfaces.

Soil characteristics controlled by terrain position and vegetation distribution have feedback effects on the soil properties that determine water availability, retention and transport (Brooks and Corey, 1964; Rawls and Brakensiek, 1985). For example, water infiltration in semiarid areas is directly related to soil characteristics which are mediated by depositional processes, plant litter, soil gas production (Gile et al., 1981; Abrahams and Parsons, 1991; Wilcox et al., 2003b) and to some extent by the influence of fauna living under vegetation mounds (e.g., burrowing animals). Soil hydraulic properties, such as conductivity and moisture retention, play a critical role in the partitioning of precipitation into infiltration, runoff, evapotranspiration and deep percolation. Soil controls on the water balance ultimately affect the moisture availability for plants and the excess water for transport through the hillslope and channel system (e.g., Porporato et al., 2002; Milne et al., 2002; Caylor et al., 2005). Soil profile development via weathering processes of parent material also determines the soil depth available for moisture storage (Dietrich et al., 1995). As soil properties vary along a hillslope due to catenary processes and in a watershed due to vegetation patterns, we anticipate that strong interactions and feedback mechanisms will exist between ecohydrological dynamics and soil formation.

In this study, we discuss ecohydrological controls on root zone water fluxes and soil development in semiarid regions, with a focus on watersheds with complex terrain. The paper is organized as follows. Section 2 presents a review of the vegetative controls on soil development, with examples presented from a conifer-shrub ecotone in a small basin in New Mexico. In section 3, we describe the study catchment in more detail. An estimate of soil infiltration capacity for the two ecosystems is derived in Section 4 by using standard pedotransfer functions. Section 5 utilizes the vegetation and soil properties to parameterize an energy balance algorithm and one-dimensional vadose zone model for the two opposing hillslopes ecosystems. We investigate the effects of landscape position, vegetation, and soil properties on root zone water fluxes, including moisture and pressure profiles, deep percolation and evapotranspiration. In Section 6, we discuss the interaction between hydrologic dynamics and soil development in semiarid regions and point to critical measurements necessary in this emerging research area.

2.2 Ecohydrology and Soil Formation Processes

The role of different ecosystems in the distribution, persistence and movement of water has been of mutual interest to ecologists and hydrologists for many decades. More recently, the emerging field of ecohydrology attempts to link the work by hydrologists and ecologists to construct a more complete understanding of the ecological relevance of the water cycle and vice versa (Rodrguez-Iturbe, 2000). As plant-water interactions occur on complex landscapes, the study of ecohydrology requires consideration of abiotic factors (climate, soils, terrain) that control water fluxes and mediate vegetation dynamics. While several abiotic controls have been recognized, the effects of topography and soil development on

plant dynamics and the feedbacks of vegetation on landscape and soil morphology have not received as much attention. Furthermore, to our knowledge, the long-term linkages between plants and soil formation processes as a control on short-term ecohydrological fluxes have not been investigated in water-limited ecosystems.

The interactions between hydrologic, geomorphologic and ecosystem processes in semiarid basins are best discussed with the aid of a conceptual diagram in Figure 2.1 The schematic presents three stages in the development of a small, semiarid basin with time progressing downwards. The basin initially develops from an alluvial fan surface, which is incised due to erosional processes. Note that the west to east channel orientation leads to opposing north-facing and south-facing slopes with initially identical runoff production (Figure 2.1.a). Aspect variations in the opposing slopes lead to differential solar radiation altering the energy and water balance at the soil surface (Bonan, 2002). Topographic convergence of soil water also leads to preferentially wet or dry regions in the basin. In Figure 2.1.b, variations in moisture created by the effects of solar radiation and terrain convergence lead to preferential plant establishment in a distinctive pattern associated with terrain aspect. The vegetation pattern is typically repeated in sequences of north- and south-facing slopes in semiarid regions, in particular where climate promotes ecosystem coexistence (McAuliffe, 1984; Aide and VanAuken, 1985; Wondzell et al., 1996).

The established vegetation typically consists of a more mesic plant species in the north-facing slope and a more xeric community in the south-facing slope. The head slope area in Figure2.1.b is characterized by an increased flow convergence and a range of solar radiation, effectively serving as a dynamic boundary between the two ecosystems. Differential plant establishment has important

consequences on the hydrologic dynamics in the opposing hillslopes, in particular if the species have variations in canopy and root characteristics (e.g., mesic conifer versus xeric shrub). For example, evapotranspiration fluxes in Figure 2.1.b can vary in the opposing ecosystems due to plant water uptake strategies. The plants also lead to variations in soil development above an identical parent material. Soil profiles along the north-facing hillslope are typically deeper and have a larger percentage of organic matter, silt, clay and calcium carbonate over the soil depth (Figure 2.2; McMahon, 1998). Furthermore, the combined effects of soil conditions and vegetation lead to variations in runoff and erosion, shown in Figure 2.1.c as an increased drainage density along the south-facing hillslope.

This conceptual evolution of a semiarid basin is based upon field observations, soil analysis and mapping conducted by McMahon (1998) and our own studies. Basin evolution is the result of relationships between climate, hydrology and geomorphology, mediated by the effects of coexisting plants in the opposing slopes. Vegetation controls on soil formation lead to variations in hydraulic properties that reinforce differences in moisture, runoff and erosion in the two slopes. While the vegetation influences on landscape evolution are interesting, we limit this study to identifying the vegetative controls on soil development and its effects on root zone water fluxes. In the following, we describe three vegetation-mediated processes that lead to the development of arid and semiarid soils: (1) moisture fluxes, (2) material deposition and erosion, and (3) calcium carbonate horizon development. We then describe the potential for feedback between soil formation, hydrologic fluxes and ecosystem processes occurring in semiarid rangelands.

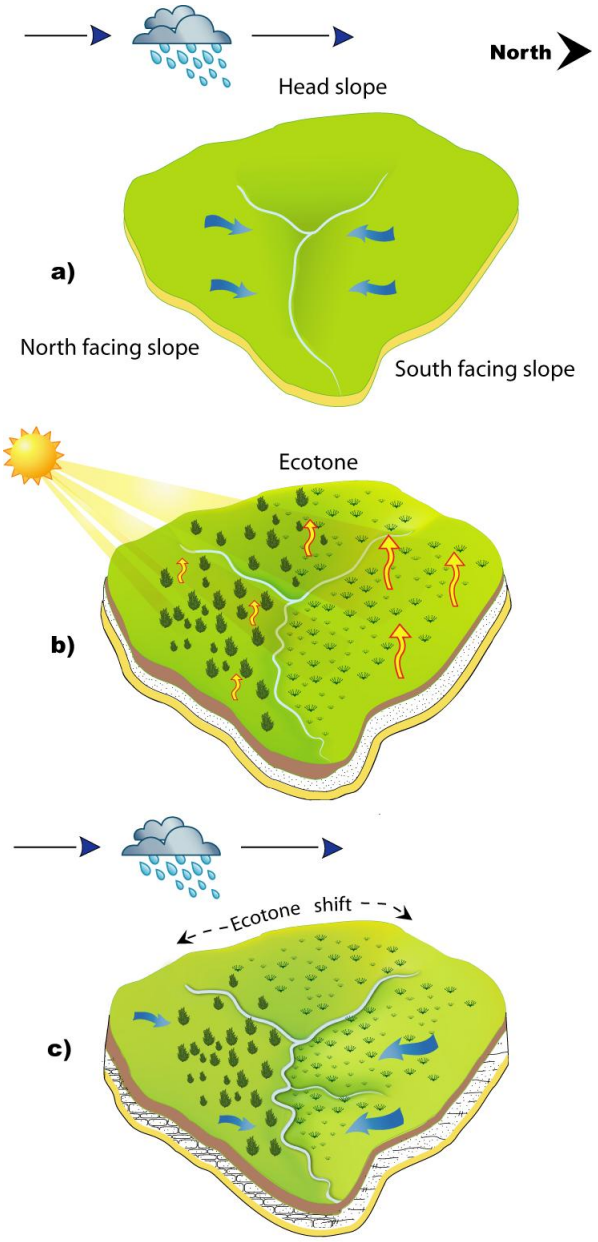

Figure 2.1: Conceptual evolution of a semiarid alluvial fan with opposing hillslopes and an ecotonal boundary. The area corresponds to a small drainage basin with *Juniperus monosperma* (oneseed juniper) on the north-facing slope and *Larrea tridentata* (creosote bush) on the south-facing slope. (a) Initial alluvial fan dissection and formation of main channel leading to opposing hillslopes and head slope area. Note the lack of soil development in the two slopes. (b) Development of major channels and steeper incision leading to further differentiation of opposing hillslopes. Variation of incident radiation due to aspect results in differential moisture conditions which leads to preferential vegetation establishment, with a north-facing mesic and south-facing xeric species. Caption continues in next page.

(c) Continued alluvial fan development with increased channel incision and secondary drainages on the south-facing slope, with associated changes to the hillslope profile convexity. Long-term establishment of different plant communities impacts soil development, including organic matter, silt, clay and $CaCO_3$ profiles. In addition, runoff and erosion (blue arrows) vary in the two slopes. Soil characteristics, vegetation and hydrologic fluxes reinforce soil pedogenesis and lead to feedback effects on the occurrence of distinct vegetation. Ecotonal shifts between mesic conifer and xeric shrub species occur on the head slope due to climate and soil water variations.

Figure 2.2: Soil profile measurements in opposing hillslope ecosystems: north-facing juniper savanna hillslope (SL-1) and south-facing creosote bush-grass hillslope (SL-5) (after McMahon, 1998). Refer to Figure 2.3 for soil characteristics and Figure 2.4 for profile locations.

2.2.1 Root Zone Moisture Fluxes

Moisture fluxes in the root zone of arid and semiarid soils are primarily controlled by precipitation patterns (e.g., Milne et al., 2003; Reynolds et al., 2004). The partitioning of rainfall into runoff, infiltration, evapotranspiration and deep percolation is dependent on precipitation regime. For example, the timing of rainfall occurrence relative to plant growth determines the infiltration consumed by shallow roots versus the amount leading to deep storage (Scott et al., 2000; Porporato et al., 2002). In the southwestern US, the bimodal distribution of precipitation in the summer monsoon and winter season results in distinctive soil moisture patterns (Milne et al., 2003). During the winter, low intensity, long duration rainfall events during periods of low plant activity lead to steady, slow infiltration into and below the root zone. During the monsoon, small convective storms lead to high intensity, short duration rains which have a reduced opportunity to percolate deep in the profile, due to the low soil infiltration capacity (Bhark and Small, 2003) and high evapotranspiration (Kurc and Small, 2004). As a result, monsoon moisture fluxes tend to be limited to the upper soil profile and are readily accessible to shallow roots.

Seasonal precipitation patterns and moisture conditions also determine vegetation establishment. For example, Lauenroth et al. (1994) noted that small differences in soil water content can have significant effects on plant germination. The timing of moisture fluxes is critical for plant growth, seed dispersal and water stress (Reynolds et al., 2004; Ludwig et al., 2005). As a result, moisture availability can control plant structure, composition and density (Singh et al., 1998; Kerkhoff et al., 2004). Established plants have significant feedbacks on root zone moisture via several mechanisms. One effect is the changing soil conditions created

by the presence of plant litter. Dead biomass near the plant base alters soil temperature and moisture retention of the canopy patch (e.g., Breshears et al., 1998; McClain et al., 2003; Wilcox et al., 2003b). The presence of shallow fine roots and deep root networks also lead to macropores affecting infiltration (Seyfried, 1991; Gibbens and Lenz, 2001; Schenk and Jackson, 2002). Another important effect is the increased net precipitation in a canopy patch due to vegetation stemflow and runon from intercanopy patches (Martnez-Mesa and Whitford, 1996; Reid et al., 1999). Increased plant water from stemflow and runon, coupled with higher moisture retention in litter layers and preferential flow along macropores can lead to canopy patches which act as islands of fertility in semiarid landscapes (Schlesinger and Pilmanis, 1998).

Hydrologic patchiness induced by the spatial patterns of canopy and intercanopy spaces is also mediated by vegetation controls on root water uptake during transpiration (Feddes et al., 2001; Scott et al., 2000; Cruiziat et al., 2002). Differences in adaptation of desert plants lead to multiple strategies for extracting available water from the root zone (Rodrguez-Iturbe et al., 2001b). Both spatial and temporal partitioning of rainfall can occur, with coexisting species adapted to coping with seasonal distributions of rainfall or variations in moisture with soil depth. Plant spatial root distributions, phenology and function dictate the location and timing of water uptake. Since plants in arid and semiarid regions are especially adapted to water stress (Pockman and Sperry, 2000), root water uptake can lead to significantly low moisture contents and highly negative matric potentials. Recent work by Walvoord et al. (2002) suggests that long-term water fluxes in deep vadose zones can be directed upwards toward the root zone. In addition, hydraulic redistribution by plant roots in response to water deficits can lead to complex moisture patterns within the root zone (Burgess et al., 1998;

Seyfried et al., 2005). As a result, vegetation can impact moisture redistribution in both the vertical and horizontal directions. Since plants have roots of varying geometries and distributions (Schenk and Jackson, 2002), plant transpiration can have significant spatial and temporal controls on soil moisture patterns.

2.2.2 Material Deposition and Erosion

An established plant will modify radiation, water and wind fluxes, with implications on soil characteristics, such as texture and organic content, which will in turn affect the ability of plants to extract water. Vegetation patches can serve as obstructions to runoff and wind which leads to enhanced deposition in canopies (e.g., Okin and Gillette, 2001; Breshears et al., 2003; Ludwig et al., 2005). The major sediment source for arid and semiarid soils is eolian particles arising from surrounding areas (Gile et al., 1981; McAuliffe, 1984; Birkeland, 1999). Wind-borne sediments spread widely and serve as an initial source of particles that are further redistributed by local conditions. At the hillslope scale, the deposition and transport of material is influenced by plant cover, terrain position, and overland runoff-runon processes (Reid et al., 1999; Breshears et al., 2003; Calvo-Cases et al., 2003). As a result, local sediment redistribution occurs in response to complex winds and overland flow within plant communities, potentially on sloped surfaces of varying aspect (Wilcox et al., 2003a). Water and wind-borne transport in canopy and intercanopy areas lead to differential deposition and erosion across a landscape with plant properties (canopy geometry, roughness) playing important roles.

Vegetation influences on loess deposition have been recognized as a major control on arid and semiarid soil formation (Jenny, 1958; Birkeland, 1999). One

method for assessing plant influences is via comparisons of canopy and inter-canopy soil properties. Davenport et al. (1996) discussed the conditions affecting soil formation in a pin-juniper woodland, but found little difference between canopy and bare patches due to the short plant establishment period. Over longer time periods, the effects of plant shading on solar radiation and soil temperature lead to higher moisture in canopy patches, with an increase in soil cohesion. Plant interception also influences material deposition as rainwater can contain dissolved solutes that are preferentially deposited in canopies (Abrahams et al., 2003), and since interception lowers the erosive potential of rain splash, responsible for displacing soil in bare areas (Parsons et al., 1994). Furthermore, plant canopies create higher flow resistance which lead to dust and sediment deposition (Davenport et al., 1996). As a result, plants promote deposition, while inter-canopy areas are susceptible to erosion by wind and water. Enhanced deposition leads to the creation of plant mounds and increased loess deposition (Schlesinger and Pilmanis, 1998).

Another means for assessing plant controls on soil formation is via comparisons across different ecosystems. McMahon (1998) analyzed soils in two opposing hillslopes dominated by oneseed juniper (*Juniperus monosperma*) and creosote bush (*Larrea tridentata*) in north and south-facing aspects. Several profiles were examined in each ecosystem, placed along varying slope positions. Despite having identical underlying alluvium, differences in canopy properties between the conifer (juniper) and desert shrub (creosote) have led to variations in soil development. Note in Figure 2.3 that the silt, clay and organic matter contents vary considerably between the two ecosystems, with a higher fraction of fine and organic material in the conifer slope. Table 2.1 presents the observed soil composition in each ecosystem profile. Differences in the deposition of fine material

are attributed to the effects of plant interception, flow resistance, and soil cohesion provided by moisture and root establishment. Higher organic contents in the north-facing slope are due to the decomposition of increased conifer litter. As the conditions in the canopy patch promote deposition, the organic matter is retained near the plant and incorporated into the soil along with entrapped fine particles (Ludwig et al., 2005; Belnap et al., 2005). Higher silt, clay and organic matter contents in the juniper slope suggest that soil hydraulic properties also differ between the two slopes.

Vegetation plays a critical role in determining the soil loss resulting from wind or water erosion in arid and semiarid soils. For example, plants reduce the occurrence of rain splash by decreasing raindrop energy (Parsons et al., 1994). In addition, canopy properties (e.g., moisture status, root distribution, litter layers) lead to soil stabilization not present in bare intercanopy areas. These processes can result in significant differences in erosion rates between intercanopy and canopy patches (Reid et al., 1999; Breshears et al., 2003). Sediment can be redistributed by wind and water from exposed bare surfaces to canopy patches leading to individual plant mounds (Wainwright et al., 1999). On sloped surfaces, vegetation also determines overland flow resistance which can cause differences in erosion with varying plant cover. McMahon (1998), for example, estimated grass covers of 21% and 14% for the north and south-facing slopes, as well as the distance between grass mounds, finding greater distances on the creosote slope. This difference can be significant in terms of runoff and sediment yield, as shown by Neave and Abrahams (2002) and Wilcox et al. (2003a) for similar ecosystems. Higher erosion rates from the creosote hillslope with a lower grass cover can result in more developed drainages (Figure 2.4). Furthermore, the dissection of the south-facing slope produces a more convex hillslope profile which can impact hydrologic response as compared to the more planar, north-facing slope.

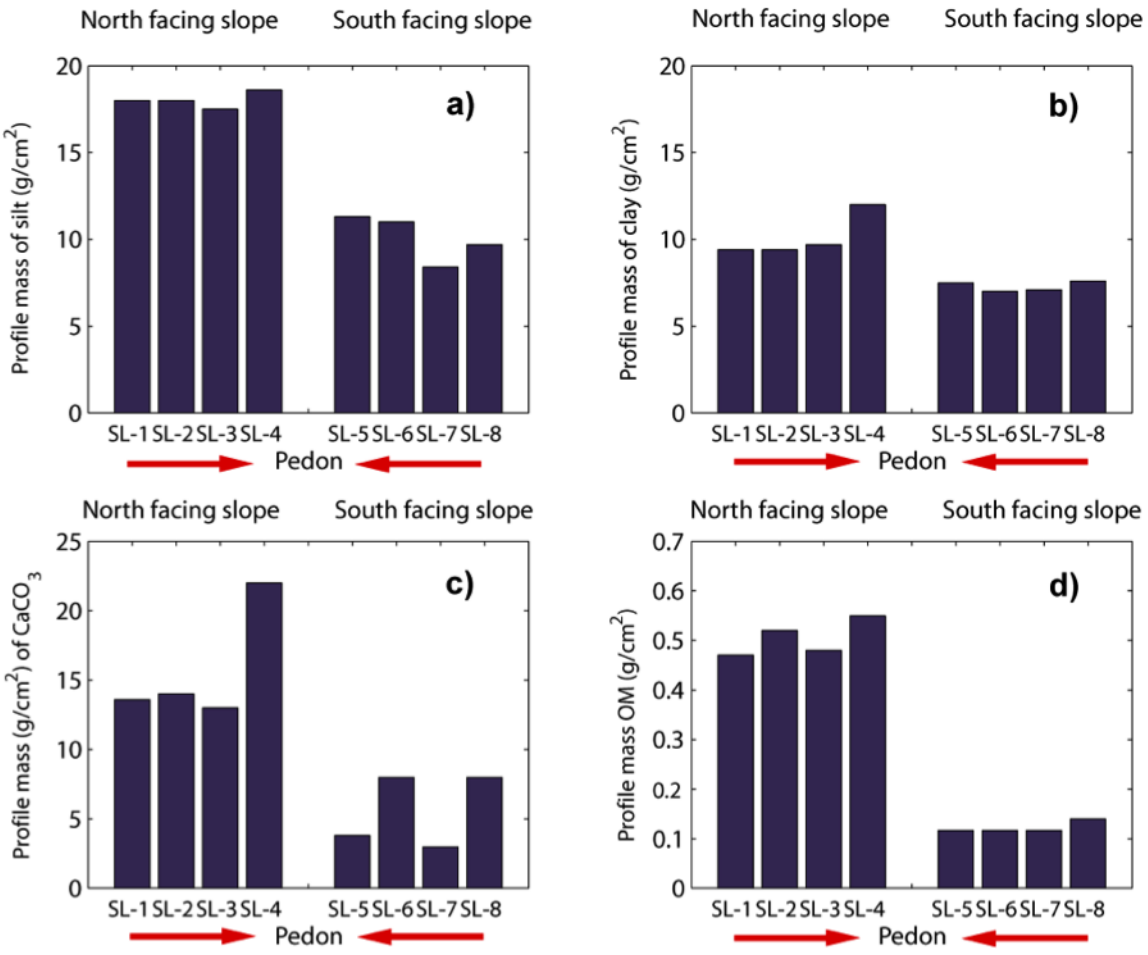

Figure 2.3: Depth-integrated soil morphological characteristics of north-facing juniper and south-facing creosote bush hillslopes from eight profiles or pedons excavated in intercanopy areas (adapted from McMahon, 1998). (a) Profile mass of silt (g/cm^2). (b) Profile mass of clay (g/cm^2). (c) Profile mass of calcium carbonate ($CaCO_3$) (g/cm^2). (d) Profile mass of organic matter (OM) (g/cm^2). Profile masses of silt and clay were integrated over the top 50 cm depth and OM content was obtained over the top 30 cm depth. Left bars correspond to the north-facing slope while right bars to south-facing slope. Arrows indicate the downslope direction in each hillslope.

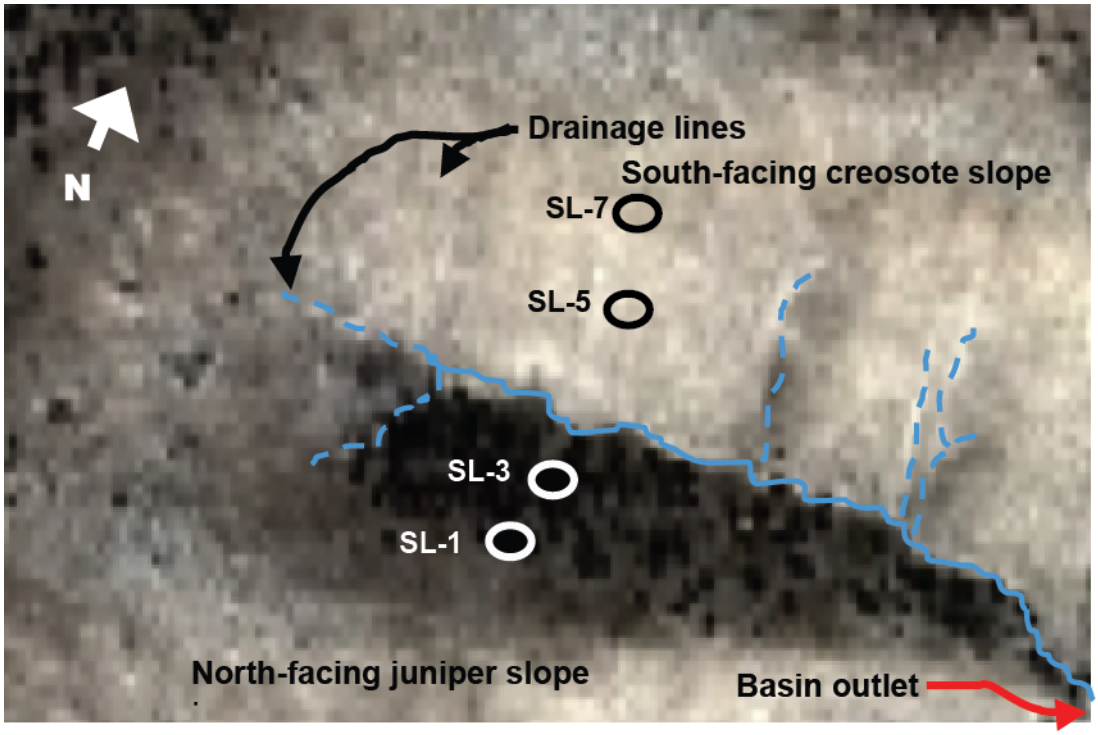

Figure 2.4: Processed ADAR (Airborne Data Acquisition and Registration) scene of the study basin illustrating the opposing ecosystems (north-facing juniper and south-facing creosote bush slopes), with approximate location of four soil profiles (SL-1, SL-3, SL-5, SL-7). Image spatial resolution is 1-m, courtesy of Sevilleta Long Term Ecological Research (LTER). Dashed blue lines represent hillslope drainages while the continuous blue line corresponds to the major channel in the catchment.

2.2.3 Calcium Carbonate Horizons

An important property of arid and semiarid soils is the development of calcium carbonate ($CaCO_3$) or calcic horizons due to moisture deficits in the soil profile (Gile et al., 1981; Goudie, 1983; Hennessy et al., 1983; Baumhardt and Lascano, 1993). $CaCO_3$ layers (caliche, calcrete) typically develop as discrete, continuous horizons with varying degrees of cementation. Initially, calcic horizons form calcareous filaments and then concretions that develop to fill the soil matrix over a certain depth. Machette (1985) classified calcic horizons based on development stage using the following attributes: (1) gravel content; (2) $CaCO_3$ distribution in the soil matrix; (3) properties such as the continuity of $CaCO_3$ coatings, presence of coalesced nodules; and (4) maximum $CaCO_3$ content. For higher stages of development, calcic horizons become indurated and the soil matrix cemented with $CaCO_3$ to form K horizons as defined by Gile et al. (1981). We utilize the term K horizon to refer to highly indurated $CaCO_3$ rich horizons. As calcic horizons develop, the soil hydraulic properties change considerably. For example, an increase in $CaCO_3$ typically leads to a decrease in hydraulic conductivity of the soil matrix and an increase in moisture retention (Shreve and Mallery, 1932; Hennessy et al., 1983). Changes in the soil hydraulic properties due to calcic horizon development can have important implications for root zone moisture fluxes and plant water uptake.

Several factors related to vegetation affect the development of calcium carbonate horizons (Shreve and Mallery, 1932). $CaCO_3$ is typically precipitated from dissolved carbon dioxide (CO_2) in pore water derived from wet and dry deposition. Increased partial pressures of CO_2 due to plant root respiration result in

an increased dissolution of calcium carbonate near the surface. Infiltration carries dissolved carbonates into the soil profile which are deposited as water is removed by evaporation and root water uptake (e.g., Yaalon, 1971; Hillel, 1998). Plant-mediated infiltration affects the deposition and mobility of $CaCO_3$, as evidenced by the distribution, occurrence and depth of calcrete horizons. Insufficient moisture fluxes due to evapotranspiration fluxes typically lead to $CaCO_3$ accumulation in the soil (e.g., low profile flushing) which can be enhanced during droughts (Schlesinger and Pilmanis, 1998). As root distribution of desert plants mediate water fluxes, the calcic characteristics (induration, lamination, hydraulic properties) can be highly controlled by vegetation. As a result, calcic horizon depth has been linked to the presence of desert plants (Shreve and Mallery, 1932), with the profile distribution related to mean annual rainfall, soil conditions, and moisture fluxes (Gile et al., 1966).

Vegetative controls on calcium carbonate horizons can be tested by analyzing soil morphology across ecosystems. McMahon (1998) presented evidence for the differential formation of K horizons in the opposing juniper and creosote hillslopes. Figure 2.3 and Table 2.1 present the depth integrated $CaCO_3$ content and the K horizon depth for the soil profiles. Note the higher amounts of calcium carbonate in the juniper hillslope are due primarily to greater CO_2 fluxes, related to denser vegetation, and higher infiltration, due to root macropores, as compared to the creosote slope. In addition, K horizons are more developed, in terms of induration and lamination, in the juniper ecosystem. This evidence suggests that long-term differences exist in the ecosystem water balance (moisture storage, evapotranspiration, deep percolation), resulting in variations in $CaCO_3$ formation for the two hillslopes. Furthermore, the presence of calcium carbonate horizons influence plant establishment and survival (Hennessy et al., 1983),

as high moisture retention at shallow depths can reduce water stress during droughts (Herbel et al., 1972). Given the frequent occurrence of $CaCO_3$ layers in arid and semiarid areas (Gile et al., 1981), it is critical to consider interactions between vegetation, soil development and root zone water fluxes in the context of potential feedbacks mediated by K horizons, as these are both influenced by plant-mediated processes and control soil hydrologic fluxes.

2.3 Study Catchment

In this study, we illustrate the effects of topographic position, vegetation and soil development on the hydrologic fluxes in two ecosystems forming part of a semiarid basin in central New Mexico. The basin is located in the northwestern corner of the Sevilleta National Wildlife Refuge, $\sim$75 km south of Albuquerque (Figure 2.5). The drainage is cut into a coarse alluvial fan deposit of the Plio-Pleistocene Sierra Ladrones Formation, consisting primarily of schist and quartzite clasts with a coarse sandy matrix (McMahon, 1998). Soils in the alluvial fans of the region are characterized by: (1) desert pavements on the upper flat surfaces, (2) sandy soil matrices, and (3) $CaCO_3$ horizons intersecting the inclined hillslope surface at various depths. County soil maps indicate that the soils in the study basin are classified as the Nickel soil series with the following properties: loamy, skeletal, mixed, thermic, Typic and Calciorthid (SCS, 1998). The drainage basin has an area of 0.034 km^2 which is dissected by an east-flowing ephemeral channel (width $\sim$1 m) dividing the north and south-facing slopes. The climate is semiarid with a mean annual rainfall of 255 mm, comprised of a bimodal rainfall regime with summer monsoon and winter storms (Milne et al., 2003). Runoff and erosion occur in response to intense summer convection and

prolonged winter stratiform rain. Winter storms can lead to a limited snowpack along the north-facing slope. The basin is similar to several drainages in the region, while its alluvial origin, orientation and geometry make it representative of semiarid basins with ecotonal boundaries (Secor et al., 1983; McAuliffe, 1994).

The most attractive feature of the basin is the opposing hillslopes hosting different ecosystems. The north-facing hillslope is composed of oneseed juniper (*Juniperus monosperma*; [Engelm.] Sarg.) and several grass species, including black gramma (*Bouteloua eriopoda*) and blue gramma (*Bouteloa gracilis*; [Willd. Ex Kunth] Lag. Ex Griffiths), while the south-facing slope is primarily creosote bush (*Larrea tridentata*; [Sesse and Moc. Ex DC.] Coville) with grass cover of fluff grass (*Erioneuron pulchellum*; [Kunth] Tateoka) and slim tridens (*Tridens muticus*; [Torr.] Nash) (McMahon, 1998). Along the head slope, an active ecotone serves as a boundary between the juniper savanna and shrub-grass ecosystems. The presence of an important number of cacti in this area is indicative of well drained soils, which is also reflected in the low soluble salts in the soil (McMahon, 1998). The ecotone is considered a dynamic feature since vegetation shifts through plant mortality and establishment are observed. For example, dead junipers are present along the head slope, possibly related to 1950s drought (Allen and Breshears, 1998). The slope angle varies accordingly to the terrain curvature and ranges from 12 to 20 °C in the basin. In general terms, the north-facing slope is planar, the head slope is concave and the south-facing slope is more convex.

The observed linkages between terrain, soil development and vegetation in the semiarid basin provide an exceptional opportunity to study the interactions and feedbacks among the different components. The major questions arising are how hydrologic fluxes interact to create preferential sites for each ecosystem, and how soil development reinforces plant establishment via changes to root

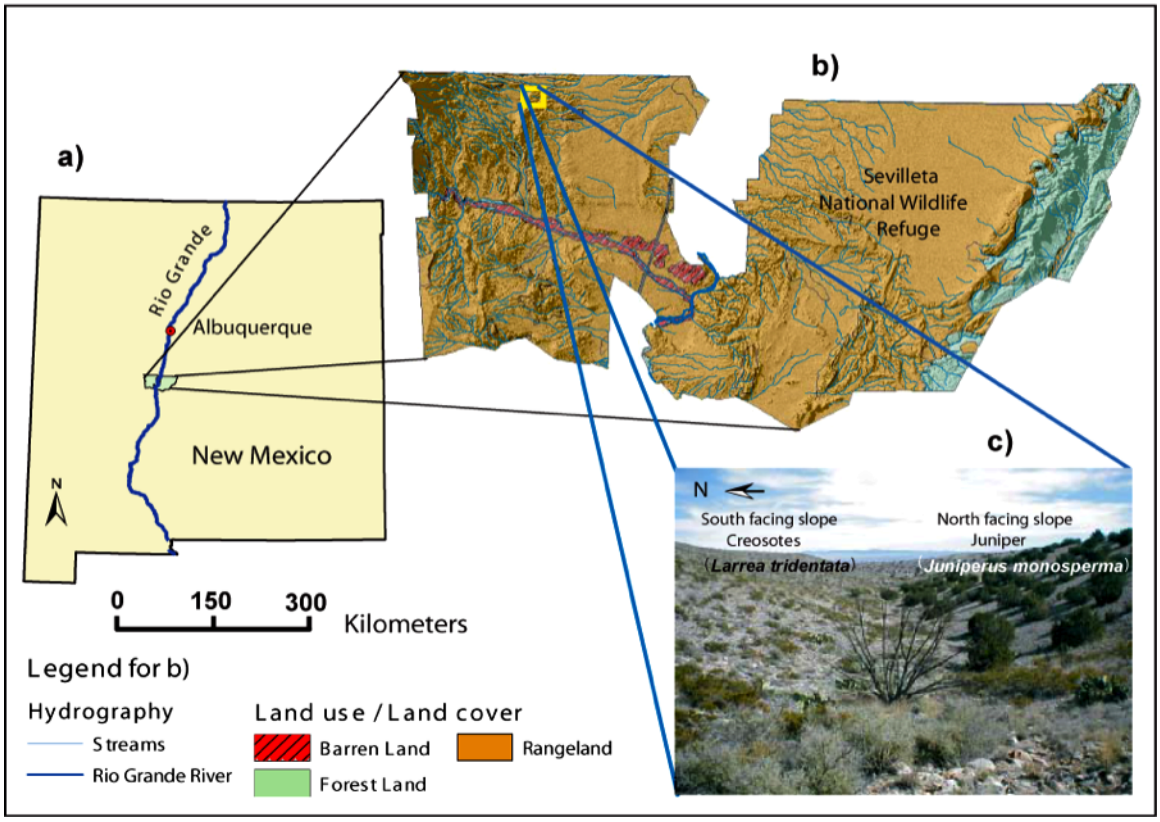

Figure 2.5: Location of study catchment in central New Mexico (Socorro County). (a) Map of New Mexico illustrating distance between Sevilleta National Wildlife Refuge (SNWR) and Albuquerque, NM, along the Ro Grande. (b) Topographic, hydrographic and soil texture variation in the SNRW with the location of study site near Sierra Ladrones (northwestern corner). (c) Photograph of study catchment taken from the head slope area looking east toward Ro Grande. Note the north-facing hillslope with individual junipers (*Juniperus monosperma*) and south-facing slope with creosote bush (*Larrea tridentata*). Other grasses, cacti and shrub species are intermixed within each hillslope. Also note the presence of a large, dead juniper tree along the bottom of the head slope area.

zone water fluxes. In the following two sections, we analyze these interactions by: (1) estimating the soil infiltration capacity in the two hillslopes using pedotransfer functions, and (2) simulating root zone water fluxes through the use of a one-dimensional vadose zone model (HYDRUS-1D, version 2.02; Simunek, et al., 1998) and an energy balance algorithm for sloped surfaces (TVET; Guan, 2005). Our aims are to identify differences in infiltration due to soil properties and examine the effects of vegetation, terrain aspect and soil development on root zone water fluxes under identical precipitation patterns.

2.4 Soil Infiltration Capacity Estimation

A critical vegetative control in semiarid areas is the effect of plants on infiltration through influences on soil, canopy and root properties. Bhark and Small (2003), for example, determined that infiltration was higher beneath canopies as compared to bare spaces in grass and shrub ecosystems. These results apply for relatively flat areas where downslope runoff is not significant, and where terrain aspect and slope position do not influence water fluxes and soil development. On sloped surfaces, we expect differences in infiltration capacity due to both plant establishment and hillslope and soil morphology. To evaluate the differences in infiltration in the opposing ecosystems, we utilize data sets from the two slope catenas (Table 2.1). Four soil profiles were examined: SL-1 and SL-3 in the north-facing slope, and SL-5 and SL-7 in the south-facing slope (Figure 2.4). Soil data required for estimating infiltration capacity from pedotransfer functions (PTFs) included soil texture, organic matter and gravel content of each horizon. We used several different PTFs to determine saturated hydraulic conductivity and matric potential; permeability; diffusivity; bulk density; and pore-size distribution of each soil horizon.

Table 2.1: Soil morphology for profiles in the opposing hillslopes: north-facing, juniper slope (SL-1, SL-3) and south-facing, creosote bush slope (SL-5, SL-7), as obtained by McMahon (1998). Refer to Figure 2.3 for soil profile location. Characteristics include soil texture, horizon description, depth from surface of bottom horizon boundary (m); bulk density (g/cm^3); sand, silt and clay content (%); gravel content for particles with diameter greater than 2 mm (% volume); and organic matter content (%).

	Text.	**Soil horizon**	**Bottom Depth** [m]	**Bulk density** [g/cm3]	**Sand content** [%]	**Silt content** [%]	**Clay content** [%]	**Gravel content** Vol. [%]	**Organic matter** [%]
SL - 1	L	A	0.04	1.75	48.13	41.34	10.53	40	1.71
	CL	Bt	0.21	1.42	37.98	41.39	20.63	20	2.7
	SL	K	0.65	1.81	67.69	19.9	12.41	40	1.11
	LS	Ck1	1.1	2.13	75.43	14.55	10.02	75	0
	LS	Ck2	1.35	2.22	89.06	6.22	4.7	75	0
SL - 3	SiL	A	0.04	1.77	48.54	41.13	10.33	40	1.65
	CL	Bw	0.15	1.5	43.57	37.82	18.61	25	2.5
	SCL	Bk	0.3	1.73	52.05	30.6	17.35	40	1.42
	L	K	0.7	1.89	67.45	18.99	13.56	40	0
	S	Ck1	1.05	2.11	72.74	14.88	12.38	75	0
	S	Ck2	1.3	2.12	77.84	10.87	11.29	75	0
SL - 5	SL	A/B	0.07	2.07	67.75	22	10.25	60	0.84
	L	Bk	0.25	2.02	64.97	19.9	15.13	60	0.86
	L	K	0.6	2.06	71.98	13.92	14.1	70	0.39
	S	Ck1	1.2	2.13	82.27	7.19	10.54	77	0
	S	Ck2	1.6	2.07	67.19	18.2	14.61	70	0
SL - 7	L	A	0.03	1.97	70.65	19.69	9.66	50	0.69
	SCL	Bjk	0.15	2.05	65.18	21.97	12.84	60	0.6
	SCL	Bk	0.33	2.04	65.99	21.43	12.59	50	0.68
	SL	K	0.8	2.11	72.9	15.39	11.71	50	0
	LS	Ck1	1.3	2.13	72.28	11.47	10.25	50	0
	LS	Ck2	1.6	2.11	78.3	10.86	10.84	50	0

Infiltration capacity is defined as the maximum rate of infiltration when the topsoil is completely saturated (e.g., Bras, 1990; Eagleson, 2002). To compute infiltration capacity (f_i) we use the Phillips equation (1) with the gravitational term (A_o) modified by Eagleson (1978) as:

$$f_i(t) = \frac{1}{2} S_i t^{-1/2} + A_o \tag{2.1}$$

$$A_o = \frac{1}{2} K(1)(1 + s_o^c) - w \tag{2.2}$$

where t is the duration of water input [T], $K(1)$ is the saturated hydraulic conductivity [L/T], so is the average, initial soil water content in the root zone [dimensionless], c is the soil permeability index ($c = (2 + 3m)/m$) [dimensionless], m is the pore-size distribution index [dimensionless] and w is a capillary rise term [L/T]. As the water table is considered deep in semiarid areas, the term w can be effectively ignored (Eagleson, 2002). S_i is the infiltration sorptivity of the soil [L/T-1/2], calculated from:

$$S_i = 2(1 - s_o)^d \{[5 n_e K(1) \psi(1) \phi_1(d, s_o)]/3m\pi\}^{1/2} \tag{2.3}$$

where d is the soil diffusivity index ($d = (c + 1)/2$) [dimensionless], n_e is the effective porosity [dimensionless], $\psi(1)$ is the saturated matric potential [L], and $\phi_1(d, s_o)$ is a sorption diffusivity parameter [dimensionless] (Eagleson, 2002). We utilized a PTF from Saxton and Rawls (2005) to estimate $K(1)$, bulk density, and volumetric soil saturation based on sand and clay content (%), organic content (%) (calculated from measurements of organic carbon for each soil horizon

using a conversion factor of 0.6), and volumetric gravel content (%) visually estimated in the field (Table 2.1). A second PTF by Rawls and Brakensiek (1985) was used to estimate m, wilting point (sw), and field capacity (sfc) for each horizon. The pedotransfer functions were used with the horizon properties to evaluate the infiltration capacity of each profile using equations (1) to (3), for a 30-min rainfall duration on a saturated soil surface that may occur during intense summer storms or prolonged winter rainfall in semiarid regions.

Estimated infiltration capacities for each horizon are shown in Figure 2.6. High infiltration capacities are found in the upper layers, with B horizons (at 0.15 m) having slightly higher infiltration than A horizons (at 0.03 m). As the depth increases, a sharp decrease in infiltration capacity is observed due to the soil properties (Bk, K below 0.33 m). Despite the fact that PTFs do not account explicitly for $CaCO_3$, variations in associated soil properties support a decrease in infiltration, with preferential saturation occurring above K horizons. The potential for the K horizon to serve as a barrier to fluid flow, due to its low infiltration capacity, is consistent with studies by Gile et al. (1981).

A comparison of the soil profiles reveals that the PTFs cannot distinguish large differences between the opposing ecosystems. However, observational evidence and soil analysis suggest that measurable differences in infiltration throughout the soil profile do occur in the two opposing slopes. For example, the stage of calcic development is higher in the juniper hillslope, indicating that infiltration rates may vary significantly below the top few centimeters. Also, note that vegetation cover has a minor impact on infiltration capacity with a higher f_i for the surface soils in the juniper slope and higher f_i in the deeper soils of the creosote slope. In addition, slope position does not seem to affect infiltration according

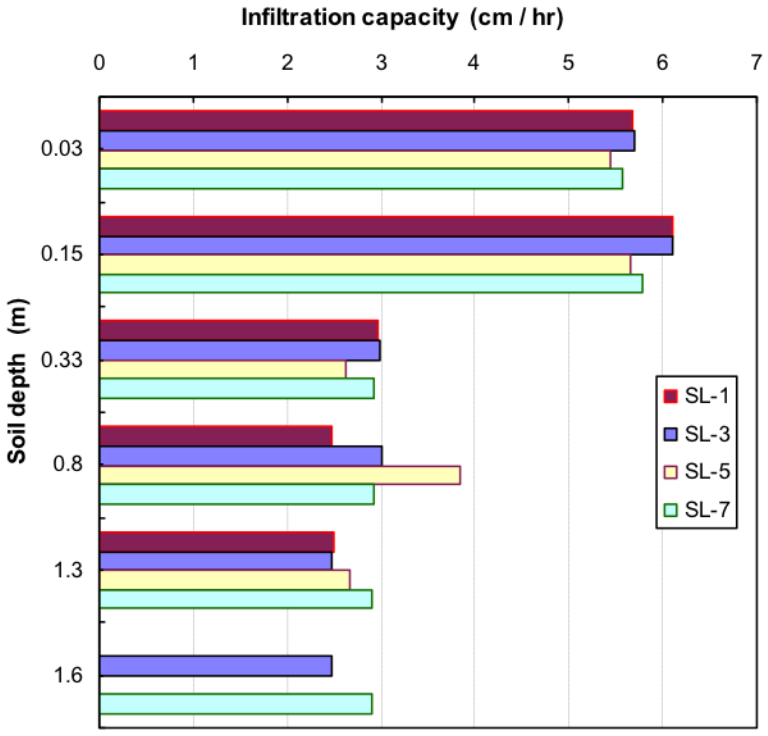

Figure 2.6: Estimated infiltration capacity (f_i in cm/hr) of the soil horizons for each profile for a 30-min saturated soil surface duration resulting from a rainfall event. SL-1 and SL-3 correspond to the north-facing juniper slope, while SL-5 and SL-7 are in the south-facing creosote bush hillslope. Each horizontal bar represents the infiltration capacity at the top of the soil horizon. For actual horizon depths, characteristics and soil profile locations, refer to Table 2.1 and Figure 2.4.

to the estimates obtained from the pedotransfer functions. Prior studies in the catchment (McMahon, 1998), corroborate that differences in soil properties along the slopes are minimal, suggesting that infiltration rates are equivalent for soils at different slope positions in the same ecosystem.

In the previous discussion, infiltration estimates from PTFs applied to the soil profiles do not account for possible preferential flow through the soil or calcrete matrix. Macropores may account for infiltration differences between the two slopes as expressed in variations of the calcic horizon depth, stage of development of $CaCO_3$ profile mass (Figure 2.3). One indication of this effect is observed in soil horizon Ck1 (0.8 m depth) of the SL-5 profile, where high infiltration capacity is due to high gravel content, which allows rapid downward percolation. As a result, it is believed that macropore flow may play a role in the two opposing hillslopes, although these effects are not accounted for in the infiltration capacity estimates. In the following, we present a series of vadose zone simulations of the fine-earth soil matrix to model hydrologic fluxes in the two ecosystems as a function of the observed soil, vegetation and terrain properties.

2.5 Root Zone Hydrologic Fluxes

Soil forming processes are strongly controlled by the amount of available water in the plant root zone, in particular for arid and semiarid regions (e.g., Gile et al., 1981; Yair and Shachak, 1987). Accurate determination of root zone water fluxes in semiarid areas requires accounting for soil and vegetation characteristics which can vary significantly over short distances (Scott et al., 2000; Walvoord and Phillips, 2004). Detailed modeling of hydrologic fluxes can provide insight on the interactions leading to soil development and plant establishment over long time

periods. In this study, we evaluate the combined effects of terrain position, vegetation and soil properties on root zone hydrologic fluxes by utilizing an energy balance algorithm for vegetated, sloped surfaces (TVET) and a one-dimensional model for vadose zone fluxes and plant water uptake (HYDRUS-1D). In the following, we briefly describe the two hydrologic models and their use in soil profile models from the two ecosystems. We then describe simulation results over an 8-year period (1996-2003) using observed rainfall forcing from a nearby weather station (Red Tank, $\sim$1km distant) in the Sevilleta National Wildlife Refuge.

2.5.1 Evapotranspiration on Vegetated Slopes using TVET

The effects of evaporation and transpiration in the two ecosystems are modeled using an approach developed by Guan (2005) for semiarid regions. The Topography and Vegetation-based surface energy partitioning model for evapotranspiration (TVET) provides realistic upper boundary conditions to root zone models such as HYDRUS-1D. The algorithm is based on an energy balance approach that accounts for the effects of surface slope and aspect on incoming solar radiation. In addition to radiation, the algorithm uses atmospheric forcing including air temperature, relative humidity, wind speed and rainfall. The energy balance at the land surface is partitioned into a vegetation canopy and bare soil based on the fractional plant cover for an ecosystem. The Penman equation is applied to calculate bare soil potential evaporation (PE), while the Penman-Monteith equation is used to compute potential transpiration (PT) (Shuttleworth, 1993). Canopy interception is also simulated to modify the incident rainfall at the surface. Ultimately, TVET produces daily PE and PT values based on meteorological data, topography and plant cover, which can be used to extract available

water from soil layers, depending on plant rooting depths and intercanopy bare soil. Vegetation can be distinguished by varying parameters such as canopy leaf area index (LAI), plant cover, stomatal resistance and plant height (Table 2.2). For the opposing hillslopes, the woody plant properties were used to parameterize the transpiration component as roots extend deep into the vadose zone (Foxx et al., 1984; Tierney and Foxx, 1987). Since grasses have shallow roots (Scott et al., 2000; Gibbens and Lenz, 2001), we assume that grass transpiration is effectively similar to soil evaporation.

Table 2.2: Vegetation and terrain parameters for the two opposing hillslope ecosystems (i.e., South-facing slope (SFS) and North-facing slope (NFS) for use in the TVET energy balance algorithm. LAI is leaf area index (dimensionless).

	Vegetation Parameters			**Terrain Parameters**			
	Plant cover [%]	Canopy LAI [-]	Plant Height [m]	Slope angle [degrees]	Latitude/Longitude [decimal degree]		Aspect [degrees]
SFS Creosote bush	7.5	1.6	1	17	-106.98	34.4	0 (S)
NFS Juniper	7.5	3.4	2	20	-106.98	34.4	180 (N)

2.5.2 Root Zone Water Fluxes using HYDRUS-1D

The potential evapotranspiration simulated by TVET is used in conjunction with rainfall forcing to model the water fluxes in the root zone using a numerical model for variably-saturated soils. HYDRUS-1D is a finite element model of vadose zone water, heat and solute transfer processes (Simunek et al., 1998).

The model simulates variably-saturated flow using the Richards equation with root water uptake captured via a sink term in different soil layers. Soil profiles can be depicted using a number of variable-depth horizons with different characteristics. Root distributions can be assigned for each horizon based on a root density profile. Soil hydraulic properties in the unsaturated media are derived from soil texture and other properties, such as organic content, using relations proposed by Brooks and Corey (1964) and van Genuchten (1980). The effects of gravel content on the soil properties cannot be captured in the model via the existing relations. As a result, the simulations considered here are for the fine earth fractions. The effects of water stress on plant uptake can be defined according to Feddes et al. (1978) or van Genuchten (1987) to simulate different plant water use strategies. A number of upper and lower boundaries and initial conditions are available in HYDRUS-1D, depending on the simulation of interest (Simunek et al., 1998). For dry semiarid soils, we selected an upper atmospheric forcing with runoff and lower free drainage conditions, and an initial state specified via soil pressure head in the two ecosytems. In other semiarid areas, HYDRUS-1D has been successfully used to simulate root zone hydrologic fluxes, deep percolation and soil water content profiles (e.g., Scott et al., 2000; Scanlon et al., 2002).

2.5.3 Model Setup

In order to test the sensitivity of the root zone water fluxes to terrain position, vegetation and soils, we designed a set of experiments using TVET and HYDRUS-1D in the opposing hillslopes. Individual models were set up for each ecosystem where landscape characteristics, boundary conditions and meteorological forcing were specified based on field observations, profile analysis and

weather data (Base case). We tested the influence of vegetation on moisture fluxes by conducting models runs which sequentially remove plant influences. In the first set (Case 1), the soil, plant and slope properties of the ecosystems were maintained as in the Base case but transpiration was removed, while maintaining soil evaporation and plant interception. In the second set (Case 2), the effects of transpiration and interception were both removed from each hillslope, leading to hydrologic fluxes controlled by rainfall, soil properties and soil evaporation. The intent of the experimental setup was to evaluate the vegetative controls on moisture fluxes in the context of the current terrain position and soil morphology.

We conducted an extensive analysis of the TVET and HYDRUS-1D models to ensure appropriate parameter selection. Here, we describe the methods for the Base case, as these include all relevant processes. The models were applied to two profiles, one in each ecosystem: SL-3 (juniper) and SL-5 (creosote). Soil hydraulic properties were based on soil texture using a neural network approach (Table 2.3, van Genuchten, 1980). For each profile, the models were run for an 8-yr period based on meteorological data from a nearby station ($\sim$1km). The atmospheric forcing for each profile was generated with TVET based on terrain and plant properties and then used as an upper boundary condition in HYDRUS-1D. A small time step was selected to ensure solution stability for the variable rain forcing. Initialization of the vadose fluxes was achieved by first setting a dry profile condition and then running the rainfall record for two sequential periods (e.g., two 8-yr periods of identical rainfall forcing). This spin-up period allowed for a dynamic equilibration of hydrologic fluxes and helped remove potential initialization errors. This method is critical since the model can be highly sensitive to the initial conditions in particular when the soil is completely dry. We used

Table 2.3: Soil hydraulic properties computed in the HYDRUS-1D model based on soil horizon texture (percentages of sand, silt, clay) for the two soil profiles (SL-3 in north-facing juniper; SL-5 in south-facing creosote bush). θ_r is residual soil water content (dimensionless), θ_s is the saturated soil water content (dimensionless), α and n are empirical parameters of the van Genuchten (1980) model (dimensionless), and K_s is saturated hydraulic conductivity (cm/day). Note that these hydraulic conductivity values do not account for gravel as performed for the infiltration capacity estimates in Figure 2.6.

	Texture	**Soil horizon**	θ_r [-]	θ_r [-]	α [-]	$\boldsymbol{n}$ [-]	K_s [cm/day]
SL-3	SiL	A	0.0431	0.3939	0.0118	1.485	24.33
	CL	Bw	0.0596	0.4009	0.0113	1.476	10.25
	SCL	Bk	0.0563	0.393	0.018	1.413	17
	L	K	0.0486	0.3832	0.0315	1.394	34.61
	S	Ck1	0.048	0.381	0.0341	1.438	44.42
	S	Ck2	0.0492	0.3786	0.0341	1.535	61.43
SL-5	SL	A/B	0.0424	0.3852	0.0331	1.412	42.12
	L	Bk	0.0511	0.384	0.0295	1.38	29.32
	L	K	0.0508	0.3799	0.0327	1.417	38.33
	S	Ck1	0.0523	0.3756	0.0319	1.695	88.48
	S	Ck2	0.0504	0.3828	0.031	1.387	32.16

results from a third 8-yr period to identify the controls of vegetation, soils and terrain on root zone water fluxes.

Soil horizons for each ecosystem profile were determined from characterizations by McMahon (1998) as presented in Table 2.3. Figure 2.7 illustrates the vertical distribution of the soil horizons along with the root density profiles for the juniper and creosote bush. Note the variable horizon depths and soil profile extents. The actual node spacing used in HYDRUS-1D is much finer than the horizon extents. Node spacing was set to 1 mm in the top 10 cm to capture soil wetting and drying, while it was progressively increased to several cm in the lower soil horizons. For each soil horizon, only the fine earth fraction was simulated, as gravel content cannot be directly incorporated into the available PTFs of HYDRUS-1D (Simunek et al., 1998). The root density values in the creosote bush profile are based on estimates from Boulanger (2004). Due to a lack of data on the root density distributions of oneseed junipers, we derived a conceptualized profile based on Tierney and Foxx (1987) and Schenk and Jackson (2002). This distribution is consistent with the following observations: (1) high density close to the surface with an exponential decrease with depth, (2) low density at the shallowest soil depths, and (3) a higher density in deeper horizons as compared to creosote bush. In addition, sensitivity tests on the juniper root density revealed minor variations in moisture fluxes if the major features are retained (e.g., exponential decay with depth after peak density near surface).

We also evaluated the most appropriate root water uptake model for each species. Based on work by Pockman and Sperry (2000) on xylem cavitation of desert plants, we selected the Feddes et al. (1978) model for simulating the juniper transpiration and the van Genuchten (1987) S-shape model for creosote

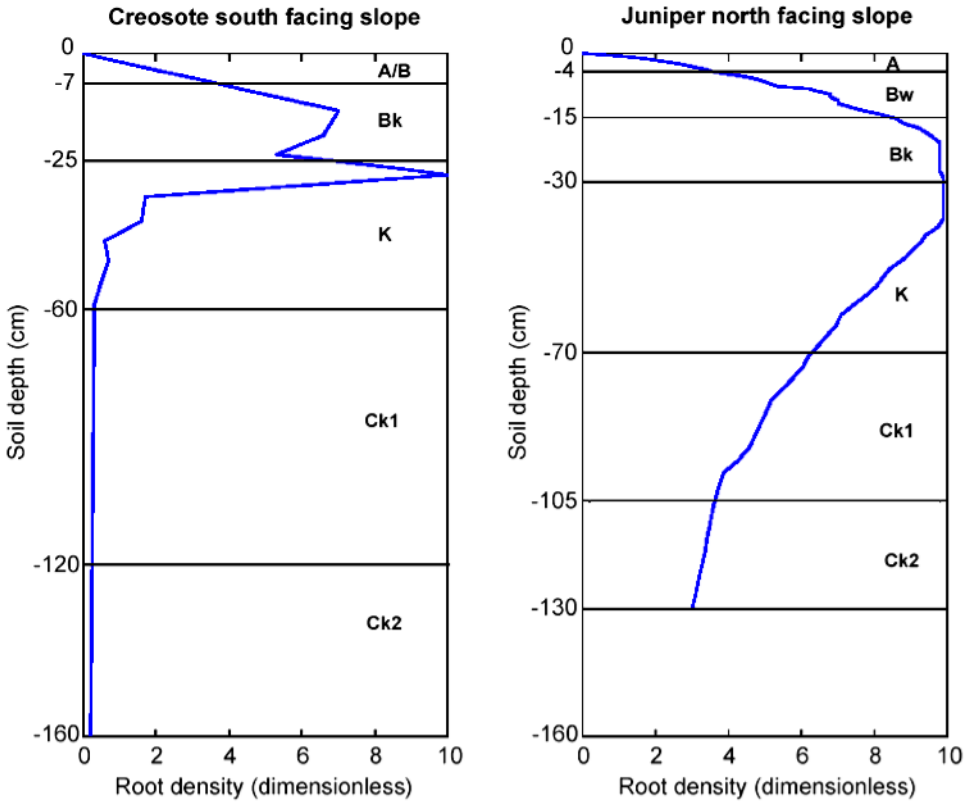

Figure 2.7: Soil profile horizon depths and conceptual root distributions for creosote bush (left) and juniper (right) along the south-facing and north-facing hillslopes, respectively. The x-axis represents the root density distribution for the soil profile where 10 is the maximum root density and 0.1 is the minimum root density. The y-axis depicts soil profile depth, while the horizontal lines within each profile identify boundaries between soil horizons.

water uptake. Table 2.4 lists the input parameters and values, while Figure 2.8 presents the uptake functions used in the different ecosystems. Note that the Feddes et al. (1978) model allows juniper to transpire at a maximum rate over a broad range of matric potentials. Reductions in transpiration occur linearly for both low (below -10 MPa) and high water contents (above -2 MPa). This model is reasonable for oneseed juniper as xylem cavitation has been observed to increase quickly for soil pressures greater than -10 MPa in absolute terms (e.g., -15 MPa) (Pockman and Sperry, 2000). On the other hand, the van Genuchten (1987) model allows limited creosote transpiration for negative soil water pressures, which is consistent with an observed exponential decline in water uptake in creosote bush as water contents decrease (Pockman and Sperry, 2000).

Table 2.4: Root water uptake model parameters for juniper and creosote bush ecosystems. The Feddes et al. (1978) parameters are: P0, pressure head value below which roots start to extract water (cm); Popt, pressure head value below which roots extract water at the maximum rate (cm); P2, limiting pressure head below which roots no longer extract water at the maximum rate (cm); P3, pressure head value below which root water uptake ceases (cm), usually at the wilting point; and r2, potential transpiration rate (cm/day). The S-shape model parameters are: P50, pressure head at which extraction rate is reduced by 50% (cm); and P0*, fitting parameter in an exponential response function associated with water stress (dimensionless).

Vegetation	**Feddes Model**					**S-shape Model**	
	P0 [cm]	**Popt** [cm]	**P2** [cm]	**P3** [cm]	**r2** [cm/day]	**P0*** [-]	**P50** [cm]
Juniper	-10	-25	-80000	-130000	0.5	-	-
Creosote bush	-	-	-	-	-	3	-20000

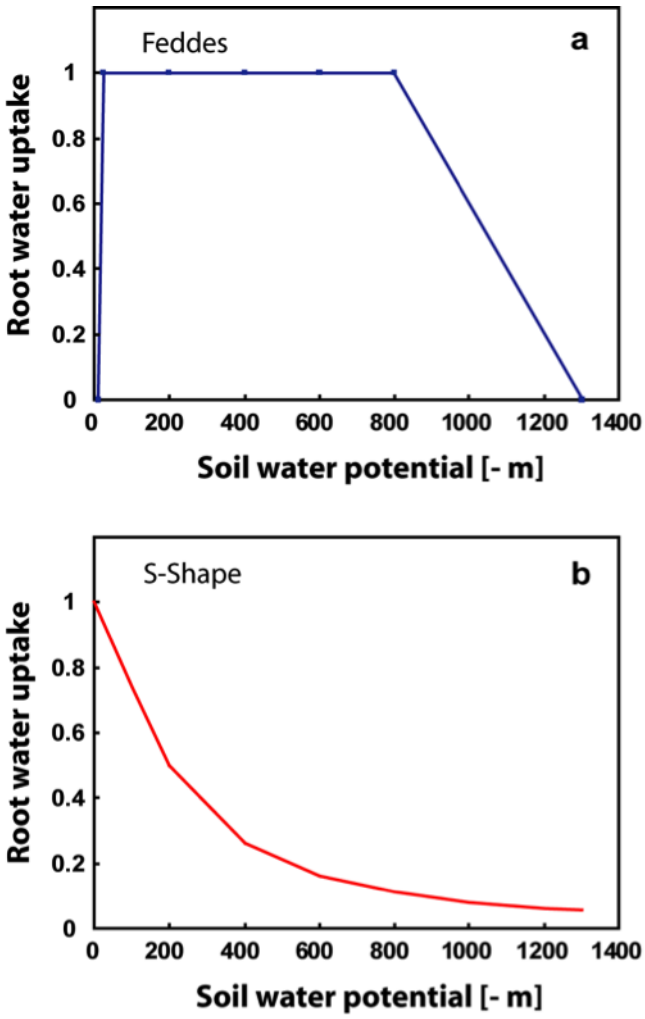

Figure 2.8: Root water uptake models for the (a) north-facing juniper trees (Feddes et al., 1978) and (b) south-facing creosote bush (van Genuchten, 1987) obtained by matching with xylem water pressure observations from Pockman and Sperry (2000). Note that the root water uptake varies with the soil water potential (in units of negative meters). The root water uptake is scaled from 0 to 1. Zero values imply no root water uptake, while one represents the maximum rate of water uptake (no soil limitation to root uptake).

2.5.4 Soil Water Content and Matric Potential Profiles

For the 8-yr simulation period, we evaluated the differences in soil water content, soil water pressure, evapotranspiration and deep percolation in the two soil profiles parameterized for each ecosystem. In the following, we emphasize comparisons for the Base case runs, which capture plant controls (interception, transpiration) on hydrologic fluxes. In addition, we evaluate the effects of the two vegetation species as a function of soil profile depth, taking into account the long-term influences of plant establishment on soil development. Note that results incorporate differences in terrain position and vegetation through the TVET forcing and in soil morphology and root distribution through the HYDRUS-1D vadose zone simulations.

Figure 2.9 presents a comparison of the spatial and temporal volumetric soil water content distributions for the two ecosystems. Note that the observed precipitation (cm/day) is quite variable and consists of storm pulses throughout the year with larger amounts during the summer monsoon. Both ecosystem soil profiles are sensitive to rainfall forcing with a larger response observed in the upper horizons (Figures 2.9b, c, d). For the deeper horizons, the variability in soil water content decreases considerably (Figures 2.9e, f, g) due to the dampening of the rainfall pulse by the soil matrix. In addition, the temporal decay of the soil water pulse varies with depth, ranging from weeks (upper horizons) to months (lower horizons). Minor differences between the ecosystems are observed for the upper horizons (A, B) as higher moisture retention is present for the juniper slope. As depth increases, differences in the $CaCO_3$ horizons (K, Ck) and root distribution lead to larger changes in soil water content (Figure 2.9e). Note that the creosote soil water content at 86 cm responds to large rain events exceeding

4 cm, while the juniper soil does not allow percolation to this depth (Figure 2.9f). This is consistent with more developed K and Ck horizons in the juniper ecosystem which limit water movement deep into the profile (Shreve and Mallery, 1932; Hennessy et al., 1983).

Soil water pressure, or matric potential, is important for determining the ability of plants to extract soil water. Figure 2.10 compares the matric potential variations for the two ecosystems. Note that highly negative matric potentials indicate plant water stress. Although upper horizons (A, B) show more variability and frequency in the change of matric potential values (Figures 2.10b, c), they experiment shorter excursions of negative matric potential with smaller amplitudes as compared to lower horizons (K, Ck), which have several long periods of severe water stress (Figures 2.10d to g). Differences are observed in the matric potential for each ecosystem across a range of depths, due to the varying nature of the root water uptake models. Junipers are capable of extracting water until a high threshold pressure is reached beyond which uptake ceases, as evidenced by the constant dry conditions in the deep horizons. Creosote bush, on the other hand, can transpire under highly stressed conditions but at lower than maximum rates (Pockman and Sperry, 2000). As a result, the creosote profile experiences smaller negative matric potentials, except for extended dry periods where transpiration can continue to deplete soil water. These results are consistent with the capacity of creosote to overcome high negative matric pressures and tap water in deeper K horizons (Shreve and Mallery, 1932).

Soil water content and matric potential values can be utilized to establish model-based water retention curves for each ecosystem. Figure 2.11 presents the ecosystem water retention curves at 20 cm depth (Bk horizons in both profiles). Over this horizon depth, the maximum root density in both plant species

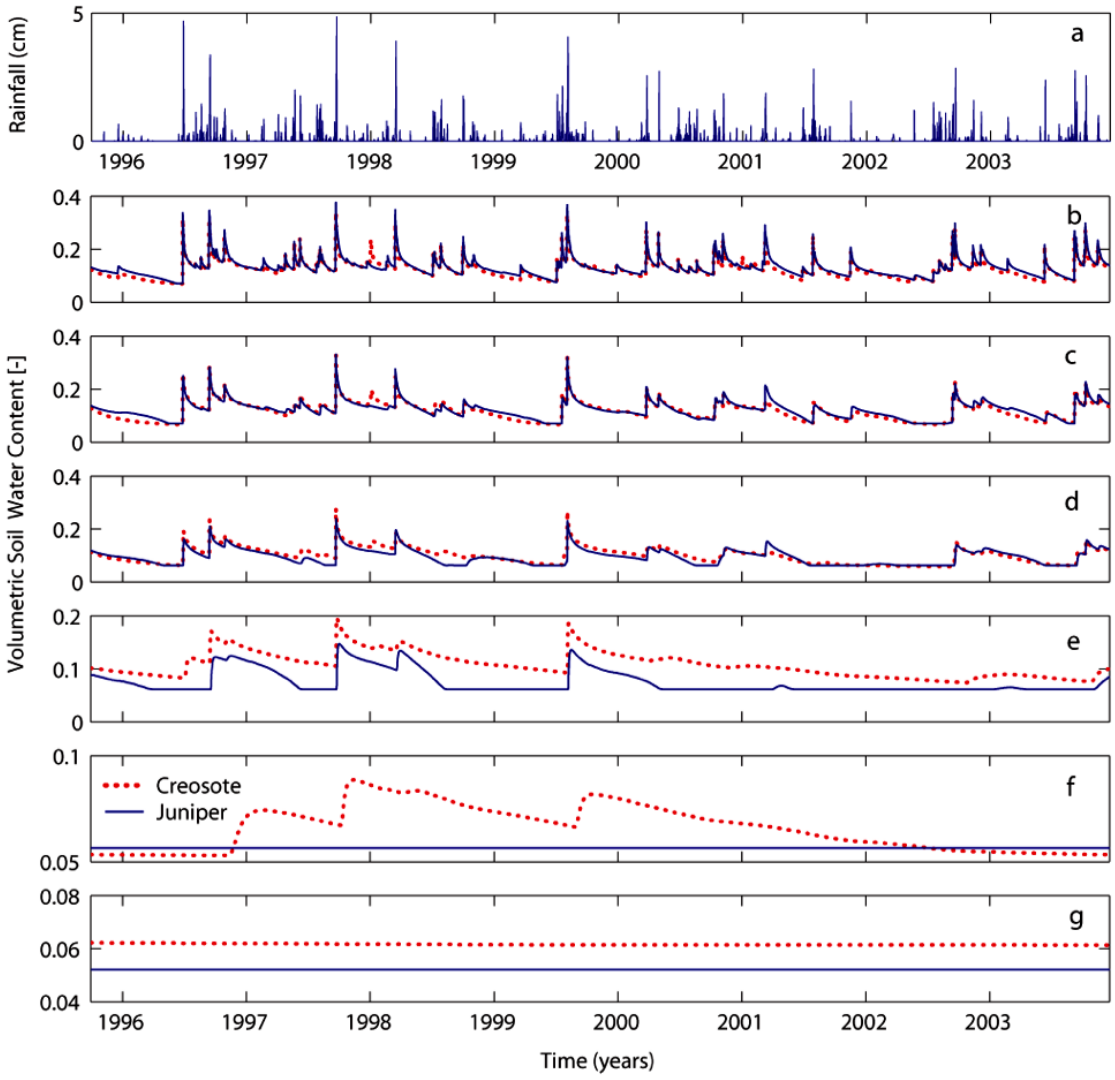

Figure 2.9: Volumetric soil water content [-] of the fine earth fraction as a function of soil depth and time for the creosote and juniper ecosystems. (a) Rainfall forcing during the simulation (cm/day). (b) Soil water content at 10 cm (Bk horizon for the creosote, Bw horizon for the juniper). (c) Soil water content at 20 cm (Bk horizons). (d) Soil water content at ∼30 cm (upper K horizons). Note that nodes at this depth are coincident with the greatest plant root density in the soil profile (Figure 2.7). (e) Soil water content at 50 cm (lower K horizons). (f) Soil water content at 86 cm (Ck1 horizons). (g) Soil water content at 126 cm (Ck2 horizons). Note that the scale of the y-axis changes with depth to clearly show behavior in each soil horizon and differences between vegetation species.

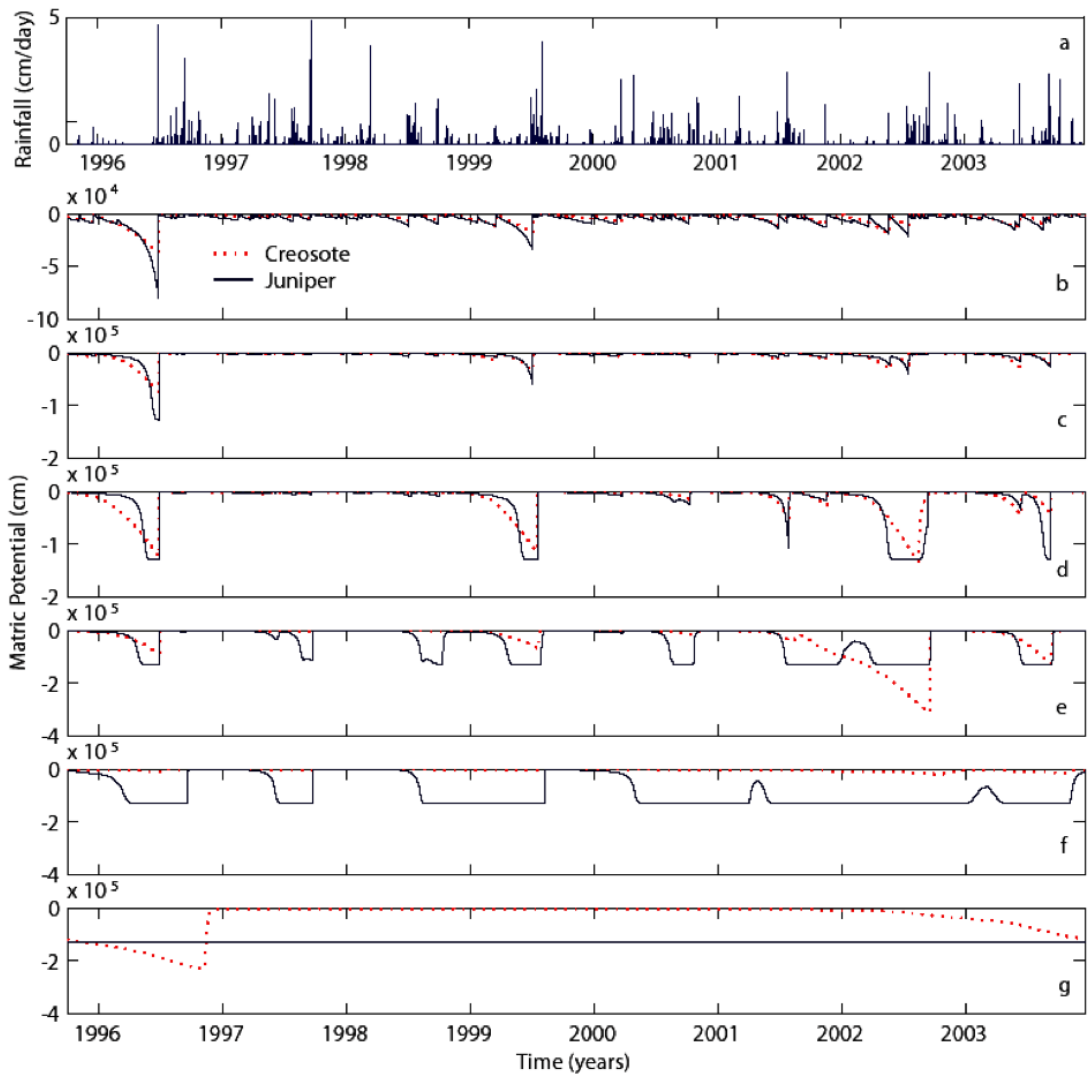

Figure 2.10: Matric potential (cm) as a function of soil depth and time for the creosote and juniper ecosystems. (a) Rainfall forcing during the simulation (cm/day). (b) Matric pressure heads at 10 cm (Bk horizon for the creosote, Bw horizon for the juniper). (c) Matric pressure heads at 20 cm (Bk horizons). (d) Matric pressure heads at ∼30 cm (upper K horizons). (e) Matric pressure heads at 50 cm (lower K horizons). (f) Matric pressure head at 86 cm (Ck1 horizons). (g) Matric pressure heads at 126 cm (Ck2 horizons). Note that the scale of the y-axis changes with depth to clearly show behavior in each soil horizon and differences between vegetation species.

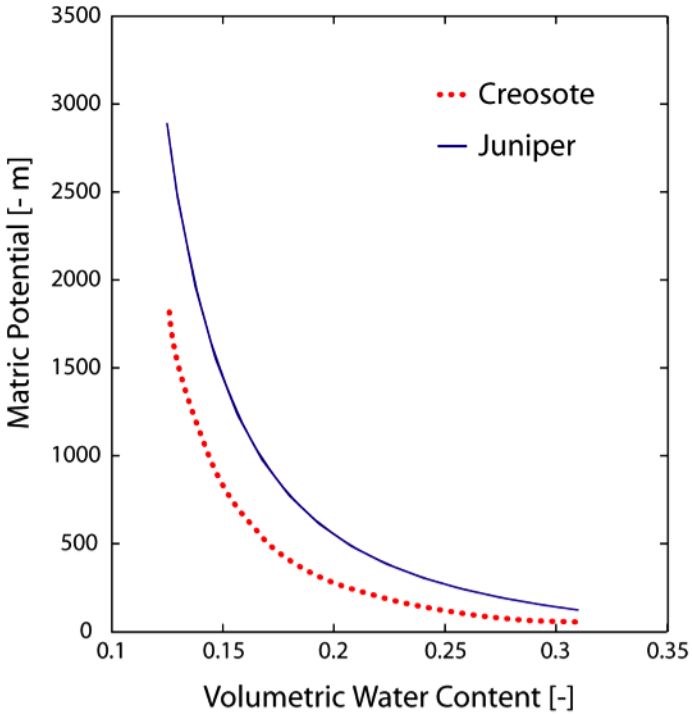

Figure 2.11: Simulated soil water retention curves for the creosote and juniper soils at 20 cm depth (Bk horizon) based on both wetting and drying periods of the soil horizon. Hysteresis of the soil water fluxes and gravel content were not considered in the model-based soil water retention curves. Note the upper and lower limits in water content and matric potential depict the range of conditions experienced during the 8-yr simulation.

is depicted in the model (Figure 2.7). Note that the north-facing juniper slope demonstrates higher moisture retention as compared to the south-facing creosote slope due to the soil horizon characteristics (e.g., clay and silt) and the dynamic effects of root uptake. The higher moisture retention in the juniper ecosystem is consistent with a simulated decrease in downward percolation into the deeper horizons. These results are also consistent with modeled water retention curves for the two hillslopes obtained by McMahon (1998).

2.5.5 Evapotranspiration Fluxes

The variations in soil water content and matric potential in the two ecosystems are also reflected in differences in evaporation and transpiration for each profile. Figure 2.12 compares the potential evaporation (PE) and transpiration (PT) computed by TVET to the actual evaporation (AE) and transpiration (AT) simulated by HYDRUS-1D, plotted as cumulative amounts over the simulation. Major differences between the potential and actual rates are due to water availability in the surface soils (evaporation) or in the deep soil horizons (transpiration). Given the semiarid climate, the potential evaporation and transpiration are quite high, exceeding 100 cm/year. Note that the south-facing creosote slope experiences a higher PE (due to aspect) but a lower PT (due to limited leaf area) as compared to the north-facing juniper ecosystem (Figures 2.12a and b). Since PE exceeds PT given the sparse plant cover (Table 2.2), the major loss term in the ecosystems is atmospheric demand on surface soil water, with the creosote bush slope experiencing a higher potential ET (Figure 2.12c).

The actual evaporation and transpiration are quite different from potential values as water availability at the surface and over the rooting depth modifies actual rates. Note that AE exceeds AT by a factor of four (whereas PE exceeds PT by factors of 8 to 20). AE in each ecosystem is remarkably similar despite large differences in potential values, suggesting that soil properties and the high evaporative demand lead to compensating effects on surface moisture. Higher moisture retention in juniper soils allows water accumulation in the near surface, whereas creosote soils are better drained (Figure 2.9). Small variations in moisture counterbalance differences in PE and result in similar AE for the two hillslopes. Actual transpiration, on the other hand, exhibits an appreciable difference between the

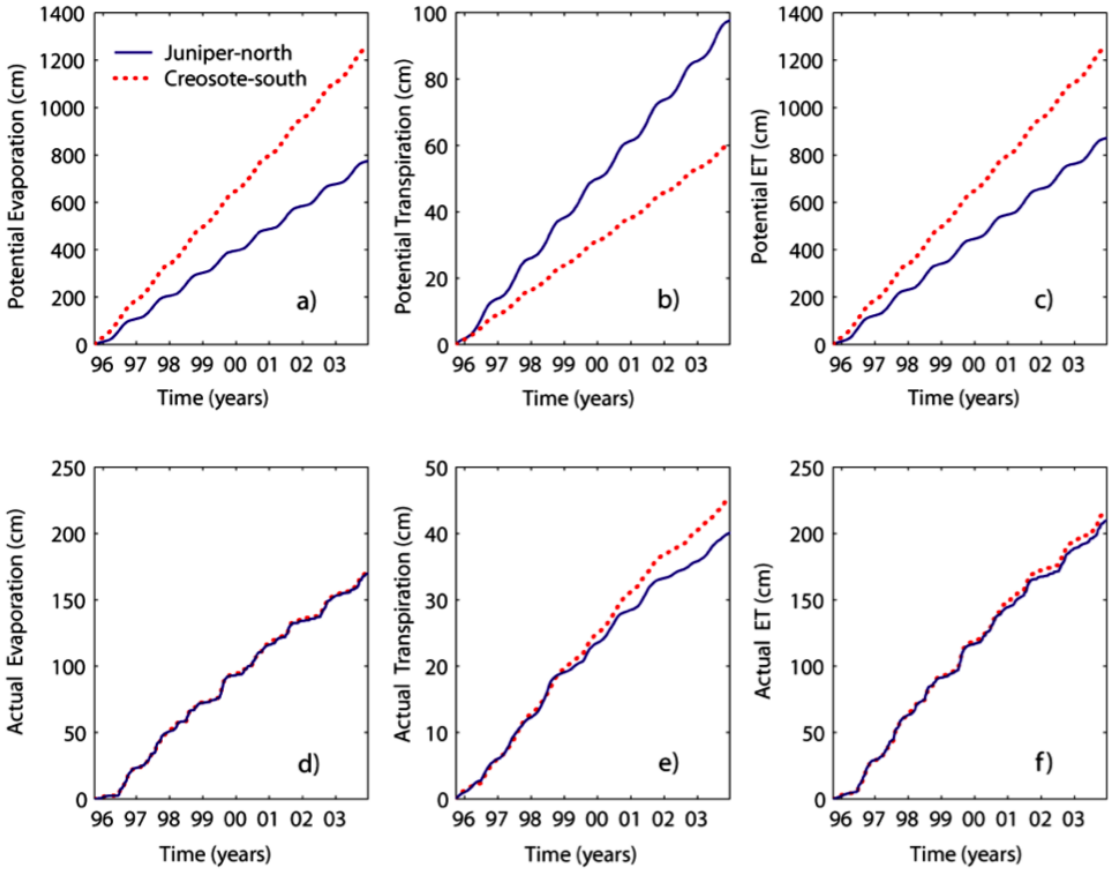

Figure 2.12: Potential and actual evaporation and transpiration estimates for the south-facing creosote bush and north-facing juniper hillslopes, plotted as cumulative depths (cm). (a) Potential evaporation from bare soil (PE). (b) Potential transpiration (PT). (c) Total potential evapotranspiration (PET). Potential values determined based on meteorological conditions, topography, and vegetation properties in TVET. (d) Actual evaporation from bare soil (AE). (e) Actual transpiration (AT). (f) Total actual evapotranspiration (AET). Actual ET values are based on the relation between atmospheric demand and soil water control in HYDRUS-1D. Computed ratios of AET to total precipitation (P) are equal to AET/P = 1 for the juniper slope and AET/P = 1.03 for the creosote slope. These ratios indicate that AET is capable of consuming the incoming precipitation and portions of the stored soil water, which is consistent with the semiarid setting under study.

ecosystems. Note that AT for creosote is a larger percentage of PT (75%) as compared to juniper (40%), suggesting that water uptake in creosote is more efficient. This transpiration efficiency is consistent with the plant capacity to extract water during dry periods despite allowing downward fluxes during wet periods (Figures 2.9 and 2.10). The combined effects of soil morphology and transpiration lead to nearly identical actual ET for the two opposing ecosystems.

2.5.6 Deep Percolation

We evaluated the vegetation controls on percolation beyond the root zone by comparing the Base case, Case 1 (no transpiration) and Case 2 (no interception or transpiration). This analysis is motivated by recent evidence suggesting that semiarid plants can control deep vadose zone fluxes (Walvoord and Phillips, 2004). Figure 2.13 shows the cumulative bottom flux for the three cases: Base case, Case 1 and Case 2 (Fig. 2.13a, b, c). Note that the Base case runs have no significant water fluxes beyond the root zone for either ecosystem. This is consistent with findings pointing to the strong plant controls on deep recharge (e.g., Seyfried et al., 2005). The removal of vegetation effects shows that transpiration has a dramatic impact on the bottom water flux (Case 1, Figure 2.13b). The bottom flux increases considerably for the creosote bush when transpiration is removed, while a smaller increase is observed for the juniper ecosystem. Since soil evaporation is maintained in Case 1, we can attribute the increase in deep percolation to a reduction in transpiration over the soil profile. In addition, excess water from the removal of transpiration that does not lead to bottom fluxes are consumed by soil evaporation due to its high potential rate. The effect of plant interception on deep percolation is minor, as shown by similarities in Case 1 (Figure 2.13b) and

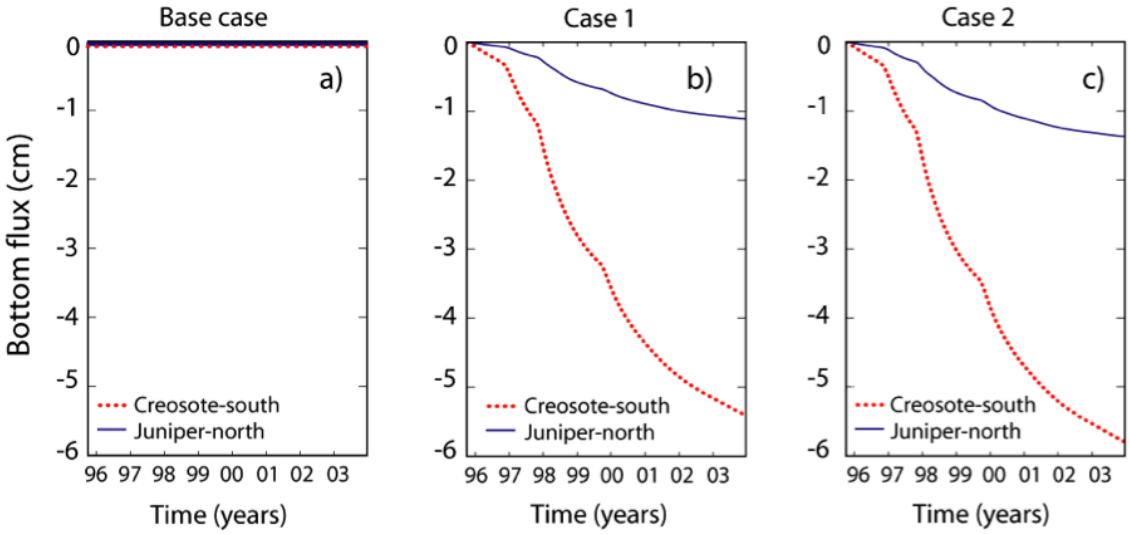

Figure 2.13: Bottom water fluxes beyond the root zone for three modeling scenarios over the simulation period, plotted as cumulative water depth (cm). Negative depth values imply downward flux. (a) Base case: vegetation transpiration and interception effects are taken into account. (b) Case 1: No vegetation transpiration. (c) Case 2: No vegetation transpiration or interception. For each scenario, the soil morphology, soil evaporation and slope conditions were maintained identical to the Base case.

Case 2 (Figure 2.13c). It is interesting to note that without vegetation effects, the differences in deep percolation are due exclusively to variations in soil properties in the ecosystems. The increased moisture retention in the juniper ecosystem due to the presence of organic matter, silt, clay and more developed $CaCO_3$ horizons lead to a lower bottom flux. However, these results do not reflect the preferential flow paths (e.g., root macropores) which may exist in juniper ecosystems and lead to percolation beyond the root zone.

2.6 Discussion and Summary

In this study, we reviewed the interactions between topography, soil development and vegetation in the context of complex semiarid rangelands, pro-

viding examples from a small drainage basin in central New Mexico exhibiting an ecotonal boundary between mesic conifer and xeric shrub species. The vegetative controls leading to differential soil formation were identified and tested via soil profile observations made in the opposing hillslope ecosystems. We assessed the effect of slope aspect, soil morphology and plant properties on the root zone hydrologic fluxes by estimating hydraulic properties using standard pedotransfer functions, and conducting simulations of vadose zone water fluxes via the use of an energy balance algorithm for sloped, vegetated surfaces (TVET) and a one-dimensional, numerical model of soil water content, matric potential and root water uptake (HYDRUS-1D). Results reveal differences in hydrologic fluxes in the two ecosystems and the controls exerted by vegetation, soil development and terrain position.

(1) Infiltration capacity estimates reveal significant variations with depth due to soil morphology, with higher infiltration in the near surface soils. Ecosystem differences suggest higher surface infiltration for junipers and greater deep infiltration in creosote bush due to the presence of organic matter, fine material and less developed $CaCO_3$ horizons in the creosote slope soils. Simulated soil water contents are consistent with the infiltration estimates, with wetter conditions observed for surface soils in the juniper slope and deeper soil layers in the creosote slope. It should be noted, however, that numerical simulations and infiltration estimates are valid for the fine earth fraction of the soil matrix and do not reflect the influences of high gravel content and macropore flow due to the presence of decayed roots or soil disturbance caused by burrowing animals. Infiltration measurements are required to validate these results and assess the effect of preferential flow in each ecosystem.

(2) Soil water content and matric potential modeling reveal spatial and temporal variations and significant differences between the two ecosystems. Soil water in upper horizons is slightly higher for the juniper soil as shown by the moisture retention curves. In the lower horizons, marked differences are observed in matric potential and water content for the two species as soil properties and root distributions vary with depth. Differences in matric potential in the K horizon suggest differential abilities of plants to tap water from deep soil horizons during water stress periods. Also, the variation in the amplitude and frequency of deep percolation for the two hillslope soils correspond to changes in profile characteristics due to differential plant effects on soil development.

(3) Potential and actual evaporation and transpiration estimates reveal interesting behavior in the two ecosystems. Simulated differences are a reflection of a combination of factors, including terrain aspect (incident radiation), soil morphology (water retention, conductivity), and root water uptake. While clear differences are observed in potential rates, compensations due to soil water content lead to similar actual rates, with a higher transpiration efficiency in the creosote ecosystem. Comparisons of the precipitation amounts with the actual evapotranspiration reveal that all incoming rainfall is consumed in each ecosystem and that portions of the stored soil water are also accessed by the creosote bush. Similarities in actual evapotranspiration in the two ecosystems suggest that differences in $CaCO_3$ development in the two slopes is a function of material deposition and moisture fluxes, rather than evapotranspiration. Matric potential in the juniper K horizon suggests greater moisture variability, which is consistent with the higher $CaCO_3$ development on the north-facing slope.

A difficulty in the analysis of interactions between topography, soils development and ecohydrological dynamics are the temporal scale differences in

each process. Short-term ecohydrological fluxes occur in the context of slowly-varying geomorphic and soil properties. Analysis and simulations conducted in this study reflect the current conditions in the semiarid basin where established plants have had a significant amount of time to impact landscape evolution and soil formation. As a result, evidence from soil differences provide an insight on long-term fluxes which may no longer be occurring in the system due to internal changes in soil properties, vegetation patterns and terrain reorganization. Nevertheless, multiple lines of evidence in this study suggest that plant establishment has led to variations in soil development which have reinforced ecosystem differences in soil water fluxes with a potential homogenization of actual evapotranspiration.

It is important to note that the conclusions of this study are based on a series of assumptions made during our modeling experiments. First, we have treated the hydrology of the two hillslopes in a simplified fashion by utilizing one-dimensional soil columns. While this can be relaxed through hillslope simulations (e.g., Simunek et al., 1999), we believe the study results are illustrative of the differences between the two ecosystems. Second, we have made simplifying assumptions on the soil profile properties, including gravel content, calcic horizon characteristics and preferential flow paths. Further work in the study basin is required to properly quantify the influence of these soil properties on vadose zone fluxes. Third, we have assumed simplified vegetation characteristics, such as plant cover, root distribution and leaf area index, which do not vary in time. Additional work is required to properly determine critical vegetation parameters for future modeling studies in the basin. Finally, we have simplified the infiltration process by assuming ponded conditions for the infiltration capacity estimates and ignoring the high gravel content on the sloped surface which

can impact soil infiltration. All of these assumptions can be refined and relaxed through more detailed modeling at the hillslope scale and improved physical representation of the study basin.

Future work in understanding the ecohydrological interactions in the semi-arid drainage basin will be directed towards obtaining improved measures of vegetation, soils, terrain properties to better parameterize hydrologic models. In addition, a network of terrain-based sensors (rainfall gauges, soil moisture probes, radiation measuring devices) is currently being installed in the two opposing hillslope ecosystems to obtain field measurements to validate modeling results. The data sets compiled from this network will be coupled with high resolution digital terrain models and remote sensing data to run a more sophisticated watershed model with ecohydrological interactions to assess the ecosystem response to changes in the climatic and hydrologic regimes.

REFERENCES

Abrahams AD, Parsons AJ. 1991. Relation between infiltration and stone cover on a semiarid hillslope, southern Arizona. *Journal of Hydrology. 122*(1-4): 49-59.

Abrahams AD, Parsons AJ, Wainwright J. 2003. Disposition of rainwater under creosotebush. *Hydrological Processes.* 17: 2555-2566.

Aide M, VanAuken OW. 1985. Chihuahuan desert vegetation of limestone and basalt slopes in West Texas. *The Southwestern Naturalist*. 30: 533-542.

Allen CD, Breshears DD. 1998. Drought-induced shift of a forest-woodland ecotone: Rapid landscape response to climate variation. *Proceedings National Academy of Science USA*. 95: 14839- 14842.

Band LE, Patterson P, Nemani R, Running SW. 1993. Forest ecosystem processes at the watershed scale-incorporating hillslope hydrology. *Agricultural and Forest Meteorology. 63*(1-2): 93-126.

Baumhardt RL, Lascano RJ. 1993. Physical and hydraulic properties of a calcic horizon. *Soil Science. 155*(6): 368-374.

Belnap J, Welter JR, Grimm NB, Barger N, Ludwig JA. 2005. Linkages between microbial and hydrological processes in arid and semiarid watershed. *Ecology. 86*(2): 298-307.

Beven KJ, Kirkby MJ. 1979. A physically-based, variable contributing area model of basin hydrology. *Hydrologic Sciences Bulletin*. 24: 43-69.

Bhark EW, Small EE. 2003. Association between plant canopies and the spatial patterns of infiltration in shrubland and grassland of the Chihuahuan desert, New Mexico. *Ecosystems*. 6: 185-196.

Birkeland PW. 1999. *Soils and Geomorphology. 3rd edition*. Oxford University Press. Oxford, UK. 430 pp.

Bonan G. 2002. *Ecological climatology: Concepts and Applications*. Cambridge University Press. Cambridge, UK. 678 pp.

Boulanger JR. 2004. *Stable isotope partitioning of evapotranspiration across a shrub-grass ecotone following a precipitation event Sevilleta National Wildlife Refuge, USA.* MS Thesis, New Mexico Institute of Mining and Technology, Socorro, NM. 66 pp.

Bras RL. 1990. *Hydrology: An Introduction to Hydrologic Science*. Addison-Wesley, Reading, MA. 643 pp.

Breshears DD, Nyhan JW, Heil CE, Wilcox BP. 1998. Effects of woody plants on microclimate in a semiarid woodland: Soil temperature and evaporation in canopy and intercanopy patches. *International Journal of Plant Science. 159*(6): 1010-1017.

Breshears DD, Whicker JJ, Johansen MP, Pinder JE. 2003. Wind and water erosion and transport in semiarid shrubland, grassland and forest ecosystems: Quantifying dominance of horizontally wind-driven transport. *Earth Surface Processes and Landforms*. 28: 1189-1209.

Brooks RH, Corey AT. 1964. *Hydraulic properties of porous media*. Colorado State University. Hydrology Paper No. 3. 27 pp.

Burgess SSO, Adams MA, Turner NC, Ong CK. 1998. The redistributions of soil water by tree root systems. *Oecologia*. 115: 306-311.

Calvo-Cases A, Boix-Fayos C, Imeson AC. 2003. Runoff generation, sediment movement and soil water behavior on calcareous (limestone) slopes of some Mediterranean environments in southeast Spain. *Geomorphology*. 50: 269-291.

Caylor KK, Manfreda S, Rodrguez-Iturbe I. 2005. On the coupled geomorphological and ecohydrological organization of river basins. *Advances in Water Resources*. 28: 69-86.

Coblentz DD, Riiters KH. 2004. Topographic controls on the regional-scale biodiversity of the south-western USA. *Journal of Biogeography*. 31: 1125-1138.

Cruiziat P, Cochard H, Ameglio T. 2002. Hydraulic architecture of trees: main concepts and results. *Annals of Forest Science*. 59:723-752.

Davenport DW, Wilcox BP, Breshears DD. 1996. Soil morphology of canopy and intercanopy sites in a Pinyon-Juniper woodland. *Soil Science Society of America*. 60: 1881-1887.

Dietrich WE, Reiss R, Hsu M-L, Montgomery DR. 1995. A process-based model for colluvial soil depth and shallow landsliding using digital elevation data. *Hydrological Processes*. 9: 383-400.

Dirnbock T, Hobbs RJ, Lambeck RJ, Caccetta PA. 2002. Vegetation distribution in relation to topographically driven processes in southwestern Australia. *Applied Vegetation Science. 5*(1): 147-158.

Dodd MB, Lauenroth WK, Burke IC, Chapman PL. 2002. Associations between vegetation patterns and soil texture in the shortgrass steppe. *Plant Ecology*. 158: 127137.

Dunne T, Black RD. 1970. Partial area contributions to storm runoff in a small New England watershed. *Water Resour. Res.*, 6(5): 1296-1311.

Eagleson PS. 1978. Climate, soil, and vegetation. I. Introduction to water balance dynamics. *Water Resour. Res.*, 14(5): 705-712.

Eagleson PS. 2002. *Ecohydrology Darwinian Expression of Vegetation Form and Function*. Cambridge University Press, Cambridge, UK. 443 pp.

Engel VC, Stieglitz M, Williams M, Griffin KL. 2002. Forest canopy hydraulic properties and catchment water balance: observations and modeling. *Ecological Modelling*. 154: 263-288.

Feddes RA, Hoff H, Bruen M, Dawson T, de Rosnay P, Dirmeyer O, Jackson RB, Kabat P, Kleidon A, Lilly A, Pitman AJ. 2001. Modeling root water uptake in hydrological and climate models. *Bulletin of the American Meteorological Society. 82*(12): 2797-2809.

Feddes RA, Kowalik PJ, Zaradny H. 1978. *Simulation of field water use and crop yield*. John Wiley & Sons, New York, NY. 188 pp.

Fernndez-Illescas CP, Porporato A, Laio F, Rodrguez-Iturbe I. 2001. The ecohydrological role of soil texture in a water-limited ecosystem. *Water Resources Research. 37*(12): 2863-2872.

Foxx TS, Tierney GD, Williams JM. 1984. *Rooting depths of plants relative to biological and environmental factors*. Los Alamos National Laboratory, Los Alamos, New Mexico. 22 pp.

Florinsky IV, Kuryakova GA. 1996. Influence of topography on some vegetation cover properties. *Catena. 27*(2): 123-141.

Gibbens RP, Lenz JM. 2001. Root systems of some Chihuahuan Desert plants. *Journal of Arid Environments*. 49: 221-263.

Gile LH, Peterson FF, Grossman RB. 1966. Morphological and genetic sequences of carbonate accumulation in desert soils. *Soil Science*. 101: 347-360.

Gile LH, Hawley JW, Grossman RB. 1981. *Soils and geomorphology in the basin and range area of southern New Mexico-Guide book to the Desert Project*. Memoir 39, New Mexico Bureau of Mines and Mineral Resources. Socorro, NM. 222 pp.

Goudie 1983. Calcrete. In: *Chemical sediments and geomorphology: Precipitates and residua in the near-surface environment*, AS Goudie and K Pye (eds). Academic Press, New York, NY. 93-131.

Guan H. 2005. *Water above the mountain front Assessing mountain-block recharge in semiarid mountainous regions*. PhD Dissertation. New Mexico Institute of Mining and Technology, Socorro, NM. 441 pp.

Hennessy JT, Gibbens RP, Tromble JM, Cardenas M. 1983. Water properties of caliche. *Journal of Range Management. 36*(6): 723-726.

Herbel CH, Ares FN, Wright RA. 1972. Drought effects on a semidesert grassland range. *Ecology*. 53:1084-1093.

Hillel D. 1998. *Environmental Soil Physics*. Academic Press. San Diego, CA. 771 pp.

Huxman TE, Wilcox BP, Breshears DD, Scott RL, Snyder KA, Small EE, Hutline K, Pockman WT, Jackson RB. 2005. Ecohydrological implications of woody plant encroachment. *Ecology. 86*(2): 308-319.

Ivanov, V. Y., Bras, R. L., and Vivoni, E. R. 2008a. Vegetation-hydrology dynamics in complex terrain of semiarid areas. I. A mechanistic approach to modeling dynamic feedbacks, *Water Resour. Res.*, 44, W03429, doi:10.1029/2006WR005588.

Ivanov, V. Y., Bras, R. L., and Vivoni, E. R. 2008b. Vegetation-hydrology dynamics in complex terrain of semiarid areas: 2. Energy-water controls of vegetation spatiotemporal dynamics and topographic niches of favorability, *Water Resour. Res.*, 44, W03430, doi:10.1029/2006WR005595.

Jenny H. 1958. Role of the plant factor in the pedogenic functions. *Ecology*. 39: 5-16.

Kerkhoff AJ, Martens SN, Shore GA, Milne BT. 2004. Contingence effects of water balance variations on tree cover density in semiarid woodlands. *Global Ecological Biogeography*. 13: 237-246.

Kim Y, Eltahir EAB. 2004. Role of topography in facilitating coexistence of trees and grasses within savannas. *Water Resour. Res.* 40: W07505, doi:10.1029/2003WR002578.

Kirkby MJ. 1978. *Hillslope Hydrology*. John Wiley Sons. London, UK. 589 pp.

Kurc SA, Small EE. 2004. Dynamics of evapotranspiration in semiarid grasslands and shrubland ecosystems during the summer monsoon season, central New Mexico. *Water Resour. Res.* 40: W09305, doi:10.1029/2004WR003068.

Lauenroth WK, Sala OE, Coffin DP, Kirchner TB. 1994. The importance of soil water in the recruitment of Bouteloua gracilis in the shortgrass steppe. *Ecological Applications. 4*(4): 741-749.

Loik ME, Breshears DD, Lauenroth WK, Belnap J. 2004. A multi-scale perspective of water pulses in dryland ecosystems: climatology and ecohydrology of the western USA. *Oecologia.* 141: 269-281.

Ludwig JA, Wilcox BP, Breshears DD, Tongway DJ, Imeson AC. 2005. Vegetation patches and runoff-erosion as interacting ecohydrological processes in semiarid landscapes. *Ecology. 86*(2): 288-297.

Machette MN. 1985. Calcic soils of the southwestern United States. *Geological Society of America Special Paper*. 203: 1-21.

Mackay DS, Band LE. 1997. Forest ecosystem processes at the watershed scale: Dynamic coupling of distributed hydrology and canopy growth. *Hydrological Processes. 11*(9): 1197-1217.

Martnez-Mesa E, Whitford WG. 1996. Stemflow, throughfall and channelization of stemflow by roots in three Chihuahuan desert shrubs. *Journal of Arid Environments.* 32: 217-287.

McAuliffe JR. 1984. Landscape evolution, soil formation, and ecological patterns and processes in Sonoran Desert bajadas. *Ecological Monographs. 64*(2): 111-148.

McClain ME, Boyer EW, Dent CL, Gergel SE, Grimm NB, Groffman PM, Hart SC, Harvey JW, Johnston CA, Mayorga E, McDowell WH, Pinay G. 2003. Biogeochemical hot spots and hot moments at the interface of terrestrial and aquatic ecosystems. *Ecosystems.* 6: 301-312.

McMahon DR. 1998. *Soil, landscape and vegetation interactions in a small semiarid drainage basin: Sevilleta National Wildlife Refuge, New Mexico*. MS Thesis. New Mexico Institute of Mining and Technology. Socorro, NM. 174 pp.

Milne BT, Gupta VK, Restrepo C. 2002. A scale invariant coupling of plants, water, energy, and terrain. *EcoScience. 9*(2): 191-199.

Milne BT, Moore DI, Betancourt JL, Parks JA, Swetnam TW, Parmenter RR, Pockman WT. 2003. Multidecadal drought cycles in south-central New Mexico: Patterns and consequences. In: *Climate variability and ecosystem responses at Long-Term Ecological Research sites*. Greenland D, Goodin DG, Smith RC (eds). Oxford University Press. 286-307.

Milne G. 1935. Some suggested for classification and mapping, particularly for East African soils. *Soil Research*. 1: 345-347.

Moore ID, Norton TW, Williams JE. 1993. Modelling environmental heterogeneity in forested landscapes. *Journal of Hydrology*. 150: 717-747.

Neave M, Abrahams AD. 2002. Vegetation influences on water yields from grassland and shrubland ecosystems in the Chihuahuan Desert. *Earth Surface Processes and Landforms*. 27: 1011-1020.

Newman BD, Wilcox BP, Archer S, Breshears DD, Dahm CN, Duffy CJ, McDowell NG, Phillips FM, Scanlon BR and Vivoni ER. 2006. The ecohydrology of arid and semiarid environments: A scientific vision. *Water Resour. Res.*, 42, W06302, doi:10.1029/2005WR004141.

Okin GS, Gillette DA. 2001. Distribution of vegetation in wind-dominated landscapes: implications for wind erosion modeling and landscape processes. *Journal of Geophysical Research-Atmospheres. 106*(D9): 9673-9683.

Parsons AJ, Abrahams AD, Wainwright J. 1994. Rainsplash and erosion rates in an interrill area on semiarid grassland, Southern Arizona. *Catena. 22*(3): 215-226.

Pockman WT, Sperry JS. 2000. Vulnerability to xylem cavitation and the distribution of Sonoran Desert Vegetation. *American Journal of Botany. 87*(9): 1287-1299.

Porporato A, Odorico P, Laio F, Ridofi L, Rodrguez-Iturbe I. 2002. Ecohydrology of water-controlled ecosystems. *Advances in Water Resources*. 25: 1335-1348.

Rawls WJ, Brakensiek DL. 1985. Prediction of soil water properties for hydrologic modeling. In: *Watershed Management in the Eighties*. EE Jones, TJ Ward (eds). 293-299.

Reid KD, Wilcox BP, Breshears DD, MacDonald L. 1999. Runoff and erosion in a Pion-Juniper woodland: Influence of vegetation patches. *Soil Science Society of America Journal*. 63: 1869-1879.

Reynolds JF, Kemp PR, Ogle K, Fernndez RJ. 2004. Modifying the pulse-reserve paradigm for deserts of North America: precipitation pulses, soil water and plant responses. *Oecologia*. 141: 194-210.

Rodrguez-Iturbe I. 2000. Ecohydrology: A hydrologic perspective of climate-soil-vegetation dynamics. *Water Resour. Res., 36*(1): 3-9.

Rodrguez-Iturbe I, Porporato A, Laio F, Ridolfi L. 2001a. Plants in water-controlled ecosystems: active role in hydrologic processes and response to water stress. I. Scope and general outline. *Advances in Water Resources*. 24: 695-705.

Rodrguez-Iturbe I, Porporato A, Laio F, Ridolfi L. 2001b. Intensive or extensive use of soil moisture: plant strategies to cope with stochastic water availability. *Geophysical Research Letters. 28*(23): 4495-4497.

Saxton KE, Rawls WJ. 2005. *Soil Water Characteristic Estimates by Texture and Organic Matter for Hydrologic Solutions*. Software Documentation. Available online at: http://hydrolab.arsusda.gov/soilwater/Index.htm. 25 pp.

Scanlon BR, Christman M, Reedy RC, Porro I, Simunek J, Flerchinger GN. 2002. Intercode comparison for simulating water balance of surficial sediments in semiarid regions. *Water Resour. Res., 38*(12): 1323.

Schenk HJ, Jackson RB. 2002. Rooting depths, lateral root spreads and below-ground/above-ground allometries of plants in water-limited ecosystems. *Journal of Ecology*. 90(3): 480494.

Schlesinger WH, Pilmanis AM. 1998. Plant-soil interactions in deserts. *Biogeochemistry* 42: 169-187.

Scott RL, Shuttleworth WJ, Keefer TO, Warrick AW. 2000. Modeling multiyear observations of soil moisture recharge in the semiarid American Southwest. *Water Resour. Res.* 36: 22332247.

Secor JB, Shamash S, Smeal D, Gennaro A. 1983. Soil characteristics of two desert plant community types that occur in Los Medanos area of southeastern New Mexico. *Soil Science*. 136(3): 133-144.

Seyfried MS. 1991. Infiltration patterns from simulated rainfall on semiarid rangeland soil. *Soil Science Society of America Journal*. 55: 1726-1734.

Seyfried MS, Schwinning S, Walvoord MA, Pockman WT, Newman BD, Jackson RB, Phillips FM. 2005. Ecohydrological control of deep drainage in arid and semiarid regions. *Ecology*. 86(2): 277-287.

Shreve F, Mallery TD. 1932. The relation of caliche to desert plants. *Soil Science*. 35: 99-113.

Shuttleworth WJ. 1993. Evapotranspiration. In: *Handbook of Hydrology*. Maidment DR (ed). McGraw-Hill, Inc. New York, NY. 4.1 4.53.

Simunek J, Sejna M, van Genuchten MT. 1998. *The HYDRUS-1D software package for simulating the one-dimensional movement of water, heat and multiple solutes in variably saturated media*. Version 2.0. IGWMC-TPS-70. International Ground Water Modeling Center. Colorado School of Mines. Golden, CO. 202 pp.

Simunek, J, Sejna M, van Genuchten MT. 1999. *The HYDRUS-2D software package for simulating two-dimensional movement of water, heat, and multiple solutes in variably saturated media*. Version 2.0. IGWMC-TPS-53. International Ground Water Modeling Center. Colorado School of Mines. Golden, CO. 251pp.

Singh JS, Milchunas DG, Lauenroth WK. 1998. Soil water dynamics and vegetation patterns in a semiarid grassland. *Plant Ecology*. 134: 77-89.

Small EE, Kurc SA. 2003. Tight coupling between soil moisture and the surface radiation budget in semiarid environments: implications for land-atmosphere interactions. *Water Resour. Res.*, 39(10): 1278, doi:/10.1029/2002WR001297.

Stewart GH, Harrison JBJ. 1987. Plant-communities, landforms and soils of a geomorphically active drainage basin, Southern Alps, New Zealand. *New Zealand Journal of Botany*. 25(3): 385-399.

Tierney GD, Foxx TS. 1987. *Root Lengths of Plants on Los Alamos National Laboratory Lands*. Los Alamos National Laboratory, Los Alamos, New Mexico. 22 pp.

van Genuchten MTh. 1980. A closed form equation for predicting the hydraulic conductivity of unsaturated soils. *Soil Science Society of America Journal*. 44: 892-898.

van Genuchten MTh. 1987. *A numerical model for water and solute movement in and below the root zone*. Research Report no. 121. U.S. Salinity Laboratory, USDA-ARS. Riverside, CA.

van Wijk MT, Rodriguez-Iturbe, I. 2002. Tree-grass competition in space and time: Insights from a simple cellular automata model based on ecohydrological dynamics, *Water Resour. Res.*, 38(9): 1179, doi:10.1029/2001WR000768.

Wainwright J, Mulligan M, Thornes J. 1999. Plants and water in drylands. In: *Ecohydrology: Plants and water in terrestrial and aquatic environments*. AJ Baird, RL Wilby, Routledge Press. London, UK. 78-126.

Walvoord MA, Plummer MA, Phillips FM, Wolfsberg AV. 2002. Deep arid system hydrodynamics. 1. Equilibrium state and response times in thick desert vadose zones. *Water Resour Res.*, 38: doi: 10.1029/2001WR000824.

Walvoord MA, Phillips FM. 2004. Identifying areas of basin-floor recharge in the Trans-Pecos region and the link to vegetation. *Journal of Hydrology*. 292: 59-74.

Western AW, Grayson RB, Blschl G, Willgoose GR, McMahon TA. 1999. Observed spatial organization of soil moisture and its relation to terrain indices. *Water Resour. Res.* 35(3), 797- 810.

Wierenga PJ, Hendrickx JMH, Nash MH, Ludwig J, Daugherty LA. 1987. Variation in soil and vegetation with distance along a transect in the Chihuahuan Desert. *Journal of Arid Environments*. 13: 53-63.

Wilcox BP, Breshears DD, Allen CD. 2003a. Ecohydrology of a resource-conserving semiarid woodland: effects of scale and disturbance. *Ecological Monographs*. 73(2): 223-239.

Wilcox BP, Breshears DD, Turin HJ. 2003b. Hydraulic conductivity in a pion-juniper woodland: Influence of vegetation. *Soil Science Society of America Journal*. 67: 1243-1249.

Wondzell SM, Cunningham GL, Bachelet D. 1996. Relationships between landforms, geomorphic processes, and plant communities on a watershed in the northern Chihuahuan Desert. *Landscape Ecology*. 11(6): 351-362.

Yair A, Shachak M. 1987. Studies in watershed ecology of an arid area. In: *Progress in Desert Research*. Berkofsky L, Wurtele MG (eds). Rowan Littlefield Publishers. Lanham, MD. 145-193.

Yaalon DH. 1971. Soil-forming processes in time and space. In: *Paleopedology: Origin, Nature and Dating of Paleosols*. Yaloon DH (ed). Israel University Press. Jerusalem, Israel. 29-39.

CHAPTER 3

ECOHYDROLOGICAL RESPONSE TO A GEOMORPHICALLY SIGNIFICANT FLOOD EVENT IN A SEMIARID CATCHMENT WITH CONTRASTING ECOSYSTEMS

(This chapter is published as: Gutiérrez-Jurado, H. A., Vivoni, E. R., Istanbulluoglu, E., and Bras, R. L. 2007. Ecohydrological response to a geomorphically significant flood event in a semiarid catchment with contrasting ecosystems. *Geophys. Res. Lett.* **34**, L24S25, doi:10.1029/2007GL030994.)

3.1 Introduction

An increasing number of scientific studies stress the importance of measuring and understanding soil moisture dynamics and the controls exerted by vegetation [e.g., Cordova and Bras, 1981; Rodrguez-Iturbe and Porporato, 2004; Newman et al., 2006]. Vegetation plays a significant role in the partitioning of mass and energy inputs, especially for water-limited semiarid landscapes [Wilcox et al., 2003; Kurc and Small, 2004], and modifies hydrologic dynamics in ecosystems during storm and interstorm periods. In semiarid areas with terrain variability, close interaction also exists between hillslope and vegetation characteristics [Istanbulluoglu and Bras, 2005; Gutiérrez-Jurado et al., 2006] which can significantly impact local water and energy fluxes. For instance, in semiarid climates, terrain aspect can lead to establishment of different plant communities

and functional types on opposing hillslopes. Organization of steep hillslopes around the channel network can also induce overland or interflow which can become an additional water source for downslope sites [Wilcox et al. 2003; Ivanov et al. 2007], and hence modify soil moisture dynamics along slope positions. To our knowledge, few studies have addressed the effects of terrain aspect and slope on ecohydrological responses to a geomorphically significant (GS) event, defined here as a flood that alters landscape form. In this study, we present the different responses of opposing hillslopes with varying plant communities during a major flood event. We believe this is the first time that hillslope and channel responses, and the effects of ecosystem and soil characteristics, are documented in a first-order semiarid catchment. Observational analysis of this flood event has implications for understanding the impact of soil and vegetation properties on hillslope evolution. Our focus here is to demonstrate from a series of in-situ observations that soil properties and vegetation exert controls on soil moisture dynamics. We also compare runoff and erosion responses in the opposing ecosystems and tie this to the generation of a significant flood in the main channel.

3.2 Methods

3.2.1 Study Area

The study site is located in the northwest part of the Sevilleta National Wildlife Refuge (SNWR) site in central New Mexico (Fig. 3.1a). The site comprises a small ($\sim$0.1 km^2) first-order catchment dissected by an east-flowing ephemeral channel giving rise to opposing north and south facing slopes and an east facing headslope. The slopes sustain distinctive ecosystems: (1) a juniper-grass savanna on the north facing slope consisting of juniper (*Juniperus monosperma*)

and dense black grama (*Bouteloa eriopoda*); (2) a xeric shrubland on the south facing slope dominated by creosotebush (*Larrea tridentata*) with sparse fluff grass (*Erioneuron pulchellum*); and (3) an east facing headslope comprising the ecotonal boundary between the two slopes. These ecosystems exhibit differences in plant phenology, density, structure and biomass, as well as, in rooting structure and plant water uptake. Soils in the catchment are characterized by: desert pavements on the upper flat surfaces; sandy soil matrices with a high fraction of boulders and gravels; and $CaCO_3$ horizons intersecting the hillslopes at various depths [McMahon, 1998]. The climate in the area is semiarid with a mean annual rainfall of $\sim$255 mm and a bimodal rainfall regime with high intensity summer storms and lower intensity winter rains. Field observations indicate that significant runoff and erosion can occur in response to convective rainfall during the North American monsoon.

3.2.2 Hydrologic Instrumentation and Observations

An instrument network consisting of 24 water content reflectometers (WCR) and 3 tipping-bucket rain gauges was deployed along transects in the opposing north and south facing slopes (Fig. 3.1b). WCRs were placed horizontally at: 1) 10 and 20 cm soil depths to capture the vertical movement of water pulses; and 2) at open intercanopy and within canopy sites at three positions along each slope, to assess the effect of the canopy patch. As WCRs record the electrical transmissivity of the soil as a function of water content, the signal was converted to volumetric soil moisture through in-situ calibration using gravimetric sampling across a range of conditions. During the period, three rain gauges measured the

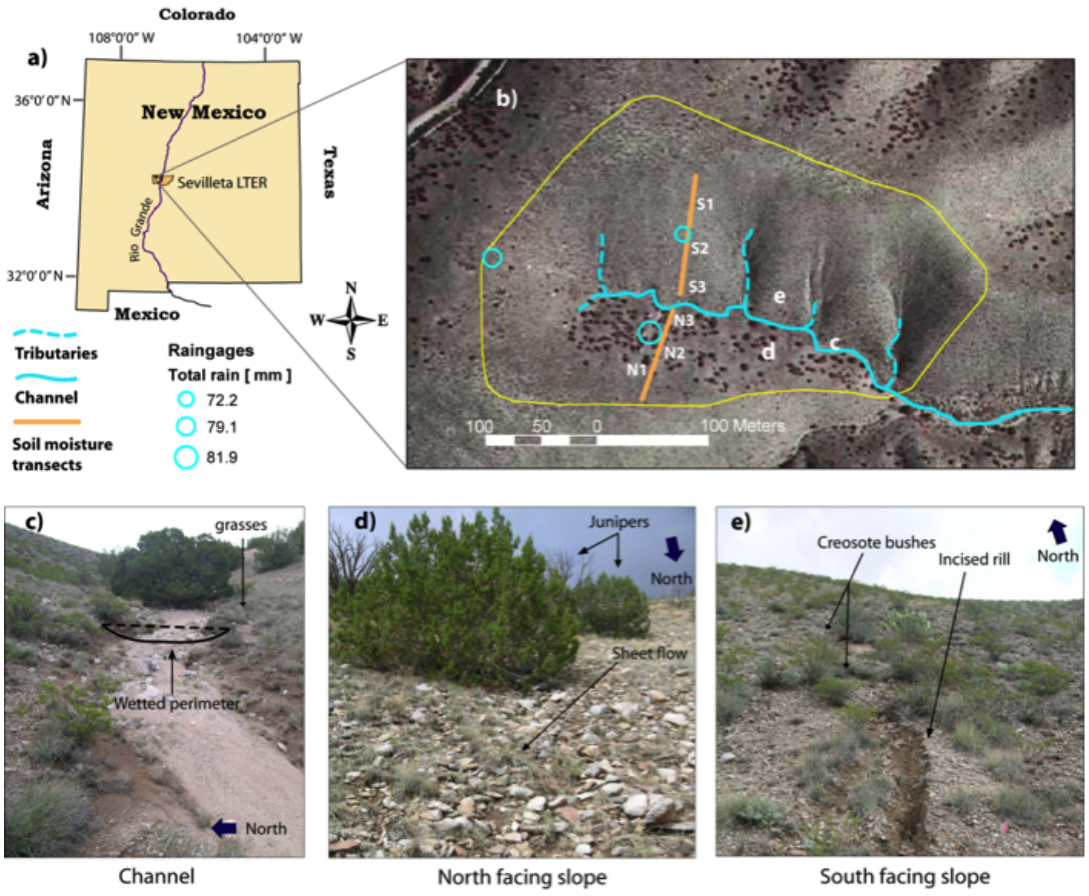

Figure 3.1: (a) Study site location in Sevilleta, NM. (b) 2-m aerial orthophoto of the study catchment depicting the boundary; the east flowing ephemeral channel; and the location of the soil moisture transects and three rain gauges. (c) Channel cross section one day after the flood event (wetted perimeter determined by fallen grasses). (d) North facing slope depicting the juniper trees and the observed evidence of overland sheet flow. (e) South facing slope with the creosotebush and a new incised rill (∼0.5 m deep).

rainfall amounts in the catchment. All the instruments recorded at 30 minutes intervals. Finally, post-flood field observations allowed us to determine the major erosional effects of the event and estimate the peak channel discharge.

3.3 Response to GS Flood Event

3.3.1 Storm Rainfall and Erosional Observations

A series of intense rainfall pulses were recorded in the study catchment from July 28 to 29, 2006, with a total accumulation of $\sim$80 mm in an 18 hour period (Figs. 3.2a,b). The total storm rainfall was approximately 1/3 of the annual precipitation at the site and was estimated to correspond to a return period between 150 and 200 years [Bonnin et al., 2004], with maximum rainfall intensities of 25 mm in a 30-min period. The sequence of rainfall events occurred during the exceptionally wet 2006 North American monsoon season in the southwestern U.S. [e.g., Magirl et al., 2007].

The storm event led to a flood response, exceeding the bankfull stage at places along the main channel. The event was clearly detected via its impact on fallen grasses in the downstream direction, as well as, the movement of soil and large clasts. Relatively large boulders ($\sim$0.3 m in diameter) were transported in the channel (Fig. 3.1b). Moreover, the flood event led to the development of several rills, $\sim$0.5 m deep and several meters in length, on the toe of the south facing slope (Fig. 3.1e), suggesting the generation of highly erosive runoff. No evidence of rill incision was found on the north facing slope, although fallen grass-cover suggested that overland sheet flow occurred in large sections ($\sim$2-3 m in width) near the slope toe (Fig. 3.1d). Furthermore, intercanopy spaces in the north facing slope showed evidence of sediment retention behind grassy mounds (not shown).

3.3.2 Hillslope Hydrologic Response

Volumetric soil water content observations at 10 and 20 cm depths obtained prior to, during, and after the flood event were analyzed to assess the effects of terrain aspect and slope position on soil moisture dynamics. Soil moisture time series (July 28 30, 2006) at intercanopy locations along each slope and in a channel site below the transects are shown in Fig. 3.2. Note that soil conditions prior to the flood event were uniformly dry at the sampling depths at most sites. Two exceptions are the south facing upslope (Fig. 3.2d) and the north facing midslope sites (Fig. 3.2e), where the shallower (deeper) layer had higher soil moisture, respectively. Differences in antecedent conditions for these two sites may be a function of local soil properties acting to retain water from a small rainfall pulse recorded $\sim$36 hours before the major flood event.

Rainfall hyetographs show a distinct double peak with rainfall distributions of 40 and 60% of the total accumulation, respectively, and a lag time of $\sim$1 h between storm pulses (Figs. 3.2a,b). Each hillslope location exhibits a response to the two peaks with a more pronounced increase in soil moisture for the upslope sites on each hillslope (Figs. 3.2c,d). This is possibly due to the proximity of these sites to the flat surface above the headslope. Note that high slopes ($\sim$20° and 17° for north and south facing slopes) can also shield these areas from an approaching storm [Ivanov et al., 2007]. Position along the slope also has a strong effect on the rising and falling limbs of the soil moisture response. Upslope positions respond faster to precipitation, but also decay at a faster rate, presumably due to the redistribution of water in the downslope direction. The downslope sites, on the other hand, exhibit slower soil moisture decays, as contributions from

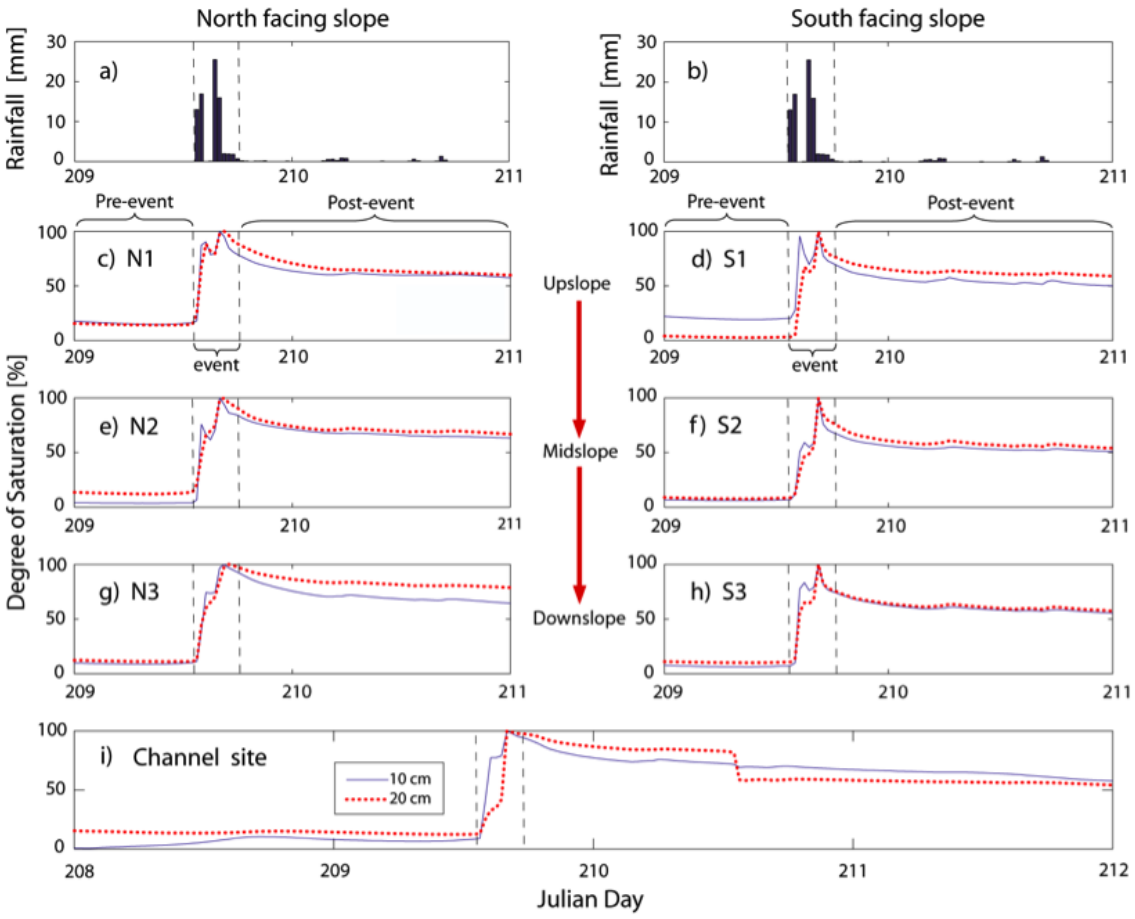

Figure 3.2: Rainfall and soil moisture observations at 10 cm (solid line) and 20 cm (dotted line) depths at each sampling point. Soil moisture is given as degree of saturation (S = θ/n, where θ is volumetric water content and n is porosity) in percent (%). (a, b) Rainfall hyetographs at two rain gauges. (c, e, g) North facing upslope (N1), midslope (N2) and downslope (N3) sites. (d, f, h) South facing upslope (S1), midslope (S2) and downslope (S3) sites. (h) Channel site.

upslope locations arrive following the end of the storm. Differences in soil moisture response between the two slopes clearly show the north facing sites remain wetter than the south facing sites, which is related to higher moisture retention due to high amounts of $CaCO_3$, silt, clay and organic matter [McMahon, 1998; Gutiérrez-Jurado et al., 2006].

Soil moisture observations in a channel site at the toe of the slopes (Fig. 3.2i) show the dynamical response in the narrow floodplain area ($\sim$1 m width), where the sediment profile quickly became nearly saturated down to 20 cm after the second peak. Saturated conditions in the channel are sustained for a longer period as compared to the slope locations, suggesting the presence of overland and subsurface flow for up to $\sim$2 hours, where visual evidence (i.e., fallen grasses) confirms the overland flow. Interestingly, the soil moisture dynamics in the deeper channel sediments exhibit a slow decay, indicating sustained water input, followed by a sharp decrease at the 20 cm depth. From these observations, we cannot infer the physical cause for this sudden soil moisture decrease.

3.3.3 Channel Hydrologic Response

Inferences of peak discharge during the flood event are available from a series of post-flood observations. Maximum flood stage was determined at 14 cross sections based on fallen grasses in the wetted perimeter and sediment deposition behind grass patches on the channel banks. Cross section geometry and reach slope were obtained through a high precision, differential GPS survey ($\sim$5 cm accuracy in x,y,z). Peak discharge (Q_p) at each section was then determined using the Manning equation, based upon roughness values estimated using Cowan [1956], which accounts for irregularities of the channel geometry,

channel obstructions and vegetation, and reach meandering. Given the uncertainties in Mannings n for the flood event, we computed Q_p for a range of possible roughness values. In general, high n were obtained for upstream sections with consistently lower estimation uncertainty, while the lower reach was characterized by low n with larger uncertainty. In addition, we derived the contributing area (A) at each cross section using delineations of a 10 m digital elevation model and visual corrections based on the 2 m orthophoto and site observations (Fig. 3.3a).

An estimate of Q_p as a function of distance from the channel head is presented in Fig. 3.3b. The flood wave likely propagated through the main channel following the first rainfall pulse (see Fig. 3.2i). Note the increasing trend in Q_p with downstream distance (linear trend of 0.3 m^3/s per 100 m, R^2 = 0.44), suggesting that transmission losses were minimized due to previous wetting from the first rainfall pulse. The mean and maximum Q_p over the channel length ($\sim$300 m) were estimated at 0.68 m^3/s and 1.54 m^3/s. Based on the site contributing area (A), the peak runoff rate (R) varied from 31 to 118 mm/hr, with a mean basin R of 60.5 mm/hr ($\pm$23.7 mm/hr). This compares well with the total rainfall of 77.7 mm averaged at the rain gauges, suggesting an exceptional runoff coefficient of 0.78 for the flood event. Note the variability in Q_p among sites is quite large ($\pm$0.4 m^3/s), but can be explained by increases in A as small tributaries enter the main channel.

Flood contributions from each slope may be inferred from the relative amounts of A along the channel. Fig. 3.3b presents the percentage of A from each hillslope at the cross section sites. Relative contributions are nearly equal from the channel head to $\sim$125 m downstream. Along with the fairly uniform

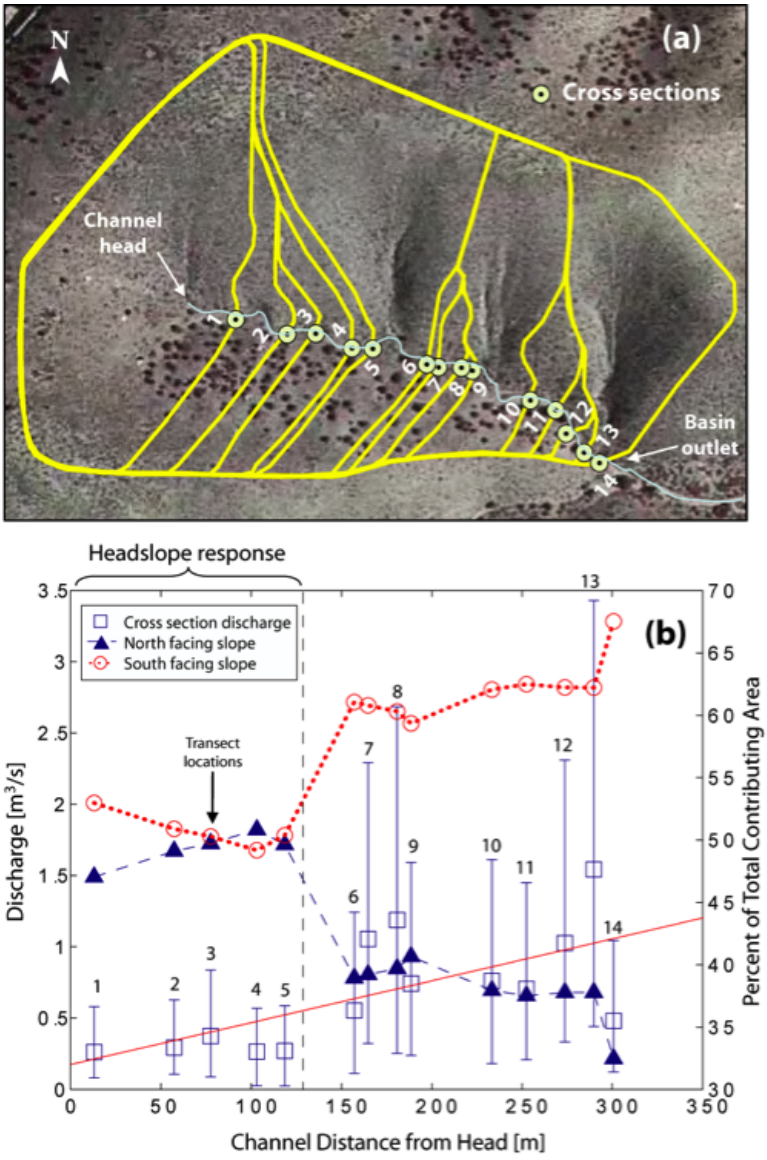

Figure 3.3: Aerial orthophoto depicting the cross section locations (labeled 1 to 14) used to estimate peak discharge and contributing areas (outlines). (b) Variation of the channel discharge (Q_p in m^3/s) and the percentage of total contributing area from each slope (%) as a function of channel distance (m). Headslope contributing area is partitioned into north and south facing segments (not shown). Solid line represents the linear regression of Q_p with channel distance. Vertical bars on the Q_p estimates represent the uncertainty arising from estimation of Mannings n at each cross section.

Q_p in this reach, this suggests the upper reach response is driven by the head-slope with lower runoff amounts generated in the slopes. Thereafter, the south facing slope is more important in terms of the total catchment area (up to 68% of A at the outlet). Due to the incised drainages on the south facing slope (Fig. 3.3a), the channel discharge increases downstream of the tributary confluences. In addition, minor discharge decreases along the main channel are observed due to local losses in the lower reach. This suggests the south facing slope dominates the flood response in the lower reach with minor contributions from the north facing slope. Clearly, the two slopes contribute different runoff amounts to the channel flood response.

3.4 Controlling Factors on the Hydrologic Response

Post-field observations indicated that different runoff production modes may exist in the north and south facing slopes. Rapid development of large rills in the south facing slope are evidence of more runoff erosion, while overland sheet flow and sediment accumulation maybe an indication of less erosion in the north facing slope. This suggests that geomorphically significant flood events may be responsible for punctuated changes in catchment morphology that differentiate landforms in the opposing slopes. Further, the different runoff modes in the opposing ecosystems seem to follow the conceptual model of Wilcox et al. [2003] for conserving and non-conserving slopes. With increased vegetation cover, the north facing slope retains a higher amount of runoff and sediment in the hillslope. Sparser vegetation cover on the south facing slope leads to a greater connection of intercanopy patches that facilitate downslope transport.

To further study the runoff production regimes, we present an analysis of the effects of slope position, soil properties and vegetation on soil moisture dynamics in the two slopes in Fig. 3.4. Analyses are based on the relation between degree of saturation (S) at the 10 and 20 cm depths for pre- and post-event conditions. The primary comparisons utilize the post-event relations as these depict soil drying or the recession behavior after complete surface saturation during the flood event. When the decay rate is faster at 10 cm depth relative to the 20 cm depth, the slope of the relation will be lower than the 1:1 line and vice versa. Furthermore, the position of the soil moisture relation with respect to the 1:1 line indicates if conditions are consistently wetter or drier at a soil depth.

The evidence at each site suggests that slope position (upslope, midslope and downslope) has important effects on the soil moisture dynamics, despite the similar soil profile properties along the slopes [McMahon, 1998]. North facing intercanopy sites (Fig. 3.4a), for example, show recession rates in the slope positions indicating downslope soil moisture redistribution. The upslope (downslope) site has a faster (slower) decay of deep water content indicating a soil moisture release (gain) along the subsurface hillslope path. Furthermore, the midslope positions in each slope (Figs. 3.4a-d) have nearly uniform soil moisture with depth and similar drying rates, suggesting these areas transmit moisture pulses downslope. While these dynamics are more typical in humid areas [Salvucci and Entekhabi, 1995], the nearly complete saturation of the slope results in hillslope activation potentially yielding subsurface runoff (or interflow) which may resurface downslope. Clearly, the relative position along the hillslope is an important control on soil moisture and runoff conditions experienced during major flood events.

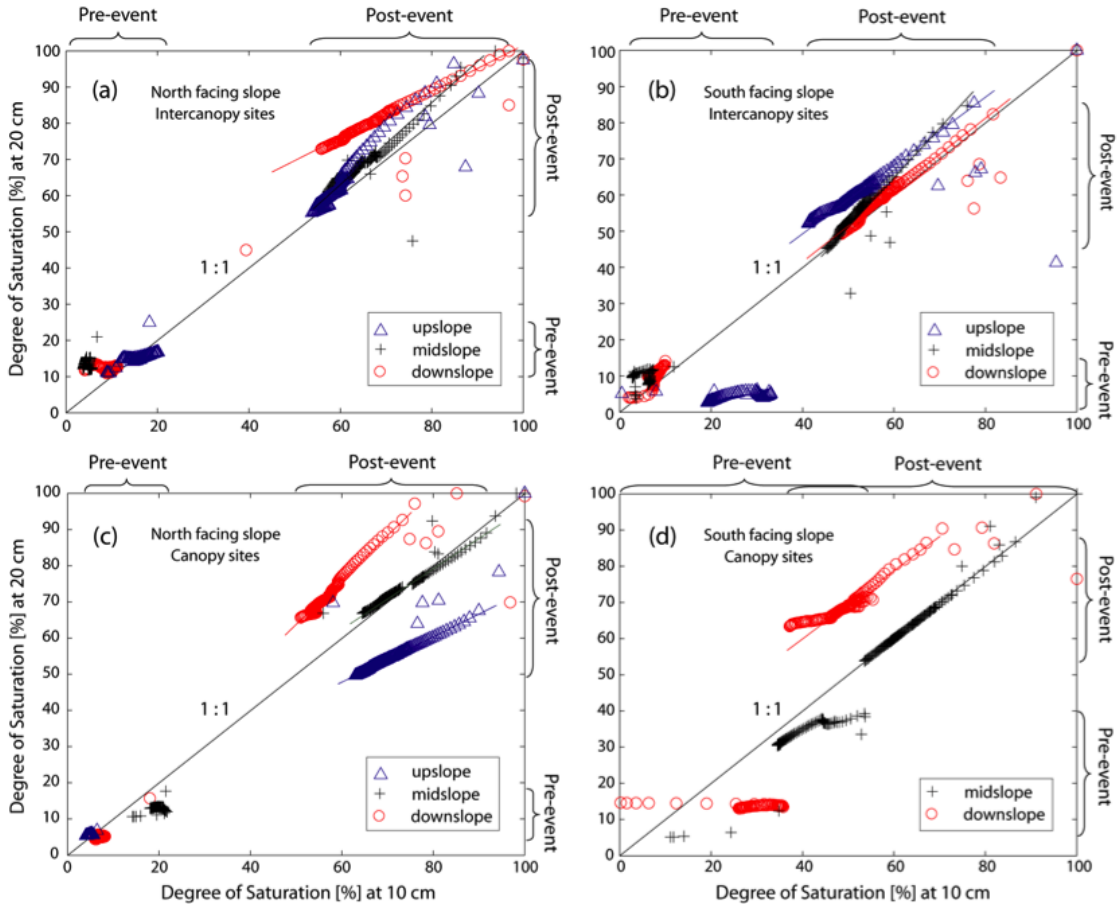

Figure 3.4: Observed relations between the degree of saturation (S in %) at 10 cm and 20 cm soil depths for the pre- and post-event conditions. (a) North facing intercanopy sites. (b) South facing intercanopy sites. (c) North facing canopy (juniper) sites. (d) South facing canopy (creosotebush) sites. The slope position effect is explored by comparing the upslope (△), midslope (+) and downslope (○) locations.

The effects of soil profile properties and the degree of connected intercanopy spaces on the runoff response can be discerned by comparing the north and south facing intercanopy sites. Note the dynamics in the south facing intercanopy site (Fig. 3.4b) differ from the north facing counterpart (Fig. 3.4a). The sparser plant cover on the south facing slope leads to uniform soil moisture with depth at the downslope site and similar recession rates, suggesting that surface runoff generated in the upper layer of the upslope sites is potentially transported downslope where it fills available storage. These observations support the notion that the south facing runoff regime favors surface flow through interconnected bare patches rather than subsurface transport and exfiltration as in the north facing slope. Since soil moisture recession rates are affected by hydraulic and water retention characteristics, differences in the two opposing slopes illustrate the impact of soil properties on the runoff generation.

The impact of the canopy patch on the soil moisture dynamics is best seen by comparing the north facing canopy and intercanopy sites (Figs. 3.4a,c). Overall, the canopy patch appears to augment the differences among the slope positions as compared to intercanopy sites. A progressive downslope shift in soil moisture conditions is observed with upslope (downslope) juniper trees having depleted (augmented) soil moisture in the lower soil layer. This behavior is possibly an indication of enhanced subsurface transport in canopy patches due to the effects of litter layers and root macropores on infiltration properties. A similar behavior is observed at the south facing canopy sites, although the upslope measurements were unavailable for comparison due to sensor malfunction.

3.5 Summary

This study documents the differential responses of opposing slopes with varying ecosystems to a major flood event in a semiarid catchment. Observational analysis of the hydrologic responses provides new insights into the interaction between terrain-soil-vegetation on modifying the spatial dynamics of soil moisture. Overall, there is a strong control of slope position on soil moisture recession due to overland and subsurface runoff redistribution. Vegetation differences have been shown to enhance the slope effects on the soil moisture dynamics along both hillslopes. Furthermore, the opposing hillslopes appear to contribute varying runoff amounts to the channel flood. Responses to this event have implications on the effects of vegetation on long-term hillslope evolution.

REFERENCES

Bonnin, GM, Todd D, Lin B, Parzybok T, Yekta M and Riley D. 2004. Precipitation-Frequency Atlas of the United States, vol 1., Semi-arid Southwest, NOAA Atlas 14, NOAA, Silver Springs, Md.

Cordova J.R., and Bras R.L. 1981. Physically-based probabilistic models of infiltration, soil moisture, and evapotranspiration. *Water Resour. Res.* 17(1): 93-106. Cowan WL. 1956. Estimating hydraulic roughness coefficients. Agricultural Engineering. 37(7): 473-475.

Gutiérrez-Jurado HA, Vivoni ER, Harrison JBJ and Guan H. 2006. Ecohydrology of root zone water fluxes and soil development in complex semiarid rangelands. *Hydrol. Process*. 20: 32893316, doi: 10.1002/hyp.6333.

Istanbulluoglu E. and RL Bras, 2005. Vegetation-modulated landscape evolution: Effects of vegetation on landscape processes, drainage density, and topography, *J. Geophy. Res*., 110: F02012, doi :10.1029 /2004JF000249.

Ivanov VY, Bras RL, and Vivoni ER. 2007. Vegetation-Hydrology Interaction over Complex Terrain, II. Energy-Water Controls of Vegetation Spatio-Temporal Dynamics and Topographic Niches of Favorability. *Water Resour. Res*., 44, W03430, doi:10.1029/2006WR005595.

Kurc SA and Small EE. 2004. Dynamics of evapotranspiration in semiarid grasslands and shrubland ecosystems during the summer monsoon season, central New Mexico. *Water Resour. Res*., 40: W09305, doi:10.1029/2004WR003068.

Magirl CS, Webb RH, Schaffner M, Lyon SW, Griffiths PG, Shoemaker C, Unkrich CL, Yatheendradas S, Troch PA, Pytlak E, Goodrich DC, Desilets SLE, Youberg A and Pearthree PA. 2007. Impact of recent extreme Arizona storms. *EOS, Transactions AGU*. 88(17): 191.

McMahon DR. 1998. *Soil, landscape and vegetation interactions in a small semiarid drainage basin: Sevilleta National Wildlife Refuge*. MS Thesis. New Mexico Tech. Socorro, NM. 174 pp.

Newman BD, Wilcox BP, Archer S, Breshears DD, Dahm CN, Duffy CJ, McDowell NG, Phillips FM, Scanlon BR and Vivoni ER. 2006. The ecohydrology of arid and semiarid environments: A scientific vision. *Water Resour. Res*., 42, W06302, doi:10.1029/2005WR004141.

Rodrguez-Iturbe I and Porporato A. 2004. Ecohydrology of Water-Controlled Ecosystems: Soil Moisture and Plant Dynamics. Cambridge University Press. 440 pp. Salvucci, GD and D Entekhabi. 1995. Hillslope and climatic controls on hydrologic fluxes. *Water Resour. Res*., 31(7): 1725-1739.

Wilcox BP, Breshears DD and Allen CD. 2003. Ecohydrology of a resource-conserving semiarid woodland: effects of scale and disturbance. *Ecological Monographs*. 73(2): 223-239.

CHAPTER 4

ECOGEOMORPHIC EXPRESSIONS OF AN ASPECT-CONTROLLED SEMIARID BASIN: I. TOPOGRAPHIC ANALYSES WITH HIGH RESOLUTION DATASETS

(This chapter was submitted for publication as: Gutiérrez-Jurado, H. A. and Vivoni, E. R. 2011. Ecogeomorphic expressions of an aspect-controlled semiarid basin: I. Topographic analyses with high resolution datasets. *Ecohydrology*)

4.1 Introduction

Vegetation organization in semiarid landscapes affects hydrogeomorphic processes such as runoff and erosion (e.g., Florinsky and Kuryakova, 2000; Nieve and Abrahams, 2002; Wilcox et al., 2003; Gutiérrez-Jurado et al., 2007). Over long periods, varying erosion rates in regions with different vegetation may leave a topographic imprint observable through coarse resolution terrain data (e.g., Istanbulluoglu et al., 2008). Nevertheless, little is known on the fine resolution (hillslope) effects of aspect-controlled vegetation patterns on the geomorphology of semiarid basins. Burnett et al. (2008), for example, showed that aspect-induced microclimatic conditions in Arizona influence erosion and weathering rates of a semiarid landscape. Gutiérrez-Jurado et al. (2007) also found that variations in vegetation can significantly alter the runoff and erosion on opposing hillslopes

with contrasting ecosystems after a large storm event. Similarly, other studies have pointed to the relation between vegetation patterns and soil development in semiarid regions (Bestelmeyer et al., 2006; Gutiérrez-Jurado et al., 2006; Wilkinson and Humphreys, 2006). Notwithstanding this progress, the interactions between vegetation and erosion processes that may feedback to landscape morphology have not been fully addressed.

In this work, we hypothesize that vegetation patterns within a semiarid basin with aspect-controlled ecosystems give rise to topographic and radiation differences that are signatures of the interactions between vegetation, soil and terrain. We argue these signatures can be detected using high resolution terrain surfaces with tree canopies derived from Airbone LiDAR (Light Detection And Ranging). Further, we hypothesize that vegetation-soil-terrain interactions occur at very fine spatial scales ($\sim$1-m) and thus are not easily detected in coarser topographic products (5 to 10-m) available at the site. This chapter is focused on the detailed analysis of the topographic expression of aspect-controlled ecosystems in a semiarid basin, and it also constitutes a preamble to Chapter 5 where we investigate the effects of topography and vegetation on solar irradiance.

4.1.1 Vegetation-soil-terrain interactions

Recent studies have discussed the identification of landform properties associated with the direct or indirect effects of vegetation (e.g., Caylor et al., 2005; Dietrich and Perron, 2006). For example, Istanbulluoglu et al. (2008) found that north facing slopes with mesic vegetation have slope and curvature properties that are distinct from south facing slopes with xeric shrublands. This observation may be due to the impact of aspect on radiation and the subsequent soil moisture

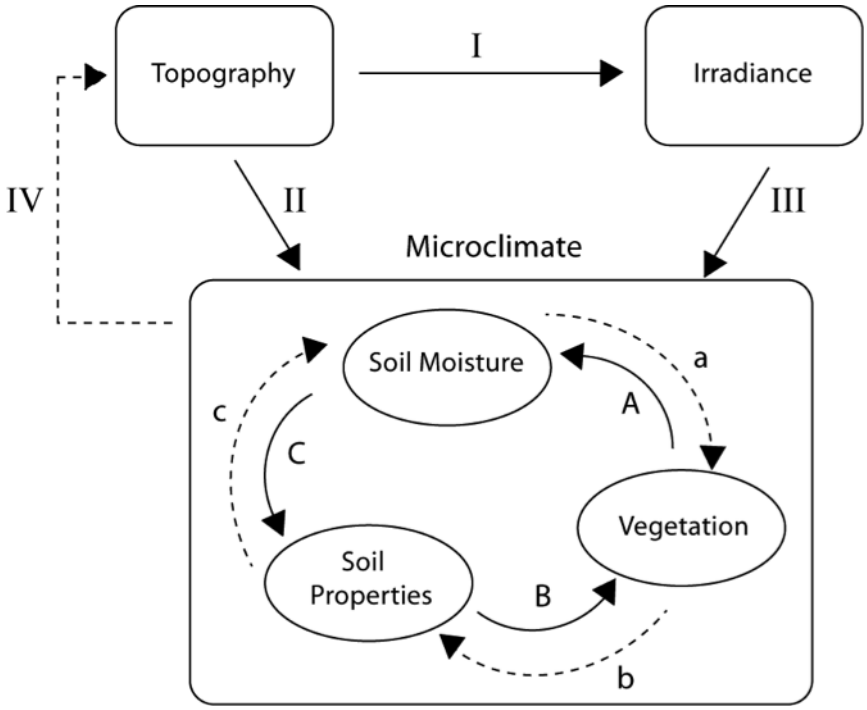

Figure 4.1: Schematic diagram depicting the influence of topography on the distribution of soil moisture, soil properties and vegetation, and its modulating effect on irradiance. The solid line arrows indicate direct effects, while the dashed line arrows illustrate feedbacks among the components. Roman numerals indicate first order effects: (I) Topography on Irradiance, (II) Irradiance on Microclimate, and (III) Topography on Microclimate. Note that microclimate feedbacks on the topographic field (IV) occur over long time scales.

dynamics and soil formation that promote different vegetation types. In addition, a feedback mechanism may exist between vegetation and the hydrogeomorphic mechanisms operating on each hillslope (Gutiérrez-Jurado et al., 2007). If these feedbacks operate over long periods, significant changes in landscape properties may lead to a topographic imprint of vegetation. Fig. 4.1 is a conceptual model of the topographic effects on the microclimatic, soil and vegetation conditions in semiarid regions, and the potential feedbacks to the terrain properties. Only a brief description of Fig. 4.1 is given here to illustrate the vegetation-soil-terrain interactions.

Differences in the water and energy balance in regions of complex terrain lead to the development of distinct microclimates which affect soil moisture, weathering and erosion processes (Carson and Kirkby, 1972; Wilkinson and Humphreys, 2006; Burnett et al., 2008). Terrain characteristics (slope, aspect, curvature) are critical determinants of the water and energy balance. For example, slope and aspect modulate the amount of exposure to direct irradiance (arrow I). Topography also affects the lateral redistribution of soil moisture and creates catenary relationships within hillslopes that affect soil development (arrow II). Since solar radiation is the main driver of the energy balance, it affects microclimate through radiation fluxes and its control on soil temperature, soil moisture and vegetation (arrow III). On long time scales, microclimate can impact terrain properties by influencing soil formation and erosion rates (arrow IV).

The interactions between soil moisture, soil properties and vegetation at a site are influenced by local microclimate (Rodrguez-Iturbe and Porporato, 2004; Bestelmeyer et al., 2006). Vegetation controls soil moisture dynamics via transpiration, shading and phenological changes (arrow A), while soil moisture influences the distribution of vegetation through plant-available water (arrow a). Soil properties can favor or inhibit vegetation species by constraining water availability (arrow B), while plants contribute to soil development through depositing organic matter content, trapping aeolian particles, and modifying soil porosity through root burrowing (arrow b). Finally, soil moisture affects the deposition and removal of materials such as $CaCO_3$ in the soil matrix and the chemical and bacterial properties of the soils (arrow C), while soil properties influence soil moisture by controlling infiltration and evaporation (arrow c).

In regions of complex terrain, special attention must be paid to the effects of aspect on solar irradiance. Radiation differences have a direct effect on the

surface energy balance, and thus on soil moisture through evapotranspiration. Contrasts in the water and energy balance may promote differential establishment of vegetation, in particular for semiarid regions where water is a limiting resource. These contrasts may also lead to soil property differences that feedback to soil moisture and thermal regimes (McMahon, 1998; Gutiérrez-Jurado et al., 2006; Burnett et al., 2008). These processes occur simultaneously in each microclimate with irradiance as the main driver of the system. Potential feedback of microclimate on topographic properties (e.g., slope, curvature) occurs over long time scales, but should be recognizable by assessing terrain metrics.

4.1.2 Terrain attributes and landform processes

Quantitative analyses of terrain attributes have become common practice with the advent of digital elevation data (Moore et al., 1991; Bras et al., 2003). Topographic analyses of slope and curvature yield substantial information on the spatial characteristics of the landscape and can be used to infer the dominant erosion processes (e.g., Tarboton et al., 1992; Dietrich et al., 1993; Tucker and Bras, 1998; Rodríguez-Iturbe and Rinaldo, 1997). For example, previous studies have shown that the convexity or concavity of a slope affects runoff and the accumulation of water in a landscape (Thorne et al., 1987; Walker and Willgoose, 1999; Wilson and Gallant, 2000; Berne et al., 2005). This effect is also present at the catchment scale, through sensitivity of the basin response to the convexity or concavity of the hypsometric distribution (Vivoni et al., 2008). While these analyses are insightful, the results can be sensitive to the spatial resolution of the topographic data (e.g., Zhang and Montgomery, 1994; Vivoni et al., 2004, 2005). Digital Elevation Models (DEMs) from different sources can also lead to divergent conclusions on the terrain properties. A number of studies address the issue

of DEM resolution on the extraction of different terrain metrics, but have been limited to relatively coarse data with pixel sizes greater than 10-m (e.g., Florinsky and Kuryakova, 2000; Kienzle, 2004; Deng et al., 2007; Erskine et al., 2007). The availability of high resolution terrain data is now increasing with differential global positioning systems (dGPS) as well as airborne and ground-based LiDAR (Slatton et al., 2007). Advanced sensing technologies allow a detailed analysis of fine-scale topographic characteristics and their relation to vegetation-soil-terrain interactions in semiarid regions.

4.1.3 Objectives and purpose

In this chapter, we analyze terrain and geomorphic attributes in a semiarid basin with different ecosystems in opposing hillslopes. We utilize three digital elevation datasets with sequentially higher spatial resolutions (i.e., 10-m, 4-m, and 1-m) to explore the hydrogeomorphic signature of the observed vegetation patterns and assess the capability of the datasets in revealing these patterns. In Part II, we explore the effect of terrain and vegetation on local microclimates by performing an analysis of incoming solar radiation. The intent of these studies is to provide insights for mechanistic models of ecogeomorphic dynamics in semiarid areas with complex terrain and to serve as a basis for interpretation of multi-year field observations made in a representative semiarid basin (see Gutiérrez-Jurado et al., 2006, 2007 for a detailed description).

4.2 Study Region and its Characteristics

The study area is located in central New Mexico within the Sevilleta National Wildlife Refuge (Fig. 4.2a). The region comprises a set of abandoned alluvial fan deposits with different degrees of incision (Fig. 4.2b,c). Alluvial fan

deposits ($\sim$2.3 km^2 in area) contain a series of nested basins with different orientations. In each basin, north and northwest-facing slopes typically contain a juniper-grass savanna ecosystem, while opposing south and southeast-facing slopes are composed of a creosotebush-grass association. Keystone species in the north-facing slopes are one-seed junipers (*Juniperus monosperma*), while south-facing slopes are creosotebush (*Larrea tridentata*). Our focus in this work is on a single headwater basin ($\sim$0.1 km^2, Fig. 4.2c) located east of the Loma Pelada fault, which has been instrumented for ecohydrological studies (Gutiérrez-Jurado et al., 2007). The climate in the area is semiarid with mean annual temperatures of 20°C and two distinct rainy seasons: a summer monsoon with high intensity, short duration events and lower intensity, winter frontal storms with occasional snow precipitation (Milne et al., 2003).

Soil profiles in north facing slopes contain higher proportions of silt, clay, organic matter content and $CaCO_3$ as compared to south facing slopes. Moreover, the north facing slope soils have stage IV calcic horizons, whereas calcic horizons in south facing soils are stage III (i.e., less developed) (McMahon, 1998). Differences in soil properties are a result of higher vegetation cover in the north facing slope, leading to: (1) trapping more dust and eolian particles; (2) producing and incorporating higher amounts of organic matter into the soils; (3) enhancing infiltration into the soil profile; and (4) increasing $CaCO_3$ precipitation due to higher CO_2 partial pressures from plant root respiration (see McMahon, 1998 and Gutiérrez-Jurado et al., 2006).

Alluvial fan deposits belong to the Sierra Ladrones Formation (SLF) from the upper Santa Fe group (Connel and McCraw, 2007) (Fig. 4.2b). They are Plio-Pleistocene in age and composed of weakly cemented, poorly sorted conglomerates originating from weathered Precambrian granites and metamorphic rocks

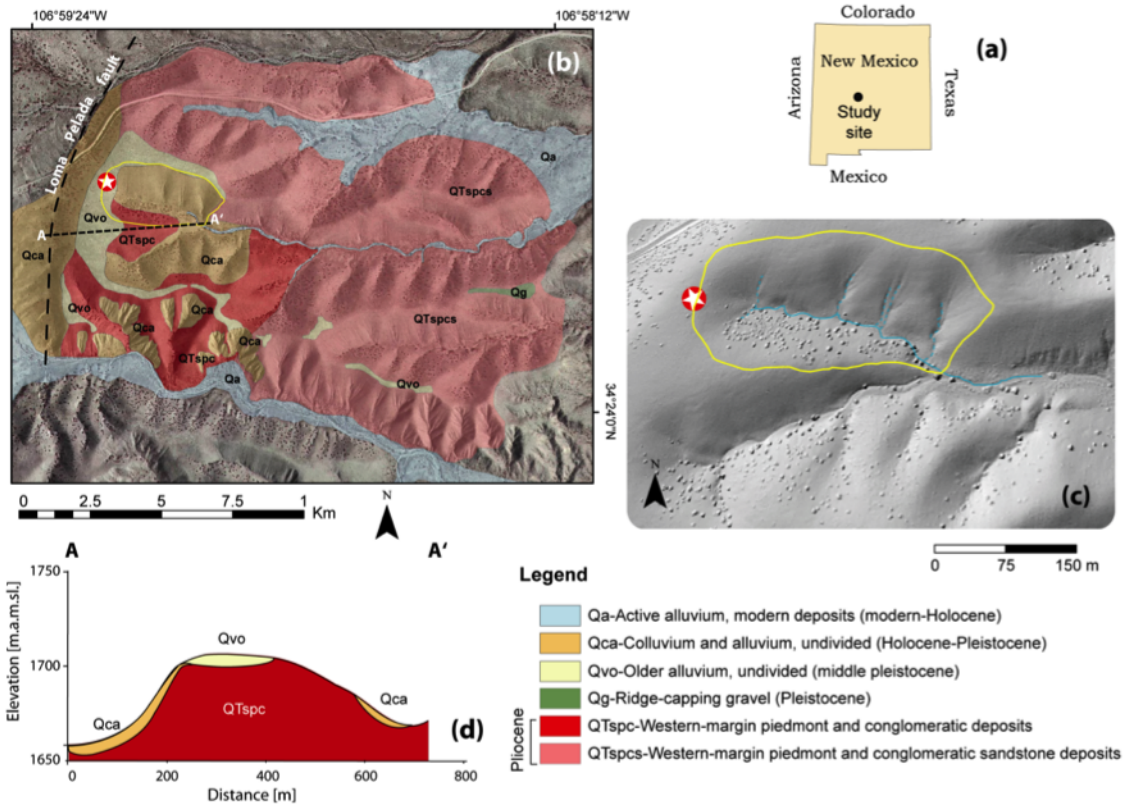

Figure 4.2: (a) Location of the study area region in New Mexico. (b) Major geologic units draped onto an orthophoto (2-m resolution) with study basin (star). Note that the alluvial fans are bounded by the Loma Pelada fault to the west. (c) Hillshade of a 1-m resolution digital surface model (DSM) of the study basin. Note the trees on north and west facing slopes as small circle-like prominences. (d) Profile section of the A-A′ transect showing the different colluvium mantles of the slopes and the younger surfaces on the alluvial fan surface.

from the Sierra Ladrones. There are five major units on the fan deposits (Connel and McCraw, 2007): (1) older alluvium on the upper surfaces ; (2) colluvium of Holocene-Pleistocene age; (3) active alluvium in the valley bottoms; (4) piedmont deposits of Plio-Pleistocene age; and (5) piedmont conglomeratic sandstone deposits. Fig. 4.2d shows a west to east transect in the alluvial fans with a commonly found vertical arrangement of the units.

4.3 Multi-resolution Datasets

In the following, we describe three topographic (DEM) datasets with sequentially improved resolutions and precision: IFSAR (10-m), dGPS (4-m), and LiDAR (1-m) available for the study basin through airborne campaigns (IFSAR, LiDAR) and a field survey (dGS).

4.3.1 InterFerometric Synthetic Aperture Radar (IFSAR)

A 10-m DEM from IFSAR was obtained from the Sevilleta Long-Term Ecology Research (LTER) site. This product was acquired by a STAR 3i system mounted on a plane, which simultaneously collects a digital terrain model and an Orthorectified Radar Image corrected for relief and other distortions. The spatial resolution of an IFSAR DEM depends on the flight altitude, leading to horizontal accuracy ranging from 1.25 to 2.5-m root mean square error (RMSE) and a vertical accuracy from 0.3 and 3-m RMSE. The IFSAR DEM used in this study has horizontal and vertical accuracies of $\sim$2.5 to 3-m. The IFSAR product is representative of readily available (standard) DEMs at coarse resolutions and has been used in prior studies in the study region (e.g., Gutiérrez-Jurado et al., 2007; Istanbulluoglu et al., 2008).

4.3.2 Differential Global Positioning System (dGPS)

A 4-m DEM was produced from a field survey using a high-precision dGPS comprised of two GB-1000 Topcon receivers with a PG-A1 precision dual-frequency, dual-constellation antenna. The survey was performed in post-processing Real Time Kinematic (PP-RTK) mode such that data is simultaneously recorded on a fixed receiver and a rover used to record points at different locations. Data post-processing was performed using the Topcon Tools v.6.04 software. A total of $\sim$10000 points were recorded across the $\sim$0.1 km^2 basin. After data quality control, however, nearly 4000 points were discarded. The precision of quality controlled points ranged in the vertical direction between 0.043 to 0.016-m and in the horizontal plane between 0.02 to 0.011-m. The resulting mean point density was estimated to be 0.6 points/m^2. We used local Ordinary Kriging (OK) with a moving window size of 8-m determined by an analysis of spatial autocorrelations, to interpolate the data points and produce a 4-m DEM for the basin.

4.3.3 Light Detection and Ranging (LiDAR)

A 1-m digital surface model (DSM) and DEM were obtained from an airborne LiDAR survey performed by the National Center for Airborne LiDAR Mapping (NCALM). The survey was carried using an Optech GEMINI Airborne Laser Terrain Mapper mounted on a twin-engine Cessna Skymaster. The laser point data was georeferenced using data from two differential GPS stations and calibrated using a two-step process consisting of: (1) a relative calibration to adjust the bore sight values of heading, roll, pitch, and scanner mirror scale to minimize systematic positional errors; and (2) an absolute calibration such that the

LiDAR DEM matches the height values of a vehicle-mounted GPS. The point density of the LiDAR grids was $\sim$4.25 points/m^2. The bare earth DEM and vegetated (with trees) DSM from the LiDAR data were produced by OK interpolation at NCALM. The bare earth LiDAR DEM will be primarily used in the analyses presented here, while Part II of the study also focuses on the vegetated LiDAR DSM.

4.4 Topographic and Geomorphic Analyses

4.4.1 Terrain attributes

Slope and aspect are first order terrain attributes extracted from a DEM and are sensitive to the DEM resolution (e.g., Kienzle, 2004; Deng et al., 2007; Erskine et al., 2007). Fig. 4.3 shows IFSAR, dGPS and LiDAR DEMs and their corresponding hillshade and aspect distributions. Two observations stand out from this comparison: (1) the effect of DEM resolution leading to a pixelated basin boundary for the IFSAR and dGPS products, and (2) the smoother appearance of the LiDAR DEM. The hillshade LiDAR DSM (i.e., vegetated product) distinctly shows the juniper trees on the north facing slope (Fig. 4.3f) and fine resolution terrain features such as rills on the south facing slope. Note that there are clear distinctions in aspect frequency among the three datasets (rose-plot histograms in Fig. 4.3g,h,i). For example, notice the wide spread of south aspect values for the dGPS, while the LiDAR shows a more restricted range in the same region.

Fig. 4.4 presents terrain attributes derived from each DEM product. The slope distribution varies considerably among the topographic datasets, with a higher range of slopes observed in the LiDAR DEM (Fig. 4.4c). The LiDAR slope field also shows steep regions in the catchment near channel heads and along the

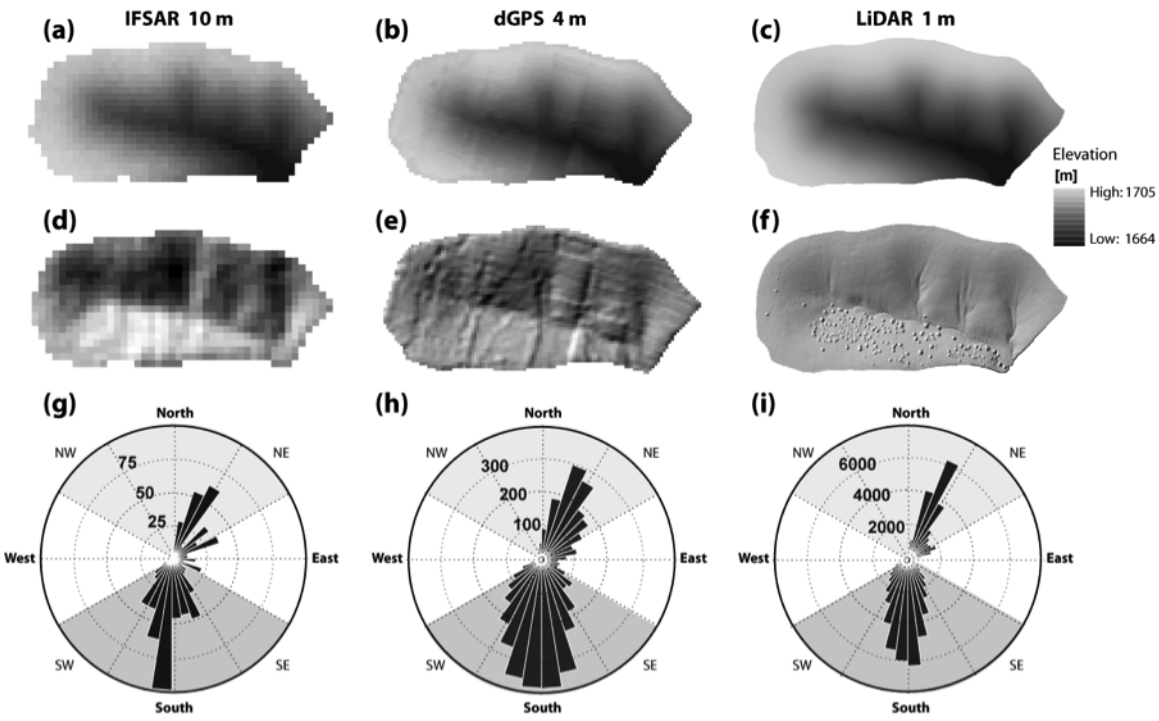

Figure 4.3: Elevations and hillshades of IFSAR 10-m DEM (a,d), dGPS 4-m DEM (b, e), and LiDAR 1-m DEM (c, f) of the study basin. (g, h, i) Rose-plot histograms of the IFSAR, dGPS and LiDAR DEMs showing the aspect distribution and frequency.

footslope of the meandering main channel. On the other hand, the IFSAR and dGPS DEMs have smoother slopes and contain artifacts arising from sampling errors. Aspect fields confirm that increasing the DEM resolution and quality improves the definition of the topographic fields. Notice the smooth transition of aspect along the hillslopes in the LiDAR DEM (Fig. 4.4f).

Although the IFSAR and dGPS DEMs distinguish the north versus south facing areas, both fail to reveal west and southwest facing regions on the hillsides of the south facing slope. Curvature distributions also reveal the level of detail present in the LiDAR DEM (Fig. 4.4i). High negative or positive values, denoting pronounced concavity or convexity, are only present in the LiDAR data as this can capture large slope changes in the basin.

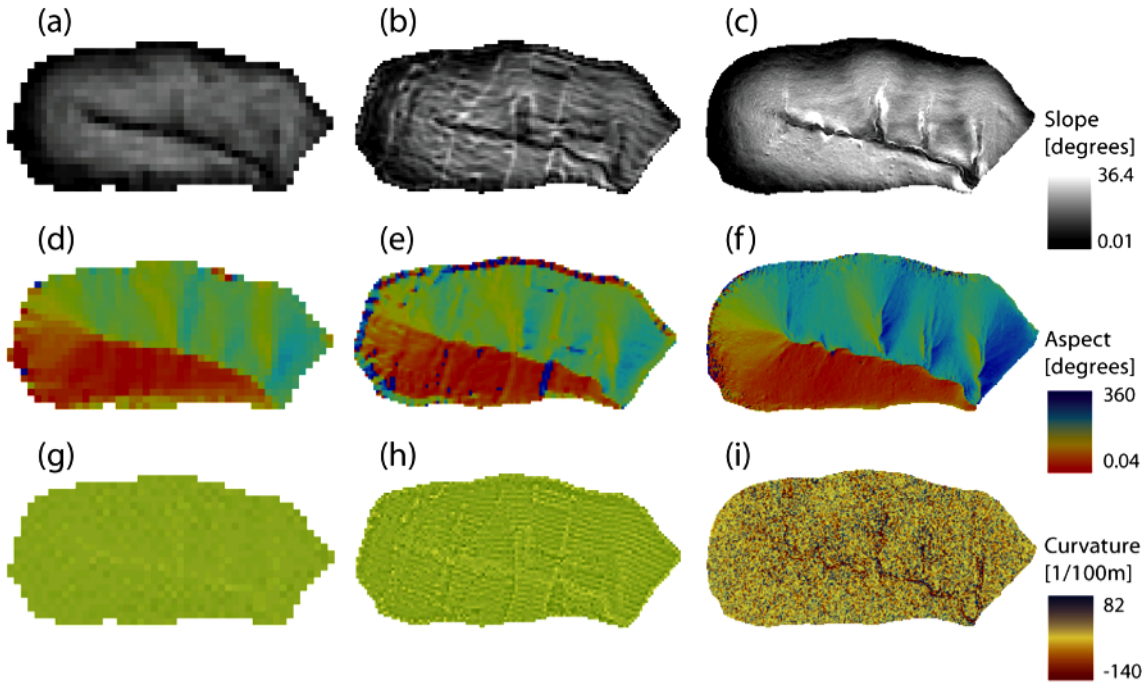

Figure 4.4: Spatial distributions of slope (a,b,c), aspect (d,e,f,) and curvature (g,h,i) for the IFSAR (left), dGPS (middle) and LiDAR (right) products.

Another hydrogeomorphic measure of the differences between the DEM products is the distribution of contributing area (A). A defines the drainage area to every point in a basin, where low A values are frequent on hilltops, increasing downslope, and with large values found along streams. Fig. 4.5 presents the A field for each DEM, classified into five categories, corresponding to an increase in order of magnitude. Each category, discussed next, is assigned a roman numeral from I (A from 0 to 10 m^2) to V ($A > 10^4$ m^2) and shown as a distinct color in Fig. 4.5.

There are notable differences in the A distribution within the basin among the products. Category I occurs at hilltops, ridges and disconnected streamside locations. In general, the DEMs agree well on the location of the low A areas. Category II ($A : 10 - 10^2$ m^2) areas are present along slopes and occupy well-defined regions only in the dGPS and LiDAR products. Category III ($A : 10^2 - 10^3$

m^2) sites are present in most of the basin for IFSAR, whereas the dGPS and LiDAR fields have locations organized into dendritic patterns resembling first order tributaries. This is a signature of a zone of transition from diffusion to fluvial dominant erosion for Category III in the dGPS and LiDAR products. Note the high occurrence of dendritic shapes on the north facing LiDAR slope, a feature that is limited in the dGPS and non-existent in the IFSAR fields. Category IV ($A : 10^3 - 10^4$ m^2) sites are arranged into linear features emerging as tributaries to the main channel. The tributary origin and extent differ for all products, becoming more realistic with increasing DEM resolution. Finally, Category V ($A > 10^4$ m^2) locations comprise the main ephemeral and meandering channel in the basin. Despite the resolution differences, the IFSAR and LiDAR products agree well on the delineation of the main channel, while in the dGPS product the main channel appears to be truncated at the middle of the basin.

4.4.2 Slope-area analysis

The classification of the A distribution was performed based on the slope-area diagram, a common tool based on sediment transport theory (e.g., Montgomery and Foufoula-Georgiou, 1993; Ijjasz-Vasquez and Bras, 1995; Istanbulluoglu et al., 2008). For example, a widely used sediment transport equation associates the local slope (S) and A as:

$$S = kA^{\theta} \tag{4.1}$$

where k is an erodibility constant and θ is a scaling exponent. θ defines the concavity or convexity in a landscape (Tucker and Bras, 1998) and describes if a

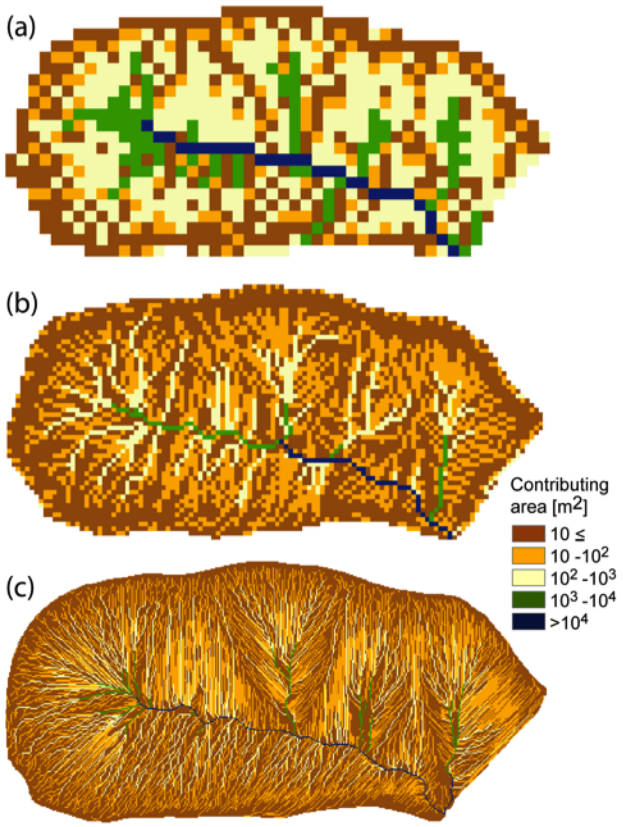

Figure 4.5: Contributing area distributions for (a) IFSAR, (b) dGPS, and (c) LiDAR products, classified into five regions.

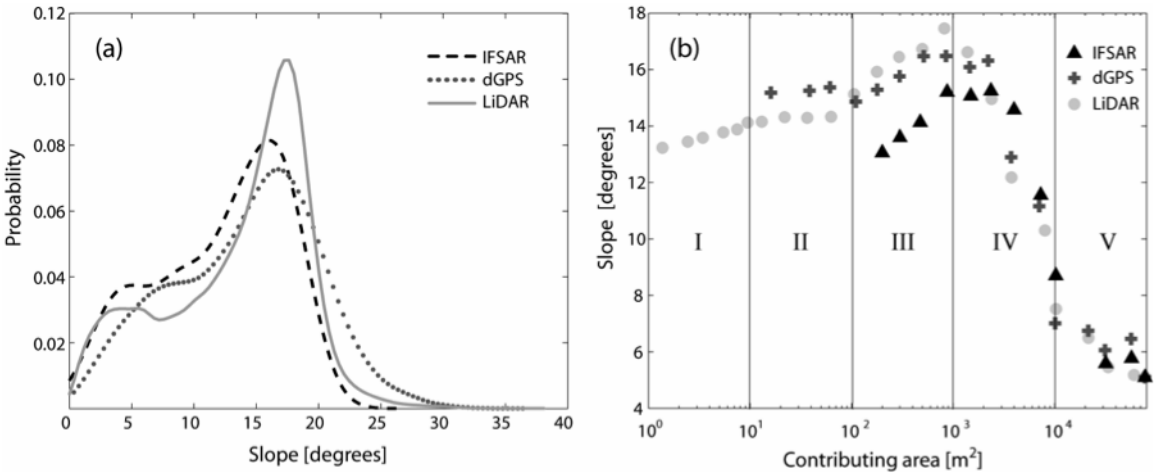

Figure 4.6: (a) Slope PDFs and (b) Slope-area diagrams for IFSAR, dGPS and LiDAR products. Note the log-scale of the contributing area (A) axis. Five scaling regimes are identified with roman numerals (I, II, III, IV and V), corresponding to Fig. 4.5.

site has diffusion ($\theta > 0$, convex) or fluvial ($\theta < 0$, concave) dominant erosion. Thus, the slope-area diagram is used to interpret different scaling regimes in θ related to erosion changes (Tarboton et al., 1992).

As a background for the slope-area analysis, we present the slope distributions for each DEM in Fig. 4.6a as probability density functions (PDFs). Slope values with high frequency occur in the range between 15° and 20°. The PDFs appear to be slightly bimodal and show approximately the same shape in each DEM. Nevertheless, the LiDAR distribution shows a more pronounced peak near 18° and bimodality is more accentuated. Note the high frequency of high slopes in the LiDAR product is due to regions near channel heads and along the footslope of the meandering channel (Fig. 4.4c). The high slopes in the dGPS ($> 20°$), on the other hand, appear to be a sampling artifact, as these are not present in the IFSAR or LiDAR products.

A comparison of the slope-area relation is shown in Fig. 4.6b for each DEM. Five scaling regimes were identified using the binned-average LiDAR data.

To derive the binned-averaged slope, a set of variable width bins were selected to capture the range of A values and ensure a sufficient sample size in each bin, as in Istanbulluoglu et al. (2008). Three regimes correspond to a diffusion-dominated sediment transport mode ($\theta > 0$, positive slope, I, II and III) and two regimes ($\theta < 0$, negative slope, IV and V) indicate fluvially-dominant erosion. When using the IFSAR and dGPS products, only three and four scaling regimes can be identified, respectively, due to the limited range of A and S in these products. Nonetheless, these regimes agree well with the LiDAR-derived classification in terms of the sign of θ. This suggests that considerable improvements are possible in extracting hydrogeomorphically distinct regions in the slope-area diagram when utilizing higher resolution datasets at the hillslope and catchment scales.

The scaling regimes in the slope-area diagram are presumed to correspond to different types of erosion in the basin. A natural question arising from these observations is: What is the physical meaning of these internal changes in sediment transport? Assuming there is abundant sediment supply in the site (Wu et al., 2006; Istanbulluoglu et al., 2008), we can use a long-term sediment transport rate (Q_s) to quantify the erosion rates in the scaling regimes. Q_s is defined as:

$$Q_s = KA^m S^n \tag{4.2}$$

where K is an erodibility constant and m and n are empirical exponents. Assuming a uniform denudation rate (D) for the basin, $Q_s = DA$, we obtain $DA = KA^m S^n$. It follows that:

$$\theta = \frac{1-m}{n} \tag{4.3}$$

θ can be calculated for each scaling regime from the slope-area diagram as follows:

$$\theta_i = \frac{\ln S_{i+1} - \ln S_i}{\ln A_{i+1} - \ln A_i} \tag{4.4}$$

where the subscript i is the nth scaling regime, ($\ln S_{i+1}$ $\ln S_i$) is the change in the value of slope (ΔS_i), and ($\ln A_{i+1}$ $\ln A_i$) is the change in contributing area (ΔA_i) in the slope-area diagram. Combining equations (4.3) and (4.4) we observe that:

$$\theta_i = \frac{\Delta S_i}{\Delta A_i} \approx \frac{(1-m)_i}{n_i} \tag{4.5}$$

Through equation (5), we can obtain values for θ_i, m_i and n_i for each regime. We can then relate changes in θ to Q_s by assessing the relative weight of the terms A^m and S^n in equation (4.2). This allows us to examine the physical reasons for the changes in regime within the basin. Table 4.1 shows the values of θ_i, m_i and n_i and the dominant parameter controlling Q_s for each regime.

As shown in Table 4.1, the value of θ for diffusive regimes (I-III) is positive and one order of magnitude less, in absolute terms, than the negative θ of fluvial regimes IV and V. Exponent m is <1 for the diffusive regimes and >1 for the fluvial dominated areas.

The value of exponent n is larger for high values of θ and decreases with lower values of θ. The terms A^m and S^n show that S^n dominates Q_s in the diffusive regimes, while A^m is more important for the fluvial areas. This comparison indicates the LiDAR field allows a clear distinction between diffusive hillslope

Table 4.1: Slope-area relation parameters in each regime.

Sediment transport	Regime	A [m^2]	θ	m	n	Dominant term in (2)
Diffusive	**I**	≤ 10	0.03	0.93	1.92	S^n
	II	10 - 10^2	0.01	0.98	1.57	S^n&A^{m*}
	III	10^2 - 10^3	0.07	0.85	2.05	S^n
Fluvial	**IV**	10^3 - 10^4	-0.4	1.79	2	A^m
	V	$> 10^4$	-0.2	1.24	1.28	A^m

* The dominant term in Equation (2) shifts from S^n to A^m in this region.

erosion ($A < 103$ m^2), where slope is a dominant factor, and concentrated, fluvial incision ($A > 103$ m^2), where contributing area controls erosion, within the opposing hillslope ecosystems.

To further explore this point, we perform a sensitivity analysis of A^m and Sn for each regime in Fig. 4.7. For regime I, S^n is much greater than A^m, therefore Q_s is dominated by the slope effect. For regime II, Q_s is controlled by S^n until A values of $\sim$70 m^2, after which A^m dominates the sediment transport. A similar transition is observed in regime III, though at values of A $\sim$1000 m^2, coinciding with the convergence of S^n and A^m. Q_s in the fluvial regimes IV and V is controlled by A^m which is overwhelmingly more important than S^n. These results show that the diffusive scaling regimes (I to III) correspond to zones in the basin being eroded mainly by steep slopes. In fluvial regimes IV and V, A is more important than slope for the mobility of sediment. Interestingly, regime II shows a transition from diffusive to fluvial erosion at A =70 m^2, where S^n remains constant, but A^m grows. This transition occurs at A values before the landscape is organized into channels and is likely associated with small rills in each hillslope, but primarily located in the south facing slope (see Fig. 4.5c). Conversely, the

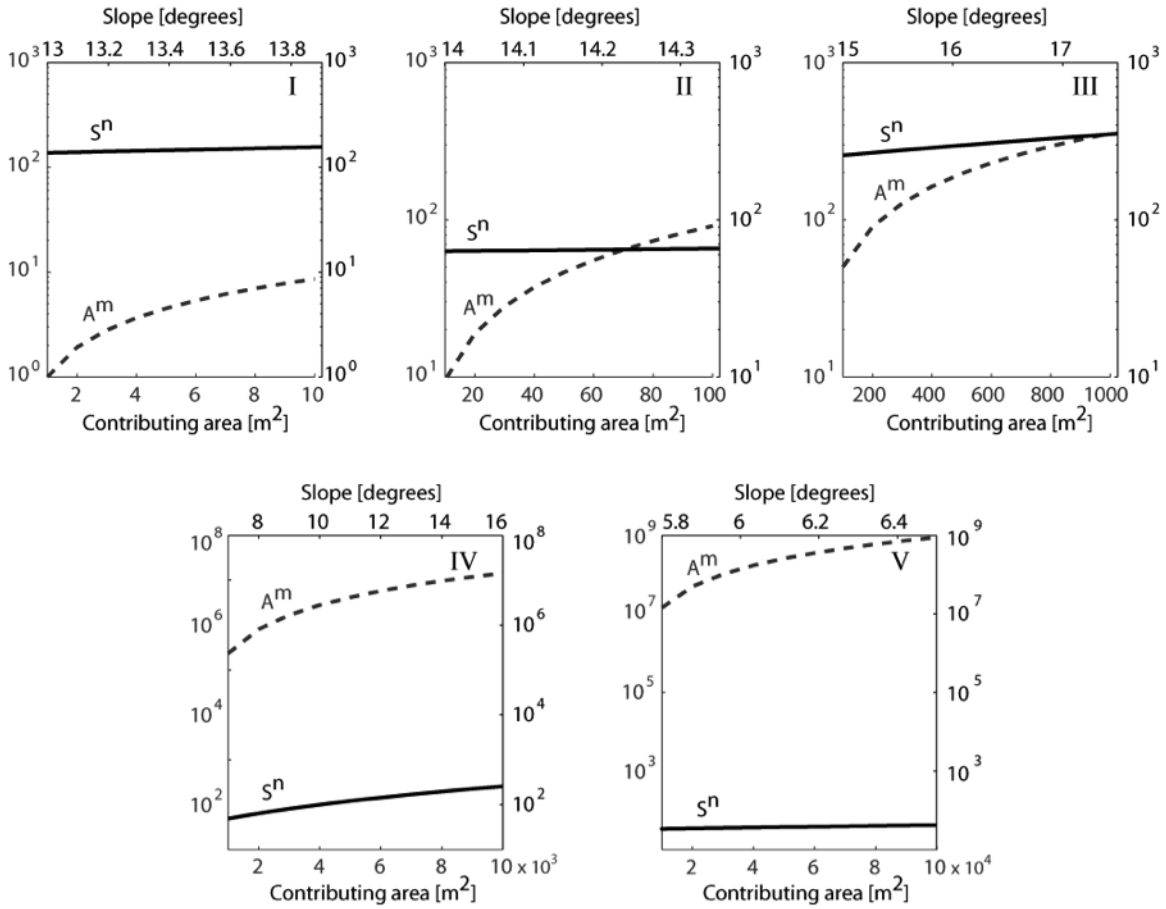

Figure 4.7: Sensitivity plots illustrating the dominance of A^m or S^n on Q_s for each scaling regime (I, II, III, IV, V). Dashed lines depict A^m as a function of contributing area (bottom x-axis), while the solid lines shows S^n as a function of slope (upper x-axis).

definite transition in sediment transport mode from diffusive to fluvial occurs at the end of regime III ($A \sim 1000$ m^2), where A^m and S^n converge, and after which A^m surpasses S^n by several orders of magnitude.

4.4.3 Curvature-area analysis

The terrain curvature or second derivative of elevation (z) is a measure of the concavity or convexity in a region and is useful for understanding hydrogeo-

morphic processes (e.g., Evans and Cox, 1999; Kienzle 2004). The total curvature is obtained as the Laplacian of z ($\nabla^2 z$) as (Bogaart and Troch, 2006; Istanbulluoglu et al., 2008):

$$\nabla^2 z = \left(\frac{\partial^2 z}{\partial x^2} + \frac{\partial^2 z}{\partial y^2} \right) \tag{4.6}$$

and can be used to identify regions where hillslope diffusion ($\nabla^2 z > 0$) dominates over fluvial sediment transport ($\nabla^2 z < 0$). A $\nabla^2 z$ value of 0 indicates no changes in slope, while large positive $\nabla^2 z >> 0$ indicate convexity and large negative $\nabla^2 z << 0$ indicate concavity. The total curvature consists of profile curvature in the downslope direction ($\partial^2 z / \partial y^2$) and planform curvature in the horizontal direction (i.e., along the contour lines, $\partial^2 z / \partial x^2$). Profile curvature is associated with advective flow, with positive values indicating flow acceleration (erosion) and negative values indicating flow deceleration (deposition). Planform curvature, on the other hand, is related to the convergence (positive values) or divergence (negative values) of flow within a landscape, indicating areas that either accumulate (convergence) or dissipate (divergence) runoff and erosion (e.g., Thorne et al., 1987; Moore et al., 1991; Evans and Cox, 1999; Schmidt et al., 2003).

Fig. 4.8a presents the curvature PDFs for each DEM product. Each PDF exhibits a normal distribution, with a larger range of values for the higher resolution products. The differences in the range of values are significant between the IFSAR and dGPS, suggesting a clear distinction from spatial resolutions of 10 to 4-m. For the dGPS and LiDAR products, the highest frequency occurs at a curvature value of 0 (no slope change) and it decreases gradually to higher negative and positive curvatures. Progressively larger ranges of the dGPS and LiDAR products suggest an advanced ability of these products to capture the fine details

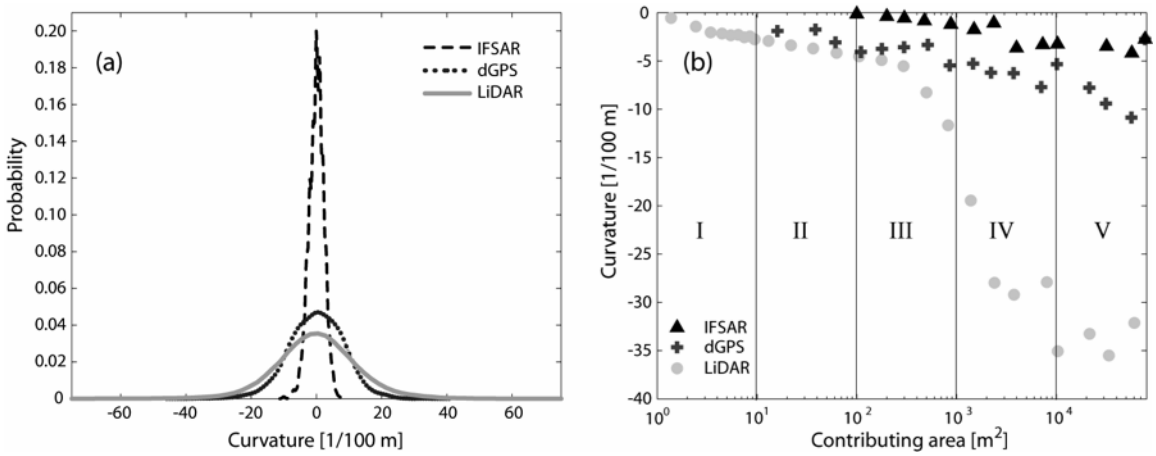

Figure 4.8: (a) Total curvature PDFs and (b) Curvature-area diagrams for the IFSAR, dGPS and LiDAR products. The roman numerals identify regimes in the slope-area diagram (Fig. 4.6).

of the basin topography, including regions exhibiting large convexity or concavity, as seen previously in Fig. 4.8g,h,i.

Curvature-area diagrams are shown in Fig. 4.8b for each product, along with the scaling regimes identified previously. Note that all the binned-average curvature values fall below 0 for all the regions (I to V), in contrast to the transition from positive to negative curvature observed by Istanbulluoglu et al. (2008) over a wider range of A. There are two reasons for this: (1) the curvature distribution is slightly skewed to the left in Fig. 4.8a, with the presence of a few extreme negative values; and (2) as contributing area (A) increases, the curvature values in a catchment become more concave (negative values), as in Boogart and Troch (2006). In general terms, total curvature declines gently with increasing A up to 300 m^2 in regime III, then declines rapidly to highly negative curvatures in regime IV, and finally attains a minimum curvature in regime V. This behavior is more evident in the LiDAR data, where high concavity is found in the main drainage and its tributaries, as shown in Fig. 4.5. A similar behavior is observed

for the IFSAR and dGPS products, although in a less accentuated fashion, as their coarser resolutions are not able to adequately capture the curvature distribution.

4.4.4 Landscape morphology in north and south facing hillslopes

To explore the differences in morphology of the opposing hillslopes, we built slope-area and curvature-area diagrams for the opposing north and south facing slopes for each product in Fig. 4.9. The slope-area and curvature-area plots show different scaling regimes (θ) bounded by vertical dashed lines. The slope-area diagram for the IFSAR product shows only three different scaling regimes, while the dGPS and LiDAR products have four and five regimes, respectively. The increasing number of regimes occurs in both north and south facing slopes at about the same A. However, the transition from diffusive ($\theta > 0$) to fluvial ($\theta < 0$) sediment transport occurs at smaller A for the LiDAR product, as compared to both the IFSAR and dGPS DEMs. This implies that using higher resolution topographic data may lead to improvements in the definition of the location of channel heads within semiarid environments.

An important difference between north and south facing slopes in the slope-area diagrams occurs in the IFSAR and LiDAR products (Fig. 4.9a,e). Previous analyses by Istanbulluoglu et al. (2008) using the IFSAR DEM indicated that north facing slopes were steeper than south facing slopes for a larger set of basins in the same region. This feature is not present, in general, within the IFSAR product for the study basin. Instead, a transition is observed near A = 600 m^2 from higher to lower S in the south facing areas as compared to north facing locations.

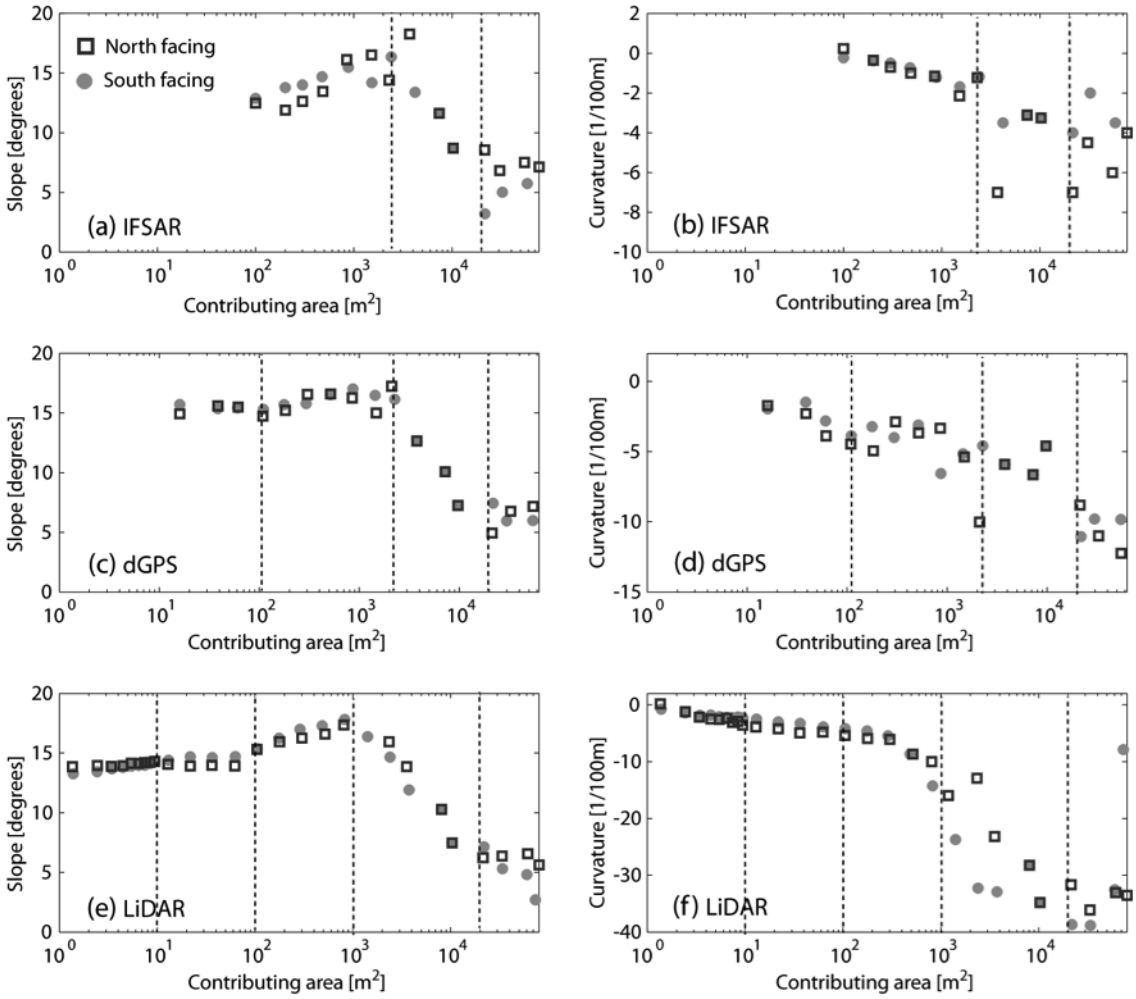

Figure 4.9: Slope-area and curvature-area diagrams of north facing and south facing slopes in the study basin for the IFSAR (a,b), dGPS (c,d), and LiDAR (e,f) products. Vertical dashed lines divide the scaling regimes, which are not necessarily coincident in all products.

In the LiDAR DEM, on the other hand, the three diffusive regimes are similar for the south and north facing slopes. Regime I shows a slightly positive θ (slightly convex) with identical north and south facing values; regime II shows essentially no trend (flat) in θ with steeper south facing slopes; and regime III has a well-defined positive θ (convex) with steeper south facing slopes. Thus, the LiDAR slope-area diagram for the study basin shows an opposite (but weak) trend to the analysis of Istanbulluoglu et al. (2008) using the IFSAR DEM. This suggests that higher resolution LiDAR data in a single site may provide a clearer depiction of morphological differences between north and south facing slopes that are related to vegetation differences.

The curvature-area plots for north and south facing slopes in Fig. 4.9 show: (1) increasing concavity with larger A and spatial resolution; (2) little consistency in the differences between north and south facing slopes across regimes for the IFSAR and dGPS products; and (3) larger and more consistent differences across all regimes for the LiDAR product. The curvature-area diagram for the LiDAR product (Fig. 4.9f) shows the following for the diffusive regimes: regime I exhibits no differences in concavity for the north and south facing slopes; regime II has slightly lower concavity for the south facing slopes; and regime III shows a sharp increase in concavity at A = 600 m^2 and a gentle negative trend for the north facing slope. Larger differences in curvature between north and south facing slopes occur after the transition from hillslope diffusion to fluvial sediment transport in regime IV between A = 1000 to 4000 m^2. In this regime, south facing curvature decreases rapidly from $\sim$-0.15 to -0.33 m^{-1}, while north facing slope decreases from $\sim$ -0.11 to -0.23 m^{-1}. This suggests that for the same fluvial regime, the erosion capacity in the south facing slope is greater than the north facing counterpart, consistent with findings of Gutiérrez-Jurado et al. (2007) and Istanbulluoglu et al. (2008).

4.4.5 Profile and planform curvature (PPC) analysis

Profile and planform curvatures depict sediment transport competence (flow acceleration or deceleration) and flow divergence or convergence, respectively. A converging-accelerating area is formed by fluvial sediment transport, while a diverging-decelerating region results from diffusion (Istanbulluoglu et al., 2008). As a result, we can use profile and planform curvature metrics to explore the geomorphic expressions in the basin in more detail. For this purpose, we introduce a profile-planform curvature (PPC) analysis based on Fig. 4.10a. The distribution of cells in the profile-planform space can be divided into four quadrants: (A) converging-accelerating, (B) diverging-accelerating, (C) converging-decelerating, and (D) diverging-decelerating. Fig. 4.10a using the LiDAR data shows a negative correlation of profile and planform curvature (R2 = -0.58). Thus, as locations become more convergent, the profile curvature becomes more concave. Note the frequency of convergent and divergent areas is similar, while there are slightly more decelerating (deposition) than accelerating (erosion) regions. Comparing quadrants A and D, we observe that diverging-decelerating areas (D, due to hillslope diffusion) are more uniformly clustered than the more disperse converging-accelerating (A, due to fluvial erosion) cells.

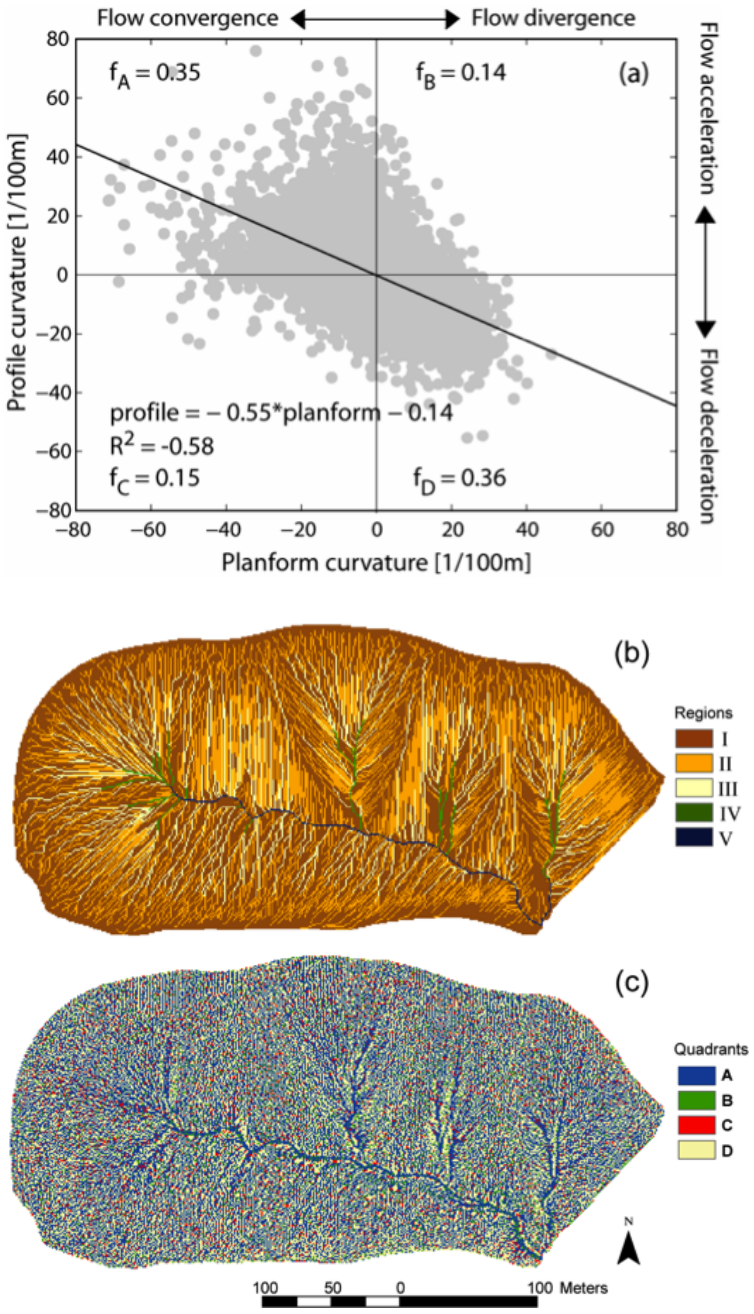

Figure 4.10: (a) Scatterplot of planform and profile curvatures (PPC) of the LiDAR product. The plot is divided into four quadrants (A, B, C, D). The letter "f" with subscripts shows the frequency of grid cells in a quadrant. The linear regression of the data and its R^2 value are shown. Spatial distributions of *A* categories (b) and PPC quadrants (c) are shown.

To visualize the quadrant areas, Fig. 4.10c presents the quadrant (A, B, C, D) distribution for each grid cell in the basin. Observe that the majority of cells correspond either to converging-accelerating (A) or diverging-decelerating (D), comprising 71% of the total area. Grid cells in the converging-accelerating space (A-blue pixels) occupy the channels in the basin (regimes IV and V) and are typically surrounded by diverging-decelerating areas (D-beige pixels). These spatial patterns suggest that sediment source areas from hillslopes (diffusive erosion in quadrant D) are in close proximity (upstream) to channels (fluvial erosion in quadrant A). On the other hand, basin areas of the diverging-accelerating and converging-decelerating quadrants (B-green and C-red pixels) appear scattered throughout the basin, lacking a clear spatial signature.

Fig. 4.11 shows PPC plots for south and north facing grid cells of the three DEM products. Negative correlations (R2) between profile and planform curvature appear in all products and is greater for north facing cells in all cases. In general, the R^2 values for north facing cells are 4 to 5% greater than south facing cells, except for the IFSAR data, where that difference grows to 13%. The frequency of the data in each quadrant is preserved in the three products, with more cells in the converging-accelerating and diverging-decelerating quadrants (A and D), than in B and C. Differences in frequency between quadrants A and D become more accentuated in the north facing cells, as compared to the south facing slope, where D has a higher frequency than A. This indicates that diverging-decelerating areas are more frequent in the north facing slope, suggesting that hillslope diffusion is a more important sediment transport mode as compared to the south facing slope. This is consistent with the field observations of Gutiérrez-Jurado et al. (2007) that suggested more diffusive erosion in the north facing slope after a major storm event.

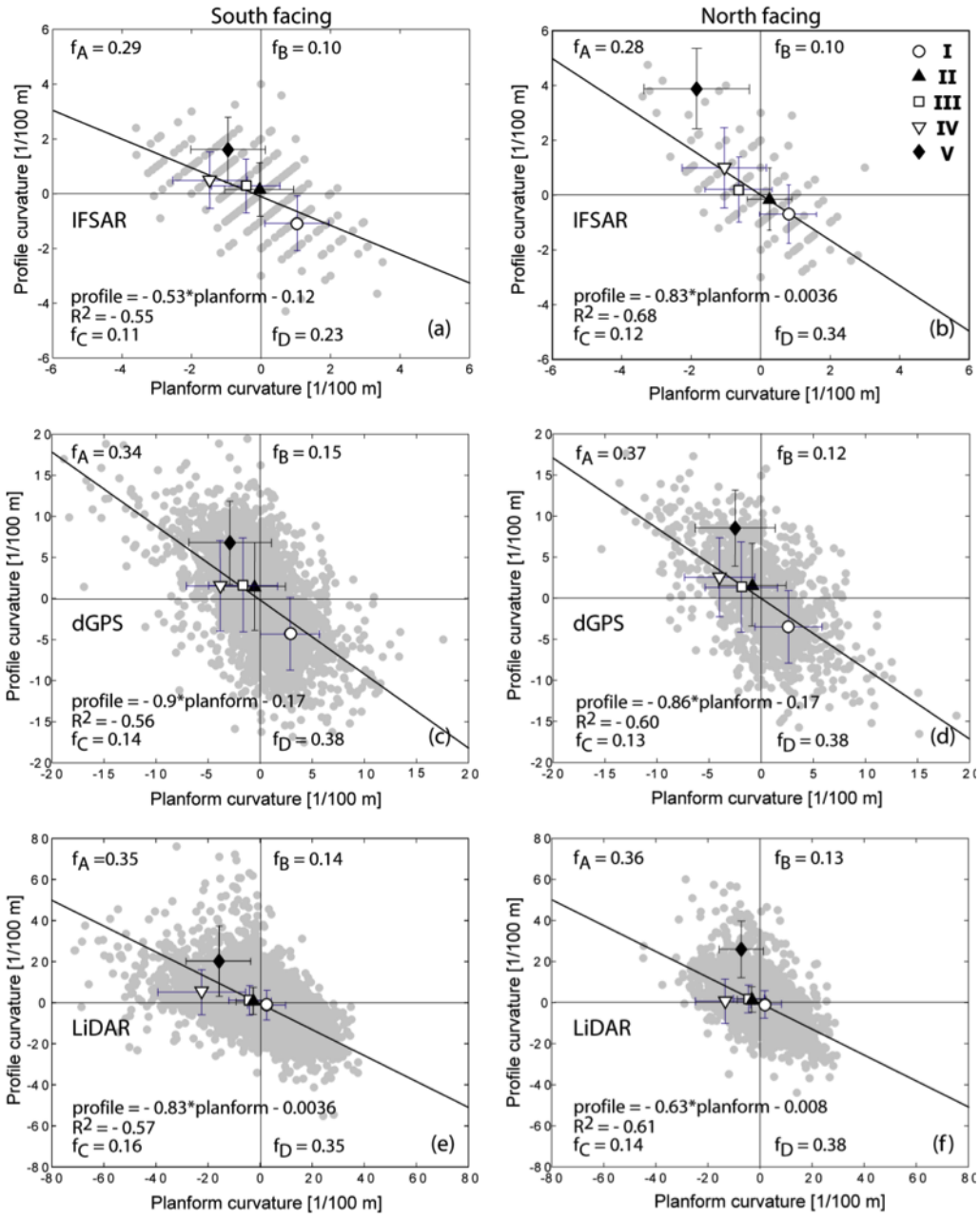

Figure 4.11: PPC analysis of the IFSAR (a,b), dGPS (c,d) and LiDAR products (e,f) for south (left column) and north (right column) facing cells. Large symbols and error bars indicate mean values and standard deviations for each regime.

Fig. 4.11 also shows the average profile and planform curvatures for each scaling regime (I to V) as symbols and its variability as error bars. Regime I site are located in the diverging-decelerating (D) quadrant, confirming these areas are formed by diffusion processes and show no clear distinctions between south and north facing slopes. Regime II is centered around the origin of the planform-profile curvature diagram, but leans towards the converging-accelerating (A) quadrant, indicating this region is mostly comprised by slightly convergent flat areas. Regime III is more convergent than regime II and presents similar values for south and north facing locations. Regime IV is considerably more convergent than the other regions. Finally, regime V is less convergent than regime IV, but has the highest profile curvature of all regimes. Note that the differences in regions are more pronounced between the south and north facing grid cells in the LiDAR data. This indicates that higher resolution data allows distinguishing features related to erosion and deposition that otherwise are obscure in coarser products. In addition, LiDAR data exhibits a more pronounced convergent-concave nature in regimes IV and V (Fig. 4.11e,f).

4.4.6 Distinguishing landscape processes in different DEM products

Based on the slope-area and curvature-area analyses, the following questions arise: Are the scaling regimes significantly different in terms of terrain attributes from each other? If so, is this valid for all DEM products? To answer these questions, we performed a multicomparison test (Hochberg and Tamhane, 1987) of the mean and standard errors of the mean slope and mean curvature for each scaling regime (I-V) for the south and north facing hillslopes (Figs.4.12 and 4.13). Note that for these analyses the mean and standard errors of scaling

regime I included values of slope and curvature of contributing areas $< 10^0$ m^2 not shown in previous plots of slope and curvature-contributing area, yielding slightly different values than those shown in Figs. 4.6, 4.8 and 4.9. In Figs.4.12 and 4.13 the circles show the mean slope or mean curvature for each regime and the bars and shaded areas illustrate the standard error at a 95% confidence interval. If the shaded areas overlap, no significant difference exists between the mean slope or curvature averaged over those different regimes. Otherwise, the regime mean is statistically different from its surrounding regimes. However, it is important to note that because the mullticomparison test does not distinguish direction in θ (i.e., $\theta > 0$ [diffusive], or $\theta < 0$ [fluvial]), the results of the analysis look mainly for differences of the regimes within each sediment transport mode. For example, the IFSAR south facing data shows no significant differences in mean slope and mean curvature between regimes II and III (Figs. 4.12a, 4.13a), while north facing data of the same product indicates that all regimes have no statistical difference in mean slope (Fig. 4.12b), but all regimes have statistical differences in mean curvature (Fig. 4.13b). In the dGPS south facing data, for example, only regimes IV and V are not statistically different, whereas for the same product the north facing data shows no significant differences between regimes II and III, III and IV, and IV and V. Observe, that for the LiDAR product, no shaded areas overlap in terms of either mean slope or mean curvature for both the north and south facing slopes (Figs. 4.12e,f and 4.13e,f). This indicates that all the regimes (I, II, III, IV, V) are statistically different from each other for both south and north facing cells for the mean slope and mean curvature. This comparison suggests that high resolution terrain data from LiDAR allow a clear (and significant) distinction of terrain attributes for different sediment transport regimes in the opposing hillslope ecosystems.

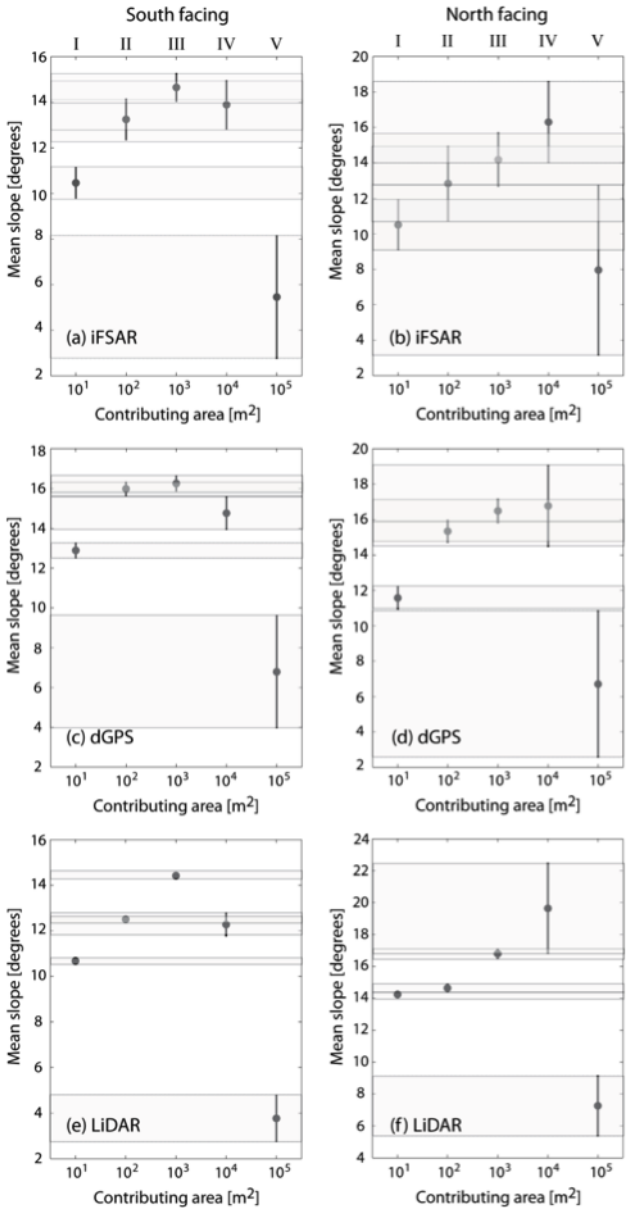

Figure 4.12: Multicomparison plots of the mean and standard errors of the mean slope for each scaling regime for south (left column) and north (right column) facing cells. Shaded areas show the standard errors within a 95% confidence interval.

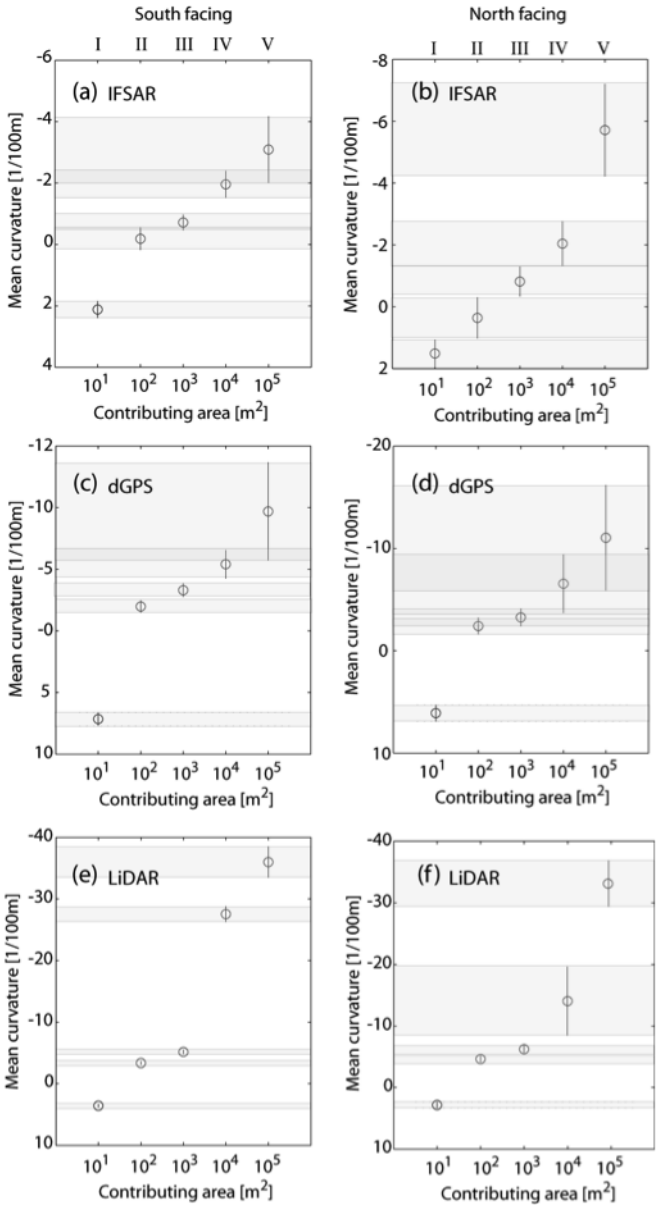

Figure 4.13: Multicomparison plots of the mean and standard errors of the mean curvature for each scaling regime for south (left column) and north (right column) facing cells. Shaded areas show the standard errors within a 95% confidence interval.

4.5 Summary

In this work, we explored the possible imprint of vegetation patterns in opposing hillslope ecosystems using terrain and geomorphic attributes. This was achieved with a set of sequentially-improved data sets to identify the resolution required to clarify the role of vegetation on the topographic form. Through this analysis, we demonstrated that terrain resolution and quality are a limiting factor on: (1) the definition of key terrain attributes (aspect, slope, curvature) affecting hydrogeomorphic processes, and (2) the identification of ecogeomorphic signatures on north and south facing hillslopes with contrasting ecosystems. Our results indicate that improving the resolution and precision of a DEM clarifies the definition of aspect and generates more realistic representations of basin boundaries, rills and meandering streams, and steep slopes. In addition, geomorphic descriptors such as concavity and convexity related to curvature are also improved. For example, the enhanced definition of the LiDAR field led to a contributing area pattern that more realistically depict the ephemeral rill network, in particular for south facing areas.

Improving the DEM resolution from the 10-m IFSAR to the 1-m LiDAR also allowed a better definition of sediment transport regimes. Slope-area analyses with the coarser data only captured the major transition from diffusive to fluvial erosion, missing the more subtle changes observed in the LiDAR product. Establishing the transition in scaling regimes is important in hydrologic and geomorphic studies since it is an indication of channel initialization (Tarboton et al., 1992; Dietrich et al., 1993; Ijjaz-Vasquez and Bras, 1995). Using the LiDAR data, we found two transitions from diffusive (dominated by slope effects) to fluvial (dominated by contributing area) sediment transport. The first transition in

regime II is believed to be an intermittent switch in sediment transport mode, primarily in the south facing slope. This occurs at contributing areas where the landscape is not yet organized into well-defined channels, but possibly contains small rills where water concentrates along hillslopes. The second transition in regime III is considered as the definite transition from hillslope diffusion to fluvial sediment transport mode, and occurs at the well-defined channel heads of the major tributaries and main channel. The first transition is not observed in the coarse resolution DEMs (e.g., Istanbulluoglu et al., 2008) indicating the LiDAR data is useful for identifying detailed processes associated with rills in semiarid basins.

Perhaps the most important finding is related to quantifying the differences between the contrasting north and south facing hillslopes, since this is central to the argument of vegetation-topographic feedbacks. Through the PPC analysis, we found that hillslope diffusion is more frequent in the north facing hillslope, as compared to the south facing slope. Furthermore, the LiDAR derived curvature-area diagram for the opposing slopes showed that the less frequent fluvial eroding surfaces on the north facing slope are less concave than their counterparts in the south facing slope and, as a consequence, are less able to promote advective flow. This agrees with the observation that vegetation on the north facing slope plays a role in impeding flow channelization (Gutiérrez-Jurado et al., 2007). The distinction between north and south facing slopes was further demonstrated by comparing the different sediment transport regimes. Using the LiDAR data, distinct morphologic characteristics for the opposing hillslope ecosystems were found more prominently for the fluvial scaling regimes. In the diffusive regimes, the LiDAR product revealed opposite (but weaker) differences between

north and south facing slopes as compared to the work of Istanbulluoglu et al. (2008) using the IFSAR DEM.

Through the various topographic and geomorphic analyses, the results of this study point to the need for high resolution datasets to detect detailed eco-geomorphic differences in semiarid areas with vegetation differences. It should be noted that the long-term signature of vegetation on topographic form is an expression of the imposed variations on the water and energy balance that operate continuously in the basin. As a result, deciphering the geomorphic effects of vegetation also requires understanding how current terrain and vegetation patterns affect microclimate and hydrologic conditions (e.g., Ivanov et al., 2008). In Part II of this study (Gutiérrez-Jurado and Vivoni, 2009), we address the radiation differences in the study basin dictated by topographic form and vegetation patterns. These works should aid in unraveling the complex interactions between vegetation, soil and terrain in semiarid landscapes with contrasting ecosystems.

REFERENCES

Badano, E. I., Caviares, L. A., Molina-Montenegro, M. A., and Quiroz, C. L. (2005), Slope aspect influences plant association patterns in the Mediterranean, *J. Arid Environments*, 62, 93-108.

Berne, A., Uijlenhoet, R., and Troch, P.A. (2005), Similarity analysis of subsurface flow response of hillslopes with complex geometry, *Water Resour. Res.*, 41, W09410, doi:10.1029/2004WR003629.

Bestelmeyer, B. T., Ward, J. P., and Havstad, K. (2006), Soil-geomorphic heterogeneity governs patchy vegetation dynamics at an arid ecotone. *Ecology*, 87(4) 963-973.

Bogaart, P. W., and Troch, P. A. (2006), Curvature distribution within hillslopes and catchments and its effect on the hydrological response, *Hydrol. Earth Syst. Sci.*, 10, 925-936.

Bras, R. L., Tucker, G. E., and Teles, V. (2003), Six myths about mathematical modeling in geomorphology, In *Prediction in Geomorphology*, Wilcock, P. and Iverson, R. (eds), American Geophysical Union, Washington DC, 63-79.

Burnett, B. N., Meyer, G. A., and McFadden, L. D. (2008), Aspect-related microclimatic influences on slope forms and processes, northeastern Arizona, *J. Geophys. Res.*, 113, F03002, doi:10.1029/2007JF000789.

Caylor, K. K., Manfreda, S., and Rodrguez-Iturbe, I. (2005), On the coupled geomorphological and ecohydrological organization of river basins. *Adv. Water Resources*, 28, 69-86.

Connel, S. D., and McCraw, D. J. (2007), *Preliminary geologic map of the La Joya NW quadrangle, Socorro County, New Mexico*, New Mexico Bureau of Geology and Mineral Resources, Socorro, NM.

Deng, Y., Wilson, J. P., and Bauers, B. O. (2007), DEM resolution dependencies of terrain attributes across a landscape, *Int. J. Geographical Information Science*, 21, 187-213.

Dietrich, W. E., and Perron, T. (2006), Is there a topographic signature of life, *Nature*, 439, 411-418.

Dietrich, W. E., Wilson, C. J., Montgomery, D. R., and McKean, J. (1993), Analysis of erosion thresholds, channel networks and landscape morphology using a digital terrain model. *J. Geology*, 101, 259-278.

Erskine, R. H., Green, T. R., Ramirez, J. A., and McDonald, L. H. (2007), Digital elevation accuracy and grid cell size: Effects on estimated terrain attribute, *Soil Sci. Soc. Am. J.* 71, 1371-1380.

Evans, I. S., and Cox, N. J. (1999), Relations between land surface properties: altitude, slope and curvature, In: Hergarten, S. and Neugebauer H. J. (eds.): *Process Modelling and Landform Evolution*, Berlin: Springer, 13-45.

Florinsky, I. G., and Kuryakova, G. A. (2000), Determination of grid size for digital terrain modeling in landscape investigationsexemplified by soil moisture distribution at a micro-scale, *Int. J. Geo. Inf. Sci.*, 14, 815-832.

Gutiérrez-Jurado, H. A., Vivoni, E. R., Harrison, J. B. J., and Guan, H. (2006), Ecohydrology of root zone water fluxes and soil development in complex semiarid rangelands, *Hydrol. Process.*, 20, 3289-3316.

Gutiérrez-Jurado, H. A., Vivoni, E. R., Istanbulluoglu, E., and Bras, R. L. (2007), Ecohydrological response to a geomorphically-significant flood event in a semiarid catchment with contrasting ecosystems. *Geophys. Res. Lett.*, 34, L24S25, doi:10.1029/2007GL030994.

Gutiérrez-Jurado, H. A., and Vivoni, E.R. (2011), Ecogeomorphic expressions of an aspect-controlled semiarid basin: II. Topography and vegetation controls on solar irradiance. *Ecohydrology* (In review).

Hochberg, Y., and Tamhane, A. C. (1987), *Multiple Comparison Procedures*, John Wiley Sons, New York, NY, 445 pp.

Holland, P. G., and Steyn, D. G. (1975), Vegetational responses to latitudinal variations in slope angle and aspect, *J. Biogeography*, 2, 179-183.

Holland, P. G., Steyn, D. G., and Fuggle, R. F. (1977), Habitat occupation by Aloe ferox Mill. (Liliaceae) in relation to topographic variations in direct beam solar radiation income, *J. Biogeography*, 4(1), 61-72.

Ijjasz-Vasquez, E. J., and Bras, R. L. (1995), Scaling regimes of local versus contributing areas in digital elevation models, *Geomorphology*, 12, 299-311.

Istanbulluoglu, E., Yetemen, O., Vivoni, E. R., Gutiérrez-Jurado, H. A., and Bras, R. L. (2008), On the topographic imprint of vegetation: Inferences from regional analysis of landscape morphology in central New Mexico, *Geophys. Res. Lett.*, 34, L14403 doi:10.1029/2008GL034477.

Ivanov, V. Y., Bras, R. L., and Vivoni, E. R. (2008), Vegetation-hydrology dynamics in complex terrain of semiarid areas: 2. Energy-water controls of vegetation spatiotemporal dynamics and topographic niches of favorability, *Water Resour. Res.*, 44, W03430, doi:10.1029/2006WR005595.

Kienzle, S. (2004), The effect of DEM raster resolution on first order, second order and compound terrain derivatives, *Transactions in GIS*, 8, 83-111.

McMahon, D. R. (1998), *Soil, landscape and vegetation interactions in a small semiarid drainage basin: Sevilleta National Wildlife Refuge, New Mexico*. MS Thesis. New Mexico Institute of Mining and Technology. Socorro, NM. 174 pp.

Milne, B. T., Moore, D. I., Betancourt, J. L., Parks, J. A., Swetnam, T. W., Parmenter, R. R., and Pockman, W. T. 2003. Multidecadal drought cycles in south-central New Mexico: Patterns and consequences. In: *Climate Variability and Ecosystem Responses at Long-Term Ecological Research Sites, Greenland*, D., Goodin, D. G., Smith, R. C. (eds). Oxford University Press: New York, NY, 286-307.

Montgomery, D. R., and Foufoula-Georgiou, E. (1993), Channel network source representation using digital elevation models, *Water Resour. Res.*, 29, 39253934.

Moore, I. D., Grayson, R. B., and Ladson, A. R. (1991), Digital terrain modelling: A review of hydrological, geomorphological, and biological applications, *Hydrol. Process.*, 5, 3-30.

Nieve, M., and Abrahams, A. D. (2002), Vegetation influences on water yields from grassland and shrubland ecosystems in the Chihuahuan Desert, *Earth Surface Processes and Landforms*, 27, 1011-1020.

Rodrguez-Iturbe, I., and Rinaldo, A. (1997), *Fractal River Basins Chance and Self Organization*, Cambridge University Press, Cambridge UK. 540 pp.

Rodrguez-Iturbe, I., and Porporato, A. (2004), *Ecohydrology of water-controlled ecosystems*, Cambridge University Press, Cambridge UK. 442 pp.

Schmidt, J., Evans, I. S., and Brinkmann, J. (2003), Comparison of polynomial models for land surface curvature calculation. *Int. J. Geo. Infor. Sci.*, 17, 797-814.

Slatton, K. C., W. E. Carter, R. L. Shrestha, and W. Dietrich (2007), Airborne Laser Swath Mapping: Achieving the resolution and accuracy required for geosurficial research, *Geophys. Res. Lett.*, 34, L23S10, doi:10.1029/2007GL031939.

Tarboton, D. G., Bras, R. L., and Rodrguez-Iturbe, I. (1992), A physical basis for drainage density, *Geomorphology*, 5, 59-76.

Thorne, C. R., Zevenbergen L. W., Burt T. P., and Butchert, D. P. (1987), Terrain analysis for quantitative description of zero order basins, Erosion and sedimentation in the Pacific Rim, *Proceedings of the Corvallis Symp.* IAHS Publ. no. 165, 121-130.

Tucker, G. E., and Bras, R. L. (1998), Hillslope processes, drainage density, and landscape morphology, *Water Resour. Res.*, 34, 2751-2764.

Vivoni, E. R., Ivanov, V. Y., Bras, R. L., and Entekhabi, D. (2004), Generation of triangulated irregular network based on hydrological similarity, *J. Hydrol. Eng.*, 9, 288-302.

Vivoni, E. R., Ivanov, V. Y., Bras, R. L., and Entekhabi, D. (2005), On the effects of triangulated terrain resolution on distributed hydrologic model response, *Hydrol. Process.*, 19, 2101-2122.

Vivoni, E. R., Di Benedetto, F., Grimaldi, S., and Eltahir, E. A. B. (2008), Hypsometric control on surface and subsurface runoff, *Water Resour. Res.*, 44, W12502, doi:10.1029/ 2008WR006931.

Walker, J. P., and Willgoose, G. R. (1999), On the effect of digital elevation model accuracy on hydrology and geomorphology, *Water Resour. Res.*, 35, 2259-2268.

Wilkinson, M. T., and Humphreys, G. S. (2006), Slope aspect, slope length and slope inclination controls of shallow soils vegetated by sclerophyllous heath-links to long-term landscape evolution, *Geomorphology*, 76, 347-362.

Wilcox, B. P., Breshears, D. D., and Allen, C. D. (2003), Ecohydrology of a resource conserving semiarid woodland: Effects of scale and disturbance, *Ecological Monographs*, 73, 223-239.

Wilson, J. P., and Gallant J. C. (2000), *Terrain Analysis: Principles and Applications*, John Wiley Sons, 469 pp.

Wu, S., Bras, R. L., and Barros, A. P. (2006), Sensitivity of channel profiles to precipitation properties in mountain ranges, *J. Geophys. Res.*, 111, F01024, doi:10.1029/2004JF000164

Zhang, W., and Montgomery, D. R. (1994), Digital elevation model grid size, landscape representation, and hydrologic simulations, *Water Resour. Res.*, 30, 1019-1028.

CHAPTER 5

ECOGEOMORPHIC EXPRESSIONS OF AN ASPECT-CONTROLLED SEMIARID BASIN: II. TOPOGRAPHIC AND VEGETATION CONTROLS ON SOLAR IRRADIANCE

(This chapter was submitted for publication as: Gutiérrez-Jurado, H. A. and Vivoni, E. R. 2011. Ecogeomorphic expressions of an aspect-controlled semiarid basin: II. Topographic and vegetation controls on solar irradiance. *Ecohydrology*)

5.1 Introduction

Understanding the effects of terrain attributes on ecologic and hydrologic properties of semiarid areas is highly relevant for a wide range of disciplines (e.g., Holland and Steyn, 1975; Kirkpatrick and Nunez, 1980; Guisan and Zimmermann, 2000; Coblentz and Riiters, 2004; Burnett et al., 2008; Bennie et al., 2008a,b; Ivanov et al., 2008a,b; Rinehart et al., 2008). In mid-latitude regions, semiarid landscapes are sensitive to the controls imposed by topography on the distribution of light, water and nutrients (Holland and Steyn, 1975; Holland et al., 1977; Badano et al., 2005; Caylor et al., 2005). In these water-limited environments, the relative abundance of vegetation is dictated by terrain-mediated energy inputs, the redistribution of available resources, and by the ecophysiological adaptations

of the plants themselves (Meentemeyer et al., 2001; Walton et al., 2005). Holland and Steyn (1975) provided a first attempt to address the effects of topographic and latitudinal variations of solar irradiance on vegetation occurrence and response. A number of studies have also recognized the influence of slope and aspect on the modification of the energy budget for mid-latitude ecosystems and its effect on soil moisture availability for plants (Ranzi and Rosso, 1995; Breshears et al., 1998; Zou et al., 2007).

The effects of terrain attributes on vegetation are complicated by the non-linear interaction of the topographic impacts on radiation and water accumulation in a landscape. To explore this, Ivanov et al. (2008b) used a distributed ecohydrological model to mimic vegetation patterns in two synthetic, semiarid landscapes (diffusion and fluvial-dominated). This exercise revealed the combined effects of slope, aspect and contributing (drainage) area on vegetation productivity for a single grass species. Aspect-controlled patterns (north versus south facing slopes) occurred in diffusion-dominated landscapes, while the vegetation distribution mimicked the channel network in the fluvial-dominated systems. Both vegetation patterns can be found in mid-latitude, semiarid regions in North America (e.g., Gutiérrez-Jurado et al., 2007; Flores-Cervantes et al., 2009), suggesting that the interplay between radiation controls (aspect) and water accumulation (fluvial network) may result in different outcomes depending on the specific setting.

In semiarid systems, systematic variations in the water and energy budgets at different terrain locations can promote the establishment of diverse plant functional types (e.g., grasses, shrubs, trees). Strong variations in ecosystem properties can, in turn, directly impact hydrologic processes, such as interception,

infiltration, and evapotranspiration, which may promote a self-reinforcing effect on the differential plant establishment (e.g., Florinsky and Kuryakova, 2000; Nieve and Abrahams, 2002; Wilcox et al., 2003; Gutiérrez-Jurado et al., 2007). As a result, terrain controls on irradiance may lead to the development of niches in semiarid landscapes that enhance ecosystem diversity as a function of aspect and slope (Kirkpatrick and Nunez, 1980; Horsch, 2003; Walton et al., 2005). Contrasting ecosystem properties in topographically complex semiarid basins can also promote differences in hydrogeomorphic processes (see, for example, Gutiérrez-Jurado et al., 2007; Istanbulluoglu et al., 2008; Corenbilt et al., 2009).

5.1.1 Vegetation-topography-radiation interactions

The effects of topography and vegetation properties on the incident irradiance have been addressed primarily at the hillslope scale (e.g., Martens et al., 2000; Breshears et al., 1998; Zou et al., 2007). Notably, Zou et al. (2007), in a systematic study of topography-vegetation cover interactions, demonstrated the effect of plant canopies in reducing near ground solar irradiance for north and south facing slopes. Nevertheless, their analysis was performed using precise north and south facing aspects and did not account for variations in aspect or slope occurring naturally in a landscape. From an ecogeomorphic perspective, it is important to study the coupled effects of vegetation and topography on solar irradiance in a complex setting that provides a range of potential vegetation niches (Wilkinson and Humphreys, 2006). Natural landscapes obtained from digital elevation models (DEMs) provide the opportunity to carefully address vegetation-topography interactions when other factors (i.e., geological substrates) can be isolated (Yetemen et al., 2009). Investigating the controls of vegetation and topography on irradiance represents a first step in unraveling the complex interactions

leading to aspect-controlled ecosystems in semiarid basins and their effects on landscape morphology (Paola et al., 2006).

Vegetation-topography-radiation interactions are considered to lead to the development of microclimates by imposing spatial heterogeneities in energy loads at canopy and intercanopy locations (Breshears et al., 1997). As discussed in Gutiérrez-Jurado and Vivoni (2009), terrain features (slope, aspect, curvature) and vegetation obstructions can lead to strong variations in the amount of irradiance reaching the surface. Topographic and vegetation controls may amplify the differences in microclimate leading to a wide range of site conditions in a relatively small area (Kirkpatrick and Nunez, 1980). For example, substantial differences in solar radiation within short distances can promote soil thermal gradients that produce varying evapotranspiration rates and affect the soil moisture status (Breshears et al., 1997, 1998). These topographically-mediated differences can also be amplified or muted by the presence of vegetation itself, through its role on radiation absorption (shading) and reflection (albedo) on a sloping terrain surface. As a result, vegetation-topography-radiation interactions in semiarid basins may reinforce the microclimate conditions that originally led to the vegetation patterns.

5.1.2 Impact of terrain resolution on simulated irradiance

The spatial resolution of the DEM used to analyze the vegetation-topography-radiation interactions directly affects the definition of surface landforms and terrain properties (e.g., Zhang and Montgomery, 1994; Deng et al., 2007). For instance, high-resolution DEMs (1-m) increase the range of slope and aspect values as compared to coarser products (Kienzle, 2004; Gutiérrez-Jurado and Vivoni,

2009). Terrain parameters (slope, aspect and sky-view) interact directly with calculations of solar irradiance, since the size, shape and orientation of obstructions modifies the exposure to the solar beam (Suri and Hofierka, 2004). Prior studies have typically used coarse resolution DEMs ($\sim$25 to 100-m) (Rich et al., 1995; McKenney et al., 1999; Fu and Rich, 2002; Dymond and Johnson, 2002; Zaksek et al., 2005; Piedallu and Ggout, 2008), though Burnett et al. (2008) obtained insolation estimates with a 3-m DEM. Radiation estimates with coarse DEMs have been used to obtain proxies for vegetation productivity and evapotranspiration, among other ecological variables (e.g., Horsch, 2003; Lassueur et al., 2006; Astrom et al., 2007; Bennie et al., 2008a; Ivanov et al., 2008b). However, an increasing number of technologies allow the production of high resolution DEMs (Slatton et al., 2007) that can be used to investigate radiation variability at fine resoultions. To our knowledge, however, there are no previous studies addressing the issue of the effect of spatial resolution on the simulation of solar irradiance in regions of complex terrain. A recent study by Montero et al. (2009) used adaptive triangular meshes for improved solar radiation modeling, but did not address the spatial resolution issue. Assessing the effect of resolution on radiation can help determine the level of detail required to capture microclimatic variations leading to ecogeomorphic differences.

5.1.3 Objectives and purpose

In Part II of this work, we analyze the topographic and vegetation effects on irradiance for a semiarid basin exhibiting aspect-controlled vegetation patterns using four sequentially improved elevation datasets. We explore the effects of aspect, slope and vegetation in the annual and seasonal radiation, with an emphasis on differences between north and south facing regions and the impact of

tree shading in intercanopy areas. Our intent is to help elucidate first order topographic and vegetation controls on the microclimate in the opposing hillslope ecosystems, as reviewed by Gutiérrez-Jurado and Vivoni (2011). This evidence can subsequently be used to improve mechanistic models of ecogeomorphic dynamics and interpret multi-year field data collected in a representative semiarid basin with aspect-controlled ecosystems.

5.2 Solar Radiation Modeling and Observations

Topographic effects on solar radiation of the $\sim$0.1 km^2 study basin within the Sevilleta National Wildlife Refuge, New Mexico, were studied using the three DEMs introduced in Part I of this work (Gutiérrez-Jurado and Vivoni, 2009): IFSAR (10-m), dGPS (4-m) and the bare earth LiDAR (1-m). In addition, a digital surface model (DSM) extracted from the LiDAR data was used to capture the effects of the conifer trees (one-seed junipers, *Juniperus monosperma*) on the north facing slope (referred to as vegetated LiDAR). These four DEM products were used as surface inputs to compute the shortwave irradiance using the Solar Radiation (SRAD) model of Wilson and Gallant (2000), as described next. The reader is referred to Gutiérrez-Jurado and Vivoni (2011) for a description of the study site and topographic products.

5.2.1 SRAD model

SRAD is a distributed model for complex terrain that takes into account the interactions of solar radiation fluxes with atmospheric and land surface characteristics (Moore et al., 1991). Fig. 5.1 presents a schematic of the SRAD model.

The amount of solar irradiance reaching the ground at any given location depends on a series of factors that operate over a range of scales (McKenney et al., 1999) spanning from global to micro-scale conditions. Global factors account for the solar beam angle of incidence and the distance traveled from the Sun to the Earth, which is dictated by latitude and time of the year. At the regional scale, several factors affect irradiance, including: (1) atmospheric attenuation (t) resulting from the reflection, absorption and scattering of the solar beam by gases, water vapor and aerosols; (2) reemission of the absorbed and scattered irradiance in the atmosphere as isotropic diffuse radiation; (3) circumsolar radiation ($Circ$) emanating from within five degrees of the solar disc; and (4) cloud attenuation (β) of the direct solar beam and diffuse irradiance. At the local scale, terrain conditions, such as slope and aspect, can alter the total irradiance (i.e., direct and diffuse) by reflection from the ground or by shading. Finally, tree canopies can reflect or absorb radiation, thus controlling the amount of irradiance received by understory vegetation and intercanopy spaces (McKenney et al., 1999; Martens et al., 2000).

To compute the potential incoming shortwave radiation (SWR) for sloping terrain, SRAD requires calibrating the model to local site conditions (e.g., McKenney et al., 1999; Wilson and Gallant, 2000). Model calculations are performed on 12-minute intervals and summed to daily fluxes for the majority of the direct, diffuse and reflected radiation fluxes (Fig. 5.1). In order to obtain realistic values, SRAD requires mean monthly values of five radiation parameters that can be calculated using nearby observations (McKenney et al., 1999; Wilson and Gallant, 2000). In this work, incoming direct and diffuse shortwave radiation data were obtained from the Sevilleta Long Term Ecological Research (LTER) Red

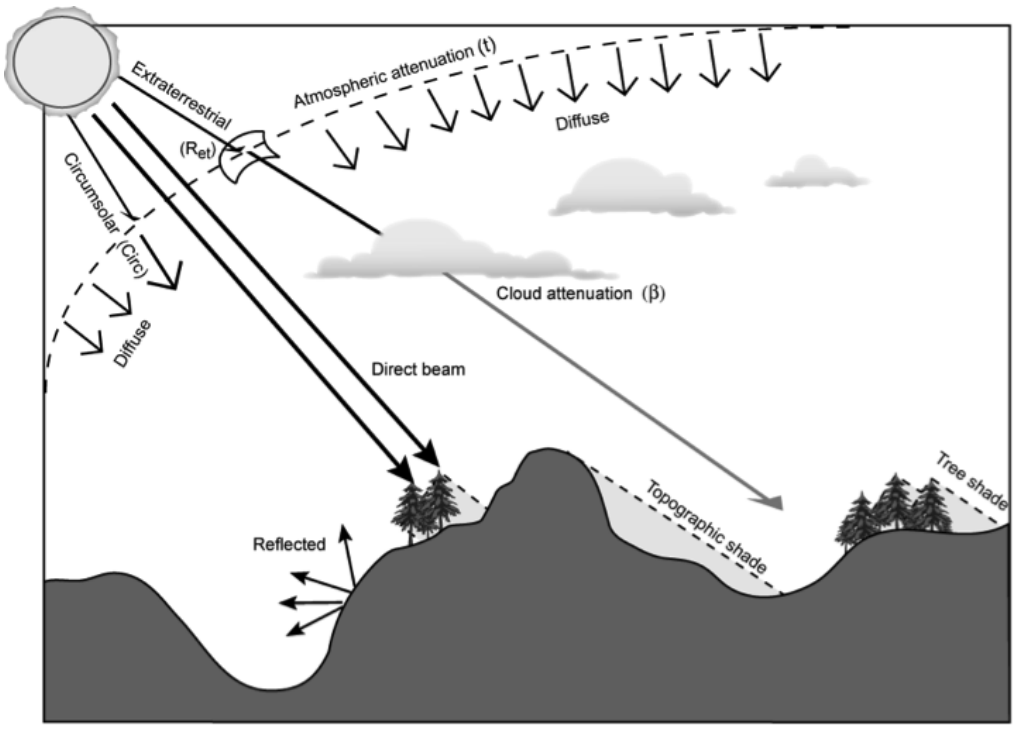

Figure 5.1: Schematic illustrating the incoming shortwave irradiance components and its attenuation: isotropic diffuse and circumsolar diffuse (*Circ*) irradiance, direct beam and reflected irradiance, atmospheric attenuation (t), cloud attenuation (β), topographic and tree shading.

Tank weather station located <1-km from the study basin (Milne et al., 2003). Table 5.1 presents the input variables and parameters necessary for SRAD. In the following, we provide a brief description of each model input.

The circumsolar irradiance is the SWR originating 5○ around the solar disc from which a coefficient (*Circ*) is derived to allow the calculation of the total incident irradiance. The coefficient *Circ* is calculated as (Wilson and Gallant, 2000):

$$Circ = \frac{R_{mth}}{24 \cdot I} \tag{5.1}$$

where R_{mth} is the mean daily observed irradiance for each month averaged over a series of years and I is the solar constant of 4.871 MJ/m^2/h. Atmospheric transmittance (t) accounts for attenuation of extraterrestrial irradiance and is calculated as the fraction of extraterrestrial irradiance observed at the ground for clear sky days minus a transmissivity lapse rate due to the thinning of the atmosphere with elevation as:

$$t = \left(\frac{R_{et}}{R_{thcs}} \right) - 0.00008 \cdot z \tag{5.2}$$

where R_{et} is the extraterrestrial irradiance from the sun incident on a horizontal plane at the top of the atmosphere, 0.00008 is the transmissivity lapse rate and z is elevation above mean sea level (z is ∼1700-m at the study site). R_{et} was calculated using the solar constant (I) and a series of geometric relations of the Sun distance and angles for each day of the year (Dingman, 2000).

Sunshine fraction (S) is the daily proportion of sunshine calculated by dividing the hours of clear sky insolation by the hours with cloudy conditions. This parameter is difficult to obtain as few weather stations directly report cloudiness

on a consistent basis (e.g., Ivanov et al., 2007). As a result, monthly variations of S were obtained from the Albuquerque International Airport station located ∼60 miles northeast of the study basin (http://www.ncdc.noaa.gov/oa/ncdc.html). The cloud transmittance coefficient (β) is a monthly fraction of attenuation of the direct and diffuse irradiance by clouds. β can be calculated as:

$$\beta = \left(\frac{R_{th}}{R_{thcs}} - S \right) \cdot (1 - S)^{-1} \tag{5.3}$$

where R_{th} and R_{thcs} are the mean monthly observed and clear sky irradiances, respectively, each averaged over several years. Clear sky irradiance is the flux of incoming radiation when the sky is completely unobstructed by clouds or dust. The calculation of R_{thcs} is somewhat problematic when there is no cloud cover data associated directly to the radiation observations. We computed R_{thcs} following McKenney et al. (1999) by: (1) obtaining the maximum radiation values for each month for all years; (2) verifying these maximum values correspond to the day of maximum insolation hours; (3) plotting the maximum daily irradiance for each month against day of the year; (4) fitting a polynomial to the data from which clear sky radiation was calculated; and (5) obtaining the mean monthly clear sky irradiance (R_{thcs}) from the polynomial interpolation.

Albedo is the fraction of incident radiation that is reflected by the land surface. This value can be measured in the field from SWR observations, or alternatively, values for albedo can be found in tables for different surfaces. In this study, albedo was implemented uniformly across the basin with seasonal changes in the summer months due to vegetation greening. We explored the sensitivity of irradiance to changes in albedo due to differences in land cover (north facing trees versus and south facing shrubs) and their effects through increased or decreased reflection.

5.2.2 Comparison between simulated and observed irradiance

The performance of SRAD was verified by comparing mean monthly radiation estimates for two years against independent observations from a pyranometer located at the flat headslope of the study basin. Fig. 5.2 shows the comparison of the observed and simulated mean monthly radiation. Observed error bars represent $\pm$ 1 standard deviation of the temporal variation within each month, whereas the simulated error bars are $\pm$ 1 standard deviation of the spatial variations at pixels in close proximity to the measurement site. In general, the simulated irradiance agrees well with the observed radiation for the winter season, but differences between the two estimates increase during the summer months. These differences in radiation between SRAD and the observations for the summer season are likely due to a poor sunshine fraction parameterization of the model. Note that the sunshine fraction parameters were derived from available data at the Albuquerque airport (60 km distant) that may not capture local cloudiness of small spatial scale during the North American monsoon (NAM) season (e.g., Ivanov et al., 2007).

Nevertheless, the SRAD estimates represent a potential maximum irradiance during the summer months and matches well with the clear-sky radiation in the study basin during this period, providing confidence in the simulated irradiance for the purposes of this study.

Table 5.1: SRAD calibration parameters.

Month	$\mathbf{R}_{th}$ * [MJ/m^2]	$\mathbf{R}_{mth}$ ** [MJ/m^2]	$\mathbf{R}_{thcs}$ *** [MJ/m^2]	$\mathbf{R}_{et}$ † [MJ/m^2]	[$\mathbf{R}_{thcs}/R_{et}$] [-]	**Circ** ‡ [-]	**Albedo** [-]	***b***†† [-]	**S***† [-]	***t***± [-]
Jan	390.1	12.8	14.2	18.7	0.76	0.11	0.2	0.62	70.1	0.62
Feb	449.5	16.2	19.3	23.7	0.82	0.14	0.2	0.67	69.1	0.68
Mar	673.3	21.7	25	30.1	0.83	0.19	0.2	0.64	73.3	0.7
Apr	779.9	26	30.1	36	0.83	0.22	0.2	0.68	80.1	0.7
May	887.7	29	33.3	39.9	0.83	0.25	0.2	0.68	80.1	0.7
Jun	886.1	29.4	34.3	41.5	0.83	0.25	0.2	0.7	83.9	0.69
Jul	841.4	27.1	33.2	40.7	0.82	0.23	0.15	0.68	77.1	0.68
Aug	758.1	24.5	30.1	37.5	0.8	0.21	0.15	0.67	75.1	0.67
Sep	656.5	21.9	25.9	32.4	0.8	0.19	0.17	0.69	78.5	0.66
Oct	561.9	17.9	21.2	26	0.81	0.15	0.2	0.67	78	0.68
Nov	413.9	13.9	16.8	20.2	0.83	0.12	0.2	0.67	73.9	0.69
Dec	364.1	11.6	13.5	17.3	0.78	0.1	0.2	0.62	69.6	0.64

* Total observed irradiance for a given month averaged over a series of years.

** Mean daily observed irradiance for a given month averaged over a series of years.

*** Mean monthly clear sky irradiance.

† Mean monthly extraterrestrial irradiance on a horizontal plane.

‡ Mean monthly value for the circumsolar coefficient.

†† Monthly cloudy irradiance transmittance value.

*† Mean monthly sunshine fraction.

± Monthly value for atmospheric transmittance.

5.3 Results and Discussions

5.3.1 Topographic and vegetation controls on annual irradiance

Annual irradiance estimates in regions of complex terrain provide a first indication of the topographic controls in the opposing hillslope ecosystems. Fig. 5.3 shows the spatial distributions of the total annual irradiance for each product: (a) IFSAR, (b) dGPS, (c) bare earth LiDAR and (d) vegetated LiDAR. In all products, the contrast in total irradiance between the south and north facing slopes is evident. This contrast is even more pronounced for the vegetated LiDAR where annual irradiance differences between north and south facing slopes can reach 8,000 $MJ/yr/m^2$. This represents an 87% reduction in irradiance for some north facing sites as compared to values on the south facing slope. In addition, there is a notable increase in complexity of the irradiance field as fine scale topographic and vegetation details are included in the DEM products. Also, note the vegetated LiDAR indicates sharp contrasts between the shaded intercanopy areas and the exposed treetops. A common feature observed in all estimates is the influence of slope in modifying the control of aspect on the irradiance. For example, the improved terrain definition in the LiDAR products indicate: (1) low irradiance in very steep slopes ($>25^\circ$) of north and west facing aspect; and (2) high irradiance on steep to moderately steep south and southeast aspect.

To provide an assessment of the effects of aspect and slope, we plotted the mean annual irradiance for each major orientation (north [315-45°], east [45-135°], south [135-225°] and west [225-315°]) against slope at 1° intervals, as shown in Fig. 5.4. The general trends observed in this analysis include: (1) irradiance for south facing areas increases non-linearly with steeper slopes, reaching a maximum at around 20°; (2) north and east facing areas show decreasing irradiance

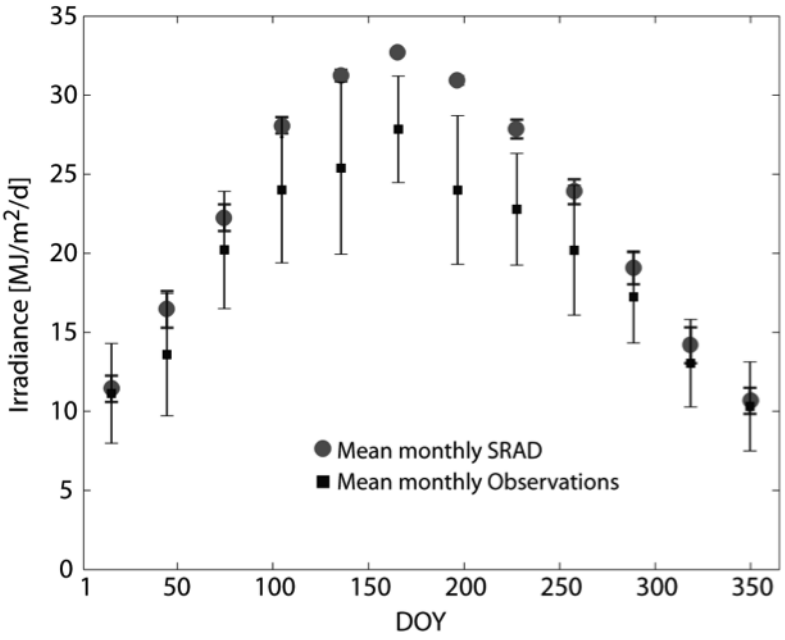

Figure 5.2: Comparison of mean monthly radiation estimates from pyranometer observations at study site (34.41 °N, 106.97 °W, 1706 m) and SRAD. Error bars depict ± 1 standard deviation. The observed values were calculated over the period 2007-2008.

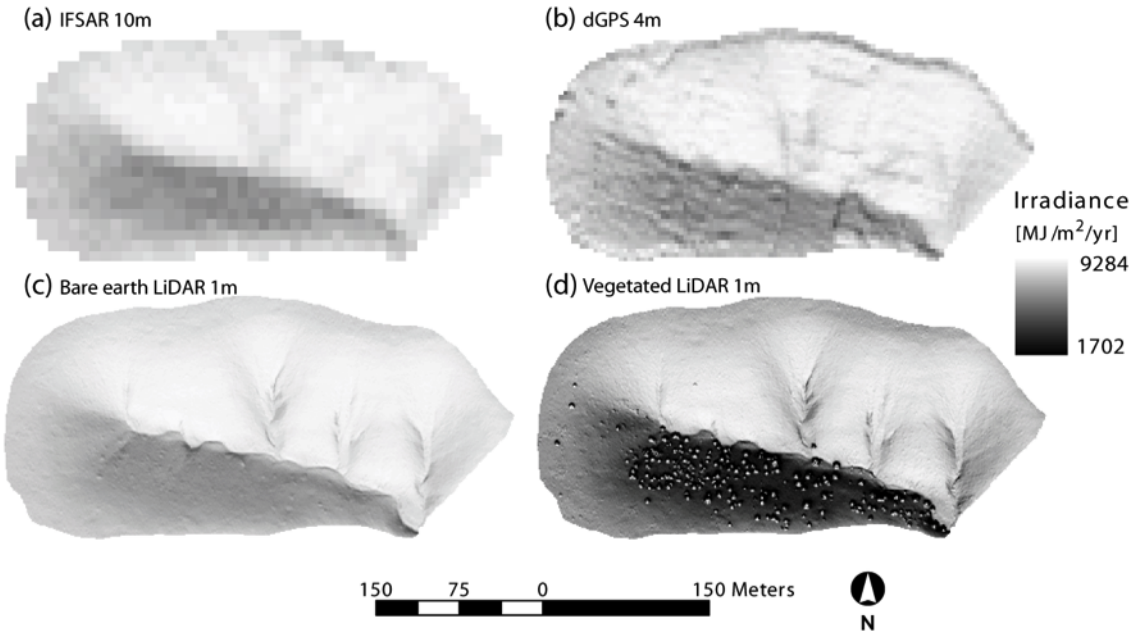

Figure 5.3: Spatial distributions of total annual irradiance ($MJ/m^2/yr$) for IFSAR (a), dGPS (b), bare earth LiDAR (c), and vegetated LiDAR (d) products.

with increasing slope that is more marked and linear for north facing sites; and (3) west facing locations do not exhibit a strong irradiance trend with slope changes. The impact of DEM resolution on annual irradiance estimates is closely tied to the range of slope and aspect values captured in each DEM product (see chapter 4). In the study basin, this effect is more prominent for north facing locations. For instance, for each increase in resolution and quality (Fig. 5.4a to c), there was an increase in the slope range ($\sim$7° for every product) and a corresponding $\sim$1000 MJ/m^2/yr decrease in minimum irradiance. As a result, annual irradiance in north facing areas linearly decreases at a rate of $\sim$140 MJ/m^2/yr per degree of slope for the IFSAR, dGPS and bare earth LiDAR products.

The effect of tree canopies on modulating the control of topographic slope and aspect on irradiance is particularly interesting. Note the rate of decrease in irradiance on the north facing slope for the vegetated LiDAR (Fig. 5.4d) is not monotonic as in the other DEM products. Three regions are apparent: (a) Region I from 0 to 15° with a similar behavior as the other products; (b) Region II from 15 to 25° with a steeper rate than in the other DEM products (and Region I); and (c) Region III with slopes $>$ 25° that show no irradiance trend with slope and exhibit very high variability. In addition, the irradiance values for the north facing slope have increasing dispersion (indicated by $\pm$ 1 standard deviation bars) with increasing slope. We interpret this variability to be a result of the complex effects of tree canopies on the north facing slope, including increasing their exposure on treetops and shading their surrounding intercanopy spaces. Though the shade and reflected irradiance produced by tree canopies should vary according to season, their impact is strong enough to alter the slope control on annual irradiance in north facing areas. These results agree well with Zou et al. (2007) who

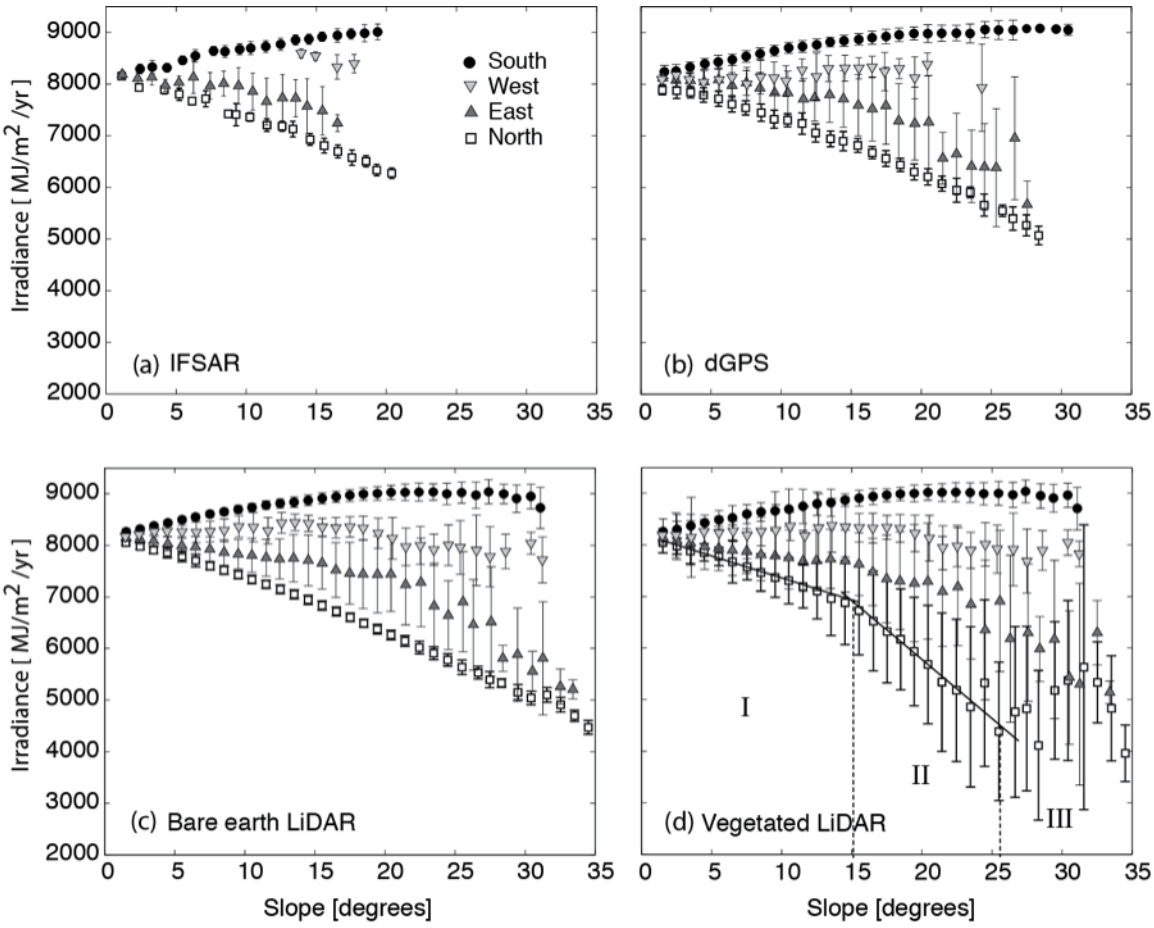

Figure 5.4: Total annual irradiance ($MJ/m^2/yr$) for IFSAR (a), dGPS (b), bare earth LiDAR (c), and vegetated LiDAR (d) products as a function of slope and aspect.

observed that the annual amount of near ground solar irradiance on north and south facing slopes is highly dependent on canopy cover.

Fig. 5.5 presents the variation of annual irradiance across all observed aspects in each DEM product. Bin-averaged annual irradiance, calculated for bin widths of 10° in aspect (denoted by the symbols), is similar among all products, though the variability in each aspect bin is different (dashed lines are ± 1 standard deviation). The coarse resolution DEMs (IFSAR and dGPS) have a more restricted range of aspect values (Gutiérrez-Jurado and Vivoni, 2009) and may miss entire east and west facing areas. Note that irradiance varies considerably within the north-northeast facing areas (larger spread), but is more uniform in the south facing regions, for all products. Clearly, north facing sites receive lower irradiance, with as much as a 2000 $MJ/m^2/yr$ difference as compared to south facing areas. Differences between the bare earth and vegetated LiDAR are evident in the north-northeast facing region, but are not reflected in the bin-averaged values. The individual sites lying outside the $\pm$ 1 standard deviation in the north-northeast facing region are particularly affected by tree shading and have reductions of irradiance as high as 5000 $MJ/m^2/yr$. This suggests that vegetation-radiation interactions in north facing areas can be substantial at the annual scale and thus merit closer inspection.

Another method to depict irradiance differences in the basin is via the use of probability density functions (PDFs) of the annual irradiance for north and south facing locations, as shown in Fig. 5.6. Interestingly, the annual irradiance distribution for south facing locations is remarkably similar for all DEMs, suggesting that coarser terrain products are adequate in regions with high radiation fluxes. Conversely, irradiance PDFs for north facing sites exhibit clear differences

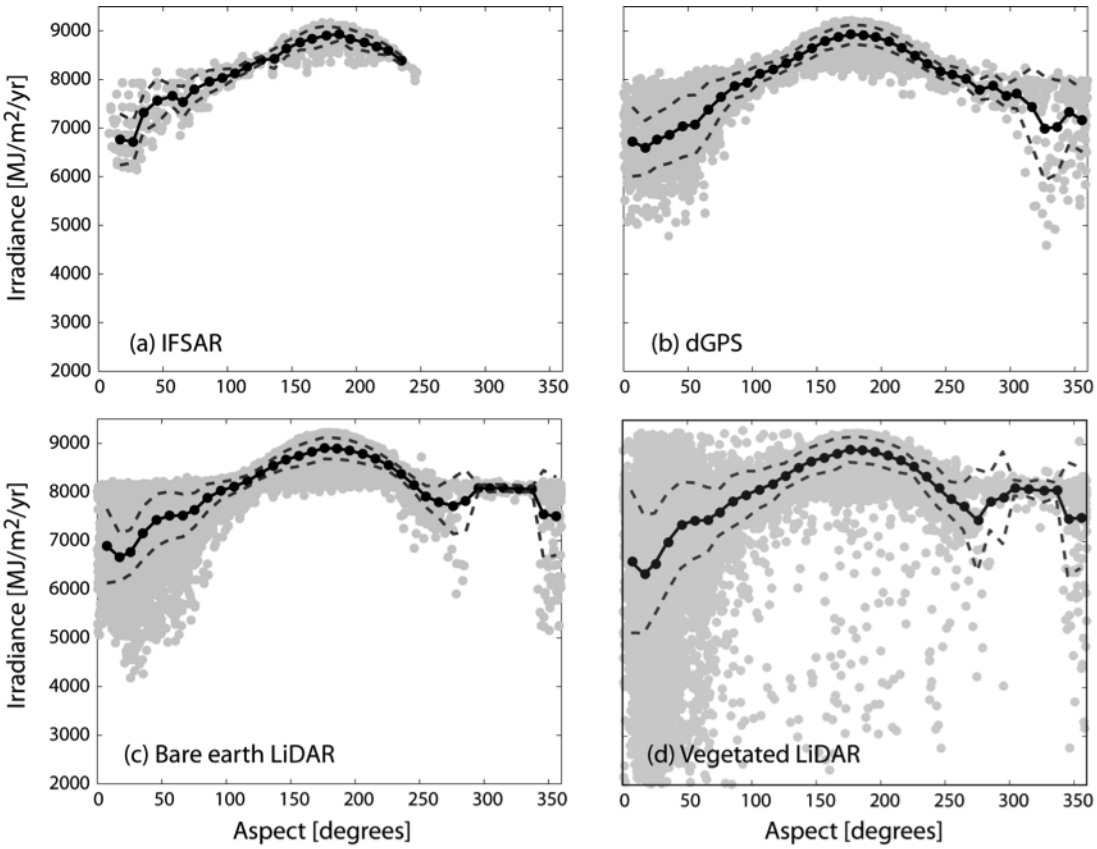

Figure 5.5: Total annual irradiance plotted as a function of aspect for each DEMs: IFSAR (a), dGPS (b), bare earth LiDAR (c), and vegetated LiDAR (d). The gray dots represent all the data, black circles show the mean irradiance for each aspect bin and dashed lines are $\pm$ 1 standard deviation.

near 6500-7000 MJ/m^2/yr and 7500-8000 MJ/m^2/yr among the DEM products. For example, north facing PDFs of the LiDAR products show a strong bimodality reflecting the slope distribution, as shown in Gutiérrez-Jurado and Vivoni (2009). This bimodality is muted in the dGPS product and nearly identical in the IFSAR DEM. The effect of tree canopies in the vegetated LiDAR (Fig. 5.6c) is limited to north facing areas and results in an overall dispersion of irradiance, with higher and lower values near the tails of the distribution, and a decrease in the bimodality. This suggests the tree canopies increase the spatial variability in the north facing irradiance. Lower irradiance values (<6000 MJ/m^2/yr) are due to tree shading effects on intercanopy spaces, while the higher irradiances (>8000 MJ/m^2/yr) result from the exposure of south-facing treetops (Fig. 5.3d).

5.3.2 Seasonal variability of topographic and vegetation controls

Since aspect-derived contrasts in irradiance are known to vary with seasons (e.g., Walton et al., 2005; Zou et al., 2007), we assessed differences in daily irradiance in Fig. 5.7 for the spring equinox (DOY 80), summer solstice (DOY 172) and winter solstice (DOY 355), where DOY is day of year. In the northern hemisphere during the summer (winter) solstice, the Earth is tilted towards (away from) the Sun, leading to more (less) intense and longer (shorter) irradiance. During the spring equinox, the angle of the direct sun beam is intermediate and irradiance values fall between the summer and winter solstices. Visually, the largest differences between north and south facing areas for the unvegetated DEMs (IFSAR, dGPS, bare earth LiDAR) occur during the winter solstice, and the smallest variations for the summer solstice. However, this contrast is not observed for the vegetated LiDAR, where the largest differences take place during

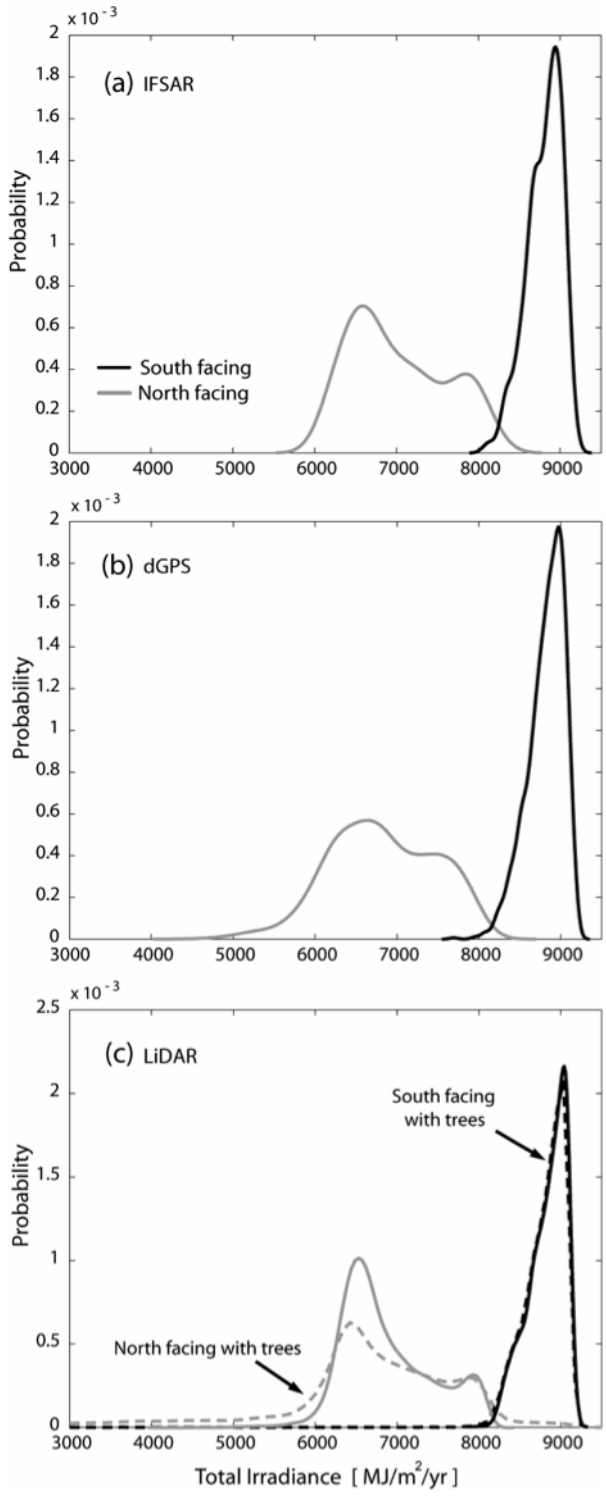

Figure 5.6: Probability density functions (PDFs) of total annual irradiance for IFSAR(a), dGPS (b), and LiDAR (c) products for south facing (black line) and north facing (gray line) slopes. Dashed lines in (c) illustrate the effects of tree shading and reflection.

the spring equinox. Note the dramatic impact of the trees during the various seasons, generally leading to lower irradiance in the north facing slope and increasing its spatial variability considerably. While the increase in DEM resolution and accuracy improves seasonal irradiance estimates, the effect of the tree canopies overwhelms this improvement, leading to a more pronounced impact on the irradiance field. This suggests that tree height and cover information is essential for assessing microclimate conditions in semiarid basins with differences in vegetation patterns.

Fig. 5.8 presents the combined effect of aspect and slope on the daily irradiance for three DEM products (IFSAR, dGPS and vegetated LiDAR). We omit the bare earth LiDAR since the vegetated version best exhibits irradiance differences among the slopes. Clear aspect controls are observed for the spring equinox and winter solstice, with increasing (decreasing) irradiance with slope for the south (north) facing locations. These results closely parallel the annual irradiance dependence on slope and aspect, but yield greater slope and aspect differences during the winter solstice. The controlling effects of aspect and slope on irradiance nearly disappear during the summer solstice in the IFSAR and DGPS DEMs and are greatly reduced in the vegetated LiDAR. Nevertheless, the tree canopies influence the irradiance during the summer solstice, in particular for the steeper slopes, by reducing irradiance in the north and west facing locations (Fig. 5.8h). The largest impact of the tree canopies occurs, however, during the spring equinox (Fig. 5.8g), instead of the winter solstice. This is primarily due to the pronounced decrease in irradiance with slope in north facing locations and suggests that the spring tree shading is more important in reducing the irradiance than in the winter time, when most of the shade is due to topographic effects. This has important ecological implications as the spring irradiance is closely related to

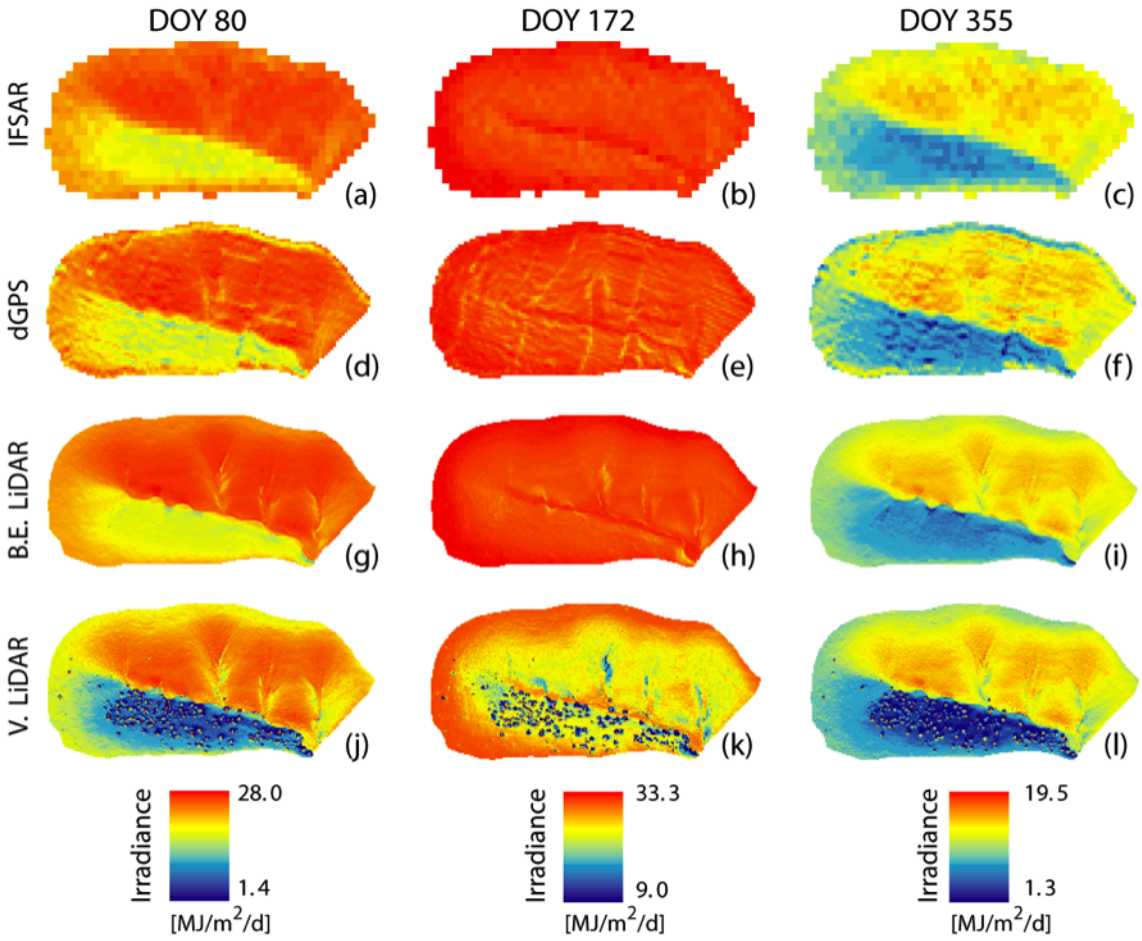

Figure 5.7: Spatial distributions of daily irradiance for each DEM (top to bottom: IFSAR, dGPS, bare earth LiDAR and vegetated LiDAR), for spring equinox (right column), summer solstice (middle column), and winter solstice (left column). Note that for each DOY, the four product maps were adjusted to the maximum range of values observed among the products for comparison purposes.

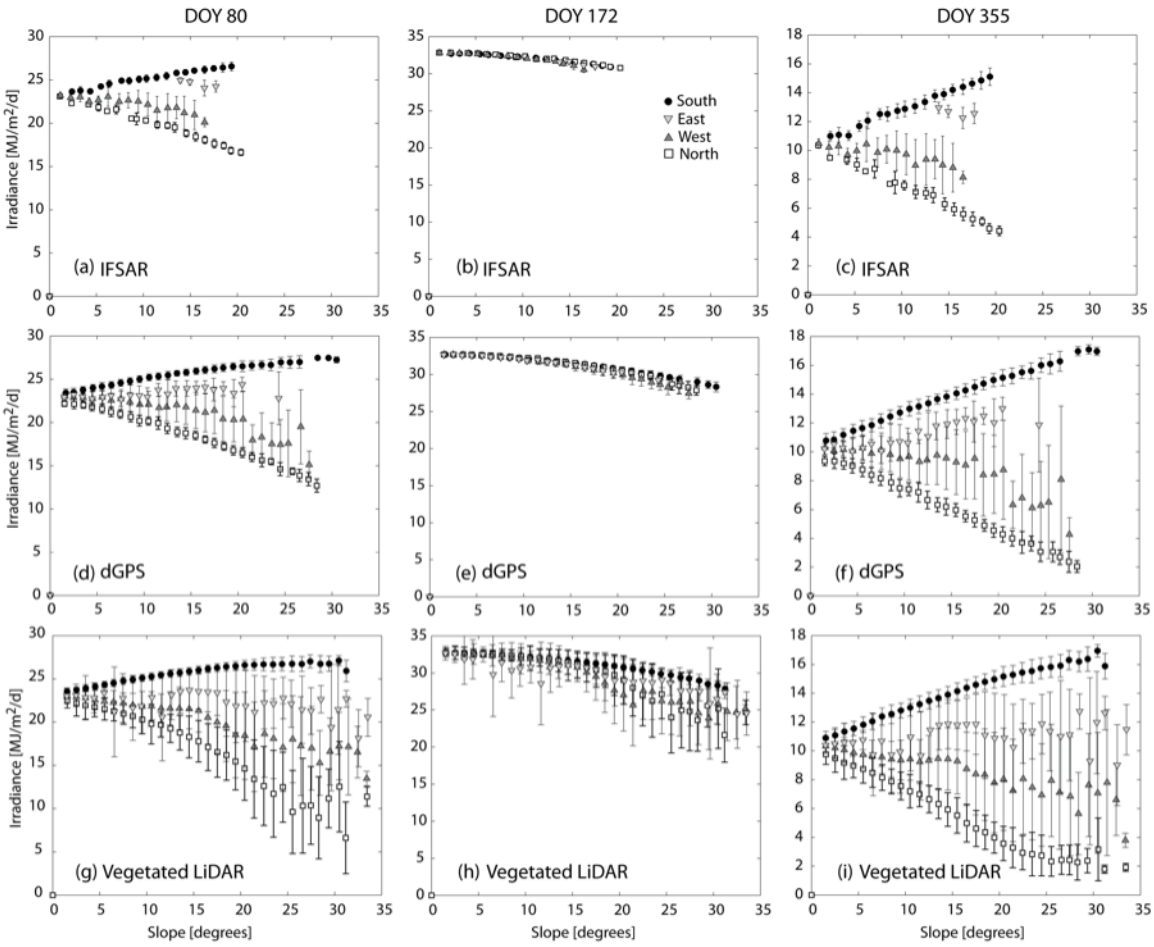

Figure 5.8: Daily irradiance as a function of slope for each DEM product (top to bottom: IFSAR, dGPS, and LiDAR), for spring equinox (right column), summer solstice (middle column), and winter solstice (left column). Irradiance values are grouped by aspect with different symbols.

the first pulse of grass productivity in intercanopy areas (Pennington and Collins, 2007; Ivanov et al. 2008b). Clearly, the availability of unvegetated and vegetated terrain products allows distinguishing tree versus topographic (slope and aspect) controls on the seasonal irradiance in the study basin.

5.3.3 Vegetation-irradiance interactions as a function of tree cover and albedo

An important question is the potential of vegetation feedbacks to the local radiation field as a function of tree cover (Breshears et al., 1998; Gutiérrez-Jurado et al., 2006). We explore this by inspecting mean irradiance differences (MID) during the year in two sampling areas (SA) with distinct tree cover percentages: (1) SA1 with 28% tree cover, and (2) SA2 with 12% tree cover. Fig. 5.9a shows the two sampling areas in the north facing slope selected for this analysis. We evaluate the effect of tree radiation sheltering by subtracting the bare earth LiDAR radiation from the vegetated LiDAR radiation for each day in the year and for each SA as:

$$\text{MID} = R_{veg} - R_{bare} \tag{5.4}$$

where R_{veg} and R_{bare} are the irradiances averaged over all intercanopy spaces in each SA after masking out the tree cells determined using an algorithm by Forzieri et al. (2009). Fig. 5.9b shows the MID calculated for each day of the year for the two SAs. A negative MID indicates that the SA experiences a reduction in radiation because tree shading overwhelms any potential increases in reflection to the ground due to the tree albedo. For this analysis, the albedo values in Table 5.1 were assumed. In both sampling areas, the trees reduce the amount of irradiance throughout the year, leading to a net loss of radiation that is greater during the summer season than the winter. The sampling area with higher tree cover (SA1) receives consistently less irradiance during the year, with SA1 and SA2 loosing $\sim$310 and $\sim$220 MJ/m^2/yr, respectively. This implies that a 16% increase in canopy cover from SA2 to SA1 leads to a 40% decrease in annual

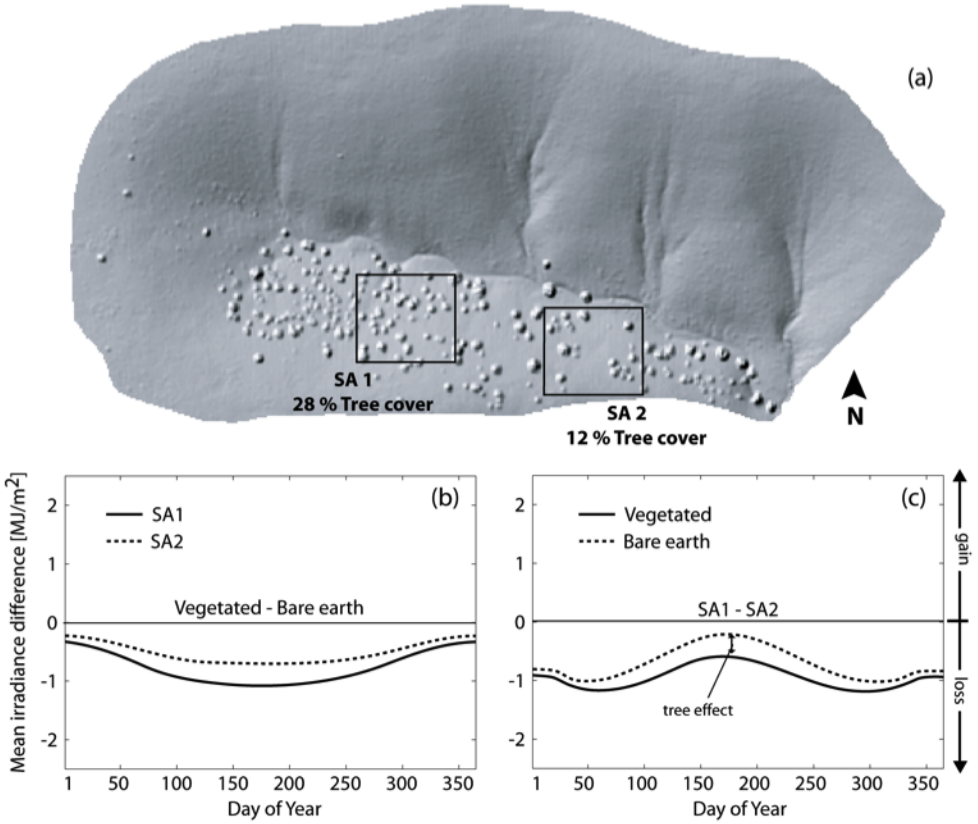

Figure 5.9: (a) Digital surface model depiciting two sampling areas (SA) with different tree cover percentages: SA1 = 28% and SA2 = 12%. (b) Mean irradiance difference between vegetated and bare earth sample areas. (c) Mean irradiance difference between SA1 and SA2 for vegetated (solid line) and bare earth LiDAR (dotted line).

irradiance. These results indicate that the trees affect the total amount of irradiance received by intercanopy spaces, depending on the tree cover and the day of the year. Overall, the denser tree cover in SA1 was more efficient in reducing the irradiance as compared to the sparser SA2 area.

To evaluate the combined effects of terrain attributes and tree cover, we subtracted the mean irradiance from the two SA for each product (vegetated and bare earth LiDAR) as:

$$\mathrm{MID}_{veg,bare} = R(\mathrm{SA1})_{v,b} - R(\mathrm{SA2})_{v,b} \tag{5.5}$$

where R(SA1) and R(SA2) represent the areally-averaged irradiance for the intercanopy areas in each SA, and v and b depict the vegetated and bare earth products (Note that MID_{veg} is related to $\mathrm{R(SA1)}_v$ and $\mathrm{R(SA2)}_v$ only, similarly for $\mathrm{MID}_b are$). MID_{veg} and MID_{bare} are the solid and dotted lines in Fig. 5.9c, respectively. Temporal differences between MID_{veg} and MID_{bare} (depicted as the area between the solid and dotted lines) capture explicitly the role played by tree canopies on the irradiance, independent of variations in topographic conditions among the two sampling areas. Note that the combined effects of changes in topographic conditions among the two SAs and a 16% increase in tree cover from SA1 to SA2 produce a net loss of radiation of $\sim$300 MJ/m^2/yr (MID_{veg}). By removing the effect of the trees (MID_{bare}), a net annual irradiance loss of $\sim$220 MJ/m^2/yr is observed, which is a 26.6% increase in irradiance as compared to MID_{veg}. It is interesting to note that the temporal variations in MID_{veg} and MID_{bare} reveal that the effect of the tree canopies on the irradiance is greatest during the summer period. Furthermore, the effect of topographic shading

is largest during spring and fall seasons, suggesting that the impacts of terrain attributes and vegetation cover on irradiance are asynchronous during the year.

The impact of tree reflection was further assessed by performing a sensitivity analysis of the surface albedo. Prior results assumed a spatially uniform albedo with temporal fluctuations during the summer season (Table 5.1). For this analysis, a spatially variable albedo was used based on vegetation differences (trees versus grasses/shrubs). Tree albedo was held constant at a value of 0.15 due to its evergreen nature, while the grass and shrub albedos were varied according to seasonal phenology (Table 5.1). Fig. 5.10a and b illustrate the impact of the spatially variable albedo (dotted lines) with respect to the uniform albedo (solid lines). Results indicate a slight decrease in irradiance when using a spatially variable albedo for both SA1 and SA2, especially during the summer (Fig. 5.10a), but a small irradiance gain in SA1 during winter. The decrease in irradiance in the summer is due to the lower albedo of the trees (from $\sim$0.2 to 0.15 in April to September) resulting in less radiation reflected back to the intercanopy spaces. The small increase in the winter for SA1 is likely due to the higher cover, suggesting slightly higher tree reflection to the intercanopy space at this tree density for this sun beam angle. The impact of albedo on the tree effect (i.e., the difference between MID_{veg} and MID_{bare}, Fig. 5.10b) is minimal, but exhibits the trends described for summer and winter seasons. This suggests that using a spatially variable albedo amplifies the observed differences in radiation in the opposing slopes.

5.3.4 Individual tree locations and canopy radiation

The opposing hillslope ecosystems show irradiance differences at seasonal and annual scales, despite their close proximity. As a result, the tree locations

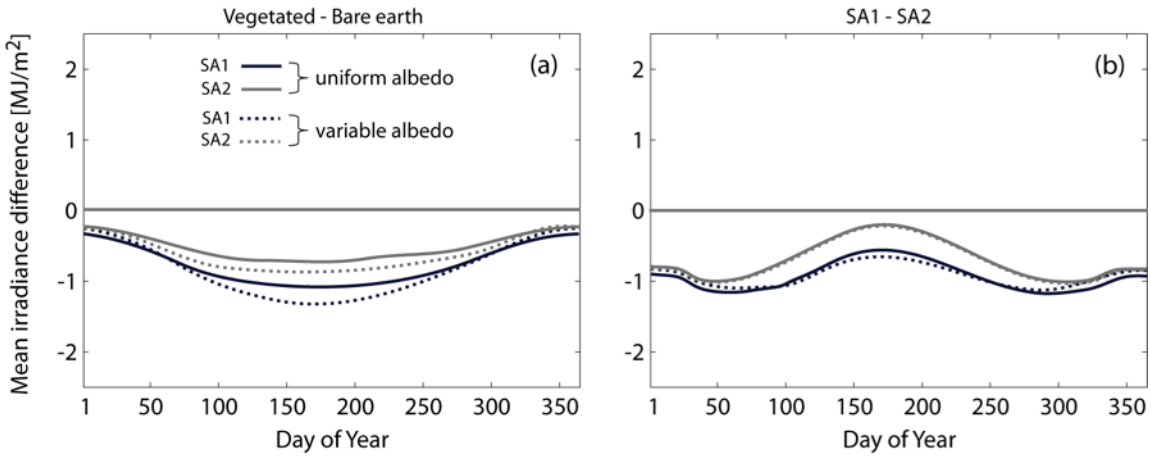

Figure 5.10: Sensitivity analyses for a spatially uniform albedo (solid lines) and a variable albedo as a function vegetation differences (dotted lines). (a) Mean irradiance differences between vegetated and bare earth sample areas. (b) Mean irradiance difference between SA1 and SA2 for vegetated (solid line) and bare earth LiDAR (dotted line).

within the study basin should be controlled by aspect and to a lesser extent by slope. Fig. 5.11a graphically shows the tree locations with respect to aspect and slope in polar coordinates, with the distance from the origin representing the surface slope (0 to 40°). The majority of the trees are clustered in the north-northeast region between 0 and 50° in aspect and along slopes between 15 and 25°. This suggests a preferential location (or topographic niche) for conifer trees related to the irradiance received at a site. This observation supports the analysis of Ivanov et al. (2008b) which indicated that grass species in this climate had preferential locations depending on radiation amounts. The range of slopes with trees also coincides with Region II in Fig. 5.4d, indicating that the steepening of the irradiance trend in the north facing areas is due to tree sheltering.

Tree canopies at specific locations constitute a protuberance in the terrain with defined canopy aspects and slopes. Fig. 5.11b shows the mean annual irradiance received by tree canopies in the basin as a function of aspect. Distance

from the origin indicates the amount of irradiance on the trees themselves for each aspect bin (10° degree bin width). In general, the portions of the canopies facing north receive the least radiation ($\sim$4000 MJ/m^2/yr) and parts facing south receive the highest irradiance ($\sim$9000 MJ/m^2/yr). Similarly, the spatial variability ($\pm$ 1 standard deviation within each aspect bin as bars) is greater for north facing sides and decreases approaching the south facing parts. As a result, we would expect that intercanopy areas on the north facing slope looking directly towards the south facing sides of a tree canopy experiences higher amounts of canopy reflectance. This effect can combine with lower shading in certain intercanopy areas of the north facing hillslope to result in a net increase of radiation throughout the year. This behavior would contradict the general trend of decreased irradiance in the north facing hillslope and is only likely to occur under very special circumstances. For example, this may explain the small increase in irradiance in SA1 (higher tree density) during the winter season (Fig. 5.10a).

Finally, we used the vegetated LiDAR to explore the relation of tree canopy height with three topographic attributes: aspect, slope and curvature. We used tree height, extracted using an algorithm by Forzieri et al. (2009), to classify canopies into three sizes: small ($<$1-m), medium (1 to 2.5-m), and tall ($>$ 2.5-m). For each category, we calculated the probability of tree occurrence as a function of aspect, slope, and curvature in Fig. 5.12. Clearly, there are no differences in the tree height distribution with aspect as all trees are located on the north-northeast slopes. Nevertheless, the range of aspect values in which trees occur slightly increases with tree height. Slope appears to have an effect on the distribution of tree height with smaller trees ($<$1-m) located in a more restricted range of slopes (15 to 21°) as compared to medium size trees (13 to 26°) and tall trees (5 to 30°). Note that small and medium trees have normal distributions of tree occurrence with

slope, while tall trees exhibit a bimodal distribution such that they are located either on gently sloping terrain (5 to 12°) or steep slopes up to 30°, with the majority located around 20°. With respect to curvature, we find that: (1) the majority of small and medium size trees are found on planar terrain and have almost equal chances of finding tree on convex and concave locations; and (2) a few tall trees are located in concave areas (negative curvature), where soil water tends to concentrate, while the rest are found in more convex locations (positive curvature) associated with a diverging hillslope (Gutiérrez-Jurado and Vivoni, 2009). While we would expect that tall trees be found in concave areas with water accumulation, this may not occur for all tall trees if they grow to a size that depends less on the local conditions of the terrain (concave or convex) by reaching out farther with a larger root system. Further exploration of this topic is warranted through the use of high-resolution topography-vegetation datasets.

5.4 Summary

Opposing hillslope ecosystems in mid-latitude, semiarid regions exhibit clear differences in vegetation composition and hydrogeomorphic properties. These differences are driven by variations in the energy budget in which solar irradiance plays an important role. Quantifying irradiance contrasts between the north and south facing hillslopes is a first approximation to unraveling the complex interactions leading to the observed ecogeomorphic patterns. In this study, we used a distributed solar radiation model and a set of sequentially improved elevation datasets to explore the vegetation-topography-radiation interactions in a basin in the Sevilleta National Wildlife Refuge. Previous studies addressing the effects of slope and aspect on annual irradiance state that polar (equator) facing

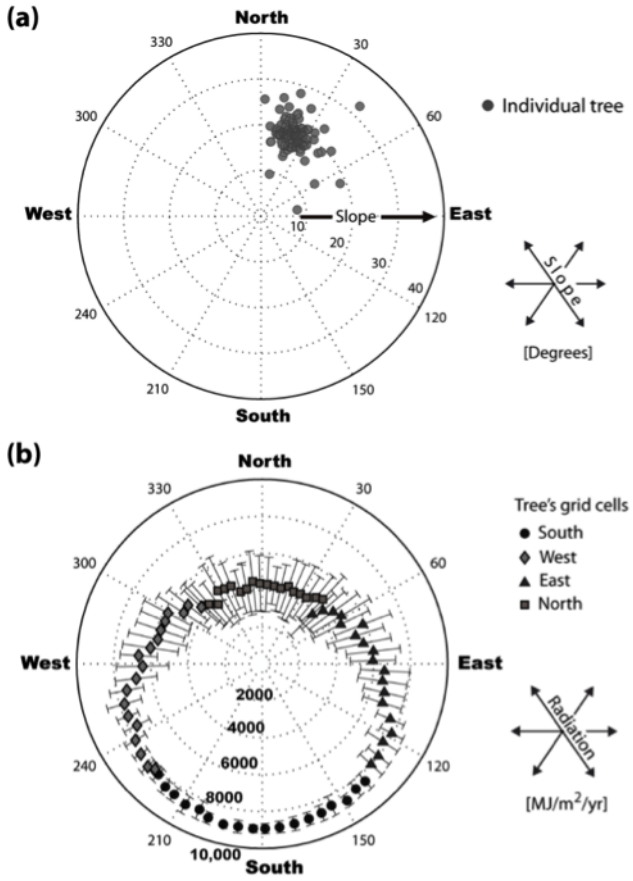

Figure 5.11: (a) Location of each individual tree as function of aspect and slope. (b) Bin-averaged total annual irradiance for each tree aspect, separated into south (circles), west (diamonds), east (triangles) and north facing (squares) sites. Error bars depict $\pm$ 1 standard deviation in each bin. The magnitude of irradiance [MJ/m^2/yr] increases radially outwards.

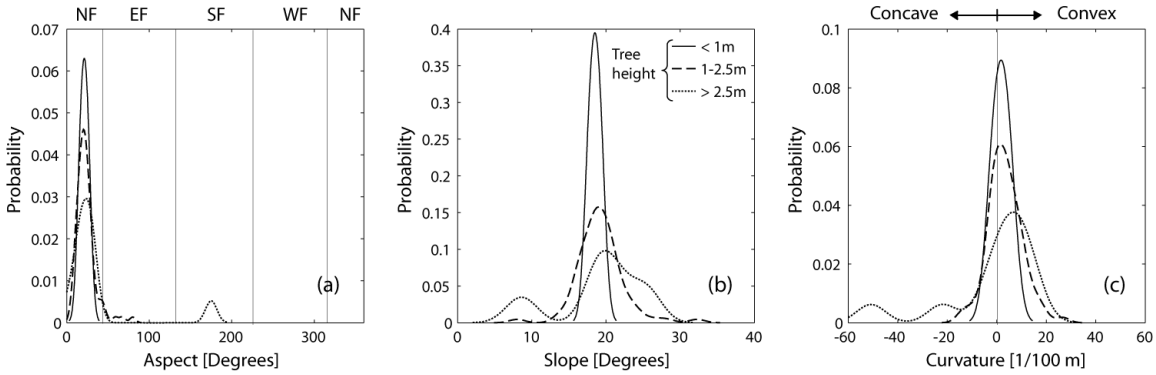

Figure 5.12: Probability density functions (PDFs) of tree height and location with respect to aspect (a), slope (b), and curvature (c). The solid line is for trees of 1m or less height, the dashed lines is for trees between 1 and 2.5 m height and the pointed line is for trees taller than 2.5 m. In plot (c) negative curvatures indicate concave terrain, whereas positive values indicate convex terrain.

areas receive less (more) radiation with steeper slopes (Rich et al., 1995; Breshears et al., 1998; Zou et al., 2007). Our analysis on the effects of topography on irradiance supports prior studies and demonstrates that the slope-aspect effect on irradiance in the study basin is more prominent for the north facing areas, leading to a linear decrease rate of $\sim$140 MJ/m2/yr per degree increment of slope. In addition, the pronounced effect of slope on the north facing areas is augmented when the effect of the tree canopies is considered, leading to large reductions in total annual irradiance due to tree sheltering.

Assessing the performance of the various DEM products on the calculation of irradiance allowed us to elucidate the impact of spatial resolution on the vegetation-topography-radiation interactions at the basin scale. In general, improving the definition of terrain features (i.e., aspect, slope and curvature) by increasing the DEM resolution and quality leads to the amplification of the irradiance contrasts in the basin. However, annual irradiance estimates for south facing areas are remarkably similar for all DEMs, suggesting that coarser terrain products are adequate in regions with high radiation fluxes. On the other hand,

radiation fluxes on north facing locations are significantly improved with each increase in resolution (i.e., IFSAR to dGPS, dGPS to LiDAR). Moreover, adding the tree effects as obstructions in the irradiance estimates results in an increase of the spatial variability of radiation on the north facing hillslope and a significantly lower irradiance in the intercanopy spaces occupied by grasses. As a result, high resolution data with tree cover information is essential for properly assessing microclimatic conditions within semiarid basins that exhibit contrasting vegetation patterns.

Seasonality in irradiance for water-limited ecosystems in areas of complex terrain is important in explaining the vegetation contrasts between opposing slopes (Dymond and Johnson, 2002; Badano et al., 2005; Walton et al., 2005). The fundamental premise is that the amount of radiation incident on the slopes varies through the seasons providing more or less energy input for evapotranspiration demands (Breshears et al., 1998). For a basin in the northern hemisphere, we would expect to observe greater differences in irradiance between the north and south facing slopes in the winter and the smaller differences during the summer. This behavior in seasonal irradiance occurs in all DEMs except the vegetated LiDAR product, where the largest irradiance differences between north and south facing slopes are found in the spring. The deviation from the expected results effectively shows the impact of tree canopies in reducing the irradiance of their surrounding intercanopy areas. Given the grass community established between the conifer trees (Gutiérrez-Jurado et al., 2007), this finding has important implications on the radiation and thermal regime experienced during the spring growing season for the grasses. For instance, tree shading may help conserve soil moisture in the grassy intercanopy areas of the north facing hillslope, allowing for a more vigorous vegetation response in the spring.

The conifer trees (*Juniperus monosperma*) are the only plant species fully captured by the LiDAR dataset in our study basin. Thus, the modeling of irradiance with tree canopy effects allowed us to examine in detail the potential feedback of conifers on irradiance. For two selected sampling areas with varying tree cover percentage, we found that irradiance in intercanopy areas is reduced depending on the density of tree cover and the time of the year. In this study, we limited our analysis to the actual tree distribution on the north facing slope of the study basin. However, further investigation on the effect of spatial distribution of the canopies in adjacent basins may be required to clarify vegetation-radiation interactions in a broader setting (Martens et al., 2000). Another issue regarding the effect of the trees on irradiance would be the proportion of radiation reflected from the different aspects of the canopy surface. For example, we observed that on average a conifer tree can receive twice as much radiation on the surface facing south as compared to the canopy portions facing north. This explains why we observed greater variability in irradiance on the north facing slope of the vegetated LiDAR product.

An analysis of the spatial distribution of trees in relation to three topographic attributes (aspect, slope, curvature) showed: (1) tree locations are restricted to north facing areas and are normally distributed within the north-northeast region regardless of size; (2) small trees occur at restricted ranges of slopes (15-21°), while taller trees can be located either on steep or gentle slopes; and (3) the majority of the trees are located on slightly convex locations, while a few tall trees take advantage of the concave locations where water can accumulate in the landscape. The analysis of the spatial occurrence of conifer trees with respect to terrain attributes merits further investigation through a larger dataset (sample size) in the study region. Given the larger range of terrain and vegetation conditions in

the broader region (Istanbulluoglu et al., 2008), this analysis is more likely to obtain generalized trends between tree establishment and terrain properties in this aspect-controlled ecosystem. In particular, a fruitful avenue for investigation is to link this observational dataset with numerical ecohydrological modeling (Ivanov et al., 2008a,b) in order to identify the underlying mechanisms (for example, lateral soil moisture redistribution through run-on or subsurface transport) that are responsible for the observed vegetation patterns.

In conclusion, the multiple analyses on the vegetation-topography effects on irradiance in the basin supports the hypothesis that the ecosystem patterns are primarily a result of aspect-controlled irradiance, where slope and tree spatial arrangements are a second order controls on irradiance. We also conclude that the conifer trees effectively promote a negative feedback with irradiance that may self-reinforce their occupation of the north facing slope. If this feedback is strong enough to perpetuate the contrasting vegetation patterns between the slopes, this would constitute an unequivocal key to the observed ecogeomorphic expressions.

REFERENCES

Astrom, M., Dynesius, M., Hylander, K. and Nilsson, C. (2007), Slope aspect modifies community responses to clear-cutting in boreal forests, *Ecology*, 88(3), 749-758.

Badano, E. I., Caviares, L. A., Molina-Montenegro, M. A. and Quiroz, C. L. (2005). Slope aspect influences plant association patterns in the Mediterranean, *J. Arid Environments*, 62, 93-108.

Bennie, J., Huntley, B., Wiltshire, A., Hill, M.O., and Baxter, R. (2008.a), Slope, aspect and climate: Spatially explicit and implicit models of topographic microclimate in chalk grassland, *Ecological Modelling*, 216, 47-59.

Bennie, J., Hill, M.O., Baxter, R., and Huntley, B. (2008.b), Influence of slope and aspect on long-term vegetation change in British chalk grasslands, *Journal of Ecology*, 94, 355-368.

Breshears, D. D., Rich, P. M., Barnes, F., and Campbell, K. (1997), Overstory-imposed heterogeneity in solar radiation and soil moisture in a semiarid woodland, *Ecological Applications*, 7(4), 1201-1215.

Breshears, D. D., Rich, P.M., Barnes, F.J., and Campbell, K. (1998), Effects of woody plants on microclimate in a semiarid woodland: soil temperature and evaporation in canopy and intercanopy patches, *Int. J. Plant Sci.*, 159, 1010-1017.

Burnett, B. N., Meyer, G. A., and McFadden, L. D. (2008), Aspect-related microclimatic influences on slope forms and processes, northeastern Arizona, *J. Geophys. Res.*, 113, F03002, doi:10.1029/2007JF000789.

Caylor, K. K., Manfreda, S., and Rodriguez-Iturbe, I. (2005), On the coupled geomorphological and ecohydrological organization of river basins. *Adv. Water Resources*, 28, 69-86.

Coblentz, D. D., and Riitters, K. H. (2004), Topographic controls on the regional-scale biodiversity of the south-western USA. *J. Biogeography*, 31, 11251138.

Corenbilt, D., and Steiger, J. (2009), Vegetation as a major conductor of geomorphic changes on the earth surface: toward evolutionary geomorphology, *Earth Surf. Process. Landforms* 34, 891-896.

Deng, Y., Wilson, J. P., and Bauers, B. O. (2007), DEM resolution dependencies of terrain attributes across a landscape, *Int. J. Geograph. Inf. Sci.*, 21, 187-213.

Dietrich, W. E., and Perron, T. (2006), Is there a topographic signature of life, *Nature*, 439, 411-418.

Dingman, L. S. (2000), *Physical Hydrology, 2nd edition*, Prentice Hall, 365 pp.

Dymond, C. C., and Johnson, E.A. (2002), Mapping vegetation spatial patterns from modeled water, temperature and solar radiation gradients, *J. Photo. Remote Sens.*, 57, 69-85.

Flores-Cervantes, J. H., Vivoni, E. R., Istanbulluoglu, E., and Bras, R. L. 2009. Feedback between grass distribution and land surface form. *Proceedings of the National Academy of Sciences of the United States of America*. (in review).

Forzieri, G., Guarnirei, L., Vivoni, E. R., Castelli, F., and Preti, F. 2009. Multiple attribute decision making for individual tree detection using high-resolution laser scanning. *Forest Ecology and Management*. (in Review).

Fu, P., and Rich, P.M. (2002), A geometric solar radiation model with applications in agriculture and forestry. *Computers and Electronics in Agriculture*. 37,25-35.

Guisan, A., and Zimmermann, N. E. (2000), Predictive distribution models in ecology, *Ecological Modelling*, 135, 147-186.

Gutiérrez-Jurado, H. A., Vivoni, E. R., Harrison, J. B. J., and Guan, H. (2006), Ecohydrology of root zone water fluxes and soil development in complex semiarid rangelands, *Hydrol. Process.*, 20, 3289-3316.

Gutiérrez-Jurado, H. A., Vivoni, E. R., Istanbulluoglu, E., and Bras, R. L. (2007), Ecohydrological response to a geomorphically significant flood event in a semiarid catchment with contrasting ecosystems. *Geophys. Res. Lett.* 34, L24S25, doi:10.1029/2007GL030994.

Gutiérrez-Jurado, H. A., and Vivoni, E.R. (2011), Ecogeomorphic expressions of aspect-controlled semiarid basins: I. Topographic analyses with high resolution datasets. *Ecohydrology*. (In review).

Holland, P. G., and Steyn, D. G. (1975), Vegetational responses to latitudinal variations in slope angle and aspect, *J. Biogeography*, 2, 179-183.

Holland, P. G., Steyn, D. G., and Fuggle, R. F. (1977), Habitat occupation by Aloe ferox Mill. (Liliaceae) in relation to topographic variations in direct beam solar radiation income, *J. Biogeography*, 4(1), 61-72.

Horsch, B. (2003), Modelling the spatial distribution of montane and subalpine forests in the central alps using digital elevation models, *Ecological Modelling*, 168, 267-282.

Ivanov, V. Y., Bras, R. L., and Curtis, D. C. (2007), A weather generator for hydrological, ecological, and agricultural applications, *Water Resour. Res.*, 43, 10, W10406, doi: 10.1029/2006WR005364.

Ivanov, V. Y., Bras, R. L., and Vivoni, E. R. (2008a), Vegetation-hydrology dynamics in complex terrain of semiarid areas. I. A mechanistic approach to modeling dynamic feedbacks, *Water Resour. Res.*, 44, W03429, doi:10.1029/2006WR005588.

Ivanov, V. Y., Bras, R. L., and Vivoni, E. R. (2008b), Vegetation-hydrology dynamics in complex terrain of semiarid areas: 2. Energy-water controls of vegetation spatiotemporal dynamics and topographic niches of favorability, *Water Resour. Res.*, 44, W03430, doi:10.1029/2006WR005595.

Istanbulluoglu, E., Yetemen, O., Vivoni, E. R., Gutiérrez-Jurado, H. A., and Bras, R. L. (2008), On the topographic imprint of vegetation: Inferences from regional analysis of landscape morphology in central New Mexico, *Geophys. Res. Lett.* 34, L14403, doi:10.1029/2008GL034477.

Kienzle, S. (2004), The effect of DEM raster resolution on first order, second order and compound terrain derivatives, *Transactions in GIS*, 8, 83-111.

Kirkpatrick, J. B., and Nunez, M. (1980), Vegetation-radiation relationships in mountainous terrain: eucalypt dominated vegetation in the Risdon Hills, Tasmania, *J. Biogeography*, 7, 197-208.

Lassueur, T., Joost, S., and Randin, C. F. (2006), Very high resolution digital elevation models: do they improve models of plant species distribution?, *Ecological Modelling*, 198, 139-153.

Martens, S. N., Breshears, D. D., and Meyer, C. W. (2000), Spatial distributions of understory light along the grassland forest continuum: effects of cover, height, and spatial pattern of tree canopies, *Ecological Modeling*, 126, 79-93.

Meentemeyer R.K., Moody A., and Franklin J. (2001), Landscape-scale patterns of shrub-species abundance in California chaparral: The role of topographically mediated resource gradients, *Plant Ecology*, 156, 19-41.

McKenney, D. W., Mackey, B. G., and Zavitz, B. L. (1999), Calibration and sensitivity analysis of a spatially-distributed solar radiation model, *Int. J. Geographical Information Science*, 13, 49-65.

McMahon, D. R. (1998), *Soil, landscape and vegetation interactions in a small semiarid drainage basin: Sevilleta National Wildlife Refuge, New Mexico*. MS Thesis. New Mexico Institute of Mining and Technology. Socorro, NM. 174 pp.

Milne, B. T., Moore, D. I., Betancourt, J. L., Parks, J. A., Swetnam, T. W., Parmenter, R. R., and Pockman, W.T. 2003. Multidecadal drought cycles in south-central New Mexico: Patterns and consequences. In: *Climate Variability and Ecosystem Responses at Long-Term Ecological Research Sites*, Greenland, D., Goodin, D. G., Smith, R. C. (eds). Oxford University Press: New York, NY, 286-307.

Montero G., Escobar J.M., Rodriguez E., Montenegro R. (2009), solar Radiation and shadow modelling with adaptive triangular meshes, *Solar Energy*, 83, 998-1012.

Moore, I. D., Grayson, R. B., and Ladson, A. R. (1991), Digital terrain modelling: A review of hydrological, geomorphological, and biological applications, *Hydrol. Process.*, 5, 3-30.

Nieve, M., and Abrahams, A. D. (2002), Vegetation influences on water yields from grassland and shrubland ecosystems in the Chihuahuan Desert, *Earth Surface Processes and Landforms*, 27, 1011-1020.

Paola, C., Foufoula-Georgiou, E., Dietrich, W. E., Hondzo, M., Mohrig, D., Parker, G., Power, M. E., Rodriguez-Iturbe, I., Voller, V., and Wilcock, P. (2006), Toward a unified science of the Earths surface: Opportunities for synthesis among hydrology, geomorphology, geochemistry, and ecology, *Water Resour. Res.*, 42, W03S10, doi:10.1029/2005WR004336.

Pennington, D. D., and Collins, S. C. (2007), Response of an aridland ecosystem to interannual climate variability and prolonged drought, *Landscape Ecology*, 22(6), 897-910.

Piedallu, C., and Gégout, J. (2008), Efficient assessment of topographic solar radiation to improve plant distribution models, *Agricultural and Forest Meteorology*, 148, 1696-1706.

Ranzi, R., and Rosso, R. (1995), Distributed estimation of incoming direct solar radiation over a drainage basin, *Journal of Hydrology*, 166, 461-478.

Rich, P. M., Hetrick, W. A., and Savings, S. C. (1995), *Modelling topographical influences on solar radiation: manual for the SOLARFLUX model*, LA-12989-M, Los Alamos National Laboratories, Los Alamos, 33 pp.

Rinehart, A. J., Vivoni, E. R., and Brooks, P. D. (2008), Effects of vegetation, albedo and solar radiation sheltering on the distribution of snow in the Valles Caldera, New Mexico, *Ecohydrology*, 1, 253-270.

Slatton, K. C., Carter, W. E., Shrestha, R. L., and Dietrich, W. (2007), Airborne Laser Swath Mapping: Achieving the resolution and accuracy required for geosurficial research, *Geophys. Res. Lett.*, 34, L23S10, doi:10.1029/2007GL031939.

Suri, M., and Hofierka, J. (2004), A new GIS-based solar radiation model and its application to photovoltaic assessments. *Transactions in GIS*, 8 (2), 175190.

Walton, J. C., Martinez-Gonzalez, F., and Worthington, R. (2005), Desert vegetation and timing of solar radiation, *J. Arid Environments*, 60, 697-707

Wilcox, B. P., Breshears, D. D., and Allen, C. D. (2003), Ecohydrology of a resource conserving semiarid woodland: Effects of scale and disturbance, *Ecological Monographs*, 73, 223-239.

Wilkinson, M. T., and Humphreys, G. S. (2006), Slope aspect, slope length and slope inclination controls of shallow soils vegetated by sclerophyllous heath-links to long-term landscape evolution, *Geomorphology*, 76, 347-362.

Wilson, J. P., and Gallant, J. C. (2000), *Terrain Analysis: Principles and Applications*, John Wiley Sons, 469 pp.

Yetemen, O., Istanbulluoglu, E., and Vivoni, E. R. 2009. The implications of geology, soils, and vegetation on landscape morphology: Inferences from semi-arid basins with complex vegetation patterns in central New Mexico, USA. *Geomorphology*. 116: 246-263.

Zaksek, K., Podobnikar, T., and Ostir, K. (2005), Solar radiation modelling, *Computers & Geosciences*, 31, 233-240.

Zhang, W., and Montgomery, D. R. (1994), Digital elevation model grid size, landscape representation, and hydrologic simulations, *Water Resour. Res.*, 30, 1019-1028.

Zou, C. B., Barron-Gafford, G. A., and Breshears, D. D. (2007), Effects of topography and woody plant canopy cover on near-ground solar radiation: Relevant energy inputs for ecohydrology and hydropedology. *Geophys. Res. Lett.*, 34, L24S21, doi:10.1029/2007GL031484.

CHAPTER 6

ON THE OBSERVED ECOHYDROLOGIC DYNAMICS OF A SEMIARID BASIN WITH MICROCLIMATIC INDUCED ECOSYSTEMS

6.1 Introduction

The study of topographic-hydrologic-vegetation interactions is a complex issue (Tromp-van Meerveld and McDonnell, 2006) due to the number of nonlinear processes operating on their many interrelations (Ivanov et al., 2008a). For the same reason, understanding the coupling of terrain patterns with vegetation and water fluxes can reveal important constraints on the distribution and adaptability of vegetation to a variable range of environmental conditions. Additionally, grasping a comprehensive knowledge of vegetation-water relations as affected by complex terrain would help clarify the role of plants in the water balance of montane catchments (Brooks and Vivoni 2008). For example, Wang et al., (2011) showed that vegetation species and slope aspects significantly influence the water budget in the soil-vegetation-atmospheric continuum. Yet, these complex interactions are poorly understood, and have not been systematically quantified.

In semiarid areas with complex topography the modification of regional climatic and hydrologic regimes provide niches for particular vegetation communities in conditions that otherwise would not permit their establishment and persistence (Ivanov et al., 2008b). For instance, it has been acknowledged that

plant form and community structure are highly determined by environmental parameters, regardless of genetic constraints (Parsons and Moldenke, 1975). Furthermore, the contrasting effects of topographic-aspect on the modification of environmental variables to which vegetation is highly sensitive, give way to the emergence of coexisting ecosystems with recognizable distinct aridity tolerances, that in normal conditions would be separated by large expanses of terrain and/or significant differences in altitude. In this context, the study of naturally occurring environmental gradients in areas of complex topography provide ideal conditions to understand how changes in land surface processes might impact the current ecologic, hydrologic and energy balance dynamics of semiarid ecosystems (Turnbull et al 2010.d). In the following sections we elaborate on the importance of studying environmental gradients in topographic complex locations, and highlight the benefits of a conceptually holistic approach that seeks to explain vegetation, climatic and terrain contrasts effects on the hydrology of semiarid catchments with contrasting slope aspects and vegetation communities.

6.1.1 Slope aspect and vegetation relations

In areas of complex terrain, topography creates niches of favorability for the vegetation communities best adapted to the local microclimatic and soil water conditions (Liang et al., 2006; Ivanov et al., 2008.a.b). For example, Armesto and Martinez (1978) in a study of vegetation structure slope aspect relations attributed differences in vegetation composition to a nonlinear moisture trend following variations in aspect, where the equator-facing slopes were clearly identified at the xeric end. This arrangement of vegetation with terrain slope and aspect is a global phenomenon that is particularly common to areas of mid-latitude regions

(Mooney et al., 1975; Armesto and Martinez, 1978). To date, many studies have reported this phenomenon in a wide variety of places around the globe (Cottle, 1932; Cantlon 1953; Holland and Steyn, 1975; Mooney et al., 1975; Parsons and Moldenke, 1975; Parsons, 1976; Holland et al., 1977; Armesto and Martinez, 1978; Kutiel 1992; Kutiel and Lavee, 1999; Sternberg and Shoshany, 2001; Desta et al., 2004; Badano et al., 2005; Gutiérrez-Jurado et al., 2006; Astrom et al., 2007; Bennie et al., 2008.b; Chmura 2008; Gallardo-Cruz et al., 2009; Warren 2010). Figure 6.1 provides an example of clear vegetation differences between equator-facing and pole-facing slopes at three different latitudes within the north-American continent. In the three cases shown in Figure 6.1, the more mesic vegetation is found in the pole-facing slopes, while the more xeric vegetation is found on the equator-facing slopes. Replicates of this pattern of mesic versus xeric vegetation communities coexisting with each other in slopes of different aspect are present at both north and south hemispheres all around the globe. Mooney et al., (1975) provides an example of this documenting the co-occurrence of homologous plant community types across a gradient of slope-aspect terrains in climatically comparable regions of North and South-America.

6.1.2 Topographic induced ecohydrologic units

The conspicuous effect of aspect on vegetation species composition, distribution, and biomass production (Liang et al., 2006; Bennie et al., 2008.a; Chmura 2008; Gallardo-Cruz et al., 2009) is tightly coupled to the local modification of microclimatic variables such as temperature and relative humidity (Desta et al., 2004; Bennie et al., 2008.a). For example, in semiarid basins of central New Mexico slope-aspect differences lead to dissimilar energy loads from solar radiation that ultimately result in the existence of diverse microclimates within

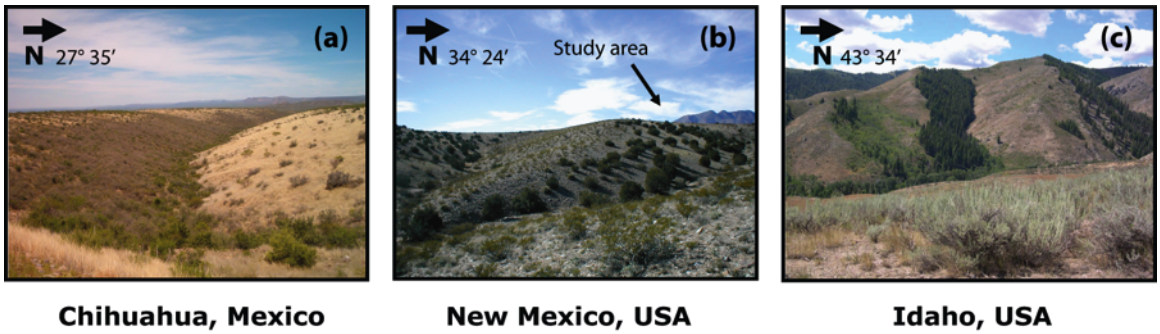

Figure 6.1: Semiarid basins with contrasting vegetated slopes along a latitudinal gradient in North America showing vegetation types organized by aspect; (a) slopes of central Chihuahua, Mexico with deciduous woody vegetation on the north facing slopes and grasses and shrubs on the south facing slope; (b) slopes in central New Mexico, US, with Juniper trees and grasses on the north facing slopes and shrubs and grasses on the south facing slopes; (c) slopes near Anderson Ranch, Idaho, US, showing conifer trees on the north facing slopes and grasses on the south facing slopes (reproduced with permission from Thayne Tuason, Central Washington Native Plants, http://www.cwnp.org/).

a single catchment (Gutiérrez-Jurado et al., 2011). The microclimatic diversity imposed by topography in these catchments promotes the co-occurrence of distinct ecosystems with sharp boundaries and well-defined geomorphic attributes (Gutiérrez-Jurado et al., 2007, 2011.a; Istanbulluoglu et al., 2008). In turn, the arrangement of particular geomorphic and ecologic attributes in the hillslopes of water limited regions result in distinct hydrologic dynamics within the basins (Gutiérrez-Jurado et al., 2007). In synthesis, the combination of singular microclimatic conditions with well-defined vegetation structure and composition on different slopes within a single catchment gives rise to what we define as topographic induced ecohydrologic units. To better illustrate the concept of topographically induced ecohydrologic units we present a 2D diagram of hypothetical opposing semiarid slopes in Figure 6.2. This conceptual model is based on observations and previous work by McMahon (1998) and Gutiérrez-Jurado and others (2006, 2007) in basins from Central New Mexico. Although some of the

terrain-vegetation conditions depicted in Figure 6.2 reflect local conditions from New Mexico study basins, the schematic attempts to represent in general terms the contrasting vegetation-hydrologic-terrain interactions found elsewhere. The graphic presents a cross section of opposing pole, versus equator-facing slopes of a first-order catchment with marked vegetation and soil profile contrasts. In the pole-facing slope a well developed soil profile is accompanied by an extensive mesic conifer-grass vegetation cover. In the equator-facing slope a sparse xeric shrub-grass vegetation community accompanies a less developed soil profile. The pole facing soil shows a clear A horizon (dark brown), a thick B horizon (light brown), and a K-Ck horizon. The equator-facing soil presents an intermittent and irregular A horizon, a thin B horizon and a shallow K-Ck horizon. The differences in soil profiles between the slopes reflect distinct hydraulic properties, such as higher infiltration capacities (I_c) and deeper infiltration fronts on the pole facing slopes resulting from the thicker A and B horizons and the deeper Ck horizons (Gutiérrez-Jurado et al., 2006).

The schematic also shows how the expressed differences in vegetation and terrain properties between the slopes impact water fluxes (triangles) and storages (rectangles) in each system (Wang et al., 2011; Segal 1985). For example, a markedly larger (sparser) canopy cover in the pole (equator) facing slope resulting from the more extensive (meager) and mesic (xeric) vegetation cover, increases (decreases) its rainfall interception capacity, surface ponding time, and augments (reduces) the shallow infiltration (Inf_s) and the resistance of the soil to runoff (Q) and erosion (Gutiérrez-Jurado et al., 2007). The schematic shows a slightly larger Evapotranspiration (ET) on the equator facing slope than at its counterpart, with a larger contribution of soil evaporation (E) than transpiration

from shrubs (T_s) and grasses (T_g) (Boulanger, 2004). On the other hand, soil moisture storage is larger on the pole facing slope due to the more developed soils (i.e. thicker B horizons) (McMahon, 1998). While the conceptual ecohydrologic model of the opposing slopes aims to convey a simplified picture of terrain-vegetation-hydrologic interactions and their effects on the water fluxes and storages, also provides a parsimonious framework on which several hypotheses can be tested. For instance, the elements of the system represented with solid lines will be directly addressed and quantified in this study, whereas elements represented with dashed lines will not be quantified and will remain open questions to be addressed by further efforts.

In this study we pose the hypothesis that once the ecohydrologic dynamics of a place have been established, a series of feedback mechanisms emerge on each distinctive ecohydrologic unit, reinforcing its dynamics and modifying its environment to optimize the resources surrounding them. To test this hypothesis we conducted a field study in a first order basin of central New Mexico with nearly exact pole (north) vs. equator (south) facing slopes, and clear vegetation and terrain contrasts. We use observations from a network of sensors deployed along slope transects throughout the basin to quantify the spatio-temporal dynamics of energy and water fluxes of opposing north and south facing slopes. The first question we try to address is how do the observed differences in terrain properties and land-surface cover alter the energy balance of the slopes?, then we go on to ask how do the topographically mediated energy balance combined with the current ecosystem properties affect water fluxes into and out from the slopes?, and finally we attempt to summarize in a parsimonious way, how do the observed terrain-vegetation interactions translate into the hydrologic dynamics of the catchment. Our aim is to unveil the underlying mechanisms responsible

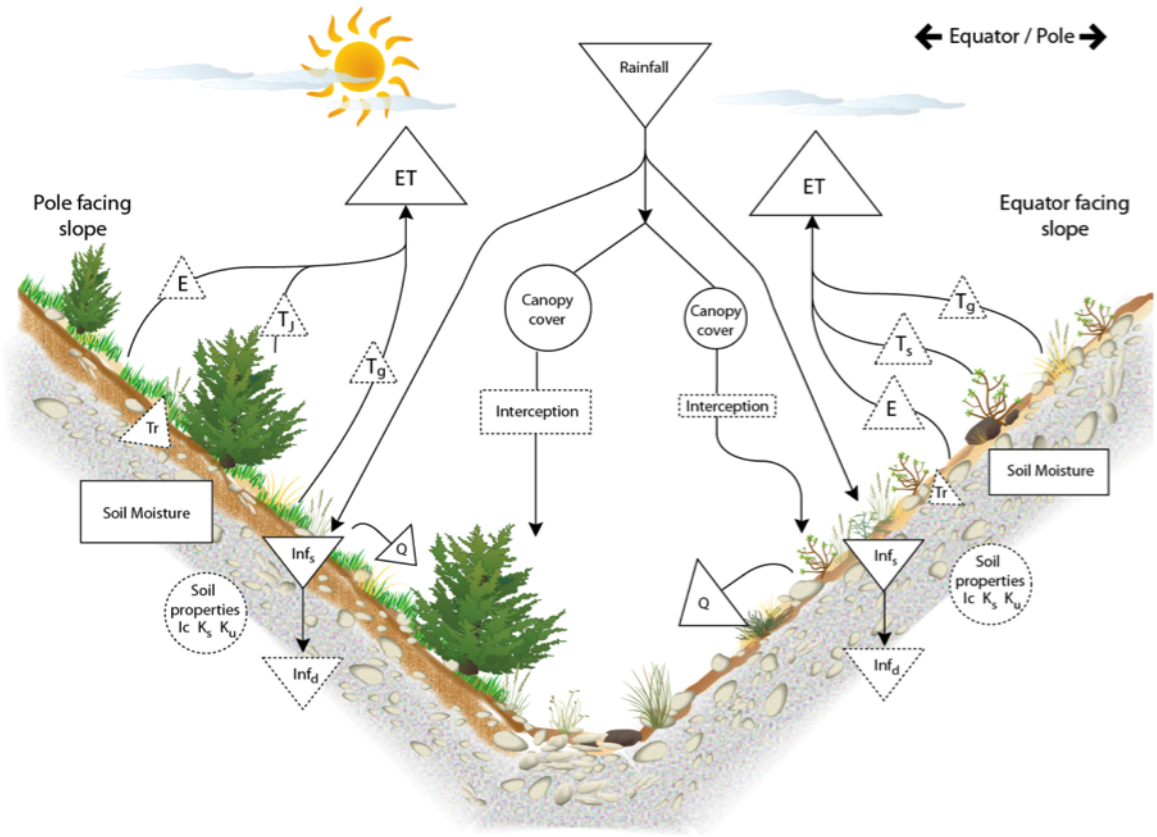

Figure 6.2: Schematic of water fluxes and storages of hypothetical opposing semi-arid slopes exhibiting differences in soils and vegetation composition and cover. The pole (equator) facing slope shows a thicker (thinner) A and B soil horizons with a deeper (shallower) calcic horizon, and a denser (sparser) and more mesic (xeric) vegetation cover. Water fluxes are represented by triangles pointing towards the direction of flux; water storages are represented by rectangles; system properties are depicted with circles. The size of each element attempts to illustrate the differences of fluxes, storages, and properties between the opposing slopes. The elements of the system represented with solid lines will be directly addressed and quantified in this study, whereas elements represented with dashed lines will not be quantified.

for the ecohydrologic patterns observed in the opposing slopes of the study basin. Along this way we will address the following specific questions:

1. To what extent topographically imposed terrain properties and processes (e.g., slope-aspect, vegetative cover, soil characteristics, and energy fluxes) modify the regional climatic regime (i.e., air and soil temperatures, air vapor pressure, near ground atmospheric momentum transfer) in the opposing slopes?

2. Are the residence times and dynamics of soil moisture significantly different between and within each slope-ecosystem?

3. Are the soils of the continuum NFS-EFS-SFS following a consistent trend in soil moisture and temperature and to what extent?

4. How does vegetation cover, soil structure, and slope position affect the production of runoff?

5. Are ET fluxes different between the contrasting slope-ecosystems and to what extent?

6. Are vegetation properties of the contrasting slopes reflected in the soil moisture-ET relations?

7. How are the hydrologic dynamics of the slopes affecting the water balance of each ecosystem?

This paper is organized as follows: In section 2 we describe in detail the materials and methods used in the study, including: a comprehensive description of the study area, the network and arrangement of instrument systems and transects, the study period length, the availability and characteristics of the field data, and the methods and techniques used to process and analyze the observations. In section 3 we present results from comparative analyses on the topographic

modulation of the radiation balance on the slopes followed by a characterization of the microclimatic differences between the opposing slopes; next, we present a number of analyses on terrain-vegetation effects on the dynamics of soil moisture of the slopes and proceed to the quantification and characterization of rainfall-runoff relations of the opposing slopes; finally we examine the effect of energy balance differences on the measured evapotranspiration of the slopes followed by analyses of soil moisture-evapotranspiration differences between the north and south-facing slopes. In section 4 we discuss the implications of the observed energy and hydrologic dynamics for the ecosystem properties and their possible feedbacks to the water balances and land-surface dynamics of the opposing slopes, and briefly summarize the role of terrain-vegetation interactions on the modification of land surface properties in advantage of distinct ecohydrologic dynamics and their corresponding vegetation communities.

6.2 Materials and Methods

6.2.1 Description of study area

The study area is a headwater basin or catchment ($\sim$0.1 km^2, Figure 6.3b; in this study the words catchment and basin are equivalent and used interchangeably) located in the northwestern corner of the Sevilleta National Wildlife Refuge, in central New Mexico (Figure 6.3a). The basin is part of a set of abandoned alluvial fans that give rise to a series of nested basins with various degrees of incision and characteristic vegetation contrasts resulting from different hillslope aspects (Figure 6.3b; Gutiérrez-Jurado et al., 2010). The study basin is basically

comprised of three aspect slope-aspects (north, south and east) with unique hydrologic, ecologic, and geomorphic properties. Vegetation structure and composition in the basin is clearly associated to variations in aspect, from which essentially two ecosystems emerge: a mesic Juniper-grass savanna on the north facing slope (NFS), and a xeric creosote shrubland on the south facing slope (SFS). In this basin the east facing slope (EFS) acts as the ecotone between the NFS and SFS ecosystems. Vegetation composition in the NFS is dominated by one-seed junipers (*Juniperus monosperma*; 20 % cover) in association with hairy and black gramma (*Bouteloa spp.*; 21% cover), while in the SFS, creosote bush (*Larrea tridentata*; 7.8% cover), mariola (*Parthenium incanum*; 6.6% cover), fluff grass (*Erionuron pulchellum*; 7% cover) and slim tridens (*Tridens muticus*; 6% cover) are the keystone species (McMahon, 1998).

The climate in the area is semiarid with mean annual temperatures of 20°C and two distinct rainy seasons: a summer monsoon with high intensity, short duration events and lower intensity, winter frontal storms with occasional snow precipitation (Milne et al., 2003). The hydrology of the study basin is strongly influenced by the distinct properties of the soils of the three slope-aspects (Gutiérrez-Jurado et al., 2006). In general terms, the soils of the study basin are composed of sandy matrices and $CaCO_3$ layers, some of which can intersect the inclined hillslope surface at various locations (Gutiérrez-Jurado et al., 2006).

McMahon (1998) documented remarkable morphological differences among the soils of the three slopes. In general, NFS soils have higher percentages of fines (i.e., silts and clays), organic matter and $CaCO_3$, as compared to SFS and EFS soils. The presence, stage of induration, development and depth of the $CaCO_3$ layers in the soils are all dependent on the magnitude and direction of soil moisture fluxes.

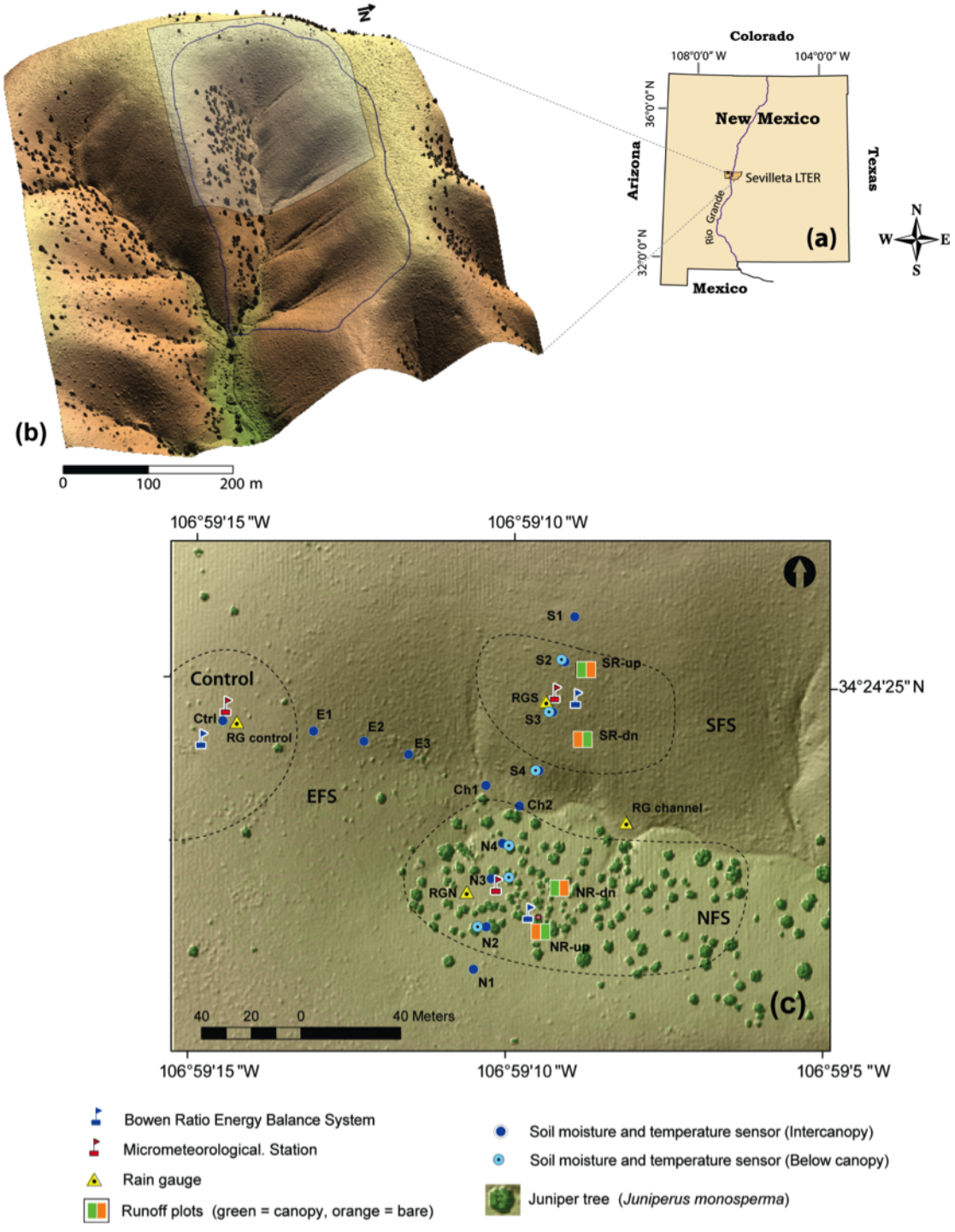

Figure 6.3: (a) Location of the Sevilleta National Wildlife Refuge within the state of New Mexico; (b) 3-D view of the study catchment with its boundary highlighted by a blue line, and showing the Juniper trees as black dots; (c) hillshade map of the study basin showing the location of the instruments (shaded area in (b)). Caption continues in next page.

The green circles on the map are Juniper trees; the blue flags depict the location of the BREBs; The red flags depict the location of the mMets; the blue solid circles show the location of an intercanopy soil moisture (SM) and soil temperature (ST) sensor, while the dotted light blue circles show the location of SM and ST sensors below canopies; the yellow dotted triangles show the raingages locations; the bicolored rectangles show the locations of the runoff plots sets, in which the green subrectangles are plots with trees or shrub canopies inside, and the orange subrectangles are plots with no trees or shrubs. The nomenclature of the sensors for each $\theta - T_s$ transect are identified with an N for the NFS, S for the SFS and E for the EFS, followed by a number indicating the position within the slope and increasing in the upslope direction. Figs. b and c were produced using a 0.5m resolution Digital Elevation Model derived from airborne LiDAR courtesy of the National Center for Airborne LiDAR Mapping (http://www.ncalm.org).

Therefore, variation in one or more properties of the soil $CaCO_3$ horizons reveal variations in the hydrologic properties of the slopes. Field observations in the soils of the study basin exposed substantial differences in the depth and stage of the $CaCO_3$ horizons among the soils of the three aspect slopes (McMahon, 1998; Gutiérrez-Jurado et al., 2006). For example, the depth to the $CaCO_3$ on the NFS soils is greater than that of the SFS soils, indicating deeper infiltration fronts on the NFS. On the other hand, the amount of $CaCO_3$ on the soils of the headslope (EFS) decreases in the downslope direction, suggesting flushing of the $CaCO_3$ by higher moisture fluxes in the soil. On the other hand, differences in soil properties between the north and south facing slopes are a result of higher vegetation cover in the NFS, leading to: (1) more dust and eolian particles trapping; (2) producing and incorporating higher amounts of organic matter into the soils; (3) enhancing infiltration into the soil profile; and (4) increasing $CaCO_3$ precipitation due to higher CO_2 partial pressures from plant root respiration (see McMahon, 1998 and Gutiérrez-Jurado et al., 2006). The soils of the headslope (EFS) do not follow the same patterns of the NFS and SFS soils. The EFS soils are for the most part well

drained soils and have decreasing $CaCO_3$ accumulation and at a greater depth moving downslope along the axis of the headslope.

6.2.2 Hydrologic instrument network

A network of instruments measuring hydrologic variables were deployed in the study basin to quantify the effect of terrain and vegetation in the dynamics of water and energy fluxes of the slopes. The instruments are grouped by systems and include: Bowen Ratio Energy Balance systems (BREB), micrometeorological stations (mMet), soil moisture (θ) and soil temperature (T_s) transects ($\theta - T_s$), and runoff plots (RP). Figure 6.3c shows the precise location of the instruments in the study basin obtained via a differential global positioning system (dGPS) survey. The arrangement of the instruments was designed in a way that permits the analysis of differences between the NFS and SFS by: 1) direct comparison of their data, and; 2) by benchmarking the data of the slopes to the data of a control location (Control) −in the upper flat surface above the EFS, where there is no effect of slope and aspect −when appropriate. As a result, the instruments systems are arranged as follows: there is one BREB, and one mMET for each one of the NFS, SFS and Control; there is one $\theta - T_s$ per slope (NFS, SFS and EFS) and three additional θ and Ts sampling locations, one at Control (labeled Ctrl), one at the channel head (labeled CH1) and one in a channel bed (labeled CH2) at the intersection of the NFS and SFS $\theta - T_s$; there are two sets of RP (2 runoff plots per set) for the NFS and SFS; finally, in addition to the raingages located at each mMET site, there is a raingage on a bank along the channel downstream of the $\theta - T_s$. A more detailed description of the instruments systems and their components are given in the following subsections. All data from the network of

sensors has been subject to quality control procedures, to avoid usage of unreal and extreme values in the analyses.

6.2.3 Study period and data availability

The period of observations in the study basin is shown in Figure 6.4, along with time series of daily rainfall and mean daily θ at the Control. Note that the length of data availability varies with instrument system. The longest period of data availability ($\sim$3.5 years) correspond to the mMets and $\theta - T_s$ (07/14/2006 - 12/31/2009), following the RP sets (07/07/2008 - 12/31/2009) and the BREB systems (08/07/2008 - 12/31/2009) with little less than $\sim$1.5 years of data. The study period commences in the middle of an exceptionally wet summer in 2006 (Gutiérrez-Jurado et al., 2007) when a sequence of unusually high pulses of rains sustained θ at levels close to saturation during that summer (Figure 6.4) and which moisture was not completely depleted until a year later. Note that throughout the duration of the observations the basin underwent various cycles of wet and dry periods. Characteristic wet peaks occur during the early to late summers from monsoonal rains and rewetting appears between the late fall to early winters with dry episodes intertwined in between. It is also noteworthy to observe the rapid θ recessions for summer peaks as opposed to the slow winter θ peak recessions, suggesting a seasonal control on the depletion rates of θ. Further analyses of θ, energy balance and micrometerological variables exploring this seasonal effects are presented in the results section.

6.2.4 Soil moisture and soil temperature networks

Volumetric soil moisture (θ) and soil temperature (T_s) were measured at two depths (10 and 20 cm) at canopy and intercanopy patches using CS-616 water

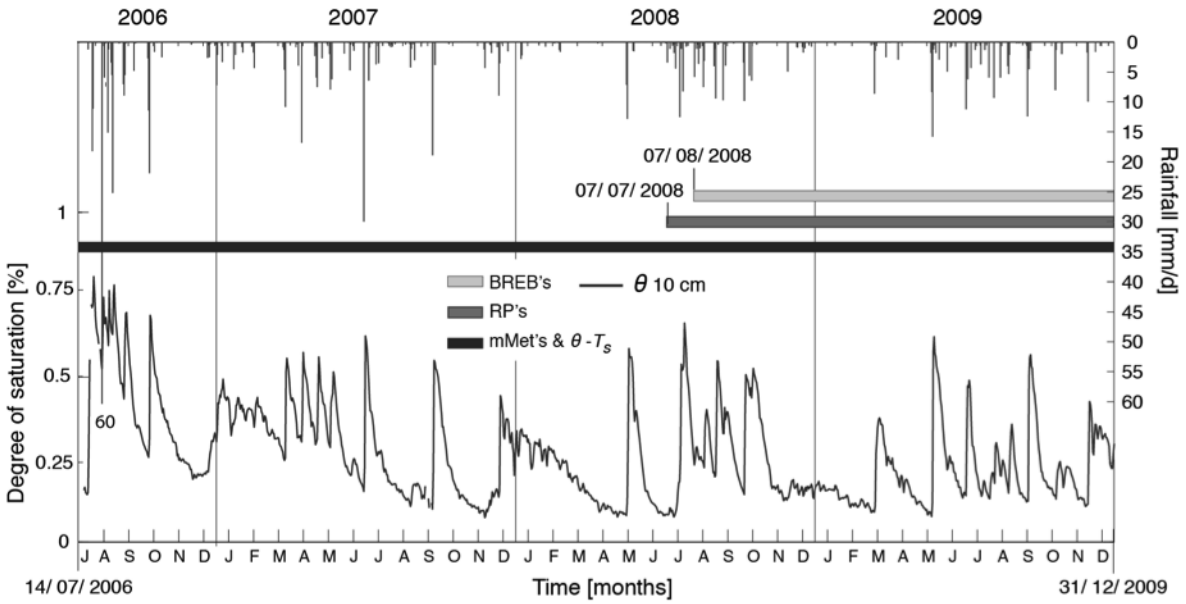

Figure 6.4: Shallow (10 cm) soil moisture (θ) and rainfall time series at the Control for the entire study period. The horizontal bars define the availability of data for the $\theta - T_s$ transects and mMet stations (black), BREB (light grey), Runoff plots (grey).

content reflectometers (WCR) for θ and 107-L temperature probes for T_s, both sensors from Campbell Scientific. The WCR and 107-L probes were placed in pairs parallel to the surface at each monitoring location and depth. θ and T_s were measured at 1 minute intervals and 30 min averages were recorded. In the following lines we provide detailed descriptions of the WCR and their operating principles.

WCR measure the resistivity of the soil to an electrical current, which is a function of the moisture content. The resistivity values obtained by the WCR were transformed to volumetric soil moisture (θ [m^3/m^3]) using a gravimetric calibration procedure. Due to the high heterogeneity of the soils gravel content, site-specific calibration of the sensors was performed on a number of sites. The calibration procedure included taking soil samples to the laboratory at various dates to determine: the gravimetric moisture content, the dry bulk density and

the soil porosity. The site-specific soil properties and calibration parameters for the θ monitoring locations are shown in Appendix D. For the locations where no site-specific calibration was performed, parameters from the nearest location were used and tested for coherence in θ results. The 107-L temperature probes do not require calibration. In this study we report values of volumetric soil moisture referred hereafter as θ, and soil moisture degree of saturation referred from now on as θ_s. The values for T_s are reported in °C.

6.2.5 Micrometeorology

A number of micrometeorology variables were measured on the NFS, SFS and Control locations (Figure 6.1c) using standard weather stations represented hereafter with the acronym mMet. At each mMet the following variables were recorded at 30 min. intervals into a C-1000 datalogger from Campbell Scientific: relative humidity (RH) in [%], air temperature (T_a) in [°C], windspeed (μ) in [m s^{-1}], wind direction (WD) in [degrees], rainfall (R) in [mm], and incoming shortwave radiation (SW_{in}) in [Wm^{-2}]. In order to characterize the micrometeorology of the NFS, SFS and Control locations and to investigate the effect of topography on the microclimatic differences of the opposing slopes we performed comparative analyses using time series of mean daily values for T_a, μ, and vapor pressure deficit (VPD; calculated using RH and T_a). Additionally, we included time series of mean daily T_s values for representative locations of the opposing slopes into the analyses mentioned above.

6.2.6 Runoff

Runoff was measured using runoff plots (RPs) deployed on the north and south facing slopes. The arrangement of the RPs on each slope is detailed in Fig-

ure 6.3. The RPs consist of 4x2 m exclusion plots connected to a flume where flow elevation is measured using Global Water WL400 pressure transducers located inside a stilling well. The flumes are of the HS type (Brakensiek et al., 1979), have horizontal floors and are made of fiberglass. In each plot runoff is collected in PVC tubes then funneled down a 2-ft long chute sloped 2° to the flume. The chutes, plot walls, and flume-supporting boxes are made of acrylic. Plot walls are buried 4-6 deep depending on terrain conditions. More details on the dimensions and design of the RPs are shown in Appendix C. Elevation values recorded in the flumes were converted to discharge (Q_s) values using a quadratic equation derived from a series of rating curves from the literature (Gwinn and Parsons, 1976). The resulting Q_s values were subject to quality control procedures to remove the effect of sensor drifting and sensor malfunction from the original data.

6.2.7 Energy balance and Bowen ratio

The energy balance at the land surface is described by the equation:

$$R_n + G + H + \lambda E = 0 \tag{6.1}$$

where R_n is the total net radiation on the surface in [Wm^{-2}], G is the soil heat flux in [Wm^{-2}], H is the sensible heat flux in [Wm^{-2}], and λE is the latent heat flux in [Wm^{-2}]. In this study we measured R_n and G directly and calculated H and λE using the Bowen ratio (β) method (Bowen 1926). The methods and equipment used to obtain each component of the energy balance are described in the following subsections.

6.2.7.1 Radiation

The four components of the radiation balance −shortwave incoming (SW_{in}), shortwave outgoing (SW_{out}), longwave incoming (LW_{in}), and longwave outgoing (LW_{out}) −were measured on the NFS, SFS and Control with identical double-sided CNR1 net radiometers. CNR1 radiometers measure the four components of the radiation balance using double-sided pyranometers for SW_{in} and SW_{out}, and double-sided pyrgeometers for the LW_{in} and LW_{out} (Campbell Sci., 1998). The radiometers were installed horizontally at ∼2 m height from the ground and away from any nearby obstruction on the Control and SFS locations, and as far away from Juniper trees as possible on the NFS. Because the radiometers were placed horizontally, corrections to account for the slope and aspect effects on the radiation components of the NFS and SFS were performed following a method by Tian et al., (2001). Details on the equations used for the correction of the radiation terms are given in appendix A. After correction of the corresponding shortwave and longwave radiation measured on the NFS and SFS, the net shortwave (SW_n), net longwave (LW_n) and total net radiation (R_n) for the three sites were calculated by subtracting the outgoing from the incoming components (i.e., $SW_n = SW_{in} - SW_{out}$, $LW_n = LW_{in} - LW_{out}$, and $R_n = SW_n - LW_n$). Finally, the albedo was also calculated using the ratio $alb = SW_{in}/SW_{out}$.

6.2.7.2 Soil heat flux

Soil heat flux density was measured at 5 cm depth below canopies and bare earth patches at each BREB location (NFS, SFS and Control) following a calorimetric based approach (Fritschen and Simpson, 1989). In this method, G

is obtained by adding the soil heat flux (G_p) at a reference depth (i.e., 5 cm) to the change in energy stored in the soil layer (CES) above the reference depth (Kimball et al., 1976). The appropriate measurements for soil heat flux calculations were done using REBS soil heat flux plates, temperature probes and Campbell Scientific water content reflectometers CS-616. Site-averaged values of all ground-surface variables for each location were calculated based on the weighted percent cover of canopy versus bare soil surface following Kurc and Small (2002). This was done using the equation:

$$v = fv_c + (1 - f)v_b \tag{6.2}$$

where v is a generic character that can be replaced to represent, soil temperature (T_s), soil water content (θ), or soil heat flux (G), the subscripts c or b indicate canopy or bare soil respectively, and f is the fractional canopy cover.

6.2.7.3 β and the Sensible and Latent heat fluxes

β is the ratio of sensible-heat (H) exchange to latent-heat (λE) exchange (Dingman 2000) and can be obtained as:

$$\beta = \frac{H}{\lambda E} = \frac{P \cdot c_a \cdot dT_a/dz}{(\lambda_v \cdot 0.622) \cdot /de/dz} \tag{6.3}$$

where P is atmospheric pressure in [kPa] taken as a constant for a constant height, c_a is the air heat capacity in [MJ kg^{-1}K^{-1}], λ_v is the latent heat of vaporization in [MJ kg^{-1}], 0.622 is the ratio of the gas constants for air and water vapor, dT_a/dz is change in air temperature (T_a) with height (z) in [°C m^{-1}], and de/dz is change in air vapor pressure (e) with height (z) in [kPa m^{-1}]. To obtain β in

the field we used identical REBS temperature and humidity probes mounted on an automated exchange mechanism (AEM) that switches the vertical location of the probes to eliminate potential bias on the sensors readings due to condensation and heating effects (Fritschen and Simpson, 1989). The vertical separation of the probes and specific set up for each monitoring location (i.e., NFS, SFS and Control) is shown in Table 6.1, and the approximate fetch (i.e., β sampling area) is shown in Figure 6.3c with dotted lines. Each fetch was calculated based on the height of the instruments relative to each other and to the height of vegetation, and the prevailing wind directions for each location (Figure 6.5) following (Nie 1992). β (equation 6.3) can be combined with the energy balance (equation 6.1) to obtain λE and H as:

$$\lambda E = -\left(\frac{R_n + G}{1 + \beta}\right) \tag{6.4}$$

$$H = -(R_n + G + \lambda E) \tag{6.5}$$

Table 6.1: Deployment set up for each Bowen Ratio Energy Balance system.

BREB system	**AEM separation distance** [m]	**Lower arm height** [m]	**Average canopy height*** [m]
Control	1.05	0.5	0.2
NFS	1.65	2.2	1.7
SFS	1.66	0.86	0.4

* Average canopy height was estimated from individuals within a 5 m radius.

Each of the components of β and the energy balance (i.e., BREB) were subject to strict quality control procedures. Errors in the quantified fluxes inherent to the BREB method for arid conditions were found and discarded following a

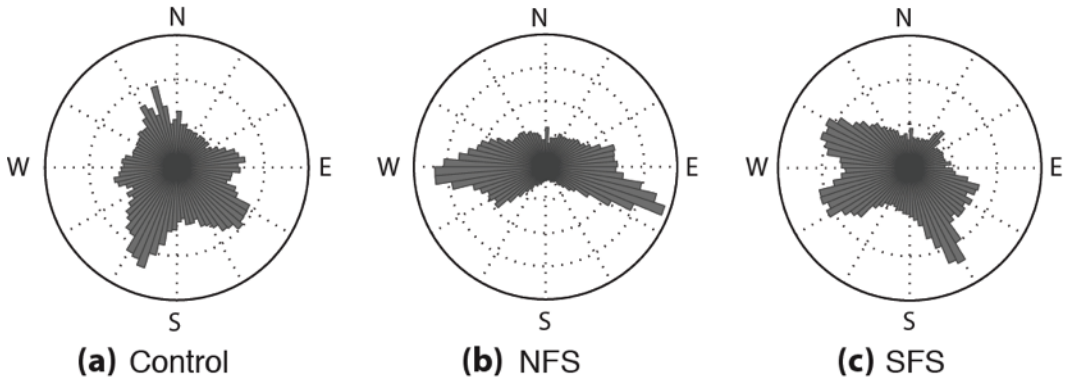

Figure 6.5: Rose plots of the predominant wind directions measured at the (a) Control; (b) NFS; and (c) SFS mMet stations respectively.

method by Perez et al., (1999). The resulting values for each of the four energy-balance components were examined for coherence and comparisons with values obtained in other locations of similar characteristics yielded good agreement (Kabat 1997; Kurc and Small 2002). Finally, to examine the causes of potential ET differences among the three locations we calculate and report values of midday available energy ($R_n - G$) and midday average values of the evaporative fraction (EF). (i.e., fraction of the available energy used to produce latent heat; equation 6.6). In this study we calculate midday values from 10:00 a.m. to 4:00 p.m.

$$EF = \frac{1}{1+\beta} \tag{6.6}$$

6.3 Results

6.3.1 Topographic modulation of seasonality on the radiation balance

The annual cycle for each radiation component is shown in Figure 6.6. Incoming shortwave radiation (SW_{in}) shows the most striking differences of all radiation components among the three locations (Figure 6.6a-c). The annual cycle of

SW_{in} shows a strong sinusoidal pattern with the highest values during the summer months and the lowest during the winter months (Figure 6.6b). This SW_{in} sinusoidal pattern is oppositely affected by the combined slope-aspect properties of the terrain; while the SW_{in} seasonal variation in SFS is dampened, on the NFS is greatly amplified. Because in all cases (i.e., NFS, Control, and SFS) SW_{out} is only minor compared to SW_{in}, and because LW_n is relatively constant throughout the year in the three locations, the resulting R_n preserves the same pattern of the SW_{in}. As a result, during the lowest SW_{in} period from mid-October to late February, the daily energy flux from R_n for the NFS is negative ($<$0 MJ/d), for the Control is close to neutral (i.e., $\sim$0 MJ/d), and for the SFS remains positive and high ($\sim$7-8 MJ/d). This topographic modulation of the seasonality in R_n is also reflected on the albedo of the three locations; on the NFS there is a strong increase in albedo during the winter months, a slight increase is noted for the Control, and a slight decrease is shown for the SFS during the same period.

To further explore the slope-aspect modulation effect on the seasonality of the different radiation components we calculated diurnal seasonal averages of each radiation component for each location. In this study we distinguish four seasons: Summer (Jun. 21-Sept. 23), Fall (Sept. 23-Dec. 21), Winter (Dec. 21- Mar. 21), and Spring (Mar. 21-Jun. 21). For each season of the year, significant differences in diurnal average incoming radiaton ($\overline{SW_{in}}$) among the three locations were found (Figure 6.7a-d). In all the cases $\overline{SW_{in}}$ follows a consistent pattern: SFS shows significantly the highest $\overline{SW_{in}}$ throughout the year, followed by the Control and with the NFS showing always the lowest $\overline{SW_{in}}$ values. Notably, $\overline{SW_{in}}$ in the SFS shows little variability throughout the year compared to the Control and NFS locations, where a strong $\overline{SW_{in}}$ seasonal variation is observed. This has a strong effect on $\overline{R_n}$ given that $\overline{LW}$ differences between the sites are minimal

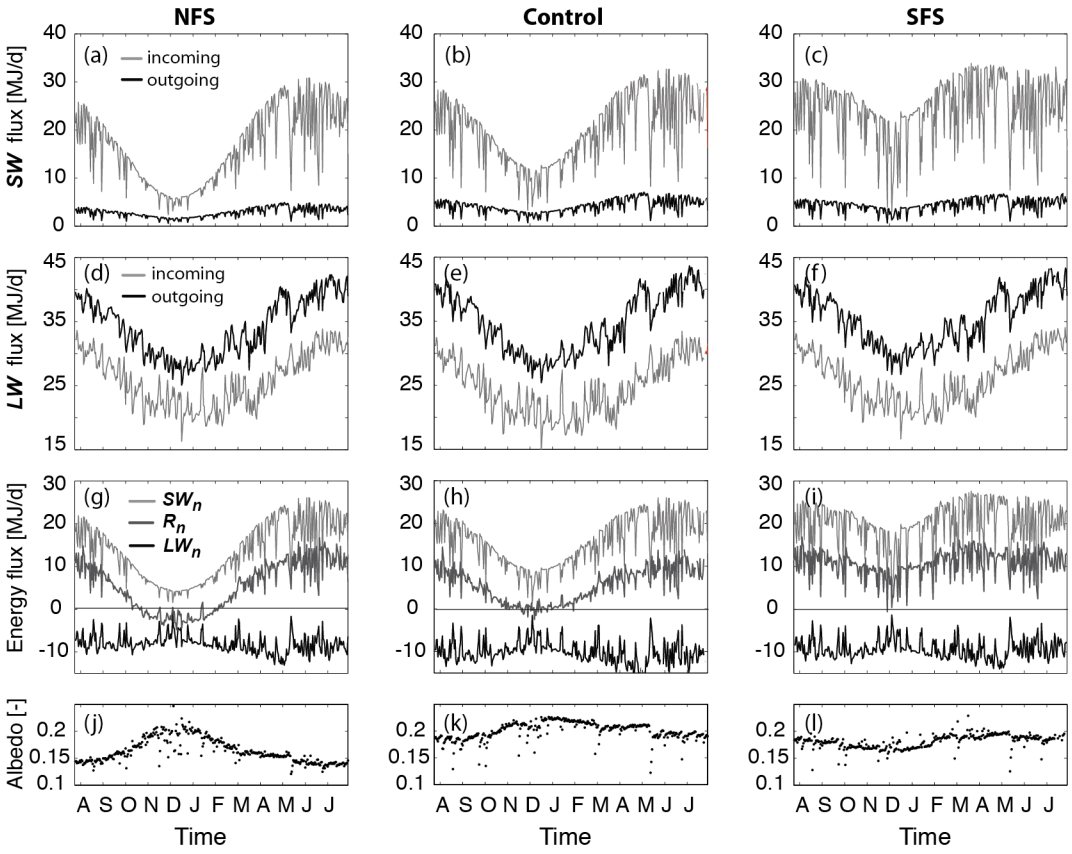

Figure 6.6: Typical annual variation of the radiation balance components for each BREB location: (a,b,c) show the shortwave components for the NFS, Ctrl, and SFS; (d,e,f) show the Longwave components for the NFS, Ctrl, and SFS; (g,h,i) show the R_n, SW_n, and LW_n components for the NFS, Ctrl, and SFS; (j,k,l) show the variation in albedo for the NFS, Ctrl, and SFS.

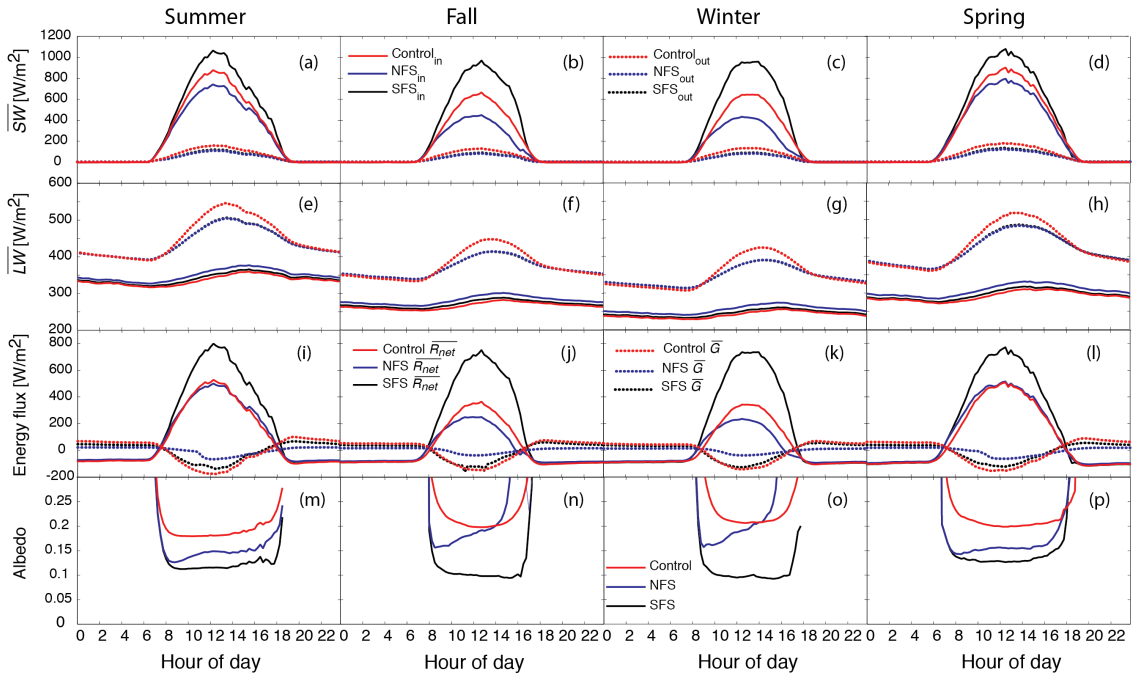

Figure 6.7: (a h) Diurnal cycle seasonal averages of the slopes (blue-NFS, black-SFS, red-Control) for each radiation balance component (shortwave-first row; longwave-second row); (i-l) Diurnal energy flux cycle seasonal averages of the NFS (blue line), SFS (black line) and Control (red line), where solid lines depict the net radiation (R_n) and dotted lines show ground heath fluxes (G); (m-p) Diurnal cycle seasonal averages of albedo for the NFS (blue line) SFS (black line) and Control (red line).

compared to the $\overline{SW}$ component (Figure 6.7e-h). Overall, the general pattern on the effect of aspect on the radiation balance of the slopes shows that north facing slopes enhance seasonal differences specially through the fall and winter times, while the effect of aspect on the south facing slopes is to dampen the seasonal variability in R_n. These results provide evidence supporting the hypothesis that energy balance differences resulting from increased (reduced) seasonal variability towards north (south) facing slopes act as a main driver of the ecohydrologic differences expressed in the opposing slopes.

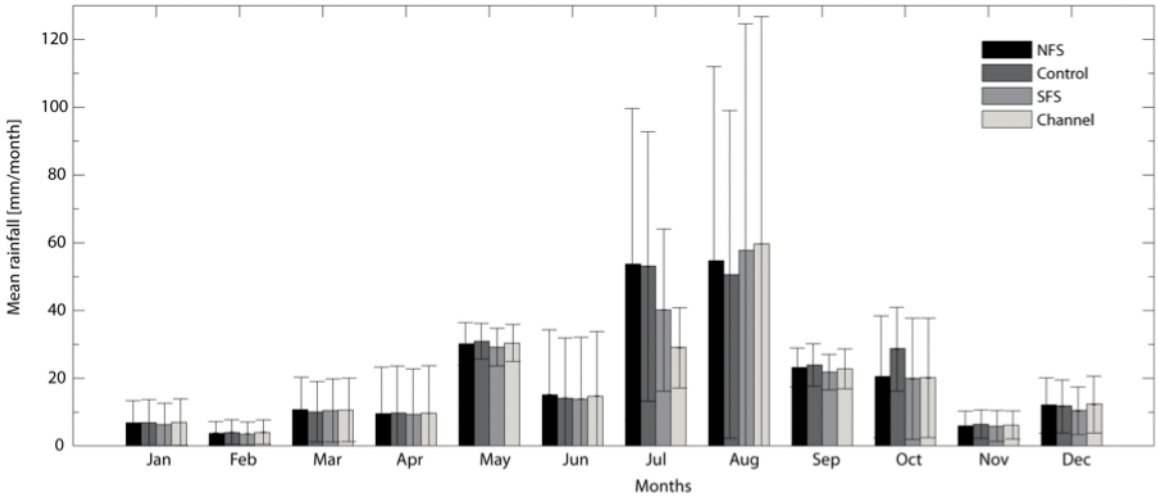

Figure 6.8: Monthly averages of rainfall for each raingage deployed in the study basin; NFS (black), Control (dark grey), SFS (light grey), Channel (white). The vertical lines show $\pm$ one standard deviation.

6.3.2 Micrometeorology of the slopes

In this section we show the differences in micrometeorology among the Control, NFS and SFS. We evaluate the effect of terrain slope and aspect on the modification of rainfall patterns, air and soil temperature, vapor pressure deficit, and windspeed at a screen height of $\sim$2m from the local surface.

6.3.2.1 Rainfall variability

Figure 6.8 shows the variation of the mean monthly rainfall and corresponding standard deviations for each raingage in the study basin. Although the period of record in the basin is relatively limited ($\sim$3.5 yrs), a number of temporal rainfall patterns can be readily recognized. For instance, the largest proportion of the annual precipitation falls within the months from May to October, while from November to April mean monthly rainfall is lower than 15 mm and exhibits little variability compared to the months with high rain amounts. The influence of the

North American monsoon can be clearly observed during the summer months where the mean monthly averages for July and August rise above 50 mm (i.e., $\sim \frac{1}{4}$ of the mean total annual rain). An important aspect of Figure 6.7 is that shows the spatial variability of the rainfall within the study basin. Generally, mean monthly rainfall values for all the locations in the basin (i.e., NFS, Control, SFS, and Channel) are very similar. Nevertheless, our records show there can be substantial differences in mean monthly rainfall among the four locations during the summer months. This is particularly pronounced for the month of July, when differences among all locations are largest, and in some instances can account for as much as 50% reduction in rainfall (NFS-Control vs. Channel). It is possible that these differences are related to a combination of the directionality of the rainfall and some topographic sheltering (Ivanov et al., 2008.b).

6.3.2.2 Topographic induced microclimatic differences

To investigate the effect of topography on the microclimatic variations of the opposing slopes, we plotted the NFS and SFS differences (Δ) with respect to the Control (e.g., Δ_{NFS} = NFS - Control, and Δ_{SFS} = SFS - Control), of the mean daily values for the following variables (Figure 6.9b-e): air temperature ($\overline{T_a}$, in [°C]), shallow (10cm) soil temperature ($\overline{T_s}$, in [°C]) at the midslope intercanopy (N3 and S3) and canopy (cN3 and cS3) locations, vapor pressure deficit ($\overline{VPD}$, in [Δ%]), and wind speed (i.e., momentum transfer) ($\overline{\mu}$, in [Δ%]). To serve as a reference for the interpretation of the micrometeorological comparisons, Figure 6.9a shows the time series of daily SW_{in} at the Control for all the study period. For $\overline{T_a}$, $\overline{T_s}$ and $\overline{VPD}$, there is an apparent seasonal effect on Δ_{NFS} (Figure 6.9b,c and d). $\overline{T_a}$ and $\overline{VPD}$ Δ_{NFS} follow closely the variations in SW_{in}, reaching peak (positive)

values in the summer months (i.e., June through August) and finding their lowest (negative) numbers during the late Fall and Winter months (i.e., November to February). On the other hand, $\overline{T_a}$ and $\overline{VPD}$ Δ_{SFS} do not follow the seasonal pattern of their counterparts. Instead, Δ_{SFS} $\overline{T_a}$ shows an overall negative trend, with positive values through the first year and half (Aug-2006 to Dec-2008) and negative values in the last year of data (2009), while Δ_{SFS} $\overline{VPD}$ shows consistently positive values, fluctuating around 8% Δ throughout the whole study period. In a similar manner, Δ_{NFS} $\overline{\mu}$ and Δ_{SFS} $\overline{\mu}$ (Figure 6.9e) do not follow a seasonal pattern during the study period but rather show consistently negative values, which fluctuate around -20% for Δ_{SFS} $\overline{\mu}$ and around -50% for $\Delta_{NFS}\overline{\mu}$. Perhaps the graph that best reflects the modulating effect of topography on the seasonality of the microclimatic patterns of the slopes is that of $\Delta\overline{T_s}$ (Figure 6.9b). Both Δ_{NFS} and $\Delta_{SFS}\overline{T_s}$ show a strong seasonal signal but with opposite effects, with negative (Δ_{NFS}) and positive (Δ_{SFS}) differences growing towards the winter months and decreasing to a minimum ($\Delta_{SFS} \approx 0$ & $\Delta_{NFS} \approx 0$) when approaching the summer months. It is worth noting that during large periods of the winter, $\Delta\overline{T_s}$ between NFS and SFS can be as large as 10 °C. Also, note the different effect of canopy cover on the opposing $\Delta\overline{T_s}$, while on the NFS the Juniper canopy dampens the seasonal signal by preserving Δ_{NFS} more or less constant ($\sim$ -3 °C), on the SFS the shrub canopy follows the same seasonal pattern of the intercanopy Δ_{SFS}.

6.3.3 Soil moisture dynamics of the slopes

To assess the differences in soil moisture dynamics of the slopes at the root zone ($\sim$0-25 cm depth), and to address the question on how the combined effects of topography (i.e., aspect and slope position) and land cover properties (i.e., vegetation cover and soil properties) affect the hydrologic behavior of the slopes, we

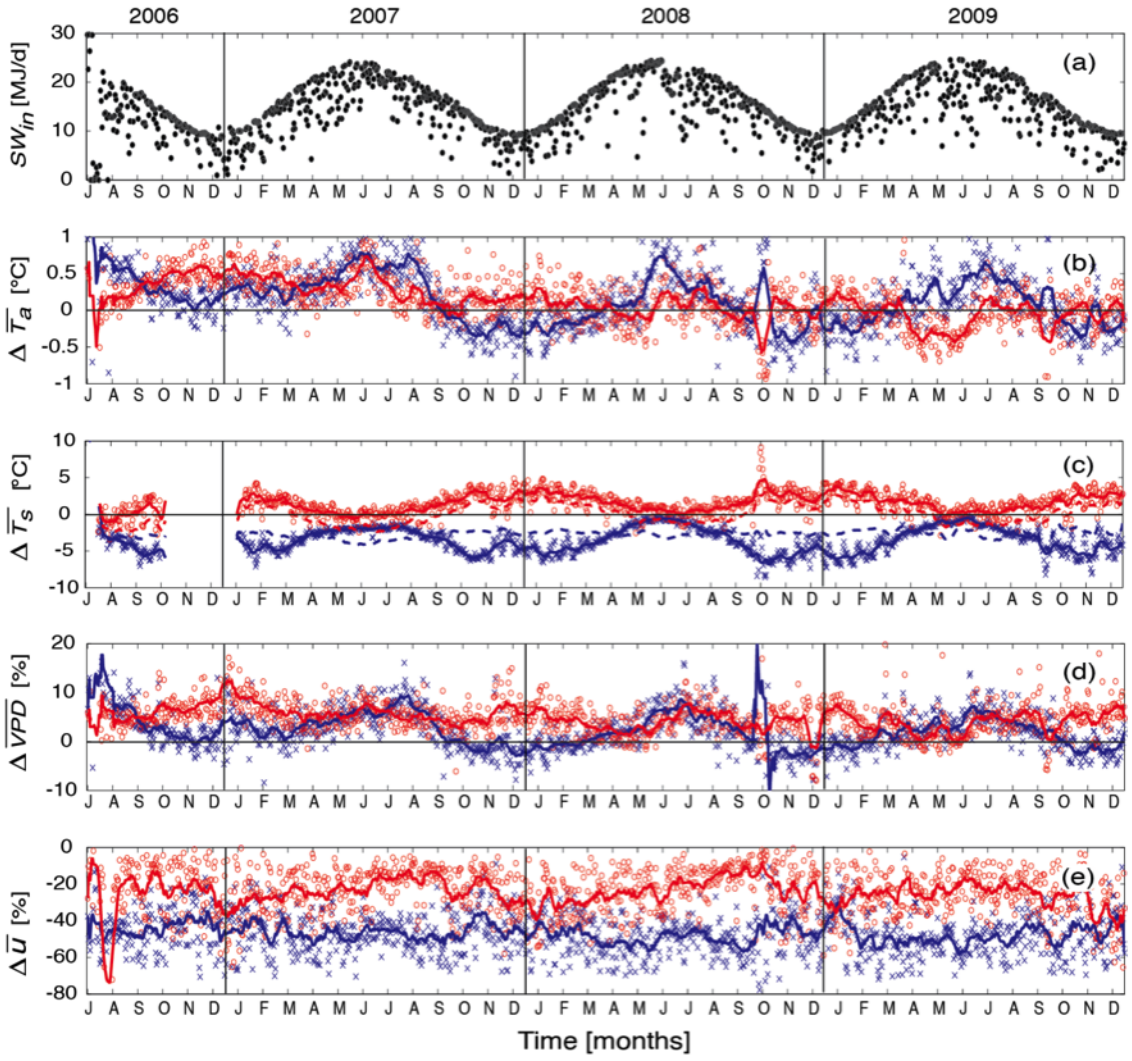

Figure 6.9: Comparative time series of micrometeorological variables from NFS (blue crosses) and SFS (red circles) observations with respect to the Control. (a) Incoming shortwave radiation (SW_{in}) at Control; (b) Difference in mean daily air temperature ($\Delta\overline{T_a}$) in [°C]; (c) Difference in mean daily shallow (10 cm) soil temperature ($\Delta\overline{T_s}$) in [°C]; (d) Percent [%] difference in mean daily vapor pressure deficit ($\Delta\overline{VPD}$); (d) Percent [%] difference in mean daily windspeed ($\Delta\overline{\mu}$). The solid lines in (b-e) show a 15 days moving average of the NFS (blue) and SFS (red) observation differences (Δ) with respect to the Control in each variable. The dotted lines in (c) depict the $\Delta\overline{T_s}$ 15 days moving averages below the canopies of Junipers (blue) and Creosotes (red).

conducted a series of analyses based on time series of soil moisture for ∼3.5 years of data. Figure 6.10 shows soil moisture time series given as degree of saturation (θ_s) for five representative locations within the study basin (Figure 6.10b-f), and a hyetograph from the raingage at the Control to aid in the interpretation of the data (Figure 6.10a). The dynamics of θ_s from the time series reveal a clear drying trend for the study period. This trend is stronger at the Control and NFS locations (Figure 6.10b, and d), partly because it is apparent that the soils at these places preserved the moisture pulses from the 2006 summer and 2006-2007 winter rains for longer time. For the NFS a noticeable interception effect from the Junipers is observed on θ_s when comparing the intercanopy (θ_{si}) and canopy (θ_{sc}) data. This interception effect is not observable however, for the Creosote shrubs on the SFS. On the contrary, θ_{sc} on the SFS shows responses even for short amounts of rainfall that θ_{si} does not see, which may be an indication of canopy interception-funneling and stemflow rainfall concentration of the Creosote shrubs (Martinez-Mesa and Withford, 1996). A distinct feature of the EFS and SFS θ_s series is the null differences between the moisture observed at 20 and 10 cm depth for all rainfall amounts. On the other hand, Control and NFS θ_s series do show differences between the observations at 10 and 20 cm for moderate-to-low rainfall events, with a highly responsive θ_s at 10 cm and slight to non-responsive 20 cm θ_s. The differences in the responses of θ_s with depth to the magnitude of rainfall between Control-NFS and EFS-SFS soils indicate different infiltration behaviors and merit a more detailed exploration looking at all the θ_s monitoring locations.

6.3.3.1 Topographic-vegetation effects on soil moisture residence times

Seasonal averages of soil moisture decay curves after significant rainfall events (>7mm) were computed for each sampling location and the resulting time

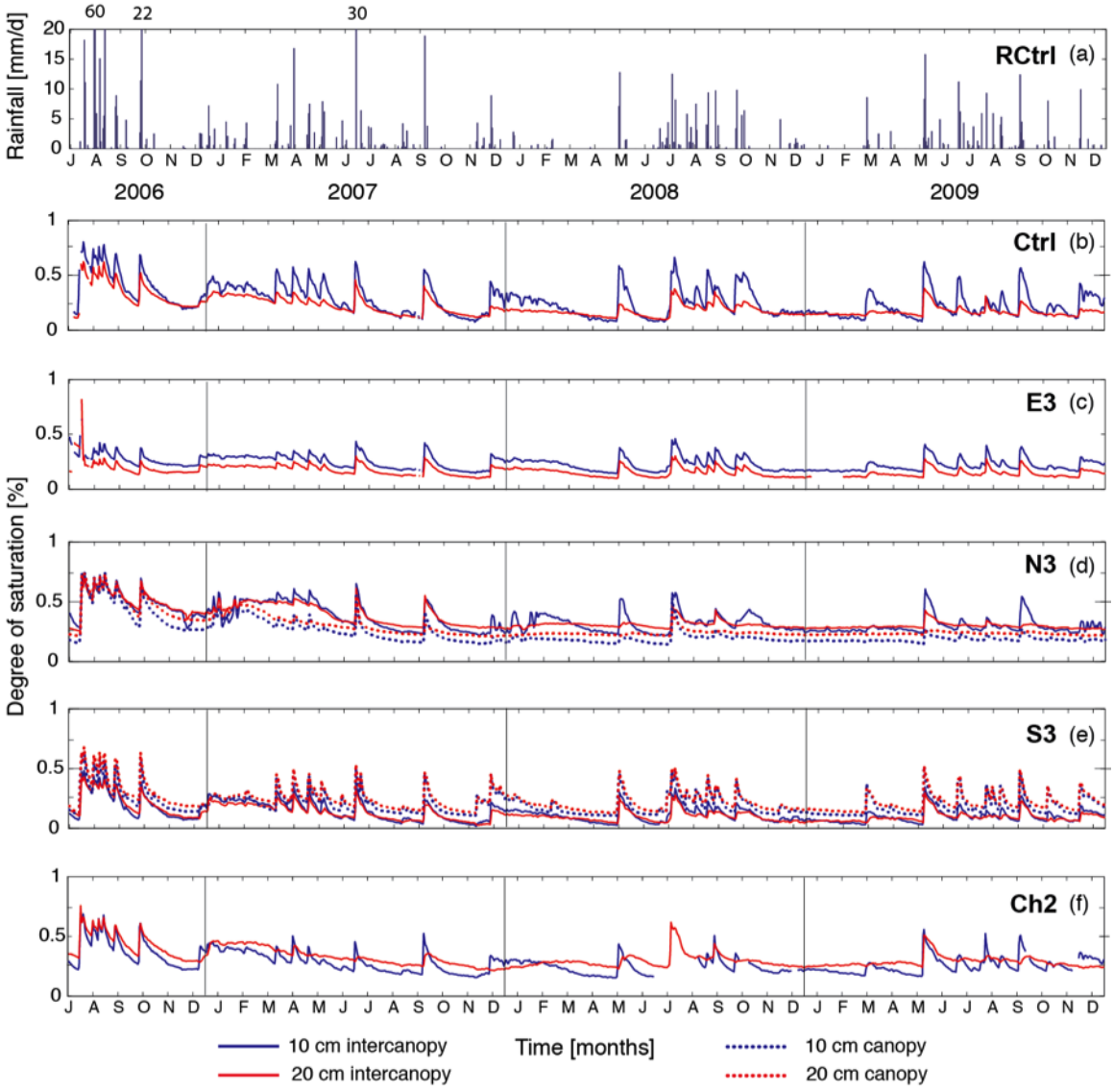

Figure 6.10: Time series of rainfall (a) and soil moisture (b,c,d,e,f) at 10 cm (blue lines) and 20 cm (red lines) depths, at intercanopy (solid lines) and below canopy (dotted lines) locations within the NFS. The soil moisture is shown as degree of saturation ($S = \theta/n$, where θ is volumetric water content and n is porosity) in percent [%].

constants (τ) plotted as surrogates of rainwater residence times. The results are shown in Figure 6.11. In general, soil-moisture residence times (i.e., τ) vary significantly with season, aspect and slope position and at intercanopy and below-canopy locations at 10 cm depth within the soil. For instance, during the summer, τ is in average 2 days longer for the north-facing soils for all slope locations compared to the south-facing soils at the same slope positions. Differences between SFS and NFS τ decrease notably during the Fall when all intercanopy τ approximate the value of τ at the Control location. On the other hand, the largest differences observed between NFS and SFS soils occur during the spring time, with τ diverging as much as 5 days between the top slope positions on the NFS and SFS. It is also in the springtime when differences in τ with slope position within a single ecosystem are larger. For instance, τ differences for both the EFS and SFS top and bottom slope locations are as large as $\sim$4.5 days, while differences for the same locations along the NFS can account for $\sim$3.5 days. In general, the effect of the canopies on the dynamics of soil moisture is to reduce τ for both, NFS and SFS. However, the largest differences between canopy and intercanopy τ occur during the spring time, where they will depend on slope position, with the bottom locations showing the greatest differences (e.g., 5 days on the SFS and 3 days on the NFS). In summary there appears to be a strong control of seasonality and topographic location (i.e., location on the slope) on the dynamics of soil moisture residence times that can be related to the expected variations in ET and drainage (e.g., soil properties) imposed by topographic and vegetation factors.

6.3.3.2 Temporal stability of θ and T_s

To examine the terrain (slope-aspect-soils) and vegetation effects on the spatial and temporal patterns of θ and T_s, we performed temporal stability anal-

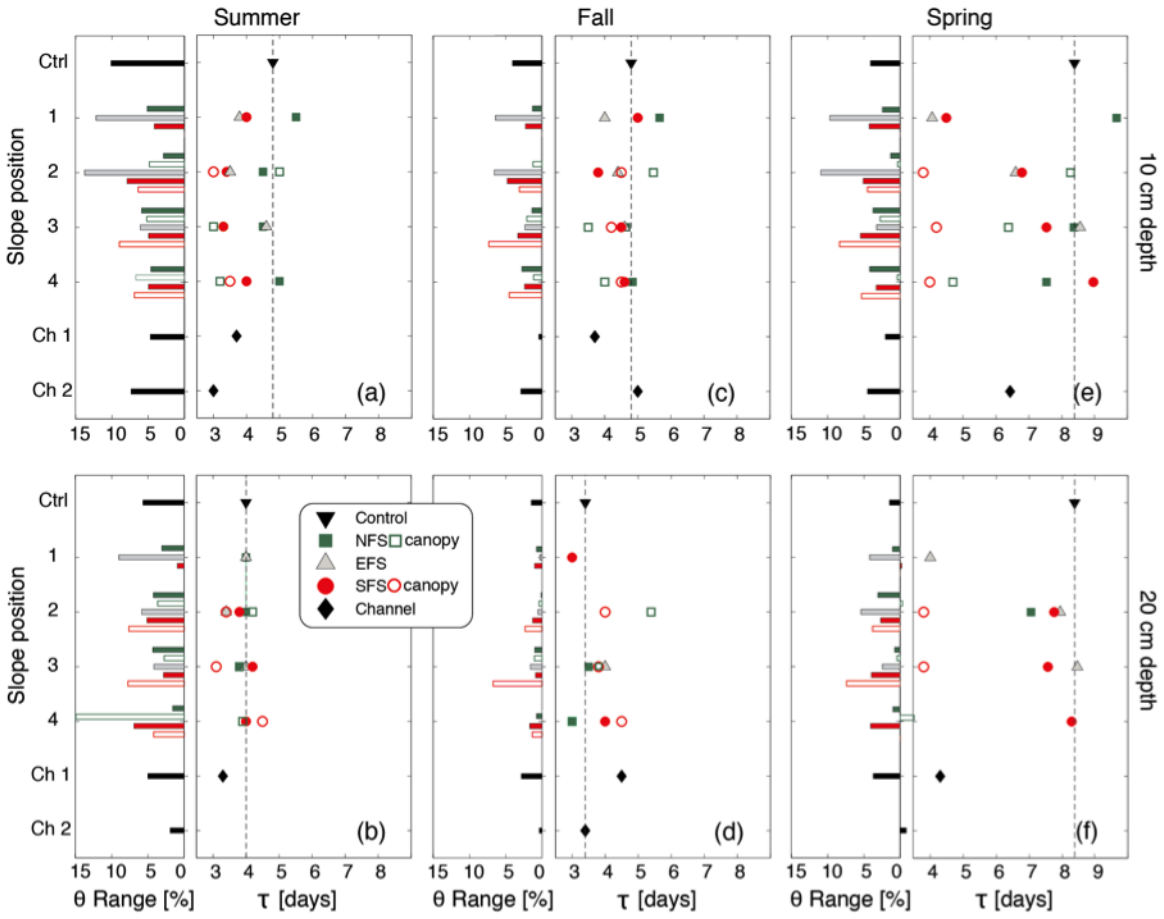

Figure 6.11: Plots of volumetric soil moisture (θ) residence times (τ) in [days] and their corresponding θ range in [%] for all the sampling locations (black triangle-Control, solid green squares-NFS intercanopy, open green squares-NFS below canopy, gray triangles-EFS, solid red circles-SFS intercanopy, open red circles-SFS below canopy, black diamonds-channel locations), organized by seasons (summer-left column, fall-mid column, spring-right column) and soil depth (10 cm depth-first row, 20 cm depth-second row). The coloring of the bars showing the volumetric θ range follows the same order of their symbol counterparts.

yses for all the monitoring points of the $\theta - T_s$ transects, following a similar approach to those by Lin (2006), Martinez-Fernández and Ceballos, (2003) and Grant et al., (2004). We calculated the time average ($\overline{\delta_i}$) of relative difference for the mean daily θ in degrees of saturation ($\overline{\delta_i}(\overline{\theta_s})$) and mean daily T_s ($\overline{\delta_i}(\overline{T_s})$) using the method of Vachaud et al., (1985) modified to explicitly account for the relative difference of each monitoring site with respect to the Control values, as follows:

$$\overline{\delta_i} = \frac{1}{m}\sum_{j=1}^{m}\delta_{ij} \tag{6.7}$$

$$\delta_{ij} = \frac{v_{ij} - v_{Ctrl\cdot j}}{v_{Ctrl\cdot j}} \tag{6.8}$$

where, m is the number of monitoring days, δ_{ij} is the value of the subject variable v (i.e., $\overline{\theta_s}$ or $\overline{T_s}$) at a given depth, at site i, and on measurement day j, and $v_{Ctrl\cdot j}$ is the value of the subject variable at the Control on day j. For these analyses, positive values of $\overline{\delta_i}(\overline{\theta_s})$ ($\overline{\delta_i}(\overline{T_s})$) indicate higher $\overline{\theta}_s$ ($\overline{T}_s$) values year round relative to the values at the Control; likewise, negative $\overline{\delta_i}(\overline{\theta_s})$ ($\overline{\delta_i}(\overline{T_s})$) indicate lower $\overline{\theta}_s$ ($\overline{T}_s$) values than those at the Control, irrespective of measurement time. Additionally, the standard deviation (σ) for each $\overline{\delta_i}$ was calculated as a way to identify the most time stable locations (i.e., lowest $\sigma(\delta_i)$) (Vachaud et al., 1985; Lin 2006).

Figure 6.12 presents joint $\overline{\theta}_s$ and $\overline{T}_s$ time stability plots, showing $\overline{\delta_i}(\overline{\theta_s})$ vs. $\overline{\delta_i}(\overline{T_s})$ and their corresponding $\sigma(\delta_i)$ for (a) 10 cm and (b) 20 cm soil depths for all sampling locations. In these plots each point is labeled with numbers relative to their slope position (Figure 6.3). Note a missing value for the 10 cm N4 location in the plot space as a result of anomalous high temperature readings not detected

by the quality control procedures of the data. The graphs neatly illustrate the effect of topographic location and vegetation cover on the temporal stability of $\overline{\theta}_s$ and $\overline{T}_s$. There is a clear progression in $\overline{\delta_i}(\overline{\theta_s})$ and $\overline{\delta_i}(\overline{T_s})$ values from NFS to EFS and SFS locations; with the NFS points located at the wetter and cooler end of the spectrum (upper left quadrant) followed by the EFS points, with $\overline{\delta_i}(\overline{\theta_s})$ values similar to those on the NFS and $\overline{\delta_i}(\overline{T_s})$ values close to the Control, and finally SFS points, located at the drier and warmer end of the spectrum (lower right quadrant). This result is consistent with the transition in vegetation type (i.e., mesic to xeric), cover, and soils documented by McMahon (1998) and Gutiérrez-Jurado et al., (2006).

In general, the temporal stability plots reveal less stable (larger $\sigma(\delta_i)$s) and more clustered data points for each group (i.e., NFS, EFS, SFS) at 10 than at 20 cm. This is an indication that the soils become more hydrologically heterogeneous going deeper into the root zone. Interestingly, the EFS and intercanopy SFS data points exhibit some spatial organization for both $\overline{\theta}_s$ and $\overline{T}_s$ within the slope that is preserved at both depths. In the SFS intercanopy points the soils become drier progressing from the top to the bottom of the slope, and preserve the same pattern in $\overline{\delta}_i(\overline{T}_s)$. In the EFS points there appears to be a transition from a very Control-similar top-slope E1 location to a wetter and warmer upper midslope E2 location to a finally drier lower midslope E3 location. On the other hand, the effect of slope position on the NFS data points is overridden by the heterogeneity imposed by vegetation. Note the stabilizing influence of the Juniper canopies on the consistency of soil temperature for both depths (10 and 20 cm). Furthermore, an interception effect of the canopy on the NFS points is also apparent, with two of the three canopy monitoring locations at both depths permanently drier than the Control and the rest of the NFS points. Finally, the

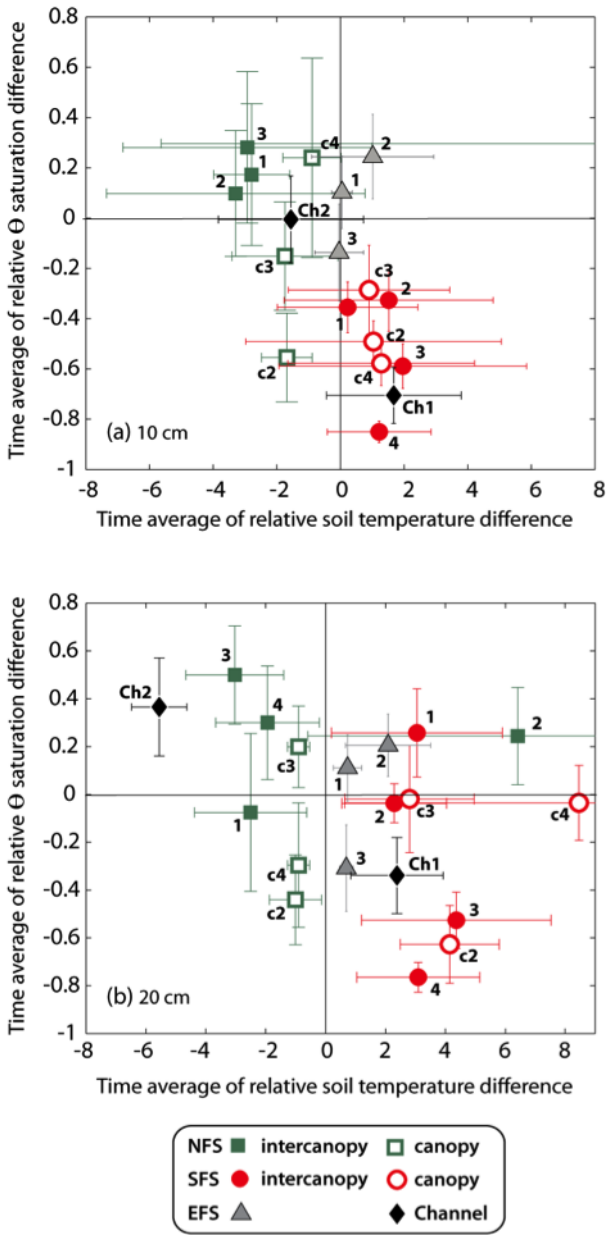

Figure 6.12: Joint temperature and θ saturation time stability plots showing the time average of relative difference in soil temperature ($\overline{\delta_i}(\overline{T_s})$) plotted vs. the time average of relative difference in θ saturation ($\overline{\delta_i}(\overline{\theta_s})$) for (a) 10 cm and (b) 20 cm soil depth for all sampling locations. Green solid (open) squares depict NFS intercanopy (canopy) locations, red solid (open) circles depict SFS intercanopy (canopy) locations, grey triangles depict EFS locations, and black solid diamonds show the location of the channel banks sampling points. Numbers next to data points indicate slope location. Vertical lines show $\pm$ one standard deviation in $\overline{\delta_i}(\overline{\theta_s})$ and the horizontal lines show $\pm$ one standard deviation in $\overline{\delta_i}(\overline{T_s})$. All points are plotted relative to the temperature and θ values of the Control location (i.e., 0,0 coordinate in the plots).

channel points exhibit markedly different $\overline{\theta}_s$ and $\overline{T}_s$ behaviors. While the channel head (Ch1) clusters well with the SFS data in the warmer and drier quadrant, the channel bank (Ch2) resembles more the NFS intercanopy points. This may be an indication of differences in hydrologic connectivity for different sections along the channel.

6.3.4 Runoff on the opposing slopes

To characterize the differential runoff (Q) responses to rainfall (P) in the opposing north and south facing slopes we present a suite of analyses on the reported $\sim$1.5 years of Q data. Tables 6.2 and 6.3 show summaries of the characteristics for each runoff event recorded at each runoff plot (RP) during the study period, and Figure 6.13 summarizes the Q behavior of the opposing slopes grouped by land surface cover type (i.e., canopy and intercanopy).

A convenient metric to compare the responses of Q to P between the slopes is the runoff ratio (Q/P) that informs the amount of P that is converted into Q (Dingman 2000). Figure 6.13.a shows the distribution of Q/P for each slope major category. For the majority of the runoff events recorded on the NFS a 13% or less of the rainfall was converted into runoff ($Q/P \leq 0.13$), and only a few times that number exceeded 20% ($Q/P \geq 0.2$). On the other hand, for the SFS plots half the events presented $Q/P \leq 0.1$, and the other half spread between 0.1 and the maximum value recorded of 0.7 Q/P. The differences in Q/P between the opposing slopes and categories are consistent with the total amounts of runoff (ΣQ_T) during the study period (Figure 6.13b). On the SFS plots ΣQ_T was 5 to 6 times higher than on the NFS plots. Similarly, SFS plots recorded a greater number of Q events than NFS plots; the highest Q frequency was registered on the

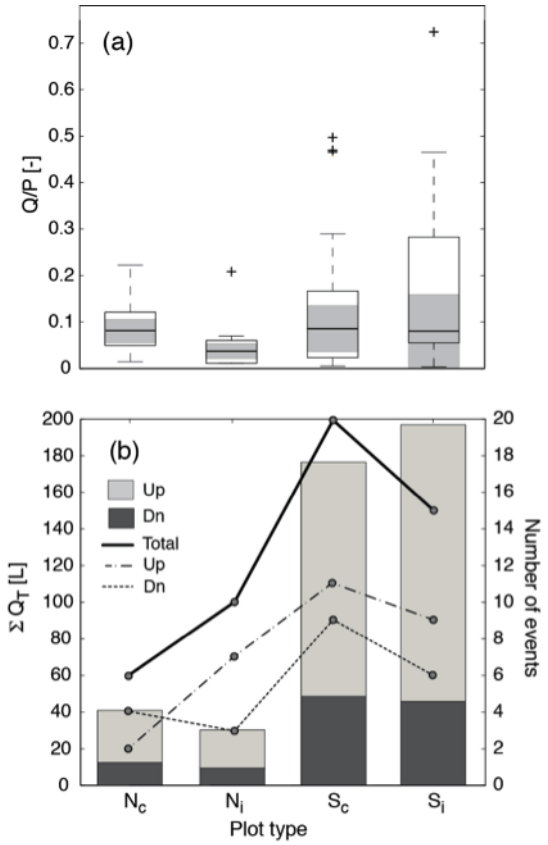

Figure 6.13: (a) Boxplots of event runoff ratio for each plot type: North facing-canopy (N_c), North facing-intercanopy (N_i), South facing-canopy (S_c), and South facing-intercanopy (S_i); (b) histograms of total runoff (upslope + downslope) during the RPs study period for each plot type, N_c, N_i, S_c, and S_i. Each histogram bar is divided by contribution of upslope (light gray) and downslope (gray) locations. The lines depict the number of events producing runoff for the downslope (dotted), upslope (dashed), and the total (solid) for each plot type.

Table 6.2: Characteristics of recorded runoff events on the NFS during the study period. P_E is total event rainfall, T_{LP} is time lag to peak, Q_T is total runoff, Q_P is peak runoff and Q/P is the runoff ratio. Canopy data is shown with a c and intercanopy data with int.

	Plot type		Date [mm/dd/yyyy]	P_E [mm]	T_{LP} [min]	Q_T [L]	Q_P [L/s]	Q/P [-]
NFS	Upslope	c	7/18/2008	12.5	7.3	24.1	0.129	0.22
		c	9/09/2008	10.1	8	4.3	0.019	0.05
		int	7/18/2008	12.5	7.3	6.1	0.04	0.06
		int	8/29/2008	3.8	0.3	6.9	0.009	0.21
		int	9/09/2008	10.1	8.2	5.3	0.03	0.06
		int	5/22/2009	3.3	39.5	1	0.002	0.04
		int	5/23/2009	5.1	50	1.3	0.002	0.03
		int	5/23/2009	0.2	14.2	0.1	0.002	0.04
		int	5/24/2009	1.1	8.8	0.1	0.001	0.01
	Downslope	c	7/13/2008	5.1	21.2	5.4	0.003	0.12
		c	7/18/2008	12.5	7.3	5.6	0.047	0.05
		c	9/09/2008	10.1	8	1.3	0.01	0.01
		c	4/11/2009	0.3	0.3	0.3	0.002	0.11
		int	7/18/2008	12.5	6.5	7.9	0.053	0.07
		int	9/09/2008	10.1	8.7	1	0.008	0.01
		int	5/23/2009	6.4	13.3	0.7	0.005	0.01

SFS canopy (S_c) plots (20 events), followed by the SFS intercanopy (S_i) plots (15 events), the NFS intercanopy (N_i) plots (10 events), and finally the NFS canopy (N_c) plots (6 events). Within each slope, the differences in ΣQ_T between canopy and intercanopy plots were relatively minor, $\sim$10% for the SFS plots and $\sim$25% for the NFS plots. These differences are product of the varying ΣQ_T in the upslope plots since the downslope plots showed very similar ΣQ_T between plots of the same aspect slope. Notably, in all the cases, ΣQ_T was considerably higher on the upslope plots, partly as a result of higher frequency of Q (except for N_c where the downslope plots recorded more Q events).

To further characterize and compare the runoff of the opposing slopes we calculated a number of runoff descriptors based on the analyses of runoff hydrographs (Table 6.2; Dingman 2000). In this study we present the relationship

Table 6.3: Characteristics of recorded runoff events on the SFS during the study period. P_E is total event rainfall, T_{LP} is time lag to peak, Q_T is total runoff, Q_P is peak runoff and Q/P is the runoff ratio. Canopy data is shown with a c and intercanopy data with int.

	Plot type		**Date** [mm/dd/yyyy]	$\mathbf{P}_E$ [mm]	$\mathbf{T}_{LP}$ [min]	$\mathbf{Q}_T$ [L]	$\mathbf{Q}_P$ [L/s]	**Q/P** [-]
SFS	**Upslope**	**c**	7/18/2008	15.4	7.7	21.4	0.117	0.16
		c	7/22/2008	8.7	32	2.9	0.004	0.04
		c	8/05/2008	4.1	0.3	16.6	0.026	0.47
		c	8/16/2008	7.4	12.3	1.3	0.006	0.02
		c	8/29/2008	3.8	32.2	1.4	0.009	0.04
		c	9/09/2008	10.3	8.2	25.9	0.082	0.29
		c	4/11/2009	1.7	51.2	0.1	0.002	0
		c	5/23/2009	6.5	52.2	4.4	0.006	0.08
		c	5/23/2009	6.3	11.3	27.2	0.035	0.5
		c	7/31/2009	3.8	59.5	15.5	0.061	0.47
		c	6/08/2009	11	6.8	11.3	0.045	0.12
		int	7/18/2008	15.4	7.5	8.5	0.034	0.06
		int	8/16/2008	7.4	3.2	11.2	0.01	0.17
		int	9/09/2008	10.3	8.2	28.6	0.093	0.32
		int	4/11/2009	1.7	51.2	1.1	0.003	0.07
		int	5/22/2009	3.4	40.2	3.9	0.003	0.13
		int	5/23/2009	6.5	51.8	0.2	0.002	0
		int	5/23/2009	6.3	12.3	79	0.072	1.44
		int	5/24/2009	1.4	4.2	8.8	0.004	0.72
		int	7/31/2009	11	7.3	10	0.038	0.1
	Downslope	**c**	7/18/2008	15.4	7.7	13.6	0.114	0.1
		c	8/16/2008	7.4	12.8	1.7	0.012	0.03
		c	9/09/2008	10.3	8.2	15.5	0.053	0.17
		c	4/11/2009	1.7	51.5	0.2	0.005	0.02
		c	5/23/2009	6.5	53.5	0.5	0.004	0.01
		c	5/23/2009	6.3	11.5	0.5	0.004	0.01
		c	7/31/2009	3.8	59	5.1	0.036	0.15
		c	6/08/2009	11	7.2	9	0.036	0.09
		c	9/18/2009	4.4	15.7	2.5	0.008	0.07
		int	7/18/2008	15.4	7.5	7.4	0.073	0.06
		int	9/09/2008	10.3	8.2	5	0.019	0.06
		int	4/11/2009	1.7	51.5	0.1	0.003	0.01
		int	5/23/2009	6.3	11.3	25.5	0.034	0.47
		int	7/31/2009	3.8	1	2.7	0.012	0.08
		int	6/08/2009	11	7.2	5.2	0.022	0.05

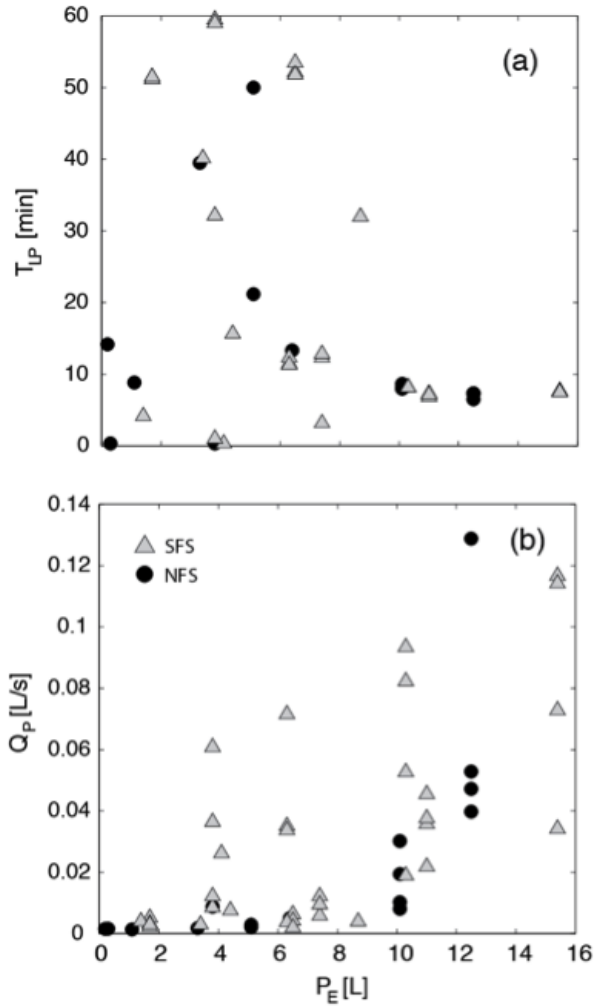

Figure 6.14: Scatter plots of (a) Time lag to peak (T_{LP}), and (b) peak runoff (Q_P) as a function of total event rainfall (P_E). Light gray triangles are SFS data points and black solid circles are NFS data points.

between total event precipitation (P_E) to the time lag to runoff peak (T_{LP}; Figure 6.14a), and to runoff peak (Q_P; Figure 6.14b). Although the relationship between P_E and T_{LP} looks cumbersome, there seems to be a threshold-like pattern of response between these two variables; for very large P_E ($\geq$ 10mm) there is a consistent and almost constant response in T_{LP} (10 min). The relation between P_E and Q_P is not less cumbersome for the SFS, however, the threshold pattern also appears between these variables. For $P_E \leq 3$ mm SFS Q_P yield values of ≤ 0.01 Ls^{-1}, while for $P_E \geq 3$ mm there is an increasing trend of Q_P with a wide range of values (0.01 - 0.12 Ls^{-1}). Finally, NFS Q_P seems to follow a more or less clear positive exponential relation with Q_P.

6.3.5 Evapotranspiration and Energy Fluxes

The quantification of the evapotranspiration (ET) and the differences in energy fluxes at each location is central to this study. Figure 6.15 shows time series of rainfall at the Control (a), ET (b) and midday evaporative fraction (EF) at each location (c), and the control based differences in midday available energy ($\Delta R_n - G$; d), and daily sensible heat flux (ΔH) between the opposing NFS and SFS (e). Careful inspection of Figure 6.15b reveals that ET in the NFS (ET_{NFS}) is always lower than ET at Control ($ET_{Control}$) and SFS (ET_{SFS}), except for a short period between April and May 2009. While ET_{SFS} and $ET_{Control}$ are very similar for the most part, there are slight differences during the summer and parts of the fall and winter time. From the late spring (i.e., early June) to the late summer (i.e., late August) the responses of $ET_{Control}$ to significant ($\geq$5 mm) rainfall pulses are stronger than those of ET_{SFS}, posibly, a result from higher momentum transfer, since the Control location is more exposed to higher windspeeds (Figure

6.9e). On the contrary, slightly larger ET_{SFS} is shown during the fall and winter months, reflecting the larger SFS available energy ($R_n - G$) for λE transfers registered during these periods. Because ($R_n - G$) is always larger on SFS, EF_{SFS} was lower than the similar EF_{NFS} and $EF_{Control}$ trouhgout the year. The modulating effect of topography on the energy fluxes leading to different ET rates in the opposing slopes is clearly shown in Figure 6.15d and e. Differences in both, midday ($R_n - G$) and H reach a minimum (≤ 2 MJ) during late spring trhough early summer and peak (≥ 6 MJ) during late fall and early winter. Because the differences in H mimic those of ($R_n - G$), and considering the influx of water for the opposing slopes close to equal, then, the observed differences in ET are proportional to the differences in ($R_n - G$).

6.3.6 Water balance at the slopes

Analyses of ET and soil moisture relations shown in Figure 6.16 exhibit marked contrasts between NFS and SFS. Figure 6.16a shows the fraction of ET contributed by soil moisture ($\Delta\theta$/ET) at 10 and 20 cm, and the total ET for each season. Two observations stand out from this Figure: first, seasonal ET totals and $\Delta\theta$/ET on both slopes follow a sinusoidal pattern, which in the case of $\Delta\theta$/ET dampens with depth; second, the seasonal sinusoidal pattern of $\Delta\theta/ET_{SFS}$ is in phase with seasonal ET totals, contrary to the ET out of phase $\Delta\theta/ET_{NFS}$. While $\Delta\theta/ET_{SFS}$ diminishes with decreasing seasonal ET, $\Delta\theta/ET_{NFS}$ increases, and vice versa. The opposite behavior of $\Delta\theta$/ET between the NFS and SFS is a clear indication of distinct ET soil-water pools through the seasons for each slope. Our data suggests that during the summer the majority of the NFS ET is taken from the topsoil (i.e., 0-7 cm), and as time progresses and the topsoil moisture is depleted the ET demand is then supplied by deeper soil moisture. On the other

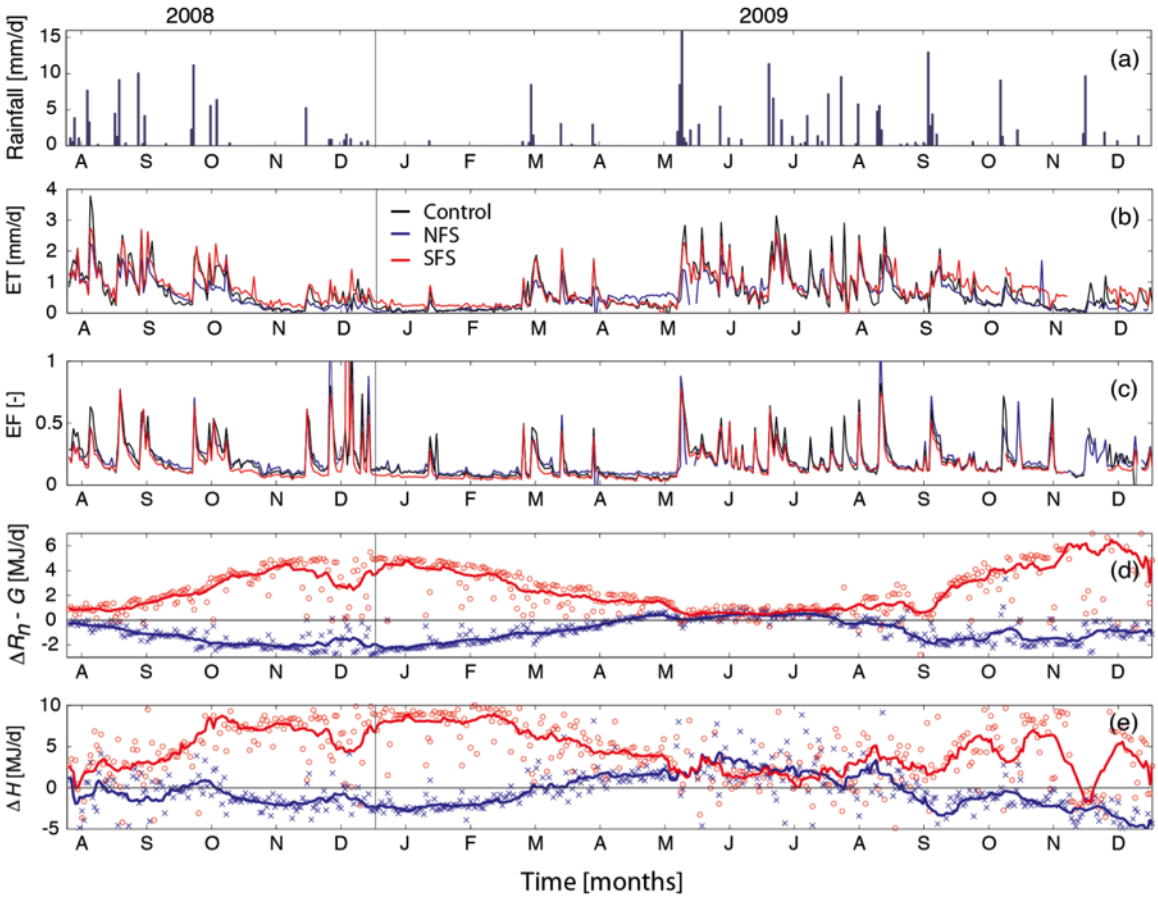

Figure 6.15: Time series of: (a) rainfall at the Control; (b) evapotranspiration (ET); (c) midday evaporative fraction (EF); Control based differences in midday available energy ($\Delta R_n - G$) for the NFS (blue) and SFS (red), and; Control based differences in total daily sensible heat (ΔH) for the NFS (blue) and SFS (red) locations.

side, the contribution of the shallow soil moisture to the SFS ET seems to follow the seasonality of rainfall contributing more water to ET when there is more rainfall.

The opposite behavior of $\Delta\theta/ET$ between the NFS and SFS is a clear indication of distinct ET soil water pools of the slopes throughout the seasons. To further explore the observed θ-ET relations we constructed a climograph for the NFS and SFS (Figure 6.16b) in a similar way to those shown by Mahmood and Vivoni (2011). To construct the climographs we plotted $\Delta\theta/P$ as a function of ET/P. In this study $\Delta\theta/P$ is the amount of soil water evaporated (removed) from a particular depth (e.g., 10 and 20 cm) shown as a fraction of the total season rainfall; and, ET/P is the amount of ET shown as a fraction of the rainfall on a season. That is, for $ET/P<1$ some rainfall was stored, for $ET/P \approx 1$ all rainfall is removed by ET, and for $ET/P > 1$ the system (i.e., NFS or SFS) is using stored water from previous seasons or years. In other words, the plot informs about the water balance of the soil at a particular depth as a function of the water balance (i.e., storage status) of the system. Additionally, we used arrows to connect the data points in the climograph to depict the seasonal trajectories of the water balance on the opposing slopes. Because as in $\Delta\theta/ET$ (Figure 6.16a) the behavior of $\Delta\theta/P$ for each slope is very similar between depths (i.e., only dampens from 10 to 20 cm) we only connected the 10 cm datapoints. Note distinct seasonal trajectories on the water balance (i.e., ET/P) of the opposing slopes: on the NFS the Summer and Fall rainfall (i.e., moonson rainfalls) supply enough water for ET demands ($ET/P \approx 1$) while Winter and Spring rains do not suffice the ET demands and stored water might be used ($ET/P > 1$); on the other hand, for the SFS only the moonson rains fell during the summer seem to meet the ET demands

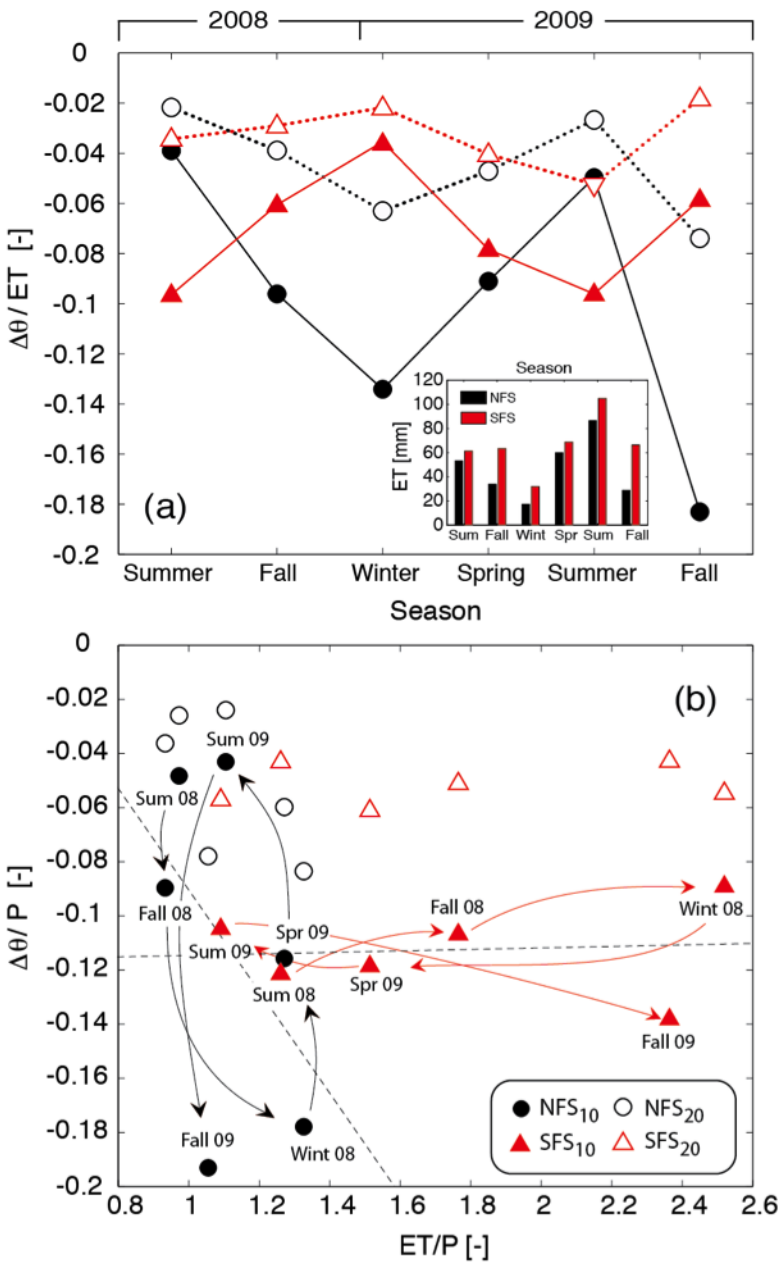

Figure 6.16: (a) Average fractional contribution of soil moisture to ET ($\Delta\theta/ET$) plotted for every season, slope (circles (NFS), and triangles (SFS)), and monitoring depth (solid lines-symbols (10 cm), open symbols dashed-lines (20 cm)). Inset plot shows the total ET for each season on NFS (black) and SFS (red). (b) Seasonal climograph of the mean slope $\Delta\theta/P$ as a function of ET/P for NFS (circles) and SFS (triangles) observations at 10 cm (solid) and 20 cm (open) soil depths. For reference, the dashed lines show the linear regressions for NFS10 (diagonal) and SFS10 (horizontal) data, and the arrows depict the seasonal trajectories of $\Delta\theta/P$ vs. ET/P.

(ET/P$\approx$1) while the rest of the year ET far exceeds rainfall inputs (ET/P$\gg$1), specially during Fall and Winter time.

Looking at the combined seasonal water balances of the soils (i.e., $\Delta\theta$/P) and the ecosystems (i.e., ET/P) the climograph shows clear differences between the north-facing and south-facing slopes (Figure 6.16b). On the SFS, ET/P varies greatly with the season (1<ET/P_{SFS} <2.5), with Winter and Fall ET exceeding by more than twice P, while $\Delta\theta$/P remains relatively constant at both depths (0.9<SFS_{10}<0.14, and 0.4<SFS_{20}<0.6). The combination of a wide range of ET/P >1 and a narrow range on $\Delta\theta$/P for the SFS indicates that regardless of how much water is removed from storage, the fraction of rainfall water contributed by θ to ET at both sampling depths is always the same, and for that reason the extra water should come from deeper soil layers. On the other hand, the variation of ET/P on the NFS is remarkably smaller than at its counterpart (0.95<ET/P_{NFS}<1.33), but the variation in $\Delta\theta$/P is notably larger on the NFS at both depths (-0.19<NFS_{10}<-0.04, and -0.8<NFS_{20}<-0.2), indicating that NFS uses considerably less storage of soil water to meet ET demands, and contrary to SFS a greater fraction of that water comes from shallow soil water storage. These differences in the seasonal system and soil water balances between the slopes reinforce the argument that NFS ET is mainly supported by shallow soil moisture, while the sources of ET on SFS vary greatly in the course of the year. It is important to note, however, that the large water imbalance on the SFS during most part of the year it is indicative of the shrubs' use of relatively deep moisture sources, well into the caliche layers of the soil profile (i.e., ¿ 2m depth). While this is feasible for the creosote shrubs and their extreme ability to extract water even from deep and highly indurated $CaCO_3$ (Duniway et al., 2010), this will require the existence of sufficient moisture reaching those depths from preferential pathways (e.g., root macropores, or

perched zones) into the caliche, possibly from large episodic rainfalls. The magnitude of this imbalance on the SFS requires further investigation, as the confirmation of this finding will imply an advanced capacity of the Creosote shrubs to produce biomass under extreme arid conditions and to significantly impact the rates of water fluxes into and out of the soils with consequences to the deep recharge on these areas.

6.4 Discussion and Summary

6.4.1 Topographic Modulated Energy Balance and Microclimate

In the study basin the energy balance of the slopes is primarily controlled by the topographic modulation of the radiation balance, on which the larger component is SW_{in} (Figures 6.7 and 6.6). Comparisons of the SW_{in} radiation of the slopes agree well with results from previous spatial radiation modeling studies in our study basin (Gutiérrez-Jurado and Vivoni, 2011) and with other studies simulating near ground SW_{in} in synthetic slopes of north and south aspects (Zou et al., 2007). Most importantly, the energy balance directly impacts ET capacities by modulating the amounts of available energy for latent heat transfers on each slope. On the NFS midday available energy differences with respect to SFS can account for as much as 8 MJ during the lower energy influx seasons (i.e., Fall and Winter), and as little as 2 MJ during the highest energy influx seasons (i.e., Spring and Summer). Comparisons between midday available energy of a grassland and shrubland from a nearby area yielded similar values to those found during the growing season (Kurc and Small, 2002).

Local land surface conditions such as soil moisture and vegetation type and cover comprise second order controls on the energy balance of the slopes

through their effects on albedo (Rinehart et al., 2007) and soil heat fluxes (G) (Kurc and Small, 2002). In our study we provide evidence of lower albedo on the NFS between the opposing slopes during the growing season. In addition, canopy cover may interact with topographic slope and aspect to amplify energy balance differences between opposing slopes. For example, previous work in our study basin, has shown that woody canopy cover of the Juniper trees on the NFS effectively decreases SW_{in} throughout the year with important implications on the variability in energy balance dynamics between NFS and SFS (Gutiérrez-Jurado and Vivoni, 2011.b). Also, Breshears et al., (1997) in a study of near-ground solar radiation along a grassland forest continuum noted that the physical presence of woody canopies reinforces spatial heterogeneity in microclimate. In this study we verified that differences in energy balance between the slopes translate into distinct magnitudes of important microclimatic variables directly influencing the rates of latent heat transfers and soil moisture residence times. For example, we recorded larger vapor pressure deficits ($\sim$10% on average) on the SFS compared to the NFS during the Winter and Spring seasons. Similarly, we found large differences in T_s ($\sim$10 °C) and moderate variability in T_a ($\sim$0.5 °C) between the opposing slopes during the periods with largest available energy divergences (.i.e., late Fall, Winter, and early Spring). The observed periodicity in microclimatic differences between the opposing slopes is in phase with the topographic amplification of seasonal energy balance differences, and therefore we confirm the hypothesis of the topographic induced microclimates in our study basin. This finding is in agreement with those from Desta et al. (2004), who reported large differences in microclimate among aspects of the four cardinal directions in a North American watershed, including significant air temperature differences between Mesic (north and east aspects) and xeric (west and southwest aspects) sites.

Ultimately the observed differences in microclimatic properties can have important ecologic and plant succession implications on the co-exisiting ecosystems of the study basin (Breshears et al., 1998), as microclimatic properties such as land-surface temperature have demonstrated to provide a feedback mechanism inducing the encroachment of shrubs into grasslands in the northern Chihuahuan desert (D'Odorico et al., 2010).

6.4.2 Topographic-Vegetation Controls on Soil Moisture Dynamics

In a study on the Mackenzie flats in the eastern Sevilleta LTER, Kurc and Small (2006) found minimal differences in shallow ($\sim$2.5 cm) soil moisture residence times ($\Delta\tau$ $<$0.5 days) between a grassland and a shrubland during the growing season (i.e., summer months). In addition, they found that the time constants for ET on both sites correlated well with their shallow θ residence times (τ) while poor relationships with deeper moisture sources were found, indicating that in these ecosystems the majority of ET during the growing season comes from shallow soil moisture stored after significant rainfall pulses. In our study area due to the slightly larger soil moisture dataset ($\sim$3.5 years) we were able to calculate τ for three different seasons (Winter τ were difficult to obtain due to the low intensity-magnitude rainfall pulses for that part of the year), at two depths and different slope positions. Our aim was to contrast the effect of topography and its potential influence on seasonal τ resulting from the observed energy and microclimatic induced differences between the slopes. Considering the differences in θ sampling depths between Kurc and Smalls study site and our slopes, the estimated summer τs on the SFS shrublands (3-4 days for this study and 2.5 days for the Eastern Sevilleta) and the NFS Juniper-grass savanna (4.5-5

days for this study and 2.8 days for the Eastern Sevilleta) seem plausible (Figure 6.11). During Fall and Spring energy balance and microclimatic differences between the slopes are essentially the same. However, the τ values for the slopes differ significantly between the two seasons (e.g., 4 to 2 days depending on position within the slope), suggesting other factors intervene in defining the rates of θ removal. We hypothesize that during the Fall the late monsoon rainfalls and the accumulated moisture of the Summer triggers a quick transpiration response of the plants on both slopes that helps maintain similar τs between the opposing slopes (Yoder and Nowak, 1999; Castellano-Perez et al., 2008; Notaro et al., 2010). However, during the Spring season only perennials (i.e., Juniper trees on the NFS and Creosote bushes on the SFS) may be actively transpiring (Oechel et al, 1972; Smith et al., 1997; Schott and Pieper 1985) due to the slow come back of annuals (i.e., grasses and other shrubs) from winter dormancy (Notaro et al., 2010). Therefore, the differences observed between Fall and Spring τ of the opposing slopes illustrate the active role of vegetation on mediating the control of the energy inputs on the rate of soil water transfers to the atmosphere. If these assertions are correct, then there is a strong legacy effect on the θ dynamics of the opposing slopes driven by the phenological constraints of the ecosystems.

6.4.3 Surface Water Fluxes on the Opposing Slopes: the case of Runoff and Evapotranspiration

A fundamental aim of this study was to quantify and contrast the water fluxes on the opposing slopes and to assess the resulting water balances in terms of the observed differences in terrain and vegetation properties. As a first consideration, recalling that both NFS and SFS have very similar rainfall inputs (Figure 6.8), therefore, the observed differences in Runoff (Q) and ET fluxes are a

result of local slope attributes in terms of energy balance, microclimate, and land surface conditions (i.e., vegetative cover, slope degree, soil development and others). Although Q in the slopes of the study basin comprise only a small percent (<5 %) of the total water inputs, the large differences observed in the recorded frequency and magnitude of Q events between the opposing slopes supports the hypothesis of distinct infiltration capacities for each ecosystem (Gutiérrez-Jurado et al., 2006), and agrees with previous observations at the study site on the differential runoff responses to large rainfall events (Gutiérrez-Jurado et al., 2007). Hydrograph analyses on the Q events recorded in this study confirm distinct rainfall-runoff dynamics between the NFS and SFS; a considerably smaller threshold in total event precipitation ($P_E < 4$L) for the SFS triggered stronger Q peak ($0.01 < Q_P < 0.06$ Ls^{-1}) discharges with more variable time lags between runoff initiation and Q_P ($0 < T_{LP} < 60$ min), while larger P_E thresholds ($P_E > 10$ Ls^{-1}) were needed to produce similar Q_P on the NFS (Figure 6.14). The unique rainfall-runoff dynamics of each slope reflect distinct erosion capacities and nutrients cycling and redistribution competences along the slopes that can have important implications on the ecology of the opposing ecosystems (Turnbull et al., 2010.a,b). It is also clear from these observations, that higher erosion rates and nutrient losses may occur on the SFS, while lower erosion and nutrients mobility are expected on the NFS.

Evapotranspiration (ET) dynamics on the study basin are highly influenced by the energy loads on each system (i.e., NFS, SFS, and Control). Therefore, the magnitudes and responses of ET to rainfall inputs vary greatly with the season (Figure 6.15). Because both ecosystems in our study basin are water limited in nature (Milne et al., 2003), the ET demand exceeds the availability of water for latent heat transfers most of the time. This is well illustrated in the very similar

evaporative fraction (EF) time series of the opposing slopes and the Control site. Nevertheless, discernible differences in both EF and ET among the three locations occur right after significant rainfall pulses during the time windows when differences in available energy ($R_n - G$) grow larger (e.g., Fall and Winter; Figure 6.15). Other studies addressing ET dynamics of semiarid areas, performed in a nearby location with flat terrain and comparable vegetation characteristics report similar ET and EF values during the growing season (Kurc and Small 2002; Kurc and Small 2007). Our study, however, addresses the quantification of ET dynamics on the opposing slopes on essentially an annual basis, and therefore we were able to show the strong seasonal effect on ET rates.

The observations on the study basin provide sufficient evidence to confirm that the water balance and the dynamics on water fluxes of the opposing slopes are highly constrained by non-linear interactions between topographic mediated ET demands, and the effect of land surface properties (more specifically slope position, vegetation type and cover and soil characteristics) in conserving or shedding important ecosystem resources (i.e., water, soils, nutrients). These findings support the conceptual model of the topographic induced ecohydrologic units proposed for semiarid catchments, in which the combination of singular vegetation-terrain characteristics creates a surface template establishing a series of feedbacks mechanisms that self-reinforce the imposed ecohydrologic dynamics of the system. The results of this study have important implications for the understanding of the potential causes and effects of vegetation changes in semiarid areas under current climate change scenarios, and provide a conceptual framework for the systematic study of different vegetation-terrain-hydrologic interactions found at other latitudes and longitudes.

REFERENCES

Zhang, W., and Montgomery, D. R. (1994), Digital elevation model grid size, landscape representation, and hydrologic simulations, *Water Resour. Res.*, 30, 1019-1028.

Armesto J. J., and Martínez J.A. (1978), Relations Between Vegetation Structure and Slope Aspect in the Mediterranean Region of Chile, *J. Ecology*, 66 (3), 881-889.

Astrom, M., Dynesius, M., Hylander, K. and Nilsson, C. (2007), Slope aspect modifies community responses to clear-cutting in boreal forests, *Ecology*, 88(3), 749-758.

Badano, E. I., Caviares, L. A., Molina-Montenegro, M. A. and Quiroz, C. L. (2005). Slope aspect influences plant association patterns in the Mediterranean, *J. Arid Environments*, 62, 93-108.

Bennie, J., Huntley, B., Wiltshire, A., Hill, M.O., and Baxter, R. (2008.a), Slope, aspect and climate: Spatially explicit and implicit models of topographic microclimate in chalk grassland, *Ecological Modelling*, 216, 47-59.

Bennie, J., Hill, M.O., Baxter, R., and Huntley, B. (2008.b), Influence of slope and aspect on long-term vegetation change in British chalk grasslands, *Journal of Ecology*, 94, 355-368.

Boulanger JR. 2004. *Stable isotope partitioning of evapotranspiration across a shrub-grass ecotone following a precipitation event Sevilleta National Wildlife Refuge, USA*. MS Thesis, New Mexico Institute of Mining and Technology, Socorro, NM. 66 pp.

Brakensiek D.L., Osborn H.B. and Rawls W.J. (1979), *Field Manual for Research in Agricultural Hydrology: Agricultural Handbook No. 224*, United States Department of Agriculture, pp. 88-125.

Breshears, D. D., Cobb N. S., Rich P. M., Price K. P., Allen C. D., Balice R. G., Romme W. H., Kastens J. H., Floyd M. L., Belnap J., Anderson J. J., Myers O. B., and Meyer C. W. (2005), Regional vegetation die-off in response to global-change-type drought., *Proceedings of the National Academy of Sciences of the United States of America*, 102(42), 15144-8, doi:10.1073/pnas.0505734102.

Breshears, D. D., Rich, P. M., Barnes, F., and Campbell, K. (1997), Overstory-imposed heterogeneity in solar radiation and soil moisture in a semiarid woodland, *Ecological Applications*, 7(4), 1201-1215.

Breshears, D. D., Rich, P.M., Barnes, F.J., and Campbell, K. (1998), Effects of woody plants on microclimate in a semiarid woodland: soil temperature and evaporation in canopy and intercanopy patches, *Int. J. Plant Sci.*, 159, 1010-1017.

Brooks, P.D. and Vivoni, E.R. (2008), Mountain ecohydrology: quantifying the role of vegetation in the water balance of montane catchments. *Ecohydrology. 1*(3): 187-192.

Campbell Scientific (2000), *CNR1 Net Radiometer Instructions Manual*, Campbell Sci., Inc., 1-23.

Cantlon J.E. (1953), Vegetation and Microclimates on North and South Slopes of Cushetunk Mountain, New Jersey, *Ecological Monographs*, 23(3), 241-270.

Castellanos-Perez, E., de Soyza A., and Donart G. (2008), Photosynthesis and water use efficiency of the association between *Larrea tridentata* (DC) Cov . and *Muhlenbergia porteri* Scribn, *Int. J. Experimental Botany*, 77, 297-320.

Chen, J., Saunders, S.C., Crow, T.R., Naiman, R.J., Brosofske, K.D., Mroz, G.D., Brookshire B.L., Franklin J.F. (1999), Microclimate in Forest Ecosystem and Landscape Ecology, *BioScience*, 49(4), 288-297.

Chmura D. 2008. The slope aspect affects the heterogeneity and growth of ground flora vegetation in deciduous temperate forest. *Polish Journal of Ecology*, 56, 463470.

Coble D. W., Milner K.S., Marshall J.D. (2001), Above- and below-ground production of trees and other vegetation on contrasting aspects in western Montana: a case study, *J. For. Ecol. Management*, 142, 231-241.

Cottle H.J. (1932), Vegetation on North and South Slopes of Mountains in Southwestern Texas, *Ecology*, 13(2), 121-134.

Desta F., Hicks R.R. Jr., Colbert J. J., (2003), Influence of topographic aspect, precipitation and drought on radial growth of four major tree species in an Appalachian watershed, *J. For. Ecol. Management*, 177, 409-425.

Desta F., Colbert J. J., Rentch J. S. and Gottschalk, K. W. (2004), Aspect Induced Differences in Vegetation, Soil, and Microclimatic Characteristics of an Appalachian Watershed, *Castanea* 69(2), 92-108.

Dingman, L. S. (2000), *Physical Hydrology*, 2nd edition, Prentice Hall, 365 pp.

D'Odorico, P., J. D. Fuentes, W. T. Pockman, S. L. Collins, Y. He, J. A. Medeiros, S. DeWekker, and M. E. Litvak. (2010), Positive feedback between microclimate and shrub encroachment in the northern Chihuahuan desert, *Ecosphere* 1(6):art17. doi:10.1890/ES10-00073.1

Duniway, M. C., J. E. Herrick, and H. C. Monger (2010), Spatial and temporal variability of plant-available water in calcium carbonate-cemented soils and consequences for arid ecosystem resilience., *Oecologia*, 163(1), 215-26, doi:10.1007/s00442-009-1530-7.

Fritschen, L. J., and Simpson, J.R. (1989), Surface energy and radiation balance systems: General description and improvements, *J. Appl. Meteorol.*, 28, 680-689.

Gallardo-Cruz, J.A., Prez-Garca, E.A., Meave, J. A. (2009), Diversity and vegetation structure as influenced by slope aspect and altitude in a seasonally dry tropical landscape, *Landscape Ecology*, 24 (4), 473-482. doi: 10.1007/s10980-009-9332-1.

Gutiérrez-Jurado, H. A., Vivoni, E. R., Istanbulluoglu, E., and Bras, R. L. (2007), Ecohydrological response to a geomorphically significant flood event in a semiarid catchment with contrasting ecosystems. *Geophys. Res. Lett.*, 34, L24S25, doi:10.1029/2007GL030994.

Gutiérrez-Jurado, H. A., and Vivoni, E.R. (2011), Ecogeomorphic expressions of aspect-controlled semiarid basins: I. Topographic analyses with high resolution datasets. *Ecohydrology* (in press).

Gwinn R. W. (1984), Chute entrances for HS, H, and HL flumes, *J. Hydraulic Engineering*, 110 (5), 587-603. doi: 10.1061/(ASCE)0733-9429(1984)110:5(587)).

Gwinn R. W. and Parsons D. A. (1976), Discharge equations for HS, H, and HL flumes, *J. Hydraulic Division*, 102 (5), 11874-11887

Holland, P. G., and Steyn, D. G. (1975), Vegetational responses to latitudinal variations in slope angle and aspect, *J. Biogeography*, 2, 179-183.

Holland, P. G., Steyn, D. G., and Fuggle, R. F. (1977), Habitat occupation by Aloe ferox Mill. (Liliaceae) in relation to topographic variations in direct beam solar radiation income, *J. Biogeography*, 4(1), 61-72.

Ivanov, V. Y., Bras, R. L., and Vivoni, E. R. (2008a), Vegetation-hydrology dynamics in complex terrain of semiarid areas. I. A mechanistic approach to modeling dynamic feedbacks, *Water Resour. Res.*, 44, W03429, doi:10.1029/2006WR005588.

Ivanov, V. Y., Bras, R. L., and Vivoni, E. R. (2008.b), Vegetation-hydrology dynamics in complex terrain of semiarid areas: 2. Energy-water controls of vegetation spatiotemporal dynamics and topographic niches of favorability, *Water Resour. Res.*, 44, W03430, doi:10.1029/2006WR005595.

Istanbulluoglu, E., Yetemen, O., Vivoni, E. R., Gutirrez-Jurado, H. A., and Bras, R. L. (2008), On the topographic imprint of vegetation: Inferences from regional analysis of landscape morphology in central New Mexico, *Geophys. Res. Lett.* 34, L14403, doi:10.1029/2008GL034477.

Kimball, B.A., Jackson, R.D., Nakayama, F.S., Idso S.B., and Reginato, R.J. (1976),Soil-heat Flux Determination: Temperature Gradient Method with Computed Thermal Conductivities, *J. Soil Sci. Soc. Am.*, 40, 25-28.

Kurc, S. and Small, E. (2004), Dynamics of evapotranspiration in a semiarid grassland and shrubland ecosystems during the summer-monsoon season, central New Mexico, *Water Resour. Res.*, 40, W09305, doi: 10.1029/2004WR003068.

Kurc, S. a, and E. E. Small (2007), Soil moisture variations and ecosystem-scale fluxes of water and carbon in semiarid grassland and shrubland, *Water Resour. Res.*, 43(6), 1-13, doi:10.1029/2006WR005011.

Kutiel P. (1992), Slope aspect effect on soil and vegetation in a Mediterranean ecosystem, *Israel Journal of Botany*, 41, 243250.

Kutiel P. Lavee H. (1999), Effect of slope aspect on soil and vegetation properties along an aridity transeat, *Israel Journal of Plant Sciences*, 47, 169178.

Lin, H. (2006) Temporal stability of soil moisture spatial pattern and subsurface preferential flow pathways in the shale hills catchment, *J. Vadose Zone*, 5, 317-340.

Martinez-Fernandez, J., Ceballos, A. (2003), Temporal stability of soil moisture in a large-field experiment in Spain, *J. Soil Sci. Soc. Am.*, 67, 1647-1656.

McMahon, D. R. (1998), *Soil, landscape and vegetation interactions in a small semiarid drainage basin: Sevilleta National Wildlife Refuge, New Mexico*. MS Thesis. New Mexico Institute of Mining and Technology. Socorro, NM. 174 pp.

Milne, B. T., Moore, D. I., Betancourt, J. L., Parks, J. A., Swetnam, T. W., Parmenter, R. R., and Pockman, W.T. (2003), Multidecadal drought cycles in south-central New Mexico: Patterns and consequences. In: *Climate Variability and Ecosystem Responses at Long-Term Ecological Research Sites*, Greenland, D., Goodin, D. G., Smith, R. C. (eds). Oxford University Press: New York, NY, 286-307.

Mooney H.A., Dunn E.L., Shropshire F., Song L. (1975), Vegetation comparisons between the Mediterranean climatic areas of California and Chile, *Flora*, 159 (5), 480-496.

Nie, D., Flitcroft, I.E. and Kanemasu, E.T., (1992), Performance of Bowen ratio systems on a slope, *J. Agric. For. Meteorol.*, 59, 165-181.

Notaro, M., Liu, Z., Gallimore, R. G., Williams, J. W., Gutzler, D. S., and Collins, S. (2010), Complex seasonal cycle of ecohydrology in the Southwest United States, *J. Geophys. Res.*, 115, 1-20. doi:10.1029/2010JG001382.

Liang, E., Shao, X., Eckstein, D., Huang, L., Liu, X. (2006), Topography- and species-dependent growth responses of Sabina przewalskii and Picea crassifolia to climate on the northeast Tibetan Plateau, *Forest Ecology and Management*, 236(2-3), 268-277. doi: 10.1016/j.foreco.2006.09.016.

Oechel W.C., Strain B.R., Odening W.R., (1972), Tissue water potential, photosynthesis, C-14-labeled photosynthate utilation, and growth in desert shrub Larrea divaricata cav. *Ecological Monographs* 42, 128141.

Parsons D.J. (1976), Vegetation Structure in the Mediterranean Scrub Communities of California and Chile, *Ecology* 64 (2), 435-447.

Parsons D.U., and Moldenke A.R. (1975), Convergence in Vegetation Structure along Analogous Climatic Gradients in California and Chile, *Ecology*, 56 (4), 950-957.

Perez, P.J., Castellvi, F., Ibanez, M., Rossell, J.I. (1999), Assessment of reliability of Bowen ratio method for partitioning fluxes, *J. Agric. For. Meteorol.*, 97, 141-150.

Rinehart, A. J., Vivoni, E. R., and Brooks, P. D. (2008), Effects of vegetation, albedo and solar radiation sheltering on the distribution of snow in the Valles Caldera, New Mexico, *Ecohydrology*, 1, 253-270.

Schott, M.R., and Pieper, R.D. (1985), Influence of canopy characteristics of One-seed Juniper on understory grasses, *J. Range Mgmt.*, 38(4), 328-331.

Seager R., Ting M.F., Held I.M., Kushnir Y., Lu J., Vecchi G., Huang H.P., Harnik N., Leetmaa A., Lau N.C., Li C., Velez J., Naik N., (2007), Model Projections of an Imminent Transition to a More Arid Climate in Southwestern North America. *Science*, 316,(5828), 1181 1184. DOI: 10.1126/science.1139601

Segal, M., Mahrer, Y., Pielke, R.A. and Ookouchi, Y., (1985), Modeling transpiration patterns of vegetation along south and north facing slopes during the subtropical dry Season, *Agric. For. Meterol.*, 36, 19-28.

Smith S.D., Monsoon R.K., Anderson J.E., (1997). *Physiological Ecology of North American Desert Plants*. Springer, New York.

Sternberg, M., Shoshany, M. (2001), Influence of slope aspect on Mediterranean woody formations: Comparison of a semiarid and an arid site in Israel, *Ecology Research*, 16, 345355.

Tian Y.Q., Davies-Colley R.J., Gong, P., Thorrold, B.W. (2001), Estimating solar radiation on slopes of arbitrary aspect, *J. Agric. For. Meteorol.*, 109, 67-74.

Thomey, M. L., Collins, S. L., Vargas, R., Johnson, J. E., Brown, R. F., Natvig, D. O., Friggens, M. T. (2011), Effect of precipitation variability on net primary production and soil respiration in a Chihuahuan Desert grassland. *Global Change Biology*, 17(4), 1505-1515. doi:10.1111/j.1365-2486.2010.02363.x

Tromp-van Meerveld, H.J., McDonnell, J.J. (2006). On the interrelations between topography, soil depth, soil moisture, transpiration rates and species distribution at the hillslope scale, *Adv. Water Res.*, 29, 293-310.

Turnbull, L., Wainwright, J., Brazier, R. E. (2010.a). Hydrology, erosion and nutrient transfers over a transition from semiarid grassland to shrubland in the South-Western USA: A modelling assessment. *Journal of Hydrology*, 388(3-4), 258-272. doi: 10.1016/j.jhydrol.2010.05.005.

Turnbull, L., Wainwright, J., Brazier, R. E. (2010.b). Nitrogen and phosphorus dynamics during runoff events over a transition from grassland to shrubland in the south-western United States. *Hydrological Processes*, 25(1), 1-17. doi: 10.1002/hyp.7806.

Turnbull L., Wainwright J., and Brazier R. E. (2010.c), Changes in hydrology and erosion over a transition from grassland to shrubland, *Hydrol. Process.*, 24, 393-414, doi:10.1002/hyp.7491.

Turnbull, L., Wainwright, J., Brazier, R. E., Bol, R. (2010.d). Biotic and Abiotic Changes in Ecosystem Structure over a Shrub-Encroachment Gradient in the Southwestern USA. *Ecosystems*, 13(8), 1239-1255. doi: 10.1007/s10021-010-9384-8.

Wang L., Wei S., Horton R., Shao M. (2011), Effects of vegetation and slope aspect on water budget in the hill and gully region of the Loess Plateau of China, *Catena*, 87, 90-100.

Warren R.J. (2010), An experimental test of well-described vegetation patterns across slope aspects using woodland herb transplants and manipulated abiotic drivers, *The New phytologist*, 185(4), 1038-49. doi: 10.1111/j.1469-8137.2009.03147.x.

Yoder, C.K., and Nowak R.S. (1999), Soil moisture extraction by evergreen and drought-deciduous shrubs in the Mojave Desert during wet and dry years, *Journal of Arid Environments*, 42(2), 81-96, doi:10.1006/jare.1999.0504.

Zou, C. B., Barron-Gafford, G. A., and Breshears, D. D. (2007), Effects of topography and woody plant canopy cover on near-ground solar radiation: Relevant energy inputs for ecohydrology and hydropedology. *Geophys. Res. Lett.* 34, L24S21, doi: 10.1029/2007GL031484.

CHAPTER 7

CONCLUSIONS

7.1 Epilogue

In this dissertation we investigated the relations between topography, vegetation, and hydrology in semiarid areas. During the development of this research and through the last part of this investigation, we used data and observations from a first order catchment with clear vegetation contrasts and almost exact north and south facing slopes and a transitional headslope facing east. In Chapter 2 we investigated the physical mechanisms affecting, soil development and hydrologic fluxes in semiarid complex terrain, using data from the study site. To accomplish this task, we assessed the effect of terrain aspect on root zone hydrologic fluxes and soil development in two ecosystems by using soil observations, hydraulic properties from pedotransfer functions, and a one-dimensional numerical model of vadose zone fluxes. In Chapter 3 we documented the differential response of the two hillslope ecosystems to a geomorphically significant flood event using field observations of rainfall, soil moisture and peak channel discharge. We illustrated the role played by slope position, soil properties and vegetation on soil moisture dynamics and runoff production after an exceptionally large rainfall event. In the subsequent chapters (Chapter 4 and 5) using a sequence of improved spatial resolution digital terrain models, we investigate the potential feedbacks of topographic form on the geomorphic processes evidenced

in opposing hillslopes, and, the expected radiation differences on the study basin hillslopes promoted by the interactions between vegetation and terrain properties. Finally, in Chapter 6 we propose a conceptual model of topographic-induced ecohydrological units as a means to explain the observed contrasts in land surface properties and processes of semiarid catchments with opposing slopes. This conceptual model is verified with $\sim$3.5 years of observations on the hydrologic and energy fluxes divergences of the opposing hillslopes, obtained with the deployment of a network of sensors. The results of Chapter 6 are discussed in light of the implications to the ecology and hydrology of semiarid areas with complex terrain.

7.2 Synthesis

To commence the investigation of topographic-vegetation-hydrologic interactions in the study basin, a set of preliminary analyses on the salient features potentially determining quantifiable differences between the opposing hillslopes were performed. A large part of these initial efforts was based upon previous work performed on the characterization of soil development, vegetation composition and structure differences in the opposing hillslopes, by McMahon (1998). Using a simple 1D modeling approach of the vertical fluxes of water on the opposing slopes, the effect of terrain aspect on root zone hydrologic fluxes and soil development in the two ecosystems was assessed. Marked differences in root zone fluxes in the north-facing Juniper and south-facing Creosote ecosystems were found. Differences in the amplitude and frequency of soil water content and pressure correspond to changes in soil profile and vegetation characteristics. For example, soil properties of the calcium carbonate ($CaCO_3$) horizons and

differential plant water uptake impact the simulated soil water pressure over an 8-year period in the opposing ecosystems. Variations in water fluxes reinforce the development of $CaCO_3$ horizons present in the soil profiles, leading to a feedback between vegetation establishment, soil water fluxes and geomorphic processes in the catchment. The results at this stage also suggested that soil properties and water fluxes could compensate for large differences in evaporative demand leading to similar actual evapotranspiration (AET) in the opposing slopes. These results motivated the quantification of water fluxes between the opposing hillslopes to verify this results at later stages in this research.

Recognizing the influence of the soils-vegetation interactions in the simulated water fluxes resulting from the 1D modeling exercises, the study basin was instrumented with a network of rain gauges, weather stations and soil moisture and temperature transects along the three basin hillslopes. This initial set of sensors captured a large summer moonson storm estimated to have a return period of $\sim$150-200 years, providing evidence on the remarkable differences in hydrologic and geomorphic responses between the opposing slopes. The unusually high water input from this storm produced observable geomorphic changes in the opposing slopes that were more dramatic on the south facing slope. Furthermore, evidence from the soil moisture records illustrate substantial differences in the recession rates of soil water along the slopes, where a strong control of slope position due to overland and subsurface runoff redistribution mechanisms is inferred. The hydrologic response to these events has implications on the effects of vegetation on long-term hillslope runoff and evolution.

Starting with the premise that vegetation effects on hydrogeomorphic processes require detailed studies at the catchment scale, we set on to look for a distinctive signature of vegetation-geomorphic interactions that could be extracted

from elevation fields in the study area. Topographic analyses using a set of terrain metrics, and a series of improved digital elevation models (DEMs) ranging from 10 to 1 m resolution, progressively revealed geomorphic differences in north and south facing hillslopes associated with vegetation contrasts. For example, less frequent fluvial erosion occurs in the more mesic juniper-grass ecosystem of the north facing slope as compared to the xeric desert shrubland of the south facing slope. Furthermore, the high resolution data (1m) from the Light Detection and Ranging (LiDAR) survey also revealed weakly steeper north facing slopes, contradicting previous work with coarser topographic products. A sensitivity analysis revealed that hillslope diffusion occurs in north facing ecosystems due to relatively higher slope, while fluvial erosion in the south facing, xeric ecosystems results from larger contributing areas. High resolution LiDAR data was also able to discriminate statistically different sediment transport regimes in north and south facing slopes due to different dominant factors. Improvements in the definition of ecogeomorphic properties confirm the need for high resolution ($<$1m) DEMs for assessing vegetation-topographic interactions at the catchment and hillslope scales. This is now increasingly feasible with the advent of LiDAR technologies, capable of surveying large expanses of terrain without compromising data quality and precision and generating sub-meter digital elevation products.

One of the primary hypothesis on which the causes for the observed differences in vegetation and morphological characteristics may rest is on the differential radiation loads between the contrasting ecosystems dictated by the effect of slope and aspect. Prior studies have been performed using coarse resolution datasets in which the effect of tree shading and other topographic obstacles could not be captured. For semiarid areas of complex terrain, faint nuances in moisture

status and radiation sheltering may signify the difference between the establishment of mesic or xeric vegetation, and an according moisture dynamics. Using a distributed solar radiation model, and the same set of sequentially improved resolution products used for exploring vegetation-geomorphic interactions, we found remarkably-enhanced irradiance fields for the study basin. The novelty produced with this study was the incorporation of a digital surface model with tree canopies, from LiDAR technology. When assessing the improvements in capturing irradiance differences in the opposing slopes, the vegetated LiDAR offered far better results in terms of the spatial distribution of irradiance and wider range of low radiation areas located on places visibly sheltered by the effect of tree canopies and natural topographic obstructions. The expected result from these improvements in the estimation of the radiation loads within the study basin was the remarkably reduced irradiance in the north facing slope throughout the year, supporting the notion that terrain aspect is a first order control on the spatial distribution of irradiance. Furthermore, tree cover and its spatial arrangement were found to be an important second order control on irradiance that can overwhelm topographic effects in specific locations and times of year. For example, differences between north and south facing slopes are maximized in the spring equinox, rather than the winter solstice, when tree shading and reflection are accounted for. North facing trees also diminish intercanopy radiation depending on tree cover and vegetation albedo, with important ecological implications for the conifer-grass association. Solar irradiance analysis helps identify the underlying topographic and vegetation controls on the energy fluxes in the opposing hillslope ecosystems, suggesting a feedback mechanism that helps reinforce the differences in vegetation establishment.

Looking for the causal effects on the observed differences in hydrologic dynamics and concurrent vegetation contrasts between the opposing aspect slopes, a conceptual model of topographic-induced ecohydrologic units was proposed and contrasted against observations from a network of water and energy fluxes sensing devices. After thorough analyses of $\sim$3.5 years of data, we obtained a clear characterization of the main hydrology and energy fluxes dynamics of the opposing slopes. Based on analyses of the magnitude of discrepancies and correlations between hydrologic forcings (i.e., rainfall, air temperature, available energy, momentum transfer) and states (i.e., soil moisture and temperature) between the opposing slopes, we found that the primary control on the observed vegetation-terrain contrasts was topographic slope and aspect through the strong influence on energy inputs affecting the water balance of the slopes. The results reveal a definite influence of topography on the accentuation of seasonal differences in energy balance between the slopes. We found that the modulating effect of topography on the energy inputs of the opposing ecosystems is driven by the amplification and dampening of the seasonal incoming solar radiation on the north and south facing slopes respectively. The next question raised is, if this observed amplification of seasonal contrasts between the opposing slopes is translated into climatic changes deviating from the regional regime, and to what extent?

Recorded micrometeorological variables at each slope revealed significant deviations of the regional climatic regime registered on the Control monitoring location above the study catchment. The reported hillslope meteorological deviations give rise to particular microclimatic properties for each slope that have a recurring and well defined periodicity. The observed behavior of climatic parameters such as, air and soil temperature, and vapor pressure deficits are in phase

with the topographic amplification of seasonal divergences in energy balance between the opposing slopes. For instance, greater vapor pressure deficits, air and soil temperatures on the SFS during the low available energy seasons (i.e., Winter and Spring) may sustain higher demands of latent heat transfers compared to the NFS. Additionally, the rates of momentum transfer recorded as windspeed are consistently and permanently lower on the NFS compared to the SFS and Control locations, due to the higher surface roughness imposed by the greater vegetation cover of the Juniper trees. In conjunction, the lower temperatures, vapor pressure deficits, and momentum transfers on the NFS imply a slower and smaller rate of latent heat transfers compared to the neighboring SFS, where the recorded microclimatic conditions suggest a more efficient environment for the rapid transfer of soil water to the atmosphere. In other words, the topographically imposed characteristics of the slopes do modify the regional climatic regime to create, in one hand, the conditions for the longer preservation of moisture and sustenance of the more mesic vegetation on the NFS and on the other hand the ideal settings for the immediate release of moisture on the SFS, generating a more arid shrubland environment.

Throughout this research it has become evident the combined effect of topography and land surface properties on soil moisture in the study basin. Soil moisture (θ) dynamics on the opposing slopes were found to be remarkably different. For instance, θ time series analyses on the NFS revealed a strong control of slope position on the infiltration, redistribution and recession rates of moisture after large rainfall events, despite having similar soil profile properties along the slope. A particularity that is not present on the SFS, where no redistribution of moisture and a more uniform behavior of infiltration and recession rates was

observed regardless of location within the slope. Analyses of soil moisture residence times (τ) showed increasing or decreasing differences between and within the slopes depending on the season. For instance, Summer τs on the NFS are $\geq$ 2 days than on the SFS for all locations, while τ differences between the opposing slopes decrease to $<$ 1 day during the Fall. However, during the spring time τ differences between and within the slopes were greatest, with values as large as 5 days. It is worth noting that the period where τ differences grow larger coincides with the time of the year where vegetation activity recovers from winter dormancy, suggesting a strong control of plants on Spring τs. Based on the evidence shown in Chapters 2, 3, 5, and 6, we found consistently higher soil moisture retention on the NFS (lower moisture recession rates, longer residence times, and higher moisture content through time) compared to the SFS. This is clearly due to the combination of soil morphological characteristics (higher fractions of fines), and a reduced ET demand resulting from lower energy influx available for latent heat transfers also evidenced in the significantly lower soil temperatures year round. Joint time stability analyses of soil moisture and temperature revealed a characteristic progression of soil moisture-temperature values along the slope aspect continuum (i.e. north-east-south facing slopes) that is preserved throughout the year, going from the wetter and cooler soils on the north facing slope to the drier and warmer soils on the south facing slope. The time stability analyses also showed that soils become hydrologically more heterogeneous with depth within the root zone. Ecologically, the consistently higher and more permanent moisture of the shallow soils on the NFS may benefit the more mesic vegetation on that hillslope.

The quantification of water fluxes into and out of the slopes was a central objective to this study. Field reconnaissance observations after an exceptional

rainfall event on the summer of 2006, and subsequent analyses on measured rainfall-runoff relations on the study basin hillslopes confirm the remarkable differences in runoff (Q) production between the contrasting ecosystems. The analyses show that Q on the SFS is produced with a smaller precipitation threshold, with higher peak discharges, more frequently, and in larger quantities than on the NFS. The more responsive rainfall-runoff relations of the SFS are consistent with the considerably lower vegetation cover and rainfall interception capacity of the shrubs, and the higher connectivity of bare ground areas compared to the land cover conditions on the NFS. Moreover, the sharp contrast in rainfall-runoff dynamics of the slopes is also expressed in the current edaphic and geomorphic properties of the study catchment, where the SFS have coarser grained soils with thinner B horizons, thin or no A horizons and more dissected slopes than its counterpart. Additionally, the observed runoff differences between the opposing slopes are in good agreement with the results from the hydrogeomorphic analyses using high resolution digital elevation data (i.e., LiDAR) and provide supporting evidence to the argument of vegetation-topographic feedbacks on polar facing slopes (i.e. north facing slopes for the northern hemisphere), where a relatively dense and mesic vegetation reduces the runoff-erosion potential, conserving more soil and nutrients that ultimately benefits the self-perpetuation of the prevailing vegetation-topographic conditions.

An important objective of this study was the quantification of Evapotranspiration (ET) on the contrasting slope-ecosystems. Our data and analyses showed that ET on the NFS was always lower than on the SFS and Control location, that this difference grows larger during the Fall and Winter seasons, and gets to a minimum during Spring and Summer time. Analyses of the seasonal trajectories of water fluxes in the study basin indicate that ET in the study catchment is highly

constrained by the dynamics of energy fluxes mediated by topographic and vegetation properties. We found that ET fluxes on each slope are strongly modulated by the incident irradiance and the resulting available energy (i.e., $R_n - G$) for latent heat transfers. Our data showed that the disparity in ET between the opposing slopes are proportional to the differences in $(R_n - G)$, and are consistent with the seasonal amplification of microclimatic divergences between the NFS and SFS.

In the study catchment soil moisture differences between the opposing slopes are modulated by ET demands and soil characteristics. Water balance analyses on the opposing slopes using soil moisture-ET relations suggest vegetation acts to mediate ET fluxes through their control on transpiration (T) and their adaptations to local conditions (e.g., rooting depth) that allow them to access soil moisture at different depths, and to create more suitable habitats (i.e., soil development, intercanopy space adjustments and competition) that ultimately provide the conditions necessary to survive under a water limited regime. The observations on the study basin clearly indicate that the dynamics of water fluxes and balances on the contrasting ecosystems are tightly controlled (highly constrained) by non-linear interactions between topographic mediated ET demands, and the effect of land surface properties (more specifically slope position, vegetation type and cover and soil characteristics) in conserving or shedding important ecosystem resources (i.e., water, soils, nutrients). These findings are in agreement with the conceptual model of the topographic induced ecohydrologic units proposed in Chapter 6. This conceptual model proposes that the combination of singular vegetation-terrain characteristics on the slopes of a semiarid basin creates a surface template modifying the regional climatic-ecologic-hydrologic regime, establishing a series of feedbacks mechanisms that self-reinforces the imposed ecohydrologic dynamics of the system. Throughout this study we demonstrate the

strong coupling between patterns of terrain, energy and water balance, resulting in the current vegetation distributions of the study basin. The mechanics on vegetation-terrain-hydrology interactions described here for water limited areas I believe may be also valid at other locations with similar environmental characteristics, although with other vegetation types. Thus, the resulting conclusions and the overall study framework could be accordingly generalizable, and therefore translated to other places.

7.3 Recommendations and future work

This work was limited to the investigation of the ecohydrologic dynamics of contrasting vegetated slopes with a brief excursion on the current geomorphic expressions and properties of opposing slopes. Although several aspects of the complex interactions on vegetation-terrain-hydrology were investigated, measurements, observations and simulation of these interactions were constrained to the shallow layers of the soil ($<$2m depth) and their connection to the land surface-atmospheric continuum. Therefore, a study connecting the hydrologic dynamics of deeper soil and the potential effect on subsurface conditions will provide a better portrait of vegetation effects on the partition and water balance of the two ecosystems. Similarly, the partition of soil water into infiltration and deep percolation was only addressed with a numerical model exercise. The verification of those results could be valuable in assessing the potential effects of vegetation-topographic relations on the recharge of aquifers underneath semiarid hillslopes with marked vegetation contrasts. Moreover, the large water imbalance on the SFS on the dry seasons shown in chapter 6 requires further investigation. The hypothesis provided in this work to explain this phenomenon asserts that the

large imbalance is product of the transpiration of the Creosote shrubs by accessing deep soil water when the shallow soil moisture has been depleted. This could be tested with transpiration measurements on a number of shrubs using sapflow techniques to contrast them with additional measurements of soil moisture or soil water pressure along a soil profile of considerable depth ($> 2m$).

An always challenging and important variable to obtain for the study of topography-ecohydrologic relations is reliable and verifiable data on the root depth and structure of the keystone species. Studies addressing this lack of proper root datasets could be of great advantage, particularly for the proper parameterization of ecohydrologic models for semiarid areas, in as much as this variable can significantly alter the results from such models.

Spatial explicit ecohydrologic models simulating the interactions of woody plants and grasses could help explain some of the variations in soil moisture observed in this study. The datasets provided in this dissertation could be used to parameterize and verify future modeling efforts of this nature. Similarly, the investigation of the spatial heterogeneity in moisture and plant resources imposed by the aggregation of woody canopies by means of modeling studies and or extensive field measurements could help to clarify observed vegetation mortality from previous droughts. This is of particular importance for the prediction of vegetation responses to increasing temperatures and more frequent and longer droughts expected as a result from global warming.

APPENDIX A

CORRECTION FOR HORIZONTALLY BASED RADIATION MEASUREMENTS ON SLOPED TERRAIN

This appendix describes in detail the methods and equations used to correct for the slope and aspect effect on the global incoming shortwave radiation measured on the slopes of the study catchment with horizontally placed net radiometers. The method is based on the equations by Tian et al., (2001) with adjustments for the calculation of the radiation balance on an instantaneous basis as opposed to the original daily based equations. According to Tian et al., (2001) the SW_{in} of a sloping surface can be calculated from:

$$G_a = Q_r + D_r + A_r \tag{A.1}$$

where G_a is the global radiation received on an inclined surface with arbitrary orientation and is equivalent to SW_{in}; Q_r is the irradiance received by the surface directly from the solar beam; D_r is the amount of diffuse radiation reaching the ground and emitted isotropically from all sky directions; and A_r is the radiation received on the surface by reflection from blocking terrain. The terms in the right hand side of equation (1) are calculated as follows:

$$Q_r = G_m \cdot R_d \cdot (1 - K_r) \tag{A.2}$$

$$D_r = G_m \cdot f_\beta \cdot K_r \tag{A.3}$$

$$A_r = G_m \cdot alb \cdot (1 - f_\beta) \tag{A.4}$$

where G_m is the global incoming radiation measured on a horizontal surface; R_d is the ratio of direct radiation on the slope (K_{ETsl}) to direct radiation on a horizontal surface (K_{ETh}):

$$R_d = \frac{K_{ETsl}}{K_{ETh}} \tag{A.5}$$

The detailed derivation of the methods to obtain the terms in eqn. (A.5) can be lengthy and complicated (Revfeim, 1978; Iqbal, 1983); for this reason, we describe the methods used in this study to compute K_{ETsl} and K_{ETh} in subsections (A.a) and (A.b) respectively. K_r is the ratio of diffuse to global radiation; f_β is a slope reduction factor accounting for the portion of the sky hemisphere above the slope surface that is blocked by the horizontal plane (Tian et al., 2001); and, alb is the albedo of the land surface calculated at each time interval using the ratio $alb = SW_{in}/SW_{out}$. The ratio of diffuse to global radiation can be calculated using the following empirical relation:

$$K_r = a \cdot K_t + b = f \cdot \frac{G_h}{H_o} \tag{A.6}$$

where K_t is the ratio of global (G_h) to extraterrestrial radiation (H_0) and a and b are empirical coefficients related to local climatic conditions. The slope reduction factor f_β is obtained by:

$$f_\beta = 1 - \frac{\beta}{180} \tag{A.7}$$

where β is the slope angle of the terrain in degrees.

A.1 Calculation of the instantaneous direct radiation on a horizontal surface

Using a series of astronomical relations to account for the effect of the varying suns beam angle incident on the earth at any given day and time of the year, the instantaneous direct radiation on a horizontal plane K_{ETh} is calculated following Iqbal (1983) as:

$$K_{ETh} = I_{sc} \cdot E_o[(\cos(\delta) \cdot \cos(\Lambda) \cdot \cos(\omega \cdot t_d) + \sin(\delta) + \sin(\Lambda)] \tag{A.8}$$

where $I_{sc} = 1367$ Wm^{-2} is the average radiation flux on a plane perpendicular to the solar beam on the upper atmosphere; E_0 is an eccentricity correction factor that accounts for the changes in the relative distance between the sun and the earth and is calculated for any day of the year as:

$$\begin{aligned} E_o \quad &= \left(\tfrac{r_o}{r}\right)^2 = 1.00011 + 0.034221 \cdot \cos(\Gamma) + 0.0028 \cdot \sin(\Gamma) \\ &\quad + 0.000719 \cdot \cos(2 \cdot \Gamma) + 0.000077 \cdot \sin(2 \cdot \Gamma) \end{aligned} \tag{A.9}$$

where r_0 is the average sun-earth distance (km), r is the actual sun-earth distance at any time (km), and Γ is day angle (degrees) calculated as:

$$\Gamma = \frac{2 \cdot \pi \cdot (J - 1)}{365} \tag{A.10}$$

where J is the julian day of the year; δ is the declination angle (degrees) that incorporates the effect of the angle between an horizontal plane on the earth and the solar beam and it is computed as:

$$\begin{aligned}\delta \quad &= \left(\tfrac{180}{\pi}\right) \cdot [0.006918 - 0.399912 \cdot \cos(\Gamma) + 0.070257 \cdot \sin(\Gamma) \\ &- 0.006758 \cdot \cos(2 \cdot \Gamma) + 0.000907 \cdot \sin(2 \cdot \Gamma) - 0.002697 \cdot \cos(3 \cdot \Gamma) \\ &+ 0.000148 \cdot \sin(3 \cdot \Gamma)] \end{aligned} \tag{A.11}$$

Λ is latitude (degrees); ω is the angular velocity of the earths rotation (15 hr-1); and, t_d is the time before or after the solar noon (S_h), in hrs and therefore is calculated as a piecewise function:

$$t_d = \begin{cases} S_h - t & \text{if } t < S_h \\ S_h + t & \text{if } t > S_h \end{cases} \tag{A.12}$$

and S_h is computed as:

$$S_h = 12 - \left(\frac{E_{rc}}{60}\right) - \left(\frac{105 - \Omega}{15}\right) \tag{A.13}$$

where Ω is the longitude of the plane, and E_{rc} is the equation of time in hrs, obtained by:

$$E_{rc} = 987 \cdot \sin(2 \cdot \beta_{rc}) - 7.53 \cdot \cos(\beta_{rc}) - \cos(\beta_{rc}) - 1.5 \cdot \sin(\beta_{rc}) \tag{A.14}$$

where β_{rc} is a day time adjustment calculated for each day (J) as:

$$\beta_{rc} = \frac{360 \cdot (J - 81)}{364} \tag{A.15}$$

A.2 Calculation of the instantaneous direct radiation on a sloping surface

The calculation of the instantaneous direct radiation on a sloping plane K_{ETsl} was performed following a method described by Dingman (2000), and based on the concept of the equivalent slope by Lee (1964). The method is based on the fact that the solar beam angle of incidence on a sloping plane at a given geographic coordinate (i.e. Lat-Long) is equivalent to the angle of incidence on a horizontal plane at a different coordinate with as many degrees removed or added to the original Lat-Long location. Slight modifications to some equations were performed to obtain instantaneous rather than daily values (for further details the reader is referred to Dingman (2000)).

K_{ETsl} is calculated by:

$$K_{ETsl} = I_{sc} \cdot E_o \cdot [(\cos(\delta) \cdot \cos(\Lambda_{eq}) \cdot \cos(\omega \cdot t_{eq} + \Delta\Omega) + \sin(\delta) + \sin(\Lambda_{eq})] \tag{A.16}$$

where Λ_{eq} is the equivalent latitude of the horizontal plane, and is obtained by:

$$\Lambda_{eq} = \sin^{-1}[\sin(\beta) \cdot \cos(\alpha) \cdot \cos(\Lambda) + \cos(\beta) + \sin(\Lambda)] \tag{A.17}$$

where α is the slope azimuth or aspect orientation (degrees clockwise from north=0); $\Delta\Omega$ is the longitude difference between the equivalent plane and the original slope (Dingman, 2000), and it is computed as:

$$\Delta\Omega = \tan^{-1}\left[\frac{\sin(\beta) \cdot \sin(\alpha)}{\cos(\beta) \cdot \cos(\Lambda) - \sin(\beta) \cdot \sin(\Lambda) \cdot \cos(\alpha)}\right] \tag{A.18}$$

t_{eq} is the equivalent time before or after the solar noon for the original sloping surface (S_{sl}), and is calculated as a piecewise function:

$$t_{eq} = \begin{cases} S_{Sl} - t & \text{if } t < S_{Sl} \\ S_{Sl} + t & \text{if } t > S_{Sl} \end{cases} \tag{A.19}$$

the value for S_{Sl} is computed by adjusting the solar noon of the original longitude (eqn. A.a.6) to the time offset of $\Delta\Omega(T_{offset})$

$$S_h = 12 - \left(\frac{E_{rc}}{60}\right) - \left(\frac{105 - (\Omega + T_{offset})}{15}\right) \tag{A.20}$$

REFERENCES

Dingman, L. S. (2000), *Physical Hydrology*, 2nd edition, Prentice Hall, 365 pp.

Iqbal, M. (1983), *An Introduction to Solar Radiation*, Academic Press, Vancouver, BC., 390 pp.

Lee R. (1964), Potential insolation as a topoclimatic characteristic of drainage basins, *Bulletin of the International Association of Scientific Hydrology*, 9, 27-41.

Tian Y.Q., Davies-Colley R.J., Gong, P., Thorrold, B.W. (2001), Estimating solar radiation on slopes of arbitrary aspect, *J. Agric. For. Meteorol.*, 109, 67-74.

APPENDIX B

FIELD OBSERVATION DATASETS

The datasets from the instruments deployed at the study basin including: the micrometeorology, soil moisture and temperature transects, Bowen Ratio energy balance systems and Runoff Plots datasets are contained in a DVD appended to the back of the Thesis document. Excel spreadsheets contain the relevant data sets: NFS0609.xls, SFS0609.xls, and Control0609xls, NFSBREB.xls, SFSBREB.xls, ControlBREB.xls, and Runoff-characteristics.xls. Each sheet has a table with site locations and variables. Appropriate tables with detailed description of the data contained in the Excell spread sheets are provided in the form of read me files: Readme-NFS.doc, Readme-SFS.doc, Readme-Control.doc, and Readme-BREB.doc.

APPENDIX C

RUNOFF PLOTS DESIGN AND DIMENSIONS

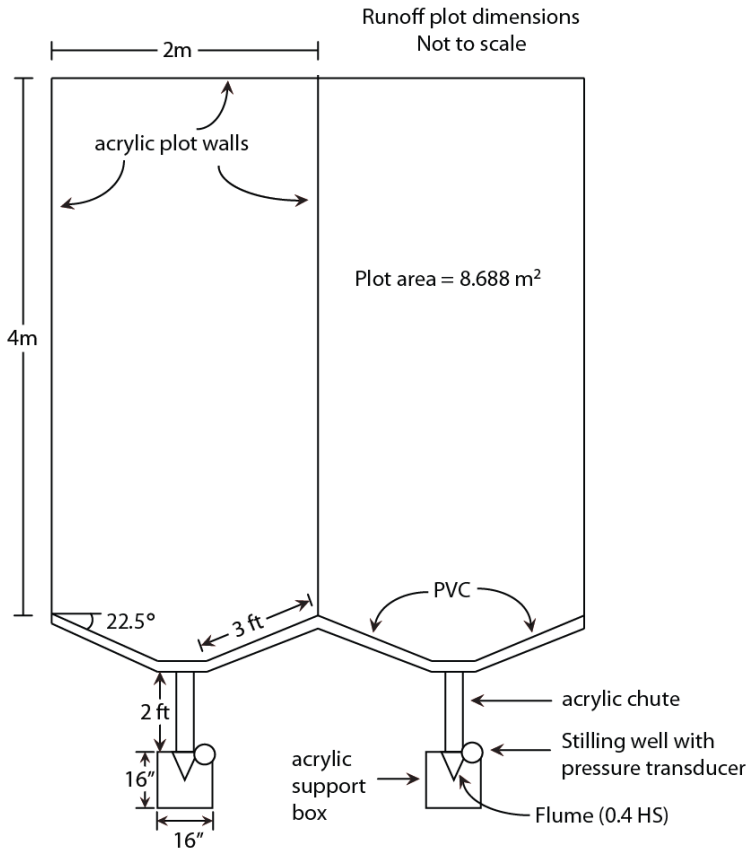

Figure C.1: Runoff plots plan view

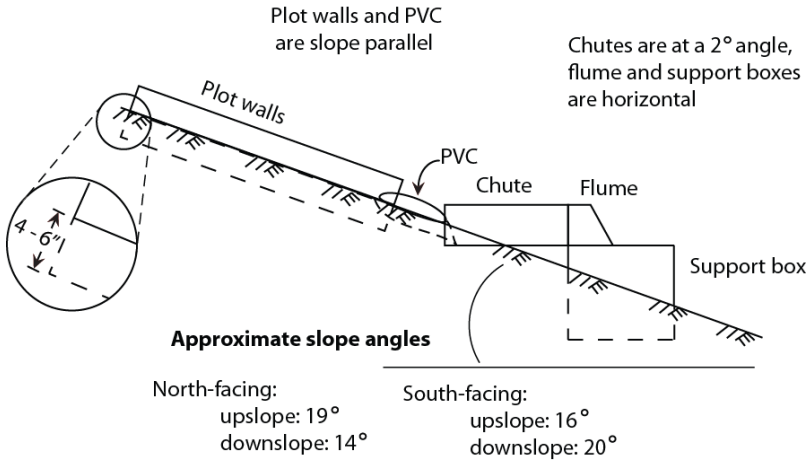

Figure C.2: Runoff plots side view

APPENDIX D

SITE SPECIFIC SOIL PROPERTIES FOR THE CONVERSION OF VOLUMETRIC SOIL MOISTURE VALUES

Table D.1: Site specific soil properties for the conversion of θ values. Dbρ stands for dry bulk density

Location	27/06/2006 Dbρ (g/cm3)	28/06/2006 Dbρ (g/cm3)	29/06/2006 Dbρ (g/cm3)	24/07/2006 Dbρ (g/cm3)	25/07/2006 Dbρ (g/cm3)	12/11/2006 Dbρ (g/cm3)	Average Dbρ (g/cm3)	Porosity [-]
E2a	1.452	1.921	1.534	1.695	-	-	1.65	0.377
E2b	1.275	1.77	1.501	1.573	-	-	1.53	0.423
E1a	1.363	1.711	1.738	-	-	-	1.604	0.395
E1b	1.133	1.709	1.707	-	-	-	1.516	0.428
CH2a	1.54	1.823	1.691	1.828	-	-	1.721	0.351
CH2b	1.523	1.875	1.472	1.732	1.633	1.677	1.652	0.377
N1a	1.399	1.845	1.582	1.641	1.482	-	1.59	0.4
N1b	1.363	1.436	1.717	1.8	1.656	1.291	1.544	0.417
cN1a	1.469	1.73	1.655	1.86	1.713	-	1.685	0.364
cN1b	0.974	1.766	1.458	1.884	1.768	1.437	1.57	0.408
N2a	1.611	1.693	1.603	1.611	1.588	-	1.621	0.388
N2b	1.505	1.546	1.713	1.739	1.542	1.555	1.6	0.396
cN2a	1.345	1.481	1.482	1.927	1.763	-	1.6	0.396
cN2b	1.115	1.766	1.446	1.817	1.567	-	1.542	0.418
N3a	1.31	1.664	1.517	1.713	1.59	-	1.559	0.412
N3b	1.505	1.552	1.666	1.664	1.856	-	1.649	0.378
cN3a	1.576	1.535	1.445	1.791	1.869	-	1.643	0.38
cN3b	1.735	1.609	1.657	1.89	1.526	1.69	1.684	0.364
N4a	1.7	1.955	1.593	1.727	1.708	-	1.737	0.345
N4b	1.735	1.983	1.722	1.716	1.8	1.621	1.763	0.335
S1a	1.381	1.815	1.888	2.092	-	-	1.794	0.323
S1b	1.452	1.476	1.477	1.942	-	-	1.587	0.401
cS2a	1.31	1.554	1.672	1.726	-	-	1.565	0.409
cS2b	1.54	1.715	1.521	1.762	-	-	1.634	0.383
S3a	1.275	-	1.575	1.807	-	-	1.552	0.414
S3b	1.292	-	1.935	1.822	-	-	1.683	0.365
cS3a	1.168	1.504	1.809	2.006	1.21	-	1.622	0.388
cS3b	1.045	1.338	1.453	1.914	-	-	1.437	0.458